AL-FARABI KAZAKH NATIONAL UNIVERSITY

UDC 54-414:628.316.12 On manuscript rights

RAKHYM AKMARAL BAKHYTZHANKYZY

Sorbents based on aluminosilicate raw materials for heavy metal ions, bisphenol-A and propranolol extraction from aqueous solutions

6D060600 – Chemistry

Dissertation submitted in fulfilment of the requirements for the degree of
Doctor of Philosophy (Ph.D.)

Scientific supervisors:
Doctor of chemical sciences, Professor
Seilkhanova Gulziya Amangeldyievna

PhD, Professor Yitzhak Mastai
Bar-Ilan University, Ramat-Gan, Israel

The Republic of Kazakhstan
Almaty, 2025

CONTENTS

INTRODUCTION 6

1 Literature review 12

1.1 Application of aluminosilicates for the extraction of various contaminants from aqueous solutions 12

1.1.1 Application of zeolites for extraction of contaminants from aqueous solutions 12

1.1.2 Application of clay materials for extraction of various contaminants from aqueous solutions 23

1.2 Methods for studying the mechanisms of adsorption of various pollutants on aluminosilicate sorbents 35

1.2.1 Instrumental physicochemical methods used for elucidation adsorption mechanisms 39

1.2.2 Effect of various factors on adsorption to elucidate the mechanisms 44

1.2.3 Overview of Theoretical Methods for Studying Adsorption Mechanisms 48

2. EXPERIMENTAL PART 64

2.1 Reagents and Materials 64

2.2 Aluminosilicate raw materials modification methods 67

2.3 Characterization of the adsorbent materials obtained 69

2.4 Adsorption experiments of studied pollutants (HM ions, BPA and PRO) onto adsorbents based on Zeolite and Clay 70

2.4.1 Adsorption experiments of studied HM ions (Pb^{2+}, Cd^{2+}, Sr^{2+}) onto adsorbents based on Zeolite and Clay 70

2.4.2 Adsorption experiments of studied organic pollutants (BPA and PRO) onto adsorbents based on Zeolite and Clay 70

2.5 Methods of modeling and statistical processing of adsorption results 71

2.5.1 Adsorption isotherm theories 71

2.5.2 Adsorption kinetic models 74

2.5.3 Calculation of thermodynamic characteristics of the adsorption process 77

2.5.4 Error function analysis of the experimental results 77

3 RESULTS AND DISCUSSION 79

3.1 Physico-chemical characterization of the obtained adsorbents 79
3.1.1 Physico-chemical characterization of the obtained Zeolite-based adsorbents 79
3.1.2 Physico-chemical characterization of the obtained Clay-based adsorbents.....92
3.2 Heavy metal ions extraction from aqueous solutions onto the adsorbents based on Zeolite and Clay 98
3.3 Investigation of optimum conditions for the adsorption of lead ions onto Clay 103
3.3.1 Effect of sorbent mass on the adsorption of lead ions onto Clay.....103
3.3.2 Effect of pH on the adsorption of lead ions onto Clay.....104
3.3.3 Effect of initial concentration and adsorption isotherms of lead ions by Clay 105
3.3.4 The effect of contact time and kinetics of Pb adsorption on Clay 108
3.3.5 The effect of temperature and thermodynamics of Pb adsorption on Clay.....111
3.3.6 The mechanism of adsorption of Pb(II) ions on Clay 113
3.4 A new approach to identify contributions of different types of interactions to adsorption mechanisms on aluminosilicates (Na-H method) 115
3.5 The study of organic pollutants extraction from aqueous solutions onto the adsorbents based on Zeolite and Clay.....118
3.6 Study of BPA and PRO adsorption mechanism on zeolite and DDAB based sorbents using Na-H method.....125
3.7 Practical application of the obtained results 129
CONCLUSIONS 138
REFERENCES 142
APPENDIX A. Flow-chart diagrams for optimal adsorbents synthesis.....167
APPENDIX B. Data for cost price calculation of modified adsorbents preparation 169

NORMATIVE REFERENCES

In this thesis references to the following standards are used:

GOST 6.38-90 Unified system of documentation. The system of organizational and administrative documentation. Requirements for documents.

GOST 7.1-84 System of standards on information, librarianship and publishing. Bibliographic description of the document. General requirements and rules.

GOST 7.1-2003 System of standards on information, librarianship and publishing. Bibliographic record. Abbreviations of words in Russian. General requirements and rules.

GOST 7.9-95 System of standards on information, librarianship and publishing. Summary and abstract. General requirements.

GOST 8.417-81 State system for ensuring the uniformity of measurements. Units of physical quantities.

GOST 7.32-2001 System of standards on information, librarianship and publishing. The research report. Structure and rules of presentation.

GOST 4233-77 Reagents. Sodium chloride. Specifications.

GOST 3118-77 Reagents. Hydrochloric acid. Specifications.

GOST 1277-75 Reagents. Silver nitrate. Specifications.

GOST 4461-77 Reagents. Nitric acid. Specifications.

GOST 4328-77 Reagents. Sodium hydroxide. Specifications.

GOST 4168-79 Reagents. Sodium nitrate. Specifications.

GOST 3773-72 Reagents. Ammonium chloride. Specifications.

GOST 83-79 Reagents. Sulfuric acid. Specifications.

GOST 4239-77 Reagents. Potassium hydroxide. Specifications.

GOST 4330-76 Reagents. Sodium carbonate. Specifications.

GOST 4140-74 Reagents. Strontium chloride, 6 aqueous. Specifications.

GOST 20490-75 Reagents. Potassium permanganate. Specifications.

GOST 4220-75 Reagents. Potassium bichromate. Specifications.

LIST OF ABREVIATIONS

BET – Brunnauer-Emmet-Teller method

BPA – bisphenol-A

Clay – Chamotte clay

C_e – equilibrium concentration

CEC – cation exchange capacity

DDAB – didodecyl dimethyl ammonium bromide

FTIR – Fourrier Transform Infrared Spectroscopy

H-Clay - Chamotte clay treated with HCl

H-Zeolite – zeolite treated with HCl

HM – heavy metal

K_d - adsorption equilibrium constant

K_t – rate constant

MAC – maximum acceptable concentration

Na-Clay – Chamotte clay treated with NaCl

Na-Zeolite – zeolite treated with NaCl

PRO – propranolol hydrochloride

q_e – adsorption capacity

SEM – Scanning Electron Microscopy

SLES – sodium laureth sulfate

s:l – solid : liquid ratio

XRD – X-Ray Diffraction

Zeolite – Shankanay natural zeolite

ΔG – Gibbs free energy

ΔH - enthalpy

ΔS - entropy

INTRODUCTION

General Description of This Work

This study focuses on developing efficient sorbents derived from aluminosilicate materials, specifically Shankanay natural zeolite (Zeolite) and chamotte clay (Clay), through modification with two surfactant types – anionic sodium laureth sulfate (SLES) and cationic didodecyldimethylammonium bromide (DDAB) – and their application in the extraction of heavy metal ions, bisphenol-A (BPA), and propranolol (PRO) from aqueous solutions. The investigation of the physicochemical and sorption properties of the synthesized sorbents has led to the proposal of a mechanism for their interaction with the chosen contaminants. Optimal conditions are created for the most successful sorbents examined in this study, and the thermodynamic and kinetic characteristics of the adsorption processes are investigated.

The Significance of This Work

Currently, water bodies contain many pollutants that are products of human activity: heavy metals, organic substances, dyes, residues of petroleum products and medicines, etc. The predominant and efficient technique for reducing the concentration of heavy metal ions in wastewater is sorption purification processes. Consequently, there is a necessity to obtain novel adsorbents that are more cost-effective than those now available in the market, while also being efficient and environmentally sustainable [1].

Natural aluminosilicate materials possess numerous features that endorse their use as sources for sorbents, catalysts, plasticizers, and reinforcing additives. Their main advantages are availability and relatively low price as compared to synthetic materials [2].

Natural aluminosilicates, in particular zeolites and clays, are known for their sorption activity concerning cations of heavy metals. Aluminosilicates can enhance their sorption activity through various chemical modifications, including ion exchange, alteration of the Si/Al ratio via direct synthesis under varying conditions, de-cationization resulting in hydrogen-enriched aluminosilicates, and dealumination through acid treatment, etc. [2].

However, natural aluminosilicates are unable to sorb negatively charged particles. Numerous contaminants possess negative charges, including viruses, bacteria, and metal anions such as chromates, nitrates, arsenates, and phosphates. The issue of wastewater contamination by endocrine-disrupting chemicals and medications containing phenolic groups is also presently significant [3]. The surfaces of zeolite and clay are changed with cationic surfactants to adsorb pollutants; these composite materials, known as surfactant-modified zeolites (SMZs) or surfactant modified clays (SMCs), have numerous applications [4]. SMZs and SMCs are organo-

aluminosilicates utilized for the extraction of organic contaminants, including petroleum products, pharmaceutical wastes, dyes, and humic acids from aqueous solutions [5,6].

Consequently, SMZs and SMCs can be considered as multifunctional amphiphilic adsorbents, efficient in the extraction of heavy metal cations and anions, as well as phenolic organic contaminants.

The Purpose of This Work

Obtaining novel efficient adsorbents based on natural aluminosilicate raw materials, in particular zeolite and Chamotte clay, and establishing the physicochemical regularities of heavy metal ions, bisphenol-A, and propranolol adsorption from aqueous solutions.

Key Research Tasks of the Thesis

- To obtain sorbents based on natural zeolite and Chamotte clay modified with an anionic surfactant – SLES or a cationic surfactant – DDAB.

- To evaluate the effect of modification on the physicochemical and sorption characteristics of the original zeolite and Chamotte clay.

- To apply the obtained adsorbents for extraction of heavy metal ions, bisphenol-A and propranolol from aqueous solutions and determine the most effective forms of sorbents for each studied pollutant.

- To analyze the kinetic and thermodynamic characteristics of the adsorption processes, as well as to establish the effect of various external parameters for Chamotte clay-Pb systems.

- To establish the interaction mechanisms of the reagents for Chamotte clay-Pb systems.

- To suggest ways of practical application of the results obtained.

Object of the Study

Sorbents based on zeolite and chamotte clay, modified with anionic surfactant – SLES or cationic surfactant – DDAB; aqueous solutions containing ions of various TM, bisphenol-A and propranolol.

Subject of the Study

Physicochemical, structural, textural, sorption characteristics of the obtained sorbents based on zeolite and chamotte clay, as well as kinetic and thermodynamic patterns of the processes of adsorption of heavy metal ions, bisphenol-A and propranolol ions from aqueous solutions.

Scientific Novelty

In this dissertation, sorbents based on natural zeolite from the Shankanay deposit (Almaty region, Kazakhstan) and chamotte clay modified with two types of surfactants – anionic SLES and cationic DDAB – have been obtained for the first time. The impact of modifying the initial materials through preliminary treatment with acid or salt on their physicochemical and sorption properties has been thoroughly investigated. The obtained new sorbents have been tested for the

extraction of heavy metal (HM) cations such as lead (II), cadmium (II), strontium (II), heavy metal anions such as permanganate and dichromate, as well as organic phenolic compounds such as bisphenol-A and propranolol. The most effective modified forms of the obtained sorbents have been determined for each pollutant.

The study established the optimal conditions for the adsorption process in the 'Clay/lead' system for the first time and determined that the mechanism of reagent interaction primarily occurs through ion exchange. A new method for evaluating the contributions of physical adsorption in pores and ion exchange to the interaction mechanism in the 'aluminosilicate sorbent/pollutant' system has been proposed, based on the analysis of identified patterns in the adsorption process and the effects of modifying the original materials on the physicochemical characteristics of the process under study. This method was evaluated on more complex systems: DDAB modified SMZs – BPA and DDAB modified SMZs – PRO.

The mechanism of interactions between surfactants and zeolite/Chamotte clay, as well as surfactants and Zeolite/Clay + HM ion, and DDAB – Zeolite, and DDAB-Zeolite + BPA/PRO, are described for the first time:

It is assumed that SLES molecules enter exchange reactions with water molecules on the Zeolite/Clay surface and are also electrostatically attracted by the excess positive charge formed by exchange cations on the mineral surface. The next SLES layer is sorbed due to the hydrophobic interaction of the surfactant "tails". Then the HM cations are sorbed due to 1) electrostatic attraction of the positively charged metal cation to the SLES sulfo group of the second layer; 2) donor-acceptor interaction between the metal ions and the free electron pair of oxygen of the SLES ethoxy group.

It is assumed that the DDAB molecule can interact with the Zeolite surface through electrostatic attraction with OH-groups adsorbed on the surface. Subsequent increase in DDAB concentration leads to bilayer formation and recharging of the Zeolite/Clay surface. Thus, the resulting DDAB bilayer leads to an excess of positive charge on the Zeolite/Clay surface, which attracts dichromate/permanganate anions. In the case of BPA, the adsorbent-adsorbate interaction mechanism may include chemisorption, electrostatic attraction, and hydrophobic interactions with the surfactant. For PRO, the adsorbent-adsorbate interaction mechanism possibly also includes physisorption.

Theoretical Significance

The theoretical significance of the results presented in the dissertation consists in establishing and analyzing the kinetic and thermodynamic parameters of the processes of adsorption of HM, BPA and PRO ions by sorbents based on Zeolite and Clay modified by surfactants; describing the chemistry of aluminosilicate-surfactant interactions, as well as sorbent-

sorptive; developing a new method for assessing the contribution of physical adsorption in pores and ion exchange to the mechanism of sorption of HM ions, as well as organic pollutants from aqueous solutions on aluminosilicate sorbents.

Practical Significance

The practical significance of the results obtained is as follows:

- It was found that Zeolite and Clay modified with SLES extract Cd^{2+} and Sr^{2+} ions by 90–97%; the original minerals without modification almost completely (98–99%) extract Pb^{2+} ions, which indicates the potential possibility of using these sorbents in the processes of water bodies purification.

- It was found that modification of acid-activated Zeolite and Clay with the cationic surfactant DDAB resulted in a notable enhancement of the sorption activity of the original minerals, with extraction rates increasing from 5% to 83%. This finding highlights the practical significance of the results for water purification processes targeting anionic forms of inorganic and organic pollutants.

- The potential for targeted delivery of medicinal compounds, specifically BPA and PRO, using the sorbents developed in this study has been demonstrated. However, further detailed research in the pharmaceutical field is essential for the practical implementation of this approach.

- The scientific results obtained in the field of physical chemistry on the establishment of kinetic and thermodynamic patterns of adsorption processes of inorganic and organic objects on aluminosilicate minerals can be recommended for implementation in the educational process: in the basic and elective courses "Applied Physical Chemistry", "Practical Chemical Kinetics", "Kinetics of Complex Processes", and "Reactivity of Solids".

Main Provisions for the Defense

1. Treatment with Na^{+}-ions increases the cation exchange capacity (CEC) of zeolite (from 616 to 624 meq/100 g) and chamotte clay (from 234 to 286 meq/100 g), whereas acid treatment decreases their CEC (to 129 and 104 meq/100 g, respectively) but enhances their specific surface area (from 4 to 39 m^2/g for zeolite and from 8 to 15 m^2/g for clay).

2. Modification with the anionic surfactant SLES increases the sorption activity of zeolite and chamotte clay (from 73% to 97% for Cd^{2+} cations and from 50% to 92% for Sr^{2+} cations om zeolite and from 68% to 97% for Cd^{2+} cations and from 41% to 64% for Sr^{2+} cations on chamotte clay) due to surface functionalization; modification with the cationic surfactant DDAB enables effective sorption of inorganic anions such as $Cr_2O_7^{2-}$ (from 5% to 80% on zeolite and from 7% to 82% on clay) and MnO_4^{-} (from 9% to 75% on zeolite and from 10% to 79% on clay) due to the formation of a positive surface charge.

3. Lead ions sorption on chamotte clay occurs mainly through ion exchange, with some contribution from physical adsorption in pores; for bisphenol-A and propranolol, enhanced adsorption on DDAB-modified zeolite is associated with surface recharging and strengthened hydrophobic interactions, the adsorption mechanism involves chemisorption and electrostatic attraction for both BPA and PRO, as well as physisorption in the case of PRO.

Personal Contribution of the Author

The author's personal contribution consists of the analysis of literature on the research topic, design and performance of the experiments on the synthesis of the surfactant modified aluminosilicate adsorbents, and adsorption of HM ions, BPA and PRO onto the obtained adsorbents, and processing of the obtained results.

Contribution to Scientific Publications Writing

Conceptualization, Methodology, Formal analysis, Investigation, Writing - Original Draft, and Visualization of data.

Approbation of the Work

The results of the dissertation were presented at such international scientific conferences as

VIII International Competition-Conference of Students' Scientific Works "Physical Chemistry – the Basis of New Technologies and Materials" named after A.A. Yakovkin. Russia, St. Petersburg. - 2019.

V International Russian-Kazakh Scientific and Practical Conference "Chemical Technologies of Functional Materials". Russia, Novosibirsk. - 2019

VI International Russian-Kazakh Scientific and Practical Conference "Chemical Technologies of Functional Materials". Almaty, Kazakhstan. - 2020

VII International Russian-Kazakh Scientific and Practical Conference "Chemical Technologies of Functional Materials". Russia, Novosibirsk. - 2021

Publications

The main results on the topic of the dissertation are presented in the form of 14 publications:

- One article in an international journal with a non-zero impact-factor (Q1, IF = 5.876) according to Web of Science database.

- One article in an international journal with a non-zero impact-factor (Q4, IF = 0.447) according to Web of Science database.

- 4 articles in scientific journals recommended by a Committee for Quality Assurance in the Field of education and Science of the Ministry of Higher Education of the Republic of Kazakhstan.

- One article in proceedings journal included in Scopus database (38%).

- One article in proceedings journal included in Web of Science database.

- 6 abstracts at international conferences.

Relation of the Thesis to Research and Government Programs

The dissertation was carried out within the framework of the scientific projects of the Ministry of Science and Higher Education of the Republic of Kazakhstan (AP08957166 and AP09260116). Also, certain research results were obtained in scientific laboratories of the Lulea University of Technology (Lulea, Sweden), Babes-Bolyai University (Cluj-Napoca, Romania) and Bar-Ilan University (Ramat-Gan, Israel).

Volume and Structure of the Thesis

The thesis consists of an introduction, three sections, conclusions, a list of references, and 2 appendices. The work is presented on 170 pages, and contains 52 figures, 30 tables, and 289 bibliographical references.

1 Literature review

1.1 Application of aluminosilicates for the extraction of various contaminants from aqueous solutions

Aluminosilicates are a class of minerals and substances distinguished by their composition of aluminum oxide (Al_2O_3) and silicon dioxide (SiO_2). These compounds exhibit a diverse range of structures, such as crystalline frameworks and layered sheets. Zeolites and clay minerals are the most prevalent forms of aluminosilicates.

Natural silicate minerals provide numerous qualities that make them highly suitable as sources for sorbents, catalysts, plasticizers, and reinforcing additives, among other applications. The primary benefits of natural materials are their widespread availability and very affordable cost in comparison to manufactured materials.

Aluminosilicates, such as zeolites and clay minerals, have received considerable recognition for their efficacy as adsorbents in diverse environmental and industrial contexts. Due to their distinctive structural properties, including a large surface area, microporosity, and ion exchange capacity, these materials are well-suited for various adsorption processes.

Zeolites possess precisely defined crystalline structures, which provide them with outstanding capacities to exchange ions and exhibit strong selectivity towards specific ions. For example, they have been successfully utilized to eliminate heavy metals such as lead and cadmium from liquid solutions by exchanging metal ions with less toxic alternatives [7]. Zeolites are also useful in the process of treating wastewater and purifying air. They can trap contaminants including ammonium ions and volatile organic compounds (VOCs) [8].

Clay minerals, such as montmorillonite, bentonite, and kaolinite, belong to a group of aluminosilicates that have a notable capacity for adsorption. Their stratified compositions and substantial surface area enable the extraction of organic pollutants and heavy metals from liquids. Research has shown that they are effective in cleaning both industrial wastewater and polluted soils [9].

Aluminosilicates have a wide range of applications, not only in environmental remediation but also in industrial processes for gas separation and catalysis [10]. Their ability to regenerate and remain stable further improves their appropriateness for sustainable and long-term use.

1.1.1 Application of zeolites for extraction of contaminants from aqueous solutions

Zeolites are hydrated aluminosilicates with cage-like structures (SiO_4 and AlO_4 tetrahedrons), an available surface of up to 100 m^2/g, and a high cation-exchange capacity. Crystals have a regular system of cavities that are interconnected by channels. Cations and water molecules remain in the channels, whereas cations are mobile and may be exchanged. They compensate for the excess negative charge of the anionic part of the zeolite's framework. Due to the "channel-

cavity" structure, these adsorbents have a well-developed inner surface that might be available for adsorbate molecules. There are around 50 types of natural and more than 150 types of synthetic zeolites used in different applications at the moment [11]. The most common type of natural zeolite is clinoptilolite.

The most abundant type of natural zeolites is clinoptilolite, which belongs to heulandite group (HEU-type). They are mostly found in specific types of sedimentary rocks (tuffs) in the form of small crystals (0.1–100 μm) associated with clays and other silicate and aluminosilicate phases of similar density[12]. The name 'heulandite' is used for samples in vugs of igneous rocks while 'clinoptilolite' for samples in sedimentary (mostly commercialized) rocks.

The crystal structure of the HEU-type zeolites [13] is characterized by a three-dimensional aluminosilicate framework consisting fundamentally of secondary building units (SBUs) of the 4–4–1 type, formed by TO_4 (T=Si, Al) tetrahedral primary building units (PBUs). Chain-like structural sub-units (SSUs) of the heulandite type originate from these SBUs and are further combined through 4.5^2-type SSUs to form structural "sheets" parallel to the (0 10). For this spatial arrangement of SSUs, the framework contains narrow four- and five-membered rings, as well as broad eight- and ten-membered rings constituting intraframework micropores (channels) capable of hosting extra-framework/exchangeable cations (e.g. Na^+, K^+, Ca^{2+}) in association with mobile H_2O molecules. The crystals of HEU-type zeolites accommodate two different systems of micropores interconnected within the lattice, the first developed along the c-axis with both eight- and ten-membered rings forming A- and B-type channels (3.3×4.6 and 3.0×7.6 Å, respectively), and the second developed along the [10 2] and the a-axis with eight-membered rings forming C-type channels (2.6 × 4.7 Å).

Clinoptilolite is the most common type of natural zeolite and is a heulandite-type zeolite. Heulandites are characterized by a three-dimensional aluminosilicate crystal lattice primarily composed of layers of 4-4-1-1 structural units: two 4-membered tetrahedron rings connected by two additional tetrahedrons. The 4-4-1-1 units form (010) layers, channels of 10-12-membered rings [14].

The study of the adsorption and X-ray structural properties of natural and synthetic zeolites made it possible to clarify the nature of their molecular sieve action [15]. The porosity of zeolites limits the entry of molecules into the internal adsorption area through the entrances known as "windows". This limitation is a result of the special crystalline structure of zeolites, which determines the main porosity. The adsorption process leads to a difference in the specific surface characteristic of zeolites due to the volumetric filling of these substances. The primary geometric characteristics of zeolites include the adsorption capacity, the effective size of the entrance window, and the nature of microvoids and channels.

Zeolites exhibit a certain selectivity with respect to various molecules, and the molecular sieve action can be expressed to varying degrees. In the case of a complete molecular sieve effect, some molecules diffuse deep into the crystal, while the diffusion of other molecules is excluded. In the case of a partial molecular sieve effect, the diffusion of individual components of a binary mixture occurs at different rates depending on the adsorption conditions.

The sorption properties of zeolite are determined by the volume of intracrystalline space (not less than 0.1 cm3/g) and pore sizes (4.5-6.5 nm). Zeolites are acid-resistant (the mineral structure begins to deteriorate at pH less than 1) and heat-resistant (up to 600°C), and are not carcinogenic, since the content of toxic elements in the mineral does not exceed 0.001 mg/g of zeolite for arsenic, lead and mercury [15].

Many studies have been devoted to estimating the adsorption activity of zeolites towards pollutants of different nature, such as heavy metal ions [16–19], inorganic anions [20–23], organic dyes [24–27], phenolic compounds [12,28–30], etc.

To increase the sorption activity, zeolites can be chemically modified by many different methods: ion exchange, varying the Si/Al ratio by direct synthesis under different conditions; decationization to obtain zeolites enriched with hydrogen, dealumination by treatment with acids, etc. The simplest modification method is ion exchange [31–34].

The acid treatment is usually performed to increase the Si/Al ratio. A low ratio causes the surface of zeolite to be hydrophilic while a high ratio causes the surface to be hydrophobic [35]. Acid-leaching with strong inorganic acids accompanied by dealumination leads to a modification in zeolite morphology by destruction of channel-blocking impurities and the development of the secondary porosity [36]. In [37] treatment of zeolite with high concentrations of HCl leads to bigger increase in Si/Al ratio in comparison to other mineral acids. The second reason for acid treatment is to create mesopores in zeolites. The primary porosity (microporosity) occurs because of the specific crystal structure of zeolite mineral grains, whereas the secondary porosity (mesoporosity) is connected with grain sizes of zeolite and other minerals in the zeolite rocks [38]. The mesopores are active surfaces for catalysis, transport channels, and adsorption of relatively large molecules.

Also, the ratio of Si to Al within a zeolite's structure is one of the most important factors when considering the applicability of a zeolite to ion exchange applications. Natural zeolites tend to be of lower Si:Al ratios, owing to the general absence of conditions necessary to form zeolites of a high Si:Al ratio in the environment. Zeolite species can be classed into three groups based on their Si:Al ratio: low Si:Al ratio (1-1.5), intermediate Si:Al ratio (2-5) and high Si:Al ratio (10 and above). Zeolites within the intermediate range tend to be the most stable species, having more heterogeneous hydrophilic surfaces within their porous crystal structure. As the ratio of Si:Al

increases, so too does the hydrothermal stability and hydrophobicity of the zeolite framework. [39]. The Si/Al ratio, in the range 3–5 modulates the ion-exchange properties of the zeolites expressed as cation-exchange capacity (CEC, which can theoretically reach 330 meq/100 g). The rather low Si/Al ratio and the consequently increased CEC render HEU-type zeolites advantageous for binding dissolved cations from aqueous solutions. The dissolved metallic cations interact with the HEU-type zeolite crystals, and they are subsequently removed from the solution, through different sorption mechanisms including principally the so-called 'ion- exchange' (which is a kind of bulk sorption, i.e. *ab*sorption into the channels of the tetrahedral framework), and also adsorption (specific and/ or non-specific regarding inner-sphere and/or outer-sphere surface complexation) and surface precipitation/co-precipitation [13].

In [40], the effect of hydrochloric acid of different concentrations (1H, 2H, 3H, 5H) on the zeolite of the Shankanai deposit was studied. Acid treatment of clinoptilolite leads to partial destruction of Si-O-Si, Si-O-Al bonds, thereby forming additional active centers on the surface and probably increasing the sorption properties. However, an increase in the acid concentration leads to dehydration of the zeolite, cationic intrasphere rearrangement and partial destruction of the structure, which can lead to a decrease in sorption activity.

Acid treatment of zeolites changes the Si/Al ratio due to dealumination, which radically changes the properties of the original substance. In addition to acid treatment, varying the silicon/aluminum ratio is possible through direct synthesis under various conditions. In 1971, Mobil developed the ZSM-5 zeolite catalyst with a high SiO2 content (R=740). Zeolites of this type are currently widely used in the processes of adsorption of substances from both aqueous solutions and gas mixtures [41–43].

Recently, methods for obtaining sorbents based on zeolites modified with substances containing various functional groups in their structure, which can act as additional active centers on the surface of the sorbent, have been widely studied. Such modifiers can be polymers, surface-active substances (SAS), acids, bases, etc. [5].

The permanent negative surface charge resulting from the prolonged isomorphic substitution of Si^{4+} by Al^{3+} cations in the tetrahedron of its crystal lattice allows the use of zeolites for the effective adsorption of metal cations (Mn^{2+}, Cr^{2+}, Pb^{2+}, La^{3+} and cationic dyes). However, they exhibit little activity towards anions [11,33,44]. Many pollutants have negative charges including viruses, bacteria, and metal anions such as chromates, nitrates, arsenates and phosphates. To adsorb such pollutants, the zeolite surface is modified with cationic surfactants; such composite materials, referred to as surfactant modified zeolites (SMZs) find many applications [4]. Surfactant-modified zeolites (SMZs) are organo-aluminosilicates, which are used to extract

organic pollutants such as petroleum products, pharmacology wastes, dyes, and humic acids from aqueous solutions [5,6].

It was found that the longer the hydrophobic chain of the cationic surfactant, the more stable the retention of the surfactant on the surface. When the surfactant exceeds the critical micelle concentration (CMC), a bilayer is formed on the surface of the zeolite [30]. The amount of surfactant fixed on zeolite depends primarily on the concentration of the surfactant in the solution. At low concentrations, the surfactant cations are bound to the outer surface of the zeolite by ion exchange with the zeolite cations until a monolayer of surfactant cations is formed. At higher concentrations, the second surfactant layer can bind to the first by hydrophobic interactions between the alkyl chains. The positively charged group of the second layer is oriented toward the aqueous solution due to the electrostatic repulsion forces of the “head” groups between the inner and outer layers (Figure 1). The formation of the second layer creates an excess of positive charge on the zeolite, which makes the process of anion adsorption possible. The authors of [42] note that with chain lengthening, surfactant molecules become more hydrophobic. They also found that the desorption of metal cations was highly dependent on the length of the surfactant chain, i.e. with chain lengthening, a greater number of metal cations are desorbed.

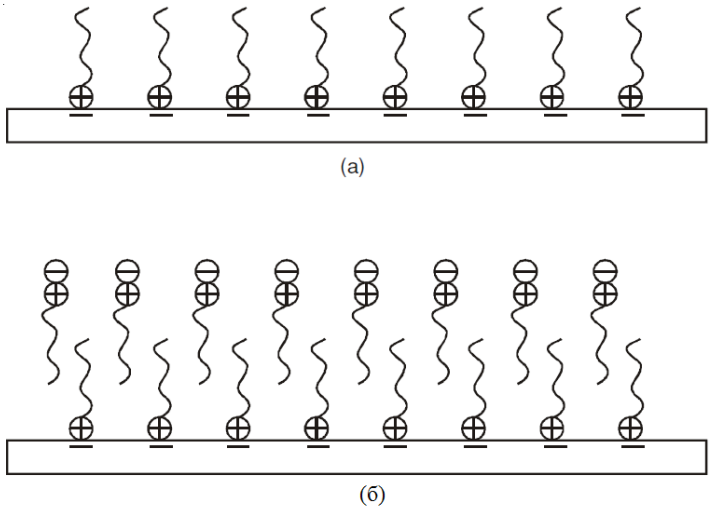


Figure 1 – Sorption of surfactant molecules in the form of a monolayer (a) and bilayer (b) [30]

The most commonly used surfactants for this purpose are quaternary ammonium compounds (QACs or quats) [25,29]. Because of their structure which includes both polar (N^+) and nonpolar (R) endings, QACs can be adsorbed on the interface, thereby decreasing surface tension. In contrast to their parent amines, they show the properties of cationic surfactants without dependence on pH [45].

QACs are used as bioactive agents owing to their very wide spectrum of biological and antimicrobial activity [45]. Due to their unique structure, positively charged QACs are commonly

used in supramolecular chemistry [45–47]. It was determined that the right choice of QAC significantly effects the supramolecular structure, in particular the cavity size of pore materials such as zeolites. To obtain new materials with a wide scope of application, QACs can also be directly embedded in the supramolecular framework.

The most commonly used QAC to enhance the adsorption properties of zeolites towards organic pollutants is hexadecyl-trimethylammonium bromide (HDTMA) [23,25,39,48–51]. It was found that the longer the tail group of HDTMA can make, the more stable it is retained on the surface of the zeolite [21]. Since the key point for the organic compounds adsorption by SMZ is precisely the change in the hydrophobicity of zeolite surface due to the surfactant, it is very important to get a stable and smooth coating. In [52] a single-chained stearyl trimethyl ammonium bromide (STAB) showed lower adsorption of emulsified oil in produced water than a double-chained organic cationic surfactant dimethyl dioctadecyl ammonium bromide. Single-chained cetyltrimethylammonium bromide (CTAB) and double-chained didodecyldimethylammonium bromide (DDAB) were compared in [53] for Semipermanent Wall Coatings in Capillary Electrophoresis. DDAB was found to form more stable coatings than similar single-chained surfactants. HDTMA and DDAB were used in [54] to modify activated carbon in order to increase adsorption of $Cr_2O_7^{2-}$. The samples containing DDAB showed higher adsorption capacities than the ones with HDTMA. Adsorption of carcinogenic polycyclic aromatic hydrocarbons (PAHs) by clinoptilolite modified with cetylpyridinium chloride (CPC), DDAB, HDTMA, and tetramethyl ammonium chloride (TMA) was studied in [55], where DDAB has shown the highest adsorption capacities due to higher hydrophobicity of double-chain organic tail.

Another advantage of using DDAB as a modifier for wastewater treatment is its high antibacterial ability. DDAB was loaded onto granular activated carbon and successfully used to deactivate total coliform, *E. coli*, and enterococci found in tertiary effluent [56].

The effective cation-exchange capacity of natural clinoptilolite can be enhanced by treating it with a 0.1 M sodium chloride solution before exposing it to surfactants. The structural characteristics of clinoptilolite impose limitations on its ability to affect the outer surface when the size of the surfactant surpasses the size of the zeolite's pores, rendering the exchange of cations on the inner surface impossible. Furthermore, the outer surface can be modified from being water-attracting (hydrophilic) to water-repelling (hydrophobic). Additionally, the charge of the outer surface can be altered from negative to positive by applying a layer of surfactants [14].

Zeolite-based sorbents used to purify wastewater from heavy metal ions (HM) deserve special attention, since high concentrations of heavy metals have a toxic effect on living organisms, leading to irreversible disruptions of biochemical processes. Even small amounts of HM entering the body cause irreparable harm, since they cannot be completely neutralized or removed. The

main sources of HM include mining, smelting, galvanic, textile, leather and battery industries. Pollutants that need to be removed from wastewater include lead, mercury, cadmium, chromium, zinc and copper. In particular, lead can destroy the hematopoietic system and disrupt the functioning of the brain, kidneys and liver, leading to anemia, encephalopathy, hepatitis, etc. Despite the fact that copper is one of the main microelements in the human body, excess copper harms the functioning of the nervous system and organs, especially the liver and gall bladder, leading to neuritis and cirrhosis [57].

Lead is among the most toxic HM for people, especially children. Lead poisoning can cause problems with cardiovascular, enzyme and reproductive systems, dysfunction of the kidneys and liver, both the peripheral and the central nervous systems are influenced by lead exposure [58]. Lead is present in tap water to some extent as a result of its dissolution from natural sources, but primarily from household plumbing systems in which the pipes, solder, fittings or service connections to homes contain lead. Polyvinyl chloride (PVC) pipes also contain lead compounds that can be leached from them and result in high lead concentrations in drinking water [59]. Adsorption methods of water treatment from lead ions have proven their efficiency [60]. Natural zeolites and clays are effective and accessible materials to use as adsorbents of different pollutants [2,61–63]. The application of natural zeolites as adsorbents of metal cations, particularly lead, has been reported in numerous studies.

Thus, Shirzadi et.al. [64] used an Iranian natural clinoptilolite for lead ions adsorption in micronized and nanoparticle forms. Kragovic et.al. [65] have observed the adsorption capacity of natural zeolite as 66 mg/g. J. Peric et.al [66] used the Croatian zeolite clinoptilolite as a natural ion exchanger and reported the high efficiency of removal for Pb (II) ions. Authors [67] utilizes zeolitic tuff from Indonesia as a novel adsorbent for Pb and Cd ions removal and the result of isotherm study based on Langmuir equation revealed that the adsorption capacity of Bantengwareng and Tegalrejo zeolitic tuff samples has a value of 416.67, 384.61 and 277.77, 243.91 mg/g for lead and cadmium, respectively. In work [68] Column experiments were performed to assess the effectiveness of zeolite and compost-zeolite mixture in removing dissolved lead (Pb^{2+}) from acidic water of pH 2.4. The maximum adsorption capacity, qo obtained for zeolite was 0.097 mg/g and 0.151 mg/g for the compost-zeolite mixture, respectively. Lead removal was attributed to ion exchange and adsorption. In other study [69] zeolite was reported as the adsorption material to remove the Pb^{2+} and Ni^{2+} from the aqueous solution and the maximum adsorption capacity of Pb^{2+} and Ni^{2+} predicted from the Langmuir model was found to be 45.00 and 28.57 mg/g respectively at 303 K.

Cadmium is a toxic element present in several industrial wastewaters, such as the production of cadmium batteries, cadmium smelting, and the manufacture of cadmium pigments [70]. The

adsorption percentage of cadmium removal by natural zeolites could be 100% based on the literature [71]. Vaca Mier et al. [72] reported Cd adsorption of 99% and higher than 90% for batch and fixed-bed column systems, respectively. A similar study for Cd adsorption in mine water achieved about 86% for strong acidic and 21% for weak acidic mine water. The low cadmium adsorption in weak acidic water was possibly because of Ca, Mg, and Mn elements which can reduce the metal adsorption capacity [73]. Even though most of the studies on cadmium adsorption are reported only with the application of natural zeolites, some authors studied cadmium adsorption by modified natural zeolites [74,75]. Cort´es-Martínez et al. [74] reported a slight decrease in Cd adsorption after the surfactant modification of about 3% for SMZ. In contrast, Nguyen et al. [75] reported an increase in Cd adsorption after another type of modification, an iron-coated modification for both batch and fixed-bed systems. They reported Cd adsorption on ICZ of 7% and 46% higher than the natural zeolite for the batch and fixed-bed system, respectively [76].

^{90}Sr is the most hazardous radioactive isotope of strontium that is produced during the normal operation of nuclear reactors. It can also spread to the environment due to fallout from nuclear accidents and nuclear weapon testing. The removal of hazardous radionuclides and the safe management of radioactive waste are of vital necessity [77].

Zeolites are used as adsorbents of cationic elements in the radioactive decontamination process of water, soil and others. In work [78] the authors determined Cs^+ and Sr^{2+} adsorption selectivity of some zeolites to know effective zeolite species for the decontamination of radioactive Cs and Sr. Among the zeolites, mordenite had the highest Cs^+ adsorption selectivity, and the selectivity had no correlation to the cation exchange capacity (CEC) of the zeolites. In contrast, Sr^{2+} adsorption selectivity of the zeolites positively correlated with the CEC of the zeolites; a simulated soil decontamination experiment of Sr from a Sr-retaining vermiculite by using Linde-type A showed decontamination rates of more than 90%. Synthetic zeolites are actively used to extract strontium from liquid media due to the same properties that make them promising sorbents for cesium: high thermal, radiation and chemical stability, selectivity to radionuclide cations, high adsorption capacity, fast adsorption and good kinetic parameters, the possibility of sintering zeolites into a stable matrix for strontium immobilization. Zeolites can be used to extract both cesium and strontium from radioactive waste at the same time [79].

The results of the study of the state of surface waters in Kazakhstan showed that in most water bodies there is an excess of the maximum permissible concentration of substances such as phenols, manganese, chromium, zinc and lead [80].

Chromium is widely used in the galvanic, and leather industries, in the creation of metal coatings and the production of chromates. Chromium can exist in six oxidation states, but in the Eh-pH (potential - pH) range of natural waters, the most important are trivalent Cr (III) and hexavalent Cr (VI). Cr (VI) (chromium trioxide, chromic acid, and dichromate) are the most toxic forms, which have a carcinogenic and mutagenic effect on living organisms. Trivalent Cr (III) (chromium oxide and chromium sulfate) is approximately 300 times less toxic than hexavalent, due to limited solubility in water, it is less mobile, and in micro quantities is an essential element for the healthy growth of an organism. Due to its high toxicity, Cr (VI) must be extracted from wastewater before discharge into the aquatic ecosystem. In recent decades, many studies have been conducted on the adsorption of chromium on zeolites, clay materials, and agricultural waste.

When it comes to Cr (VI), researchers have experimented with several techniques including ion exchange, membrane separation, adsorption, chemical precipitation, electrodialysis, photocatalytic degradation, and more [81–84]. Adsorption has emerged as the most effective technique for reclaiming harmful metals owing to its exceptional efficacy, straightforward reproducibility, wide accessibility, and the potential for regenerating adsorbents. Despite the availability of low-cost adsorbents such montmorillonite and zeolite, there is a requirement to create adsorbents that are stable, environmentally benign, and highly efficient for the retrieval of Cr(VI) from water-based solutions.

In [81], a study was conducted on the adsorption of hexavalent chromium by a sorbent based on natural zeolite modified with iron (II), grape and olive waste, and the mechanism of chromium adsorption was described. An important parameter in the description of TM adsorption is pH. The best sorption results were obtained at low pH values. At low solution acidity, the surface of the sorbents is saturated with positively charged protons, which enhances the electrostatic interaction between the sorbent and chromium anions.

There is also information on the modification of natural zeolite (clinoptilolite) and other mineral materials with lead (II) ions to extract chromium from aqueous solutions. The modified zeolite extracted 86% of dichromate anions from the solution by forming a complex compound of lead and dichromate. The adsorption capacity of the sorbent was 18.9 mg/g [82].

Thanosa *et al.* [82] used a method for the purification of wastewater from chromium (VI) ions, in which the first stage is chemical reduction to chromium (III), where many reducing agents (H2S, Fe^{2+} and Fe^{0}) were tested. First of all, chemical processes can be complex and usually require additional organic additives, which significantly hinders their practical application. Compared with such methods, photocatalysis turned out to be a more attractive, efficient and clean technology for the purification of aqueous solutions from organic pollutants and chromium [83].

Until now, few studies have been conducted on the excellent photoreduction of Cr (VI) to less toxic Cr(III) by zeolite promoted with silver nanoparticles with a well-defined morphology.

The work [83] describes the process of obtaining a zeolite modified with silver nanoparticles with subsequent irradiation with UV radiation, as well as the use of the surfactant alkyl dimethyl hydroxyethyl ammonium chloride as a secondary stabilizer. The resulting material was tested as a sorbent of dichromate anions and showed greater efficiency compared to the original zeolite.

In addition to chemical reagents, the use of natural polyaminosaccharide chitosan as a modifier is known, which is known for its chemical stability and environmental safety. Due to the content of amino and hydroxy groups in its structure, chitosan has high reactivity and selectivity with respect to HM. There is a lot of information in the literature on studies of silicon materials modified with chitosan.

The authors of [84] obtained sorbents modified with chitosan for the adsorption of heavy metal anions. A solution of potassium dichromate was used as a model solution. Several parameters influencing the adsorption process were studied, such as different proportions of zeolite and chitosan, particle size, pH, dosage, time, and interfering ions were taken into account to determine the optimal adsorption conditions. It was found that one of the most important factors influencing the adsorption process was the pH of the solution, with values of 5-6 yielding the most effective extraction of chromium ions.

Natural zeolite is organically modified with the surfactant cetyltrimethylammonium bromide (CTAB) and employed as a dual-function material for simultaneous adsorption of Cs^+ cations and $HCrO_4^-$anions from aqueous solutions [85]. CTAB-zeolite exhibited adsorption capacities of 0.713 and 1.216 mmol/g for Cs(I) and Cr(VI), respectively.

The adsorption equilibrium data of Cr(VI) from an aqueous solution on a surfactant-modified zeolite (SMZ) was determined in a batch adsorber [86]. The SMZ was prepared by adsorbing the cationic surfactant hexadecyltrimethylammonium (HDTMA) bromide on the external surface of the zeolite. The Cr(VI) was adsorbed considerably on SMZ but not on the natural zeolite. The Cr(VI) adsorption capacity of SMZ showed a maximum at pH 6 and diminished 18 and 2.7 times increasing pH from 6 to 10 and decreasing pH from 6 to 4, respectively. Desorption studies showed that Cr(VI) was irreversibly adsorbed on SMZ corroborating that Cr(VI) was chemisorbed on the SMZ. A comparison of the Cr(VI) adsorption capacities revealed that the capacities decreased in the following order: commercial granular activated carbon organobentonite > SMZ.

Many researchers reported that for chromium, anion exchange and electrostatic attraction were the main mechanisms in the anionic species of Cr ((CrO_4^{2-}; H_2CrO_4); $Cr_2O_7^{2-}$) in the pH

ranges of 1–6 and greater than 6, respectively ([87–89]. Asgari et al. [90] described the Cr(VI) adsorption on SMZ by electrostatic attraction, which can be represented as the following:

$$2SMZ + HCrO_4^- + Cr_2O_7^{2-} \rightarrow SMZ + HCrO_4^- + SMZ + Cr_2O_7^{2-} \quad (1)$$

The concentration of permanganate ion (MnO_4^-) exceeding 0.1 mg/L in water bodies reduces the biological oxygen demand of water in pools, imports undesirable taste and affects the central nervous system to the living bodies.

A review of studies on the adsorption of permanganate anions showed that activated carbons [91–94], sorbents based on mesoporous silica [95], and metal-organic frameworks [96] are most often used for these purposes.

Zeolites are used for the adsorption of manganese in the form of the cation Mn^{2+}. Thus, in the work [97] the authors the uptake capacity of Mn(II) ions by zeolite A beads was investigated for different initial Mn concentrations (100–400 mg Mn dm^{-3}) in batch mode at 25–55 °C. The obtained adsorption capacity varying from 30 to 50 mg Mn g^{-1} demonstrated a high affinity of zeolite A towards Mn(II) present in solutions.

The study of permanganate ion adsorption on zeolite may be of practical interest not only for water purification purposes but also as a modification and functionalization of the zeolite surface for adsorption of other toxic metals. Thus, in [98], a sorbent for As(V) adsorption was obtained by modifying clinoptilolite with $KMnO_4$.

Thus, zeolite-based sorbents have found wide application in the creation of sorbents for the extraction of a wide variety of contaminants from aqueous solutions.

Zeolites, characterized by their unique cage-like aluminosilicate framework and high cation exchange capacity, offer remarkable versatility in adsorbing heavy metals, organic pollutants, radionuclides, and other contaminants. Their structural features, such as interconnected channels and micropores, underpin their molecular sieve capabilities, enabling selective adsorption based on molecule size and charge.

Natural zeolites, particularly clinoptilolite, are prominent in various environmental applications due to their abundance, thermal stability, and chemical resilience. Modification techniques, including acid treatment, ion exchange, and surfactant impregnation, significantly enhance the adsorption performance by increasing porosity, altering hydrophilicity, and introducing functional groups. Surfactant-modified zeolites (SMZs) have proven especially effective in capturing anions and organic compounds, broadening the scope of zeolite-based remediation strategies.

Applications of zeolite-based materials span diverse areas, including the removal of toxic heavy metals like lead and cadmium, radionuclides such as strontium and cesium, and complex

organic pollutants. Advanced modifications, such as embedding surfactants, nanoparticles, and polymers, further enhance their efficiency and specificity. Studies highlight the adaptability of zeolites to various environmental challenges, emphasizing their critical role in addressing global water contamination issues.

Future research should prioritize optimizing modification methods, exploring multifunctional additives, and scaling applications to complex, real-world scenarios. Zeolites remain at the forefront of sustainable water treatment solutions, with ongoing innovation poised to expand their efficacy and industrial applicability.

1.1.2 Application of clay materials for extraction of various contaminants from aqueous solutions

The term *clay* is generally applied to (1) a natural material with plastic properties, (2) particles of very fine size, customarily those defined as particles smaller than two micrometers (7.9×10^{-5} inch), and (3) very fine mineral fragments or particles composed mostly of hydrous-layer silicates of aluminum, though occasionally containing magnesium and iron. Although, in a broader sense, clay minerals can include virtually any mineral of the above-cited particle size, the definition adapted here is restricted to represent hydrous-layer silicates and some related short-range ordered aluminosilicates, both of which occur either exclusively or frequently in very fine-size grades [99].

The tetrahedral sheets have a $Si_2O_6(OH)_4$ unit consisting of four hydroxyl groups surrounding every silicon atom in a tetrahedron arrangement. By comparison, an octahedral arrangement consists of Fe, Mg or Al atoms surrounded by six hydroxyl or oxygen atoms, such as in the composition of $Al_2(OH)_6$ [100].

Natural clay minerals (NMCs) have gained a wide range of applications, including agricultural applications, engineering and construction applications, environmental remediation, geology, pharmaceuticals, food processing, and many other industrial applications. This is since they are non-toxic, widespread and inexpensive.

The atomic structure of NMCs consists of two basic units, an octahedral sheet and a tetrahedral sheet. The octahedral sheet is comprised of closely packed oxygens and hydroxyls in which aluminum, iron, and magnesium atoms are arranged in octahedral coordination (Figure 2a). The second structural unit is the silica tetrahedral layer in which the silicon atom is equidistant from four oxygens or possibly hydroxyls arranged in a tetrahedron with the silicon atom in the center (Figure 2b).

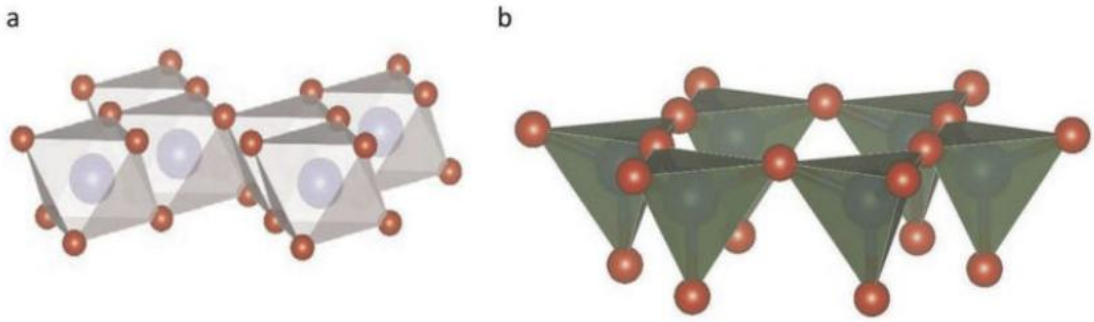


Figure 2 – Diagrammatic sketch of the octahedral (a) and tetrahedral (b) sheet.

The use of NMCs for specific applications depends on its type of structure (1.1- or 2.1-layer type) and on its chemical composition. The most important characteristic of NMCs is the cation exchange capacity (CEC). CEC is to measure the capacity of NMCs to exchange cations from the solution, which depends on the volume of the total layer charge. The presence of charge plays an important role in cation exchange and swelling properties of the minerals.

Most clay minerals produce a small amount of net negative surface charge due to isomorphic substitution. Furthermore, particle edges of clay minerals may produce charges according to the suspension pH as a result of broken primary bonds, such as Si–O and Al–O [100].

The hydrolysis of Si-OH or Al-OH bonds along the NMCs lattices supplies the surface charge. Depending on the silica structure and the solution pH, the net surface charge can be either positive or negative. The charge in NMCs occurs in two forms: structural and surface charge. The structural charge is permanent and present due to ion substitutions, which arise inside the interior of the layers. The surface charges, generally in NMCs depend on the pH value, with 2:1 layer, the surface charge is created on the basal surface of the tetrahedral sheets while the surface charge for layer type 1:1, derives from both tetrahedral and octahedral sheets. Also, the edges of both 1:1 and 2:1 layers contribute to the surface charge.

Furthermore, the presence of a number of exchangeable ions, non NMCs, soluble salts, and the quality of their texture are factors that can affect their properties and applications [101].

Clays have a wide variety of physical properties, such as fineness of particles, hardness, good plasticity, associativity, appropriate shrinkage, high refractoriness, and the capacity for surface decoration. Clays have small particle sizes and high specific surface areas as a result of their complex porous structures, which facilitate physical and chemical interactions with dissolved species. These interactions result from crystallinity, electrostatic repulsion, adsorption, and some cation exchange reactions. The high porous surface area indicates a high bonding force on the surface of the clays [100].

Based on the differences in internal layer structures, clays can be divided into two types: amorphous and crystalline. The crystalline clays possess crystal structures that can be divided into groups such as 1:1 type layer (kaolinite), 1:1 type tube (halloysite), 2:1 type layer (montmorillonite, smectite, vermiculite), the regular mixed layer type (Chlorite group) and 2:1 type layer-chain type (attapulgite, sepiolite).

Kaolinite, chemically expressed as $Al_2Si_2O_5(OH)_4$, has the theoretical components of Al_2O_3 (39.53%), SiO_2 (46.53%), and H_2O (13.94%), in the case of oxides. The chemical formula demonstrates that no substitution appears involving Si^{4+} substituted by Al^{3+} in the layer of tetrahedron and Al3+ substituted by other ions (Na^+, K^+, Zn^{2+}, Mg^{2+}, Ca^{2+}, etc.) in the layer of octahedron. Kaolinite has a 1:1 layered structure comprised of a tetrahedral SiO_4 sheet and an octahedral sheet with Al^{3+} as the octahedral cation. In kaolinite, the structure arrangement between the octahedral and tetrahedral sheets is in a ratio 1:1 and consists of kaolinite, halloysite, dickite, and anauxite. The charges between the two layers are usually balanced, and thus the clay does not swell.

Furthermore, the application of kaolinite in water treatment is growing rapidly in conjunction with other clay minerals, and H^+ ions released from the edge of the layer structure in acidic environments promote the adsorption of heavy metal ions, such as Pb(II), Cu(II), Hg(II) and Cd(II), from aqueous matrices. Some surface adsorption may also occur on the exposed tetrahedral or octahedral sheets (Figure 3) [100]. Kaolinite in raw and modified forms has been used in the removal of chromium (VI) ions, and adsorption has been reported to be highly sensitive to the Ph of the solution, with increasing adsorption from pH 1 to 7 [102].

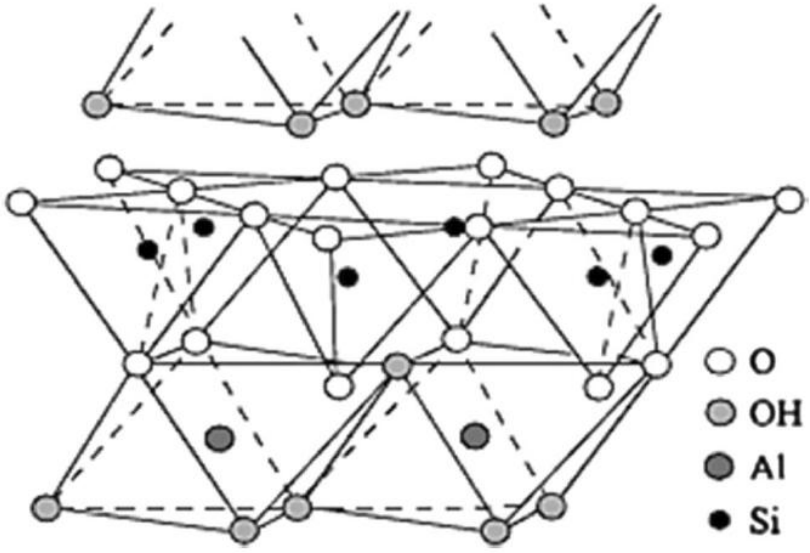


Figure 3 – The structure of kaolinite [99]

For application in heavy metal removal, the clay mineral needs to have a high cation exchange capacity (CEC) and a specific surface area. Kaolinite was reported to have the lowest CEC [102]. Thus, various methods of modification have been reported.

The pre-treatment of clay plays an important role in successful modification. In most cases, analytical-grade clay/minerals are used without purification. However, before composite fabrication, the clay/minerals are immersed in distilled water for several hours under continuous stirring or subjected to ultrasonic waves for several hours. This is to obtain a homogenous suspension and achieve the maximum swelling capacity [103].

Other studies used various modification techniques including acid treatment, and ion exchange to optimize the composite adsorption capacity before composite fabrication. Modification of clay/minerals with these methods facilitates composites fabrication, such as clay mineral-polymer composite [103].

In acid activation, hydrochloric acid (HCl) with a typical concentration of 1 M is used in the pre-treatment step to remove the minerals impurities. Then, the mixture is exposed to ultrasonic waves for several minutes to reduce the agglomeration of clay mineral particles, which increases the specific surface area. Khatamian et al. [104] reported that in the presence of sonication, the specific surface area increased for raw bentonite and iron oxide/bentonite composite by around 18% and 40%, respectively. Besides, as mentioned above, clay minerals attain CEC, which allows exchanging the inorganic cations present in the interlayer space with various materials including metals, surfactants, dyes, and humic acid to produce intercalated clays. The enhancement in adsorption capacity of the intercalated clays is mainly due to the improvement of surface hydrophobicity, and the addition of new functional groups that add new possible interaction. For instance, Ain et al. [105] claimed that the hydrophobicity of 3-acrlyamidopropyl trimethyl ammonium chloride intercalated bentonite increased, which reduced the sedimentation rate of intercalated bentonite allowing better contact between the adsorbate and the adsorbent. In addition, the study showed that despite the dramatic reduction in pore volume and specific surface area of the intercalated bentonite, the average pore diameter and pore width increased.

There have been various attempts to improve the quality and characteristics of the clays by modifying them with different techniques. Two of the common techniques in this regard are intercalation and pillaring, and acid activation.

Intercalation is the insertion of a guest species in the interlayer region of a clay mineral with the preservation of the layered structure. The material obtained is called intercalated clay. XRD measurements show that intercalation increases the spacing between adjacent layers.

Pillaring of clay minerals by various inorganic as well as organic compounds is well known. The pillaring process is generally presented as a way of increasing the accessibility of the clay

layers, but an alternative viewpoint is that it stabilizes ‘oxide’ particles of nanometer dimension that prevent aggregation by interaction with the layers.

Treatments of clay minerals with inorganic acids of rather high concentration and usually at high temperature are known as acid activation. Acid treatments of clay minerals are an important control over mineral weathering and genesis. Such treatments can often replace exchangeable cations with H^+ ions and Al^{3+} and other cations escape out of both tetrahedral and octahedral sites, leaving SiO_4 groups largely intact. This process generally increases the surface area and acidity of the clay minerals, along with the elimination of several mineral impurities and partial dissolution of the external layers.

On acid attack, the crystalline structure of kaolinite is transformed thermally to amorphous metakaolin and the octahedral Al^{3+} ions are preferentially released from the clay structure leading to formation of additional Al–OH and Si–OH bonds, without changing the original mineral structure. It has been reported that acid activation followed by thermal treatment increases the adsorption capacity to a good extent. The increase may be caused by production of finely dispersed silicon oxide from destruction of mineral structures, removal of amorphous Al or silica components, plugging surface pores or interlamellar spaces, formation of cracks and voids in the surface. After acid attack, the number of weakly acidic surface functional groups is observed to increase while the number of groups of stronger acidic character shows decreases [106].

Acid modification of kaolinite not only increases the surface acidity and specific surface area of kaolinite but also results in the production of a large number of pore structures. Bhattacharyya and Gupta [106] treated kaolinite with H_2SO_4 to further improve its properties. The modified kaolinite with H_2SO_4 opened the edges of kaolinite sheet crystals, resulting in the increased pore size and the enlarged specific surface area, and the adsorption rate constant of kaolinite for Cu(II) increased from 9.5 × 10−2 g/mg·min to 12.0 × 10−2 g/mg·min. Chai et al. [107] prepared an acid-activated kaolinite by refluxing the kaolinite in the concentrated H_2SO_4 solution. This H_2SO_4 activated kaolinite showed excellent adsorption performance on both Ni(II) and Cu(II). Moreover, the H_2SO_4 activated kaolinite possessed a higher adsorption capacity than raw kaolinite, and the maximum adsorption capacities of H_2SO_4 activated kaolinite towards Ni(II) and Cu(II) achieved 39.62 mg/g and 41.11 mg/g, respectively, while the adsorption capacity of raw kaolinite was slightly lower, showing 37.64 mg/g for Ni(II) and 40.01 mg/g for Cu(II), respectively. The improvement in the H_2SO_4 activated kaolinite should be ascribed for two reasons. First, the acid-activated kaolinite became smaller in size and appeared to be disintegrated, which increased the specific surface area by 84.58%. Second, the acid treatment with H_2SO_4 changed the surface property of kaolinite, such as the number of effective binding sites and surface negative charges.

Another way of modification reported to be effective is thermal modification. Thermal modification refers to the heating of kaolinite at a certain temperature to effectively remove H_2O molecules, carbonates, and other organic impurities attached to the pore structure of kaolinite. The disappearance of different forms of water molecules such as adsorbed water, crystalline water, and structural water can effectively increase the specific surface area and the pore volume of kaolinite, and the removal of structural water will transform it into metakaolinite, which exposes it to the generation of a large number of sites for reaction with acid. Meanwhile, its activity is enhanced and easily reacts with acid, which eventually improves the ion exchange performance and adsorption performance of kaolinite for pollutants [108].

Chamotte clay is a white heat-treated kaolin clay with stone properties, resistant to aggressive media, which contains highly dispersed hydroaluminosilicates. The clay does not require additional purification after secondary use. It can be used in industry in large quantities [109]. Chamotte is produced by the calcination of kaolinite clay in a rotary kiln. It has been used for ceramic bonding for refractories and creep-resistant applications due to its mullite content. Chamotte has also been mixed with clays to reduce the sintering stresses that produce cracks and flaws [110].

The process of the solid-phase formation of mullite from kaolinite based on the X-ray phase analysis and infrared spectroscopy data is shown in Figure 4.

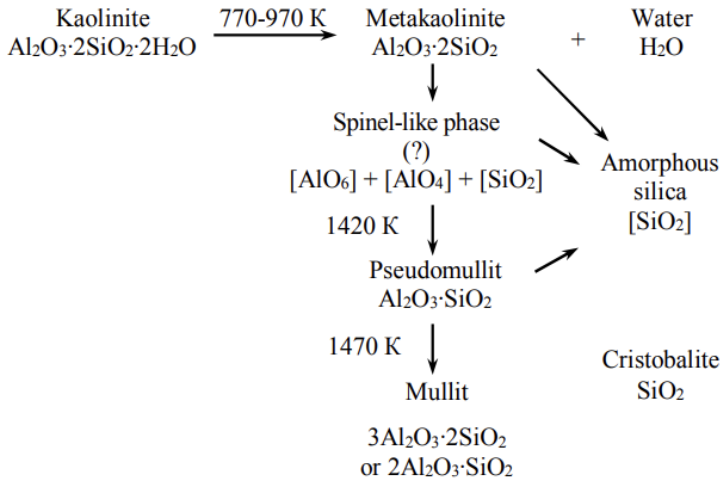


Figure 4 – A scheme of solid-phase transformation of kaolinite into mullite [111]

Based on experimental data, the thermodynamic process of kaolinite conversion can be represented as the following theoretical reactions:

$$\underset{\text{Kaolinite}}{Al_2O_3 \cdot 2SiO_2 \cdot 2H_2O} \rightarrow \underset{\text{Metakaolinite}}{Al_2O_3 \cdot 2SiO_2} + 2H_2O;$$

$$\underset{\text{Metakaolinite}}{2(Al_2O_3 \cdot 2SiO_2)} \rightarrow \underset{\text{Spinel (?)}}{2Al_2O_3 \cdot 3SiO_2} + SiO_2;$$

$$\underset{\text{Spinel (?)}}{2Al_2O_3 \cdot 3SiO_2} \rightarrow \underset{\text{Pseudomullite}}{2(Al_2O_3 \cdot SiO_2)} + SiO_2;$$

$$\underset{\text{Pseudomullite}}{3(Al_2O_3 \cdot SiO_2)} \rightarrow \underset{\text{Mullite}}{3Al_2O_3 \cdot 2SiO_2} + \underset{\text{Cristobalite}}{SiO_2}; \quad (2)$$

$$\underset{\text{Pseudomullite}}{2(Al_2O_3 \cdot SiO_2)} \rightarrow \underset{\text{Mullite}}{2Al_2O_3 \cdot SiO_2} + \underset{\text{Cristobalite}}{SiO_2}. \quad (3)$$

Total reaction:

$$3(Al_2O_3 \cdot 2SiO_2 \cdot 2H_2O) \rightarrow 3Al_2O_3 \cdot 2SiO_2 + 4SiO_2 + 6H_2O; \quad (4)$$

$$2(Al_2O_3 \cdot 2SiO_2 \cdot 2H_2O) \rightarrow 2Al_2O_3 \cdot SiO_2 + 3SiO_2 + 4H_2O. \quad (5)$$

Considering the instability of chemical mullite composition (from $3Al_2O_3 \cdot 2SiO_2$ to $2Al_2O_3 \cdot SiO_2$), Kotova et. al. [111] propose its formation from pseudo mullite (2) and (*3*) reactions, which, respectively, are reflected in total reactions (4) and (*5*).

Nonetheless, there is limited information regarding the application of Chamotte clay as an adsorbent. Reference [112] indicates that chamotte clay has been utilized as an adsorbent for the purification of biodiesel from glycerol. Additionally, Chamotte clay was employed to purify ethyl biodiesel samples derived from palm kernel oil using chemical and biological catalysis.

Literature references a material known as "fire clay," which is analogous to chamotte clay; however, the distinction is that chamotte clay is typically derived from pre-fired fire clay, whereas fire clay denotes the raw, naturally occurring substance. Still, information on this topic is limited. Consequently, fire clay adsorbents were employed for the extraction of hexavalent chromium in several studies [113,114].

In [114] the removal of hexavalent chromium from its aqueous solutions by adsorption onto fire clay and impregnated fire clay has been studied at 30°C. The adsorption process follows the Langmuir-type adsorption behavior, and the extent of adsorption is more for impregnated fire clay. It is found that electrostatic and H-bonding interactions play a key role in binding the adsorbate molecules to the adsorbent surface. The adsorption process is affected greatly by the variation in pH and temperature of the system. Low pH and high temperature favor the adsorption process.

Batch adsorption trials of Cr (VI) were performed [115] to investigate the effects of pH, contact time, initial metal ion concentration and the adsorbent dosage. Maximum chromium removal was found at pH 2.0. A kinetic study yielded an optimum equilibrium time of 90 minutes with an adsorbent dose of 2.5 g/50 mL. Results suggested that the equilibrium adsorption is described by the Freundlich model. The kinetic data of the sorption showed that the pseudo-second-order equation was the more appropriate. The results of the study indicated that fire clay

was not a suitable adsorbent for Cr (IV). Apart from the relatively long equilibrium time, the efficiency was not satisfactory.

Rathinavelu and Venkateswaran [113] investigated the adsorption behavior of Cr(VI) ions onto fire clay-TiO_2 nanocomposite and fire clay. The effect of several parameters such as adsorbent dose, contact time, initial concentration, pH and temperature has been studied. The adsorption followed pseudo second order, Elovich kinetic models. The adsorption of Cr(VI) was found to be maximum in the pH range 8-11. Adsorption on both clay and nanocomposite obey Langmuir and Freundlich models. The thermodynamic parameters ΔG^o, ΔH^o, ΔS^o have also been evaluated. Adsorptions on both clay and nanocomposite were found to be endothermic and chemisorptive in nature. Chromium removal was better with nanocomposite than with clay.

The same nanocomposites have been attempted for Pb(II) [116] and Ni(II) [117] removal. The study [116] showed that the fire clay and nanocomposite can be used effectively in the removal of Pb(II) through adsorption. Both fire clay and nanocomposite followed Langmuir, Freundlich, D-R, fairly fitted with Tempkin, Harkin-Jura and Halsey models. Pseudo second order kinetic model was followed. The sorption suggested that the adsorption is high at basic medium. Elkovich kinetic model suggested that the adsorption process is chemisorptive nature. The adsorption is also followed by intraparticle diffusion model. The calculated values of different thermodynamic parameters clearly indicated that the adsorption process with nanocomposite and clay was feasible, spontaneous and exothermic nature. This study also reveals that fire clay-TiO_2 nanocomposite exhibited higher adsorption capacity when compared to Fire Clay in its natural form.

The study of Ni(II) [117] adsorption shows that the fire clay and nanocomposite can be used effectively in the removal of Ni(II) through adsorption. The adsorption on both clay and nanocomposite followed Langmuir, Freundlich, D-R models well and fairly fitted well with Temkin model. Pseudo second order kinetic model was followed. Elkovich kinetic model suggested that adsorption process is chemisorptive nature. The adsorption is also followed by intraparticle diffusion model. The calculated values of different thermodynamic parameters clearly indicated that the adsorption process with nanocomposite and clay was feasible, spontaneous and exothermic nature. This study also reveals that fire clay-TiO2 nanocomposite exhibited higher adsorption capacity when compared to fire clay in its natural form.

Mesoporous clay ceramic pellets have been prepared by sintering silica rich low fire clay at two different temperatures (650 °C and 850 °C). The prepared ceramic pellets were characterized using FTIR, SEM, XRF, compressive strength and water adsorption capacity. The methylene blue removal capacity of ceramic pellets was investigated and it was found that the uptake capacity of pellets was found to be increasing with increase in the initial dye concentration, while it was found to be decreasing with an increase in pellet dose. Presence of co-ions and change in pH had

no effect on the removal capacity. The adsorption isotherm followed the Langmuir model while the adsorption kinetics was well described by the pseudo-second order model. A simple device that can be used in aquariums, made from stainless steel wire mesh containing the ceramic pellets has been described which can slowly yet effectively remove MB from tap water at ultralow concentrations [118].

Mesoporous clay-starch ceramic pellets have been prepared using silica-rich low fire clay and potato starch as a pore-forming agent. The ceramic pellets prepared using 30% starch, showed the highest porosity and lowest compressive strength among all the different pellets. Batch mode studies using the pellets showed higher methylene blue adsorption capacity with an increase in time and increased initial dye concentration. The adsorption capacity was found to decrease with increasing pellet dose, while pH had a negligible effect on methylene blue removal which makes them a suitable adsorbent in both acidic and basic mediums. Adsorption isotherm analysis of the process was followed by the Langmuir adsorption isotherm whereas the kinetics analysis fitted well with the pseudo-second-order kinetic model. A low-cost, simple device was made from a stainless-steel wire mesh with mesoporous ceramic pellets enclosed in it, which can easily be dipped and taken out of an aquarium and can remove methylene blue from water [119].

Besides HM cations, clay minerals-based adsorbents have been applied for retention of various pollutants, such as inorganic oxyanions [120], dyes [121,122], humic acids [123], phenolic compounds [124], pharmaceutical wastes [125,126], etc. For such applications, modification with surfactants plays a key role in the improvement of the affinity of negatively charged clay surface to adsorb anions or hydrophobic organic compounds. Clays treated with surfactants are called organo-clays in literature.

A natural kaolinite (KGa-1b) was treated with the surfactant hexadecyltrimethylammonium bromide (HDTMA-Br) to a level twice that of the cation exchange capacity (CEC) [120]. Sorption of nitrate, arsenate, and chromate by the resultant organo-kaolinite was then quantified. Sorption of each oxyanion was well-described by the Langmuir isotherm. Sorption of nitrate was the greatest, with a Langmuir sorption maximum of 24 mmol/kg, although chromate showed the highest sorption affinity of 20 L/kg. Sorption of nitrate, arsenate, and chromate on organo-kaolinite was at least two orders of magnitude greater than their sorption on unmodified kaolinite. Desorption of the bromide counterion indicated that each of the oxyanions was retained by ion exchange on an HDTMA bilayer formed on the organo-kaolinite. Chromate sorption on the organo-kaolinite was unaffected by solution pH in the range 5–9 but decreased at pH 11 due to competition of OH^- for anion exchange sites. Similarly, chromate exchange by organo-kaolinite was reduced in the presence of high background levels of chloride. Chromate was effectively retained when flowing through a packed bed of organo-kaolinite: after an input of more than 40

pore volumes, the effluent concentration of chromate was less than 10% of the input concentration, and 90% of the original HDTMA remained on the organo-kaolinite. The results demonstrate that properly prepared organoclays can remove oxyanions, as well as nonpolar organics, from contaminated waters.

Organo-clays are clay minerals modified with organic compounds, such as gemini surfactants, to enhance their properties for specific environmental applications. By transforming the naturally hydrophilic surfaces of clays into hydrophobic ones, organo-clays become highly effective adsorbents for various organic pollutants.

Gemini surfactants (dimeric surfactants), a generic name of amphiphilic molecules with two hydrophobic alkyl chains and head groups linked by a covalently bonded spacer [25], are widely employed for their physicochemical properties to single-chain modifiers with respect to surface activity, antimicrobial property and self-assembling ability, etc. Gemini surfactants with various spacers, alkyl chains and superior hydrophobic ability are popular modifiers for clay minerals, by forming complexes with a vast array of negatively charged molecules and organic components, especially for organic pollutants [127,128].

Organo-clays are particularly effective in removing organic dyes, which are a common contaminant in industrial wastewater. The primary mechanisms for dye adsorption include electrostatic interactions, hydrophobic bonding, and π-π stacking.

Studies [121] show that organo-clays modified with gemini surfactants such as 16-2-16 and 18-2-18 achieve adsorption capacities towards methyl orange (MO) as high as 276.03 mg/g and 250.00 mg/g, respectively. The adsorption process typically follows the Langmuir isotherm model, indicating monolayer adsorption on homogeneous surfaces.

The removal of anionic dyes like Congo red is enhanced by the strong electrostatic attraction between negatively charged dye molecules and the positively charged clay surfaces. Adsorption capacities can exceed 200 mg/g, depending on the surfactant structure [129].

Functionalized gemini surfactants further improve dye adsorption by introducing additional π-π and hydrogen bonding interactions. For example, surfactants with aromatic rings facilitate π-π stacking with aromatic dyes, while hydroxyl-containing surfactants enhance hydrogen bonding.

Several factors affect dye adsorption, including pH, surfactant structure, and ionic strength. Acidic conditions favor the adsorption of cationic dyes, while basic conditions enhance the removal of anionic dyes. Surfactants with longer alkyl chains and denser packing improve adsorption efficiency, but excessive ionic strength may compete with dyes for adsorption sites. Overall, organo-clays provide high efficiency and versatility for dye removal, making them a valuable tool in water treatment.

Phenolic compounds, such as phenol, chlorophenols, and nitrophenols, are common in industrial wastewater and pose significant environmental risks due to their toxicity and persistence. Organo-clays are highly effective in adsorbing these pollutants through hydrophobic interactions, hydrogen bonding, and π-π interactions [124].

Adsorption capacities for phenolic compounds often exceed 500 mg/g, particularly for chlorophenols. Adsorption kinetics generally follow the pseudo-second-order model, indicating strong chemical interactions. Isotherms align with Langmuir or Freundlich models, depending on the homogeneity of the clay surface. Factors such as pH, temperature, and surfactant structure strongly influence adsorption. Acidic conditions enhance adsorption by reducing phenol ionization and promoting hydrophobic interactions.

Humic acids, a major component of natural organic matter, cause problems such as fouling and taste issues in water. Organo-clays are effective in adsorbing humic acids due to their modified surfaces, which enable hydrophobic and electrostatic interactions [123].

The adsorption of humic acids is strongly pH-dependent. At lower pH levels, humic acids are less ionized, and hydrophobic interactions dominate. At higher pH levels, electrostatic interactions become more significant. Surfactant structure and ionic strength also play crucial roles. For example, longer alkyl chains and denser surfactant packing improve adsorption efficiency, while high ionic strength can either enhance or inhibit adsorption depending on the system.

Organo-clays are widely used in water treatment to remove humic acids, reducing issues such as disinfection byproduct formation during chlorination. Their high efficiency, cost-effectiveness, and renewability make them a sustainable solution for water purification.

Pharmaceuticals and personal care products, classified as emerging contaminants, pose significant risks to aquatic environments. Organo-clays modified with gemini surfactants are highly effective in adsorbing these pollutants due to their ability to interact with both hydrophobic and charged molecules.

Adsorption capacities for Sulfamethoxazole (SMX) on organo-montmorillonite (organo-Mt) exceed 200 mg/g, relying on hydrophobic interactions and electrostatic attractions [126]. Organo-clays achieve adsorption capacities over 130 mg/g for triclosan, with the process typically following Langmuir isotherms [125].

Ibuprofen, diclofenac, and paracetamol are also efficiently adsorbed, with removal driven by hydrophobic and electrostatic interactions.

The adsorption of pharmaceuticals onto organo-clays involves a combination of hydrophobic interactions, electrostatic attractions, hydrogen bonding, and π-π interactions. pH plays a critical role, as the ionization state of the drug and the surface charge of the organo-clay

determine adsorption efficiency. For example, acidic conditions favor the adsorption of negatively charged drugs, while basic conditions enhance the removal of positively charged compounds.

Organo-clays are increasingly used in wastewater treatment for pharmaceutical removal in hospitals, pharmaceutical industries, and municipal treatment plants. Their high efficiency, versatility, and ability to adsorb a wide range of drugs make them a promising solution for mitigating pharmaceutical pollution.

Organo-clays are versatile and highly effective adsorbents for a wide range of organic pollutants, including dyes, phenolic compounds, humic acids, and pharmaceuticals. These materials offer high adsorption capacities, cost-effectiveness, and the potential for regeneration, making them an invaluable tool in addressing global water contamination challenges. Continued research and development in this field will further enhance the applicability and performance of organo-clays in water treatment and environmental remediation.

To achieve these goals, future organo-clay adsorbent studies can be oriented to the following aspects:

1) The improvement of surfactant availability and carbon availability is a key issue for enhancing the adsorption capacity organo-clay adsorbents. Additional treatments or suitable pretreatment methods are worth exposing onto the inorganic precursors.

2) Exploiting multifunctional gemini surfactants, such as aromatic-, imino- or hydroxyl-containing modifiers with functional groups integrated and separated by suitable alkyl chain for modification, or asymmetric gemini surfactants contribute to a full utilization of additional interaction between adsorbent and the adsorbate. π-π, NH-π interactions and hydrogen bond are worth further exploration for adsorption enhancement.

3) Exploring the applicability of adsorbents in interdigitated adsorption systems or real waters (such as mixed organic pollutants, dye mixture, dye and metal ion mixture or the mixture of heavy metal ions, *etc.*), is necessary for adsorbent industrial popularization.

Thus, the diverse applications, structural characteristics, and modification techniques of clay minerals in environmental remediation, particularly for water treatment and pollutant adsorption have been comprehensively explored in this section. Clay minerals, known for their unique structures comprising octahedral and tetrahedral sheets, possess critical properties like cation exchange capacity (CEC) and high surface area, which make them versatile adsorbents. The structural diversity among clay types, such as kaolinite, montmorillonite, and chamotte, defines their functionality and application scope.

Modification techniques, including acid activation, intercalation, and pillaring, have significantly enhanced the adsorption capabilities of natural clays. These methods improve specific surface area, introduce functional groups, and optimize interaction mechanisms, such as ion

exchange, electrostatic attraction, and hydrogen bonding. Modified clays like organo-clays exhibit superior efficacy in removing a wide range of pollutants, including heavy metals, dyes, pharmaceuticals, and phenolic compounds, demonstrating the potential for sustainable and cost-effective water purification.

Future research should focus on optimizing modification strategies, exploring multifunctional surfactants, and testing these materials in real-world scenarios with complex pollutant mixtures. The findings underline the immense potential of clay-based adsorbents in addressing global water contamination challenges and highlight avenues for further development to enhance

1.2 Methods for studying the mechanisms of adsorption of various pollutants on aluminosilicate sorbents

The description of methods for determining adsorption mechanisms, as discussed in the literature, should begin with defining what an adsorption mechanism is, outlining the known mechanisms, and identifying the starting point for tackling such a complex task.

The adsorption mechanism refers to the process by which molecules, ions, or particles (known as adsorbates) adhere to the surface of a solid or liquid (the adsorbent) due to physical or chemical interactions. It involves the adsorption steps, interaction between surface intermediates, and can lead to multiple steady states based on the competition between intermediates and the reversibility of adsorption steps [130].

Types of adsorption mechanisms (Figure 5) include physical adsorption (physisorption) where weak van der Waals forces are involved; chemical adsorption (chemisorption) involving formation of chemical bonds (e.g., covalent or ionic bonds); and electrostatic adsorption that performs due to electrostatic interactions (e.g., Coulomb forces) [130,131].

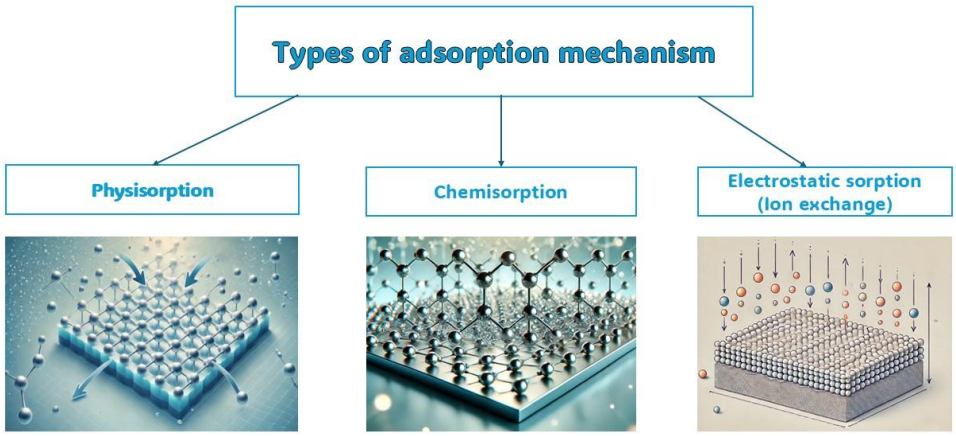


Figure 5 – Types of adsorption mechanism

Physisorption characterizes non-specific interaction between adsorbate and adsorbent, typically it occurs at low temperatures and is a reversible process with no significant change in electronic structure of adsorbate molecules. Multilayer adsorption is possible.

Chemisorption is a highly specific interaction between the adsorbate and adsorbent, usually occurs at higher temperatures, is irreversible or difficult to reverse and involves significant changes in the electronic structure. Monolayer adsorption is typical.

Electrostatic adsorption is common in ion exchange processes where adsorbate is attracted to oppositely charged sites on the adsorbent surface and occurs in systems such as clays, resins, and membranes.

There are 4 main steps in the adsorption mechanism:

1. Transport to the Surface: Adsorbate molecules travel from the bulk phase to the adsorbent surface by diffusion, convection, or migration.

2. Surface Interaction: Adsorbate molecules form physical or chemical bonds with the active sites on the adsorbent.

3. Stabilization: The adsorbate molecules are stabilized on the surface, forming an adsorption layer.

4. Equilibrium: A dynamic equilibrium is reached when the rate of adsorption equals the rate of desorption [132].

Understanding the mechanisms of adsorption is essential for advancing both the science and application of pollutant removal from water systems. Adsorption is widely regarded as an efficient and cost-effective method for eliminating contaminants such as heavy metals, dyes, pharmaceuticals, and organic pollutants. However, the success and long-term sustainability of this process depend on a detailed understanding of how these pollutants interact with adsorbent materials at the molecular level. Gaining insights into the physicochemical interactions involved—such as ion exchange, hydrogen bonding, Van der Waals forces, hydrophobic interactions, and electrostatic attractions—enables researchers to optimize operating conditions, including pH, temperature, and adsorbent dosage. This optimization ensures maximum efficiency and effective pollutant removal.

Mechanistic studies play a critical role in guiding the design and development of advanced adsorbent materials. By identifying specific functional groups or structural features responsible for high adsorption capacity, researchers can create materials with enhanced surface chemistry or customized pore architectures. Furthermore, understanding the underlying mechanisms enables the development of adsorbents with targeted affinities for specific contaminants, improving the precision and overall efficacy of water treatment technologies.

While laboratory experiments often utilize simplified systems, real-world water sources are more complex, containing diverse contaminants under varying environmental conditions. A thorough understanding of adsorption mechanisms helps predict the performance of adsorbents in these challenging conditions, ensuring they remain effective in multi-component systems where competition for adsorption sites and interference effects is common.

Additionally, studying adsorption mechanisms contributes to the sustainability and economic feasibility of water treatment processes. Insights into pollutant uptake can identify opportunities to regenerate adsorbents, reduce material wastage, and minimize secondary pollution. Moreover, a deeper understanding of desorption mechanisms can facilitate the recovery and reuse of captured pollutants, aligning with circular economy principles and reducing environmental impact.

From a scientific perspective, investigating adsorption mechanisms bridges the gap between experimental observations and theoretical modeling. This integration enhances the predictability of adsorption processes, enabling the development of models that simulate and scale up adsorption systems. These advancements are crucial for incorporating adsorption technologies into broader water treatment frameworks and ensuring their adaptability to diverse scenarios.

In summary, understanding adsorption mechanisms is not merely an academic exercise but a practical necessity for addressing the global challenge of water pollution. These insights drive innovation in material design, optimize process performance, and promote sustainable and cost-effective solutions. As such, research into adsorption mechanisms forms a cornerstone of efforts to develop and apply effective water treatment technologies.

When studying a new adsorbent–adsorbate system, the following algorithm is typically applied for the identification of the adsorption mechanism:

The first step in determining the adsorption mechanism involves studying the physicochemical and structural characteristics of the sorbents both before and after modification, as well as before and following adsorption. At this stage, instrumental methods such as IR and Raman spectroscopy, XPS spectroscopy, SEM, TEM, XRD, BET analysis, and others are typically employed. Initially, the characterization of the raw materials used as the basis for sorbent synthesis is conducted. Subsequently, the synthesized modified sorbent is characterized, and a comparative analysis of the main changes occurring after processing or interaction with the raw materials is performed.

Further studies may focus on the characteristics of the sorbents after adsorption of the pollutant to observe any changes that have occurred. This allows for the identification of interaction types, especially in cases of significant changes in IR or Raman spectra or observable alterations in morphology and texture. However, it is frequently observed in practice that no

substantial changes in physicochemical characteristics are detected. This can be attributed to the complexity of the sorbent's nature or the low concentration of the adsorbate. Therefore, relying solely on instrumental methods is often insufficient.

The second step involves investigating the effects of various factors (commonly pH, ionic strength, temperature, and others) on adsorption. External factors such as the nature of the adsorbate and adsorbent, temperature, pressure, and concentration significantly influence the adsorption mechanism. The nature of the adsorbate, including its size, polarity, and chemical reactivity, determines how effectively it interacts with the adsorbent surface. Similarly, the characteristics of the adsorbent, such as its surface area, pore size, surface charge, and chemical composition, play a crucial role in defining its adsorption capacity and specificity.

Temperature is another critical factor, as physisorption tends to decrease with rising temperatures due to the weakening of weak intermolecular forces, while chemisorption often increases with temperature because of the energy required to form chemical bonds. Pressure predominantly affects gas-phase adsorption, with higher pressures typically enhancing adsorption efficiency by increasing the number of adsorbate molecules in contact with the adsorbent surface. Lastly, the concentration of the adsorbate influences the adsorption rate; higher concentrations initially accelerate the process, but the rate plateaus once the adsorbent reaches its saturation point [133,134].

Together, these factors interact to shape the adsorption mechanism, highlighting the need to optimize conditions for specific applications.

The third step represents the modelling of experimental data using adsorption thermodynamic and kinetic models. By fitting the experimental data to known adsorption isotherm models it is possible to get some information about the mechanisms. I.e. the Langmuir model is applicable in the case of monolayer adsorption, while the Freundlich model works for multilayer adsorption. By calculating adsorption enthalpy and entropy you can tell the type of adsorption, whether it is a physical or chemical one. Adsorption kinetic models provide insights into how adsorbate molecules interact with adsorbent surfaces over time, helping to analyze adsorption rates, pathways, and controlling factors [135,136].

However, each group of methods gives different types of information about adsorption mechanisms and has its own limitations or gives questionable results. Hence, the fourth step in elucidating adsorption mechanisms is the integration of all obtained results into a comprehensive framework that describes the mechanism of interaction between the adsorbent and the adsorbed substance.

1.2.1 Instrumental physicochemical methods used for elucidation adsorption mechanisms

Instrumental techniques that facilitate the elucidation of adsorption mechanisms include all characterization methods for the studied materials, i.e., SEM, TEM, FTIR and Raman spectroscopy, XRD, ζ-potentiometry, BET analysis, thermogravimetry, and additional methods relevant to the specific adsorbent. Nevertheless, the majority of the enumerated approaches predominantly offer insights into the impacts of treatment or modification of the initial adsorbent. FTIR spectroscopy is primarily employed to determine the interaction processes between the adsorbent and the pollutant under investigation (adsorbate). This technique is especially effective for adsorption systems that contain organic molecules.

The study [137] focuses on the adsorption mechanism of ammonium onto Chinese natural zeolite. FTIR spectroscopy was employed to confirm the presence of chemical adsorption and hydrogen bonds during the interaction between ammonium and zeolite. FTIR revealed changes in characteristic bands related to O-T-O vibrations and -OH groups in the zeolite after ammonium adsorption. Shifts in these peaks in the FTIR spectrum confirmed the formation of new chemical bonds, such as hydrogen bonds between ammonium and oxygen in the zeolite, as well as stronger bonds indicative of chemical adsorption. These findings were further supported by theoretical calculations and experiments, which proved that ammonium adsorption on zeolite involves a synergy of ion exchange, electrostatic attraction, and chemisorption. Thus, FTIR spectroscopy proved to be a key tool in identifying the main mechanisms of adsorption.

The study [137] explores the adsorption mechanism of crystal violet (CV) onto halloysite that has undergone thermal and acid modifications. It identifies hydrophobic interactions between siloxane groups and the aromatic rings of CV, alongside hydrogen bonding between nitrogen in CV and silanol groups, as the primary mechanisms involved.

To clarify the adsorption mechanism, the following analytical techniques were employed:

- FTIR analysis revealed alterations in specific vibrational bands, such as those corresponding to silanol and siloxane groups, before and after the adsorption process. These observations confirmed the role of hydrogen bonding and the changes in surface groups caused by acid treatment.

- Raman spectroscopy complemented FTIR findings by detecting shifts in vibrational modes related to aromatic rings and nitrogen groups in CV. This provided additional evidence for hydrogen bonding and interactions between the aromatic rings of CV and siloxane surfaces.

- Zeta potential analysis examined the variations in surface charge as a function of pH, indicating that electrostatic interactions were not the predominant mechanism driving adsorption.

The integration of these instrumental techniques was essential for identifying and confirming the molecular interactions underpinning the adsorption process. FTIR and Raman spectroscopy offered detailed insights into the chemical transformations and bonding mechanisms during adsorption, while zeta potential measurements provided a contextual understanding of surface charge dynamics and interaction energetics.

This study [138] focuses on the selective adsorption mechanisms of Pb(II) and Cr(VI) ions using surfactant-modified and unmodified natural zeolites. By investigating the effects of surfactant modification, the researchers aimed to understand how structural, electrostatic, and kinetic factors influence the adsorption capacity and mechanism for these metal ions. The findings provide valuable insights for tailoring zeolites to optimize wastewater treatment processes.

To identify the adsorption mechanisms, various analytical methods were employed. FTIR detected changes in functional groups on the zeolite surface before and after adsorption, confirming the role of electrostatic and chemical bonding in the adsorption process. SEM revealed changes in surface morphology, showing smoother surfaces for modified zeolites and particle deposition after adsorption, which highlighted differences in adsorption behavior. XRD analysis identified structural changes and alterations in crystallinity after surfactant treatment and ion adsorption, while BET analysis measured specific surface areas and pore volumes, demonstrating how surface modifications affected adsorption capacity by altering available adsorption sites. Zeta potential measurements provided critical information on changes in surface charge following surfactant modification, explaining the enhanced adsorption of anionic Cr(VI) and its selectivity over Pb(II).

Kinetic and isothermal modeling further clarified the adsorption processes. Cr(VI) adsorption followed pseudo-second-order kinetics and was driven primarily by electrostatic forces, while Pb(II) adsorption involved both electrostatic and intrapore interactions. Isothermal analysis showed that adsorption adhered to the Langmuir model, indicating monolayer adsorption behavior.

Instrumental methods played a crucial role in elucidating complex interactions during adsorption. FTIR and SEM provided molecular and surface-level evidence for surfactant interactions and structural changes, while XRD and BET highlighted modifications in crystallinity and porosity that influenced adsorption capacity. Zeta potential analysis revealed the electrostatic mechanisms underpinning metal ion adsorption. Together, these methods demonstrate that the enhanced adsorption of Cr(VI) and Pb(II) by modified zeolites is a result of structural changes, surface charge alterations, and specific interaction mechanisms. By combining experimental data with theoretical models, the study showed that electrostatic attraction and structural modifications are key factors in improving the adsorption efficiency of surfactant-modified zeolites.

FTIR and Raman spectroscopy played crucial roles in understanding the adsorption mechanisms of chromate ions onto SMZs [139]. FTIR was instrumental in identifying molecular interactions by detecting changes in functional group vibrations. The analysis revealed structural modifications on the zeolite surface after surfactant modification, such as the appearance of new adsorption peaks corresponding to C–H stretching vibrations from the surfactant (HDTMA). These changes confirmed the attachment of the surfactant molecules to zeolite, which facilitated the formation of adsorption sites for chromate ions. Additionally, FTIR provided valuable insights into the surface chemistry, highlighting the bonding interactions between chromate anions and the positively charged head groups of the surfactant.

Raman spectroscopy complemented FTIR by offering a detailed structural analysis of the adsorbed surfactant and its interaction with chromate ions. It was particularly effective in detecting vibrational modes sensitive to molecular polarizability, which revealed the structural conformations of the surfactant, including bilayer formation and variations in the arrangement of its tail groups. Raman analysis also identified shifts in chromate peaks, such as a 30 cm^{-1} shift in the ν1 chromate peak, indicating additional Lewis acid-base interactions alongside the primary anion-exchange mechanism. Furthermore, Raman spectroscopy allowed in situ observations of wet samples, avoiding interference from water's absorption bands, making it ideal for studying chromate adsorption under real conditions.

FTIR and Raman spectroscopy provided complementary insights into the adsorption process. While FTIR identified functional group transformations and confirmed the formation of chemical bonds, Raman spectroscopy offered a deeper understanding of the structural dynamics, molecular geometry, and specific interactions of the adsorbed species. Together, these techniques demonstrated that the chromate adsorption onto SMZ involved a combination of anion exchange, surface-enhanced oligomerization, and Lewis acid interactions, providing a comprehensive molecular-level understanding of the adsorption mechanisms.

FTIR, SEM, and XRD methods were employed to identify the adsorption mechanisms of lead [Pb(II)] on natural clay and humic acid (HA) in the study [140]. Each technique played a distinct role in characterizing the interactions and understanding the molecular processes involved.

FTIR was used to identify the functional groups in clay and HA responsible for Pb(II) binding. In clay, Si–O–Si and hydroxyl (OH) groups were involved, as evidenced by shifts in their characteristic vibrational bands after Pb(II) adsorption. Similarly, in HA, functional groups like carboxylic acid, phenolic, hydroxyl, and carbonyl groups participated in ionic interactions with Pb(II). The analysis highlighted the chemical transformations and bonding that occurred during adsorption, confirming the specific molecular interactions between Pb(II) and the adsorbents.

SEM provided detailed images of the surface morphology of clay and HA before and after adsorption. For clay, the images revealed the presence of quartz and uneven Pb(II) deposition on the surface, which was indicative of ion exchange. For HA, SEM demonstrated a distinct pattern of Pb(II) deposition on its matrix. SEM imaging was crucial in visually confirming the binding of Pb(II) to the adsorbents. The EDS semi-quantitative analysis demonstrated that in the clay samples, Pb is adsorbed on the surface by replacing ions like Ca an Al.

XRD was employed to analyze the mineralogical composition of clay and HA, revealing the presence of quartz as a dominant mineral along with other components like phengite??? and montmorillonite. These minerals provided active sites for Pb(II) adsorption. The structural changes observed in the XRD spectra after Pb(II) adsorption supported the involvement of these minerals in binding processes.

Together, FTIR, SEM, and XRD provided a comprehensive understanding of Pb(II) adsorption mechanisms. FTIR elucidated molecular interactions, SEM confirmed surface-level changes and ion exchange, and XRD established the structural role of mineral components in the adsorption process. These complementary techniques highlighted the potential of natural clay and HA as effective adsorbents for Pb(II) removal.

The study [141] utilized multiple analytical methods to investigate the adsorption mechanisms of cadmium (Cd) and lead (Pb) on humic acid (HA)-iron-pillared bentonite (HA-Fe-PILC). The key methods included FTIR, XPS, SEM, XRD, BET surface area analysis, and zeta potential measurements. Among these, FTIR and XPS were critical for understanding the chemical interactions and adsorption mechanisms.

FTIR analysis was used to identify the functional groups involved in the adsorption process. The technique detected vibrations corresponding to Si-OH, Al-OH, and Fe-O groups in the bentonite structure and changes after modification with HA. New peaks at 740 and 824 cm^{-1} confirmed the successful loading of HA on Fe-PILC, which facilitated adsorption through oxidation reactions with Cd(II) and Pb(II). After metal adsorption, FTIR revealed new peaks at 1373.73 and 1292.35 cm^{-1}, attributed to the reaction of Cd and Pb with C-O groups on HA-Fe-PILC. Additionally, the disappearance or transformation of certain functional groups suggested their direct involvement in the removal of heavy metals.

XPS provided detailed insights into the surface chemistry and elemental interactions during adsorption. It confirmed the successful adsorption of Cd and Pb through the identification of Cd 2p and Pb 4f reflections, which corresponded to groups like Cd-O, Cd^0, Pb-O, and Pb^0. Changes in the C 1s and O 1s spectra indicated the interaction of metal ions with functional groups such as C=C, -C-O, and -COOH. These findings highlighted the role of surface complexation and chelation with HA molecules. Furthermore, the identification of Fe(III) states and specific shifts

in spectral peaks provided evidence of the involvement of iron in adsorption and oxidation processes.

FTIR elucidated the molecular-level bonding and confirmed the role of specific functional groups in adsorption, while XPS offered complementary information by identifying chemical states, elemental compositions, and detailed interactions. Together, these methods were instrumental in demonstrating that the adsorption of Cd and Pb on HA-Fe-PILC involved ion exchange, surface complexation, and chemical bonding, providing a comprehensive understanding of the underlying mechanisms.

In the study [142], X-ray Photoelectron Spectroscopy (XPS) and zeta potential analysis were key techniques used to elucidate the adsorption mechanism of phosphate on lanthanum-incorporated zeolite (La-Z). These methods provided detailed insights into the interaction between phosphate ions and the adsorbent.

XPS was employed to investigate the chemical states of elements and surface interactions. After phosphate adsorption, XPS detected a distinct P 2p peak at ~133.4 eV, which confirmed the successful binding of phosphate to La-Z. Additionally, changes in the La 3d and O 1s spectra indicated transformations in the lanthanum and oxygen chemical states, consistent with the formation of inner-sphere complexes. These complexes likely involved phosphate ions replacing hydroxyl groups (La-OH) on the La-Z surface, as evidenced by shifts in binding energy and changes in peak proportions.

Zeta potential measurements provided information about the surface charge of La-Z before and after adsorption. The isoelectric point (IEP) of La-Z shifted from pH 7.10 to 5.52 after phosphate adsorption. This reduction suggested specific adsorption of anionic phosphate, which increased the negative charge on the La-Z surface. The observed decrease in IEP supported the formation of inner-sphere complexes, as outer-sphere complexation typically does not affect surface charge to this extent.

Together, XPS and zeta potential analysis demonstrated that phosphate adsorption on La-Z was primarily driven by inner-sphere complexation, with phosphate ions chemically binding to lanthanum through ligand exchange mechanisms. These methods were crucial in confirming the role of La-OH groups and the specificity of the adsorption process.

The authors [143] used a combination of analytical techniques to elucidate the adsorption mechanisms of Pb(II) on HDTMA-modified bentonite clay. Among these, FTIR and XPS played significant roles in detailing the molecular and surface interactions.

FTIR was utilized to identify the functional groups involved in the adsorption process. The spectra before and after Pb(II) adsorption revealed shifts in specific peaks, such as those associated with Si–O–Si and Al–O–Si bending vibrations, indicating their participation in binding Pb(II). The

appearance of new peaks and the shifts in existing ones confirmed the formation of inner-sphere complexes, as Pb(II) chemically interacted with these groups. FTIR analysis thus provided direct evidence of changes at the molecular level due to adsorption.

XPS provided detailed insights into the chemical states and elemental interactions at the surface of the HDTMA-modified bentonite. The analysis identified the binding of Pb(II) to oxygen and silicon atoms, with shifts in binding energy confirming the formation of strong chemical bonds. XPS also indicated the reduction of electron density in the Si and Al mono-vacancies, which contributed to Pb(II) adsorption. This method verified the nature of the interaction as predominantly inner-sphere complexation, with Pb(II) occupying active sites on the modified clay.

These methods together demonstrated that Pb(II) adsorption on HDTMA-modified bentonite is primarily driven by chemical interactions rather than simple electrostatic forces. FTIR highlighted the changes in functional groups and chemical bonds, while XPS confirmed the elemental and electronic alterations at the surface, offering a comprehensive understanding of the adsorption mechanisms.

In conclusion, instrumental techniques play a vital role in elucidating the mechanisms of adsorption by providing molecular, structural, and chemical insights into adsorbent-pollutant interactions. Methods such as FTIR, XPS, SEM, XRD, and zeta potential analysis, among others, enable researchers to identify functional groups, monitor structural changes, and evaluate surface charge dynamics during adsorption. Specifically, FTIR and XPS are indispensable for revealing chemical interactions, such as the formation of inner-sphere complexes and the alteration of chemical states in the adsorbent. By integrating experimental and theoretical approaches, these methods facilitate a detailed understanding of adsorption processes, which is essential for optimizing adsorbents for environmental applications.

1.2.2 Effect of various factors on adsorption to elucidate the mechanisms

The study of various factors influencing the adsorption process is a crucial aspect of investigating new sorption systems. Identifying the optimal conditions for adsorption maximizes the efficiency of the sorbent, optimizes the process technology at all stages, and provides valuable insights into the interaction mechanisms of the materials under study.

The external factors typically analyzed in adsorption processes include sorbent mass, pollutant concentration, modifier concentration, solution pH, ionic strength, temperature, contact time, among others.

Among these factors, pH and ionic strength studies are most commonly used to reveal information about the interaction mechanisms between the sorbent and the pollutant. Additionally, investigations into temperature, adsorbate concentration, and contact time can yield significant

insights, though these often require the application of various kinetic and thermodynamic calculation methods, which will be discussed in the next chapter.

A compelling example of the application of external factor studies to elucidate chemical speciation mechanisms is presented in the work of Khan et al. [69], which explores the adsorption of lead and nickel on zeolite in aqueous solutions. The study provides valuable insights into the factors influencing the adsorption of Pb^{2+} and Ni^{2+} on zeolite, shedding light on the underlying chemical speciation mechanisms.

pH Influence plays a critical role in the speciation of metal ions and their interactions with zeolite. At low pH values (<6 for Pb^{2+} and <5 for Ni^{2+}), adsorption is primarily governed by ion exchange mechanisms due to the competition with H^+ ions. As the pH increases, metal hydroxide species dominate, resulting in inner-sphere complexation or precipitation, particularly above pH 8 for both Pb^{2+} and Ni^{2+}.

Ionic Strength impacts adsorption, especially at low pH, where it suggests that ion exchange is the predominant mechanism. However, at higher pH, the effect of ionic strength decreases, indicating that surface complexation becomes more significant.

Solid Content demonstrates that increasing zeolite content reduces adsorption per gram due to the saturation of active sites, though total adsorption increases overall.

Temperature also affects the process, with higher temperatures leading to an increased adsorption capacity, signifying an endothermic process. Thermodynamic parameters reveal that the adsorption is spontaneous and involves greater randomness at the solid-liquid interface.

Competing Ions influence adsorption rates, as coexisting cations and anions compete with Pb^{2+} and Ni^{2+}. For example, smaller cations like K^+ enhance adsorption more effectively than larger ions like Na^+ or Li^+.

Humic Acid further affects adsorption, enhancing it at low pH by forming complexes on the zeolite surface. However, at high pH, humic acid reduces adsorption due to electrostatic repulsion and complexation in the solution.

These findings clarify the interaction between zeolite and Pb^{2+}/Ni^{2+} species under varying environmental conditions. The study establishes that outer-sphere complexation and ion exchange dominate at low pH, while inner-sphere complexation becomes more significant at higher pH. Furthermore, thermodynamic data confirms the endothermic and spontaneous nature of the adsorption process, highlighting the potential for scaling zeolite-based treatments in environmental applications.

The study investigating the adsorption of 2-chlorophenol (2-CP) onto zeolite modified with cetyltrimethylammonium bromide (CTAB) [144] utilized the analysis of external factors such as

surfactant configuration, pH, temperature, ionic strength, and the kinetics of adsorption to elucidate the adsorption mechanism.

Surfactant Configuration. The study compared one-step and two-step processes, showing that a loose CTAB bilayer formed in the one-step process enhanced 2-CP adsorption compared to the compact surfactant configuration in the two-step process. This difference in surfactant arrangement on the zeolite surface influenced the hydrophobic partitioning and the availability of active adsorption sites.

pH Dependency. The adsorption of 2-CP was strongly influenced by pH. It was most effective under weakly acidic conditions (pH 3–6), where 2-CP remained predominantly non-dissociated, increasing its affinity for the CTAB-modified zeolite. At higher pH, dissociation of 2-CP reduced hydrophobic interactions and adsorption efficiency.

Ionic Strength and Temperature. Changes in ionic strength highlighted the role of ion exchange during adsorption. The study also demonstrated that temperature had a minimal impact on adsorption efficiency, making the one-step process suitable for real-world applications where temperature control might be limited.

The study concluded that the adsorption of 2-CP on CTAB-modified zeolite was a combination of hydrophobic partitioning, hydrogen bonding, and electrostatic interactions. The enhanced performance of the one-step process was attributed to the loose CTAB bilayer structure, which increased the accessibility of adsorption sites and facilitated stronger interactions between 2-CP and the surfactant's polar head groups.

By systematically studying external factors and their effects on adsorption, the research revealed that the optimal conditions and CTAB configuration significantly influence the adsorption mechanism. The findings provide a clear understanding of how surfactant modification enhances the removal of organic pollutants like 2-CP, offering a framework for designing efficient and reusable adsorbent systems.

In research [137] the study of pH influence, together with instrumental and calculation methods, played a significant role in elucidating the adsorption mechanism of crystal violet (CV) on modified halloysite. Adsorption experiments conducted over a pH range of 3 to 9 revealed that CV uptake increased with pH up to 5, after which it remained relatively constant. This behavior demonstrated that electrostatic interactions were unlikely to be the primary mechanism, as adsorption did not increase further despite the surface becoming more negatively charged. Instead, the results pointed towards hydrogen bonding and hydrophobic interactions as the dominant mechanisms.

In contrast, instrumental methods such as FTIR and Raman spectroscopy were crucial for providing molecular-level evidence of these interactions. The pH study offered an essential

macroscopic understanding of adsorption behavior, ruling out electrostatic interactions and setting the stage for deeper investigation. However, it was the application of FTIR and Raman spectroscopy that provided definitive molecular evidence, confirming the specific involvement of silanol and siloxane groups in hydrogen bonding and hydrophobic interactions. Thus, while pH analysis was critical for identifying possible mechanisms, instrumental methods were indispensable for validating and detailing these interactions at the molecular level.

The authors [138] used both the analysis of external factors and instrumental methods like zeta potentiometry to reveal the adsorption mechanisms of Pb(II) and Cd(II) on modified and unmodified zeolites. Here's how these approaches contributed:

pH Influence. The study showed that pH significantly impacts adsorption. At low pH, competition from H^+ ions reduced Pb(II) adsorption, while higher pH values facilitated hydroxide precipitation or inner-sphere complexation. Similarly, for Cd(II), pH affected the ion speciation and surface charge interactions.

Ionic Strength. Variations in ionic strength highlighted differences in adsorption mechanisms. While Cr(VI) adsorption was strongly influenced by ionic strength due to electrostatic interactions, Pb(II) adsorption remained relatively unaffected, suggesting the dominance of intrapore and chemical interactions.

Zeta potential measurements provided a direct understanding of surface charge dynamics during adsorption.

The study of external factors was essential for understanding macroscopic behaviors and trends, such as how pH, ionic strength, and temperature affect adsorption capacity and mechanisms. However, instrumental methods like zeta potentiometry offered molecular-level insights into the role of surface charge, providing direct evidence for electrostatic or non-electrostatic interactions. Together, these approaches offered a comprehensive understanding of the adsorption process, with zeta potentiometry serving as a critical tool for validating the mechanisms inferred from the analysis of external factors.

In conclusion, the analysis of external factors such as pH, ionic strength, temperature, and surfactant configuration is essential for understanding the macroscopic trends and optimizing the adsorption process. These studies help identify key parameters influencing adsorption efficiency and provide initial insights into potential mechanisms. However, instrumental methods, such as FTIR, Raman spectroscopy, and zeta potentiometry, play a pivotal role in confirming and detailing the molecular-level interactions, such as chemical bonding, surface charge dynamics, and the formation of specific complexes. The integration of both external factor analysis and instrumental techniques offers a comprehensive understanding of adsorption mechanisms, ensuring accurate

identification of underlying processes and enabling the development of efficient and targeted adsorption systems.

1.2.3 Overview of Theoretical Methods for Studying Adsorption Mechanisms

Computational Approaches for Adsorption Mechanism Analysis. An analysis of adsorption processes in interfaces between a solid and a liquid, particularly for aluminosilicate sorbents, involves a synergy of theoretical approaches. These methods enable an examination of adsorption energies, kinetics, thermodynamics, and molecular-level processes. Quantum mechanical approaches, especially Density Functional Theory (DFT), have been widely used to study adsorption at an atomic level. DFT helps estimate adsorption energies, charge transfer, and electronic structure changes upon adsorption. Solvation effects can be included through explicit or implicit solvent models, and Time-Dependent DFT (TD-DFT) is particularly useful for studying photoadsorption mechanisms.

DFT is based on the premise that the ground-state behavior of a many-electron system can be determined solely from the electron density rather than the complex many-body wavefunction. The Hohenberg-Kohn Theorems established the foundation of DFT, describing a universal density functional that determines the ground-state energy as a function of electron density. The Kohn-Sham Equations introduce an auxiliary system of non-interacting electrons that replicate the real system's electron density, significantly simplifying computations. A key component of DFT is the Exchange-Correlation Functional, which approximates electron-electron interactions. Common functionals include the Local Density Approximation and the Generalized Gradient Approximation, the latter incorporating density gradients for improved accuracy.

DFT is widely applied in adsorption studies to calculate adsorption energies, electronic structure changes, and charge transfer. In material design, it aids in optimizing sorbents by predicting surface reactivity. Implicit and explicit solvation models in DFT enable accurate simulations of solid-liquid interfaces. However, DFT has limitations, such as the inherent approximations in exchange-correlation functionals that can introduce errors in adsorption energy predictions. Its computational cost can also be high, particularly for large systems, and standard DFT does not accurately capture van der Waals interactions unless specific corrections are applied.

Molecular dynamics (MD) simulations provide dynamic insights into adsorption by modeling interactions between sorbents and adsorbates over time. MD relies on Newtonian mechanics to simulate atomic and molecular movements using predefined force fields, such as CLAYFF for aluminosilicates and TIP3P, SPC, or TIP4P for water. Newton's equations are solved numerically to predict atomic trajectories, and simulations are performed under different

thermodynamic ensembles, including NVT (constant number of particles, volume, and temperature) and NPT (constant number of particles, pressure, and temperature).

MD is particularly useful for studying dynamic adsorption processes, solvent and ion interactions, and temperature- and pressure-dependent adsorption behavior. However, its accuracy depends on the selected force field, which may not perfectly capture all interactions. Additionally, MD simulations are computationally demanding, especially for large systems or long timescales. Another drawback is that standard MD does not account for electronic structure changes, which are crucial in adsorption processes.

Monte Carlo (MC) simulations are effective in modeling adsorption equilibrium and predicting adsorption isotherms. These simulations use statistical sampling techniques to determine thermodynamic properties and adsorption behaviors. Random sampling explores adsorption sites and possible states, while the Metropolis Algorithm evaluates whether a new configuration is accepted based on energy changes and probability distributions. The Grand Canonical Monte Carlo (GCMC) method allows adsorption simulations at constant chemical potential, temperature, and volume.

MC simulations are widely used to predict adsorption isotherms, study adsorption in porous materials like zeolites and mesoporous aluminosilicates and optimize sorbents by comparing adsorption capacities. However, MC methods have certain limitations. They provide limited temporal resolution and do not capture dynamic adsorption behaviors as MD does. Configurational sampling may not explore all possible adsorption configurations, and the results can be influenced by initial parameter choices, potentially leading to biased outcomes.

Hybrid computational approaches, such as Quantum Mechanics/Molecular Mechanics (QM/MM), integrate quantum accuracy with large-scale simulations, improving computational efficiency. However, these methods come with challenges, including their complexity, the need for significant expertise and validation, and their high computational cost, particularly for large systems that require quantum calculations. Additionally, developing accurate force fields for seamless QM/MM transitions remains a challenge.

The authors [145] used a combination of experimental optimization and theoretical computation, specifically Molecular Dynamics (MD) simulations, to determine the mechanism of ammonium adsorption onto Chinese natural zeolite.

Additionally, they conducted adsorption kinetics, isotherm analysis, and thermodynamic studies to understand the adsorption behavior. The results indicated that the process followed pseudo-second-order kinetics and was best described by the Freundlich model, suggesting a multilayer adsorption process. Theoretical calculations and infrared spectroscopy further confirmed the presence of hydrogen bonding and chemisorption, highlighting the synergistic

effects of ion exchange, electrostatic attraction, and chemical adsorption as the primary adsorption mechanisms.

To determine the adsorption mechanism of heavy metals onto modified kaolin, the authors [146] employed quantum chemical simulations based on *DFT*. Specifically, they used the Dmol3 package within the DFT framework to analyze adsorption strength, charge transfer, and differential charge density. To accurately describe electron exchange, they applied the *Generalized Gradient Approximation* (GGA-PBE) exchange-correlation functional, while the DFT semi-core pseudopotential method was utilized to account for relativistic effects. Additionally, Frontier Molecular Orbital (FMO) theory and Fukui function analysis were used to evaluate the chemical reactivity of kaolin surfaces, identifying nucleophilic and electrophilic active sites. These methods enabled the researchers to understand how modified kaolin interacts with heavy metal oxides at high temperatures and to elucidate the role of electron transfer in adsorption processes.

By leveraging DFT-based quantum chemical simulations, the study provided valuable insights into the adsorption mechanisms of heavy metals onto modified kaolin at the molecular level. Theoretical methods helped clarify how surface modifications, such as intercalation-exfoliation and acid/alkali treatment, altered the adsorption properties of kaolin, making it more effective in capturing heavy metals.

One of the key findings of the study was the adsorption strength and stability of heavy metal oxides (PbO, CdO, ZnO, Cr_2O_3) on modified kaolin surfaces. DFT calculations allowed for the quantification of adsorption energy, which directly reflected the strength of interactions between the adsorbate and adsorbent. The results showed that acid/alkali modification significantly enhanced adsorption strength, particularly by creating new active sites, such as Al-defects and exposed reactive oxygen atoms, which played a crucial role in improving heavy metal retention.

In addition to adsorption strength, the study investigated charge transfer and electron interactions using *Frontier Molecular Orbital* (FMO) theory. This approach allowed the researchers to analyze HOMO (Highest Occupied Molecular Orbital) and LUMO (Lowest Unoccupied Molecular Orbital) energy levels, which are fundamental in determining electron transfer tendencies. A smaller HOMO-LUMO energy gap indicated a stronger electron transfer between heavy metals and modified kaolin, leading to enhanced chemisorption. The results revealed that Pb and Cd were more readily adsorbed at lower temperatures (900-1000°C) due to favorable electron transfer interactions, whereas Zn and Cr exhibited stronger interactions at higher temperatures (1200-1300°C), likely due to changes in surface composition and electronic properties.

The study also employed Fukui function analysis to determine how the distribution of surface-active sites changed after modification. This approach helped identify nucleophilic and

electrophilic regions on kaolin surfaces, which are essential for adsorption via electron transfer mechanisms. The formation of new oxygen species (O•) and unsaturated Al-coordination sites increased nucleophilic sensitivity, making the kaolin surface more reactive for metal oxide adsorption. The results demonstrated that acid/alkali-modified kaolin exhibited stronger nucleophilic properties, which significantly improved its ability to bind heavy metal oxides through chemical interactions.

Another critical aspect of the study was the impact of high-temperature transformations on adsorption performance. By simulating thermal decomposition processes, the authors explored how kaolin's structure evolved from metakaolin (900-1000 °C) to mullite and cristobalite (1200-1300 °C). These transformations altered the adsorption properties of kaolin, leading to a shift in selectivity. The results showed that mullite and cristobalite were more effective in capturing Zn and Cr, while Pb and Cd adsorption decreased at higher temperatures due to a decline in electron transfer induction. These findings highlighted the temperature-dependent nature of adsorption mechanisms and the importance of understanding phase transitions in kaolin to optimize its performance as an adsorbent.

Overall, the integration of DFT, FMO theory, and Fukui function analysis provided a comprehensive molecular-level understanding of how modified kaolin interacts with heavy metals under high-temperature coal combustion conditions. These theoretical methods not only explained the selectivity of kaolin for different metals but also clarified the role of surface modifications in enhancing adsorption and the mechanistic changes caused by thermal transformations. The study's findings contribute to the rational design of more effective adsorbents for heavy metal removal in environmental and industrial applications.

In [147] molecular simulations were employed to support experimental findings on the adsorption mechanism of thiocyanate (SCN^-) ions at the air-water interface. These simulations played a crucial role in clarifying the thermodynamic changes observed during adsorption, revealing the underlying driving forces and molecular-scale interactions responsible for ion adsorption behavior. By analyzing adsorption enthalpy (ΔH) and entropy (ΔS), the study challenged conventional assumptions that adsorption is driven by positive enthalpy, due to electrostatic repulsion, and positive entropy, resulting from hydrophobic forces. Instead, the simulations demonstrated that adsorption is energetically favorable due to local solvent rearrangements rather than traditional long-range electrostatic effects.

Computational models revealed that adsorbed SCN^- ions influenced the surrounding solvent density distribution, leading to a redistribution of water molecules between bulk, surface, and coordination regions. This process explained the observed negative adsorption enthalpies, as solvent molecules reoriented and reorganized locally rather than experiencing a net electrostatic

energy gain or loss. The entropy loss was attributed to the suppression of capillary waves, as adsorbed ions restricted the natural fluctuations of the liquid surface, leading to a net decrease in configurational entropy.

To achieve these insights, the study utilized molecular simulations with simplified spherical ion models as well as detailed molecular representations in the SPC/E water model. The researchers employed umbrella sampling to calculate free energy profiles for ion movement across the interface, providing spatially resolved energy maps that depicted how solvent molecules interacted with ions at different interface positions. By varying ion charge and size, the study confirmed that more polarizable and larger ions exhibited stronger adsorption tendencies. The consistency of energy and entropy trends across different ion models validated the generality of the findings.

Overall, the molecular simulations provided a microscopic perspective on adsorption mechanisms, demonstrating that thiocyanate adsorption at the air-water interface is primarily driven by local solvent reorganization and capillary wave suppression rather than by long-range electrostatic or hydrophobic forces. These results challenge traditional adsorption theories and offer valuable insights into interfacial ion behavior, with implications for fields such as environmental chemistry, biophysics, and atmospheric science.

Adsorption Isotherms, Kinetics, and Thermodynamics: Theoretical Models and Applications. Adsorption behavior is often analyzed using isotherm models, which describe equilibrium adsorption characteristics. Adsorption isotherms describe the equilibrium relationship between the amount of adsorbed substance on the surface of an adsorbent and its concentration in the solution (or gas phase) at a constant temperature. These models help in understanding adsorption mechanisms, characterizing adsorbents, and predicting their efficiency.

Several approaches exist for classifying adsorption isotherms. The most widely used models can be grouped as empirical, semi-theoretical and theoretical models (Table 1):

Table 1 – Classification of the most popular adsorption isotherm models

Model	Equation	Type	Key Features	Limitations
Freundlich	$q_e = K_F C_e^{1/n}$, where q_e is the equilibrium amount of adsorbed substance (mg/g), C_e is the equilibrium concentration in solution (mg/L), and K_F and 1/n are empirical constants	Empirical	Multilayer adsorption on heterogeneous surfaces	Does not describe adsorption saturation

Table 1 (continued)				
Dubinin-Radushkevich (D-R)	$q_e = q_m \exp(-B\varepsilon^2)$, where $\varepsilon = RTln(1+\frac{1}{C_e})$ is the Polyanyi potential, and B is a parameter related to adsorption energy	Empirical	Used for porous materials, estimates adsorption energy	Does not account for adsorption capacity saturation
Langmuir	$q_e = \frac{q_m K_L C_e}{1+K_L C_e}$, where q_m is the maximum adsorption capacity, and K_L is the adsorption equilibrium constant	Semi-Theoretical	Monolayer adsorption on homogeneous surfaces	Ignore intermolecular interactions
Temkin	$q_e = Bln(AC_e)$, where $B = RT/b$, A is the isotherm constant, and b is a parameter related to adsorption heat.	Semi-Theoretical	Accounts for adsorbate-adsorbate interactions	Limited applicability to highly porous materials
BET (Brunauer-Emmett-Teller)	$q_e = \frac{q_m C_e K_L}{(C_s-C_e)(1+(K_B-1)C_e/C_s)}$, where K_B is the interaction constant, and C_s is the saturation concentration	Theoretical	Describes multilayer adsorption, useful for surface area analysis	Not directly applicable to solid-liquid systems
Redlich-Peterson	$q_e = \frac{K_R C_e}{1+\alpha_R C_e^g}$, where K_R, α_R, g are empirical parameters	Theoretical	Combines Langmuir and Freundlich models, flexible fitting	Complex physical interpretation

Selecting an adsorption model is crucial for understanding the adsorption process. Key analytical approaches include:

1. Comparison of Model Fit to Experimental Data

- If the Langmuir isotherm provides the best fit, the process is likely monolayer and limited by available adsorption sites.

- If the Freundlich isotherm fits better, adsorption occurs on a heterogeneous surface with variable binding energies.

2. Evaluation of Adsorbent Characteristics

- The BET isotherm helps determine specific surface area and micropore volume.
- The Dubinin-Radushkevich isotherm is used for analyzing adsorption energy and porous structure.

3. Identification of Adsorbate-Adsorbent Interactions

- A high K_L value in the Langmuir model indicates strong interactions.
- The Temkin model accounts for changes in adsorption heat, providing insights into interaction strength.

4. Determination of Adsorption Type (Physical vs. Chemical Adsorption)

- Physical adsorption (Van der Waals forces) is typically described by BET and Freundlich models.
- Chemical adsorption (covalent or ionic interactions) is better represented by the Langmuir or Dubinin-Radushkevich models.

Adsorption isotherm models are essential tools for analyzing adsorption mechanisms. The choice of models depends on system properties and research goals. Combining multiple models with additional calculations (such as kinetic equations and thermodynamic analysis) allows for a deeper understanding of adsorption processes.

However, these models have drawbacks, including their tendency to oversimplify adsorption processes by assuming ideal conditions that may not apply in real systems. They also rely on empirical parameter fitting rather than first-principles calculations and have limited predictive power since they do not capture molecular-scale interactions or structural changes during adsorption.

But in order to determine the interaction mechanisms researchers often use reverse approach by fitting the experimental data to several models and by statistical analysis (correlation coefficients and error function analysis) they choose the best fitting model and then get data about the mechanisms.

The authors [144] applied isotherm model fitting to analyze the adsorption of 2-chlorophenol (2-CP) onto CTAB-modified zeolite in a one-step process, identifying key adsorption parameters and mechanisms. Among the tested models (Langmuir, Freundlich, and Dubinin-Astakhov (DA)), the DA model provided the best fit (Adj-$r^2 \geq 0.995$, MWSE ≤ 0.00473), confirming a heterogeneous adsorption process. The energy parameter (E) remained stable across temperatures, indicating that CTAB conformation on zeolite was consistent.

The study revealed that adsorption was driven by hydrophobic partitioning and electrostatic interactions, where the loose CTAB bilayer enhanced adsorption by providing additional sites.

Zeta potential and TOC measurements confirmed that the one-step process resulted in a more efficient CTAB structure than the two-step process.

Additionally, pH-dependent adsorption showed maximum uptake at pH 3–6, declining at higher pH due to 2-CP deprotonation, reducing hydrophobic interactions with CTAB.

Overall, isotherm analysis confirmed that the one-step process significantly improved adsorption efficiency compared to the two-step method, making it a cost-effective approach for water treatment.

The study [148] investigates the adsorption of Pb^{2+} ions onto Algerian treated clay, evaluating the adsorption equilibrium and determining the best-fitting isotherm model. The authors applied a comprehensive set of adsorption isotherm models to experimental data, using both linear and non-linear regression methods to determine which model best described the adsorption mechanism.

The study employed two-parameter (Langmuir, Freundlich, Temkin, Elovich, Dubinin-Radushkevich), three-parameter (Langmuir-Freundlich, Redlich-Peterson, Sips, Fritz-Schlunder, Toth), four-parameter (Fritz-Schlunder, Baudu), and five-parameter (Fritz-Schlunder) models to fit the experimental equilibrium data. Freundlich and Redlich-Peterson models provided the best fit, indicating that adsorption occurred on a heterogeneous surface rather than through monolayer adsorption. The Langmuir model showed a poorer fit, suggesting that adsorption was not limited to uniform surface sites. Higher parameter models (Fritz-Schlunder with five parameters) gave the most accurate description of adsorption behavior.

The pseudo-second-order model best described the adsorption kinetics, indicating chemisorption as the dominant mechanism. The pseudo-first-order model had a poor fit, ruling out simple physisorption. Negative enthalpy (ΔH) confirmed an exothermic adsorption process. Negative Gibbs free energy (ΔG) indicated spontaneous adsorption. Negative entropy (ΔS) suggested a reduction in randomness, supporting a specific, chemical interaction between Pb^{2+} and treated clay.

By systematically testing multiple isotherm, kinetic, and thermodynamic models, the study confirmed that Pb^{2+} adsorption onto treated clay occurs on a heterogeneous surface through chemisorption, rather than simple monolayer physisorption. The Fritz-Schlunder five-parameter model provided the best description of equilibrium behavior, and pseudo-second-order kinetics confirmed a chemical adsorption mechanism. These findings highlight the effectiveness of treated clay for heavy metal removal and provide a scientific basis for optimizing adsorption conditions in water treatment applications.

Obtaining data on the adsorption mechanism by modeling experimental data is most often done by generalizing the conclusions obtained from fitting isotherm models, kinetic models and

thermodynamic calculations. Therefore, it is also necessary to consider the known kinetic models applied for adsorption processes, as well as the main thermodynamic parameters that should be calculated to obtain information on the adsorption mechanisms.

Adsorption kinetics describe the rate at which adsorbate molecules attach to the surface of adsorbents. Kinetic models used for adsorption processes are broadly classified into:

1. *Diffusion Kinetic Models* – focus on mass transport mechanisms governing adsorption.

2. *Reaction Kinetic Models* – describe the adsorption process as a reaction between the adsorbate and adsorbent surface.

The most frequently used Diffusion Kinetic Models are the Film Diffusion model, Intraparticle Diffusion Model (Weber-Morris Model), Chemisorption Diffusion Model and Boyd Model. Diffusion models describe how adsorbate molecules move from the bulk solution to the adsorption sites. These models help in determining the rate-limiting step of the adsorption process and understanding adsorption mechanisms through mass transport analysis. Reaction Kinetic Models describe adsorption as a chemical reaction occurring between the adsorbate and adsorbent. They help in identifying adsorption mechanisms, including physisorption and chemisorption. The most common Reaction Kinetic Models are Pseudo-First-Order and Pseudo-Second-Order Kinetic Models, Elovich and Avrami models also belong to the Reaction Kinetic Models group.

The main parameters for each model are provided in Table 2.

In adsorption processes, thermodynamic parameters are crucial for understanding the feasibility, spontaneity, and nature of adsorption. The most commonly calculated thermodynamic parameters include:

1. *Gibbs Free Energy Change (ΔG°)* determines whether the adsorption process is spontaneous. It helps in predicting whether adsorption will occur under given conditions.

2. *Enthalpy Change (ΔH°)* indicates the nature of adsorption (endothermic or exothermic). Distinguishes between physisorption (low ΔH°, typically <40 kJ/mol) and chemisorption (high ΔH°, typically >80 kJ/mol).

3. *Entropy Change (ΔS°)* reflects the degree of randomness at the solid-liquid interface. Provides insight into molecular interactions between adsorbate and adsorbent.

4. *Equilibrium Constant (K)* represents the degree of adsorption at equilibrium. Higher KK values indicate stronger adsorption affinity. Used in thermodynamic equations to calculate ΔG°, ΔH°, and ΔS°.

The equations for calculating thermodynamic parameters and tips for their interpretation are summarized in Table 3**.**

Table 2 – Summary table of adsorption kinetic models

Group	Model	Equation	Mechanism	Data Obtained	Advantages	Disadvantages
Diffusion	Film Diffusion	$\frac{dC_t}{dt} = K_f(C_t - C_s)$, where C_t -adsorbate concentration in solution at time t, C_s – adsorbate concentration at the solid surface, K_f – film diffusion coefficient	External mass transfer	Film diffusion coefficient K_f, resistance estimation	Identifies external diffusion	Ignores internal diffusion
	Intraparticle Diffusion	$q_t = k_{id}\sqrt{t} + C$, where q_t – amount adsorbed at time t, k_{id} – intraparticle diffusion rate constant, C – intercept indicating boundary layer effect	Pore diffusion	Intraparticle diffusion rate constant k_{id}, mechanism identification	Distinguishes multiple steps	Cannot separate resistances
	Boyd Model	$B_t = -0.4977 - \ln(1 - F)$, where B_t is the Boyd function, $F = \frac{q_t}{q_e}$ is the fractional attainment of equilibrium adsorption, q_e – equilibrium adsorption capacity (mg/g)	Film vs. pore diffusion	Diffusion mechanism	Identifies rate-limiting step	Needs equilibrium data
	Chemisorption Diffusion Model	$q_t = q_e\left(1 - e^{(-D_e t)}\right)$, where D_e – effective diffusion coefficient	Diffusion-limited chemisorption	Effective diffusion coefficient D_e, adsorption rate	Suitable for chemisorption with diffusion control	Assumes uniform diffusion behavior
Reaction	Pseudo-First-Order	$\ln(q_e - q_t) = lnq_e - k_1 t$, where k_1 – rate constant	Physisorption	Rate constant k_1, adsorption capacity q_e	Simple, widely used	Poor fit for chemisorption
	Pseudo-Second-Order	$\frac{t}{q_t} = \frac{1}{k_2 q_e^2} + \frac{t}{q_e}$, where k_2 – rate constant	Chemisorption	Rate constant k_2, adsorption rate	Good for chemisorption	Assumes uniform adsorption energy
	Elovich	$\frac{dq_t}{dt} = \alpha e^{-\beta q_t}$, where α– initial adsorption rate, β – desorption constant	Surface heterogeneity	α, β parameters	Describes heterogeneous surfaces	Cannot predict equilibrium
	Avrami	$\frac{dq_t}{dt} = \alpha e^{-kt^n}$, Where n – Avrami exponent describing adsorption mechanism	Complex adsorption	k, n parameters	Useful for complex kinetics	Empirical limitations

Table 3 – Main thermodynamic parameters calculated for adsorption processes

Parameter	Equation	Interpretation	Significance
Gibbs Free Energy (ΔG°)	$\Delta G^0 = -RTlnK$, where ΔG^0 is the Gibbs free energy, R = universal gas constant (8.314 J/mol*K), T = temperature (K), K = equilibrium constant	ΔG° < 0: spontaneous, ΔG° > 0: non-spontaneous, ΔG° = 0 : equlibrium	Predicts feasibility of adsorption
Enthalpy Change (ΔH°)	$lnK = -\frac{\Delta H^0}{R}\left(\frac{1}{T}\right) + \frac{\Delta S^0}{R}$, where ΔH^0 is the enthalpy change, ΔS^0 is the entropy	ΔH° < 0: exothermic, ΔH° > 0: endothermic	Differentiates physisorption (ΔH°<40 kJ/mol) & chemisorption (ΔH°>80 kJ/mol)
Entropy Change (ΔS°)	$\Delta S^0 = \frac{\Delta H^0 - \Delta G^0}{T}$	ΔS° > 0: increased randomness, ΔS° < 0: decreased randomness	Describes system disorder. Often increased randomness can verify active ion-exchange processes, and decreased randomness verifies chemisorption.
Equilibrium Constant (K)	$K = \frac{q_e}{C_e}$, where q_e = adsorption capacity at equilibrium (mg/g), C_e = equilibrium concentration in solution (mg/L)	Higher K: stronger adsorption affinity	Required for thermodynamic calculations

These thermodynamic parameters provide comprehensive insight into the adsorption mechanism, spontaneity, and energy changes involved in the process.

The authors [29] conducted isotherm, kinetic, and thermodynamic studies to understand the adsorption mechanisms of Bisphenol A (BPA) onto surfactant-modified natural zeolite. Isotherm studies demonstrated how BPA molecules interact with the adsorbent surface at equilibrium. Several models were considered. The Langmuir isotherm, which assumes monolayer adsorption on a homogeneous surface, did not fit the experimental data well ($R^2 = 0.087$). The Freundlich isotherm, which accounts for adsorption on heterogeneous surfaces with varying energies, showed a better correlation ($R^2 = 0.8543$), indicating a multilayer adsorption process. The Dubinin–Radushkevich (D–R) model helped determine the nature of adsorption, revealing a mean adsorption energy of -0.226 kJ/mol, suggesting that physisorption was the dominant mechanism. The Temkin isotherm, which considers adsorbate–adsorbent interactions, provided the best correlation ($R^2 = 0.9571$), indicating that interactions between BPA and the adsorbent played a significant role in the adsorption process.

Kinetic studies helped determine the adsorption rate and mechanism. The pseudo-first-order model showed poor correlation ($R^2 = 0.123$), meaning it did not accurately describe the process. However, the pseudo-second-order model exhibited a strong fit ($R^2 = 0.9826$), indicating that chemisorption, involving electron sharing or exchange, was the primary mechanism. The high

correlation coefficient suggests that adsorption was predominantly influenced by chemical interactions rather than simple diffusion.

Thermodynamic analysis was performed to evaluate the feasibility and spontaneity of the adsorption process by calculating key parameters (ΔH°, ΔS°, and ΔG°). The enthalpy change (ΔH°) was negative (-183.39 J/mol), confirming that the adsorption process was exothermic, meaning it is more favorable at lower temperatures. The free energy change (ΔG°) values ranged from 513 to 2805 J/mol, indicating that adsorption was non-spontaneous under the studied conditions, requiring external influence. The entropy change (ΔS°) was negative (-11.08 J/mol·K), suggesting a decrease in randomness at the solid–liquid interface, meaning BPA molecules formed an organized layer on the adsorbent surface.

Thus, the Temkin isotherm best describes the adsorption process, highlighting significant interactions between BPA and the adsorbent. The pseudo-second-order model indicates that chemisorption played a key role in controlling the adsorption rate. Thermodynamic calculations showed that the process was exothermic and non-spontaneous under the experimental conditions. The D–R isotherm and adsorption energy values confirmed that physisorption was the dominant mechanism, with weak van der Waals forces playing a role.

Overall, the study suggests that both physical and chemical adsorption contribute to BPA removal, with physisorption being the predominant process. The adsorption efficiency can be improved by optimizing factors such as temperature and adsorbent dosage.

The study [149] used isotherm models, kinetics, and thermodynamics to analyze Cr(VI) adsorption on surfactant-modified activated carbon. The Langmuir isotherm ($R^2 > 0.99$) indicated monolayer adsorption, while the D–R isotherm confirmed physisorption ($E < 8$ kJ/mol). Pseudo-second-order kinetics ($R^2 > 0.99$) suggested chemisorption involvement. Thermodynamic analysis showed an endothermic and spontaneous process, favoring adsorption at higher temperatures. Overall, physisorption dominated, with electrostatic interactions playing a key role. Optimizing surfactant modification and temperature could improve Cr(VI) removal.

The study [150] applied isotherm models, kinetic analysis, and thermodynamic calculations to examine Pb(II) adsorption on natural and pretreated clinoptilolite. The Temkin isotherm best described the adsorption process, while three-parameter models like Sips and Toth provided the most accurate fit. The Dubinin–Radushkevich isotherm indicated ion-exchange as the primary mechanism ($E \approx 9$ kJ/mol). Kinetic analysis showed that the pseudo-first-order model best-described adsorption, while the pseudo-second-order model also provided a good fit. Thermodynamic calculations revealed negative Gibbs free energy (ΔG°) values, confirming a spontaneous adsorption process. The study concluded that clinoptilolite is an effective and low-cost adsorbent for Pb(II) removal.

The study [151] applied isotherm, kinetic, and thermodynamic analyses to investigate Pb(II) adsorption onto kaolinite and montmorillonite, including their acid-activated forms. Langmuir and Freundlich isotherms were used to model adsorption, with Langmuir indicating monolayer adsorption and Freundlich suggesting heterogeneous surface interactions. Pseudo-second-order kinetics provided the best fit, indicating chemisorption as the dominant mechanism.

The thermodynamic analysis in the study evaluated the feasibility and spontaneity of Pb(II) adsorption on kaolinite and montmorillonite, including their acid-activated forms, by calculating enthalpy change (ΔH°), entropy change (ΔS°), and Gibbs free energy change (ΔG°). The negative ΔH° values (-58.9 to -83.4 kJ/mol) confirmed that the adsorption process was exothermic, meaning Pb(II) adsorption was more favorable at lower temperatures. The negative ΔS° values (-116.4 to -258.7 J/mol·K) indicated a decrease in randomness at the solid–liquid interface, suggesting that Pb(II) ions formed a more stable, organized layer on the adsorbent. The negative ΔG° values (-35.8 to -79.6 kJ/mol) confirmed that the adsorption process was spontaneous under the studied conditions, though spontaneity decreased slightly with increasing temperature, aligning with the exothermic nature of the process. These findings suggest that Pb(II) adsorption was thermodynamically favorable, with acid activation enhancing adsorption strength, particularly for montmorillonite.

The study [152] applied adsorption isotherms, kinetic models, and thermodynamic calculations to investigate the removal of hexavalent chromium (Cr(VI)) using a chitosan/bentonite composite. Isotherm models, including Redlich–Peterson, best described the adsorption equilibrium, indicating a multilayer adsorption process. Kinetic studies showed that the Elovich model provided the best fit, suggesting that chemisorption dominated the adsorption mechanism. Thermodynamic analysis revealed a spontaneous (negative ΔG°) and exothermic (negative ΔH°) process, with entropy values suggesting a decrease in randomness at the solid-liquid interface. These results confirmed that Cr(VI) adsorption on the chitosan/bentonite composite primarily involved chemical interactions, making it a cost-effective adsorbent for wastewater treatment.

Adsorption isotherms, kinetic models, and thermodynamic calculations are essential tools for understanding adsorption mechanisms, evaluating adsorbent efficiency, and optimizing adsorption processes. Isotherm models help determine adsorption capacity, surface characteristics, and interaction types, distinguishing between monolayer and multilayer adsorption. Kinetic studies reveal the rate-controlling mechanisms, with pseudo-second-order kinetics often indicating chemisorption. Thermodynamic parameters, including Gibbs free energy (ΔG°), enthalpy (ΔH°), and entropy (ΔS°), provide insights into spontaneity, heat effects, and molecular organization of adsorption. The reviewed studies demonstrate that adsorption mechanisms are complex and

influenced by factors such as surface heterogeneity, electrostatic interactions, and chemical bonding. By combining multiple theoretical models with experimental data, researchers can achieve a deeper understanding of adsorption processes and enhance the efficiency of adsorbent materials for environmental and industrial applications.

Upon examining the literature, it is evident that the majority of studies on adsorption systems conventionally employ a minimum set of experimental data modeling, which includes the Langmuir and Freundlich isotherms, pseudo-first and pseudo-second order kinetic models, and the calculation of Kd, ΔG, ΔH, and ΔS for adsorption. Other models are employed in more narrowly specialized research targeted at exploring either the usage of adsorption isotherms or kinetics. Nonetheless, I would like to emphasize significant variations in the use of the modeling methodologies, which were identified in recent studies following a literature study.

A noteworthy conclusion from the study [148] is that the application of nonlinear isothermal equations in modern conditions, facilitated by various computational programs, markedly enhances the correctness of the results produced. Numerous published studies employ linear equations, raising concerns about the validity of the conclusions produced.

Simonin et al. [153] discovered that several published studies employed experimental data around the equilibrium phase when utilizing reaction kinetic models. In such instances, the pseudo-second order model typically demonstrates a favorable match; hence, the findings drawn in numerous published studies may be questionable.

The standard equation for calculating the equilibrium constant of adsorption processes is as follows:

$$K = \frac{q_e}{C_e}, \tag{6}$$

where q_e = adsorption capacity at equilibrium (mg/g), C_e = equilibrium concentration in solution (mg/L).

In the review [154] it is established that the adsorption equilibrium constant determined according to (*6*) has no physical meaning. Utilizing the equilibrium constant derived from the most appropriate adsorption isotherm model, such as the Langmuir constant (K_L), is advisable. The computation of the remaining thermodynamic parameters, including ΔG, ΔH, and ΔS, relies on the determination of the equilibrium constant, hence raising concerns over the validity of those reported in numerous published studies.

Thus, the determination of adsorption mechanisms is a rather complex and labor-intensive process, which includes the use of various methods and approaches, and also gives rise to many questions and contradictions. Analysis of the literature from the previous five years in adsorption processes reveals an increased focus on adsorption mechanisms and the methodologies for their

assessment. Therefore, obtaining data on adsorption mechanisms for new sorbent-pollutant systems and developing new approaches and methods for their determination is a very urgent task.

Conclusions of the literature review:

The literature review highlights the significant role of aluminosilicate-based sorbents, particularly zeolites and clay minerals, in the removal of various contaminants from aqueous solutions. These materials exhibit unique structural and physicochemical properties, including high surface area, microporosity, and ion-exchange capacity, which make them effective in adsorbing heavy metals, organic pollutants, and radio nuclides.

Zeolites, characterized by their crystalline aluminosilicate frameworks, offer exceptional adsorption capabilities due to their well-defined pore structures and high cation-exchange capacities. Their natural abundance and chemical stability further enhance their suitability for water treatment applications. Moreover, modifications such as acid treatment, surfactant modification, and metal impregnation significantly improve their selectivity and adsorption efficiency. Studies have demonstrated that natural and modified zeolites effectively remove heavy metal ions (Pb, Cd, Cr, etc.), organic dyes, and even radioactive contaminants like Sr-90 and Cs-137.

Similarly, clay minerals, including montmorillonite, bentonite, and kaolinite, have been widely explored for their adsorption potential. Their layered structures allow for effective pollutant binding through cation exchange, intercalation, and surface adsorption mechanisms. Modified clay materials, particularly organo-clays, exhibit enhanced adsorption of organic and inorganic contaminants by improving hydrophobicity and introducing functional groups. These modifications enable clays to capture pollutants such as pharmaceuticals, dyes, and oxyanions with greater efficiency.

Understanding the adsorption mechanisms is crucial for optimizing the design and application of aluminosilicate-based sorbents. Various instrumental techniques, including FTIR, XRD, SEM, BET analysis, and zeta potential measurements, provide insights into the physicochemical changes occurring during adsorption. Additionally, kinetic and thermodynamic modeling helps elucidate adsorption pathways, distinguishing between physisorption and chemisorption processes.

The continued development of aluminosilicate-based sorbents offers promising avenues for improving environmental remediation strategies. Future research should focus on refining modification techniques, exploring multifunctional composite materials, and scaling up applications for industrial wastewater treatment. By advancing these materials and their adsorption mechanisms, sustainable and cost-effective solutions for water purification and pollution mitigation can be achieved.

Given the increasing environmental challenges and the need for more efficient and selective sorbents, the development of novel aluminosilicate-based materials modified with surfactants is of great relevance. These hybrid systems can significantly enhance adsorption efficiency by introducing tailored functional groups, optimizing pore structures, and improving interactions with target pollutants. Detailed investigations into the physicochemical properties and adsorption mechanisms of these novel materials are essential to fully understand their potential and to establish effective strategies for their large-scale implementation in water purification technologies.

2. EXPERIMENTAL PART

2.1 Reagents and Materials

Natural zeolite originated from Shankanai deposit (Almaty region) and Chamotte clay purchased from Teplosvet Engineering LLC (Ukraine) were chosen as the objects of this study.

Three series of adsorbents based on the chosen objects were obtained (Figure 6):

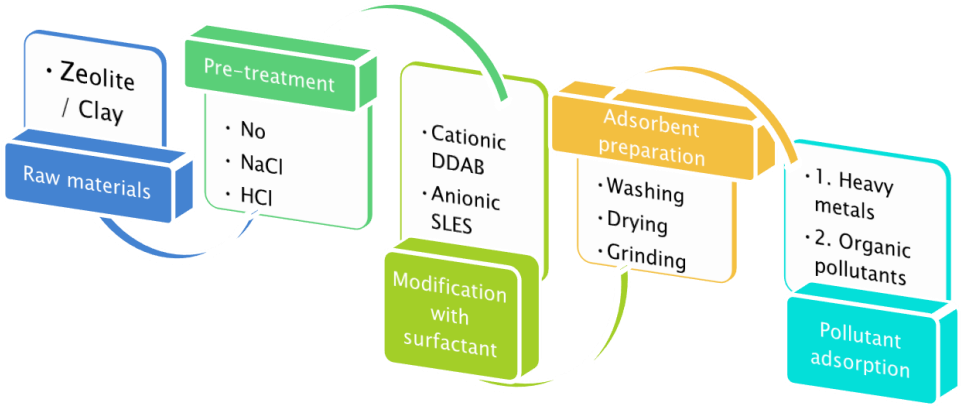


Figure 6 – Adsorbents synthesis procedure

The initial series comprises sorbents derived from zeolite/clay, modified with varying quantities of surfactants: cationic didodecyl dimethyl ammonium bromide (DDAB) or anionic sodium laureth sulfate (SLES).

The second series comprise zeolite/clay-based sorbents that have been pre-treated with a 1 mol/L NaCl solution and subsequently modified with surfactants.

The third series comprise zeolite/clay-based sorbents that have undergone acid activation with hydrochloric acid at three distinct concentrations (1 mol/L, 3 mol/L, 6 mol/L), then followed by surfactant treatment.

The modified materials were then prepared for adsorption and used to extract two types of contaminants – heavy metal (HM) ions and organic contaminants (*Figure 6*). A more detailed description for preparing composite materials is presented in Section 2.2 of this dissertation.

One of the modifiers for creating sorbents is DDAB, the structure of which is shown in Figure 7. This is a two-chain cationic surfactant with molecular parameters presented in Table 4.

The main parameter that allows us to provide information about the shape and geometry of the surfactant is the packing parameter P (7) [155]:

$$P = \frac{V_c}{A_0 l_c} \quad (7)$$

где V_c is the volume of the surfactant chain,

A_0 is the area of the head group,

l_c is the length of the alkyl chain.

DDAB has a packing parameter of 0.620 and therefore forms flat (or lamellar) structures at concentrations above the CMC [155].

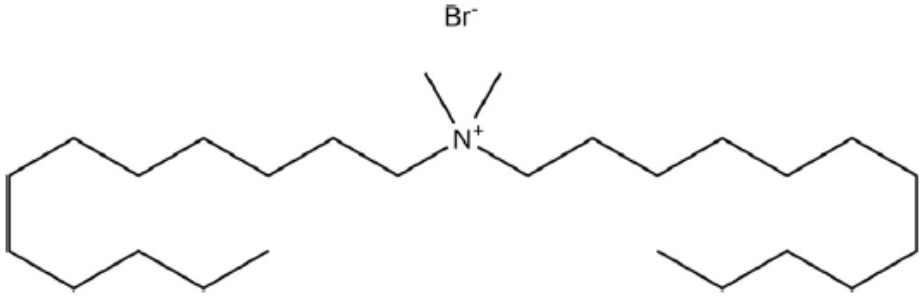


Figure 7 – Molecular structure of DDAB [155]

Table 4– Molecular parameters of DDAB [155]

Parameter	Value
l_c (Å)[a]	16,68
A_0 (Å^2)[b]	68,00
V_c (Å^3)[c]	703,70
P	0,62

[a] The length of the alkyl chain is calculated using the Tanford formula $l_c = 1.50 + 1.265$ (number of carbon atoms)

[b] The area of the head group is calculated based on the aggregation numbers of a single-chain surfactant, assuming the formation of spherical micelles

[c] The volume of the surfactant chain is obtained using the Gruen equation $V_c = 54.30$(number of CH_3) + 27,05 (number of CH_2).

The anionic surfactant sodium laureth sulfate (SLES), which is used to produce most household and technical detergents, was chosen as the second modifier. SLES is an ethoxylated form of sodium lauryl sulfate – sodium lauryl sulfate (SLS). The chemical formula of sodium laureth sulfate is shown in Figure 8 [156].

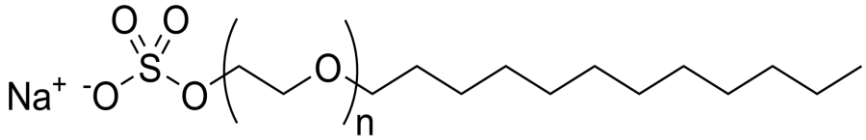


Figure 8 – Chemical structure of SLES [156]

SLES is often used in the production of detergents and personal hygiene products such as shampoo, shower gels, etc. It is milder than SLS, more biodegradable, and has lower CMC and higher surface tension [157].

Thus, the following chemicals and materials were used in this study. All reagents were purchased from LLP "Laborpharma" (ТОО «Лаборфарма) (Kazakhstan). The reagents were supplied by JSC "Khimreaktiv" (АО «Химреактив) (Russia) Merck (Germany), Sigma-Aldrich (USA), and LK (NANJING) CO, LTS (China).

1) Materials and Reagents used for Sorbent Synthesis

- Natural zeolite from the Shankanai deposit (Kazakhstan) purchased from LLP "TazaSu";
- Chamotte clay (supplier — LLP "Teplosvet Engineering", Kazakhstan);
- Sodium chloride (NaCl), 99.9%, pure grade (GOST 4233-77), manufacturer — JSC "Khimreaktiv" (Russia);
- Hydrochloric acid (HCl), 35–38%, pure grade (GOST 3118-77), manufacturer — JSC "Khimreaktiv" (Russia);
- Silver nitrate ($AgNO_3$), pure grade (GOST 1277-75), manufacturer — JSC "Khimreaktiv" (Russia);
- Sodium laureth sulfate (SLES), 70%, industrial grade (Texapon type), manufacturer — LK (NANJING) CO., LTD (China), CAS No. 68585-34-2 / 68891-38-3;
- Didodecyldimethylammonium bromide (DDAB), 98%, manufacturer — Merck (Germany), CAS No. 3282-73-3.

2) Reagents used for Sorbent Characterization

The following reagents were used for pH measurements, point of zero charge (PZC), and cation exchange capacity (CEC) determination, as well as for DDAB amount in adsorbents determination:

- Nitric acid (HNO_3), 65%, pure grade (GOST 4461-77), manufacturer — JSC "Khimreaktiv" (Russia);
- Sodium hydroxide (NaOH), pure grade (GOST 4328-77), manufacturer — JSC "Khimreaktiv" (Russia);

- Sodium nitrate ($NaNO_3$), pure grade (GOST 4168-79), manufacturer — JSC "Khimreaktiv" (Russia);

- Ammonium chloride (NH_4Cl), pure grade (GOST 3773-72), manufacturer — JSC "Khimreaktiv" (Russia);

- Sodium carbonate (Na_2CO_3), pure grade (GOST 83-79), manufacturer — JSC "Khimreaktiv" (Russia);

- Bromothymol blue (indicator), analytical grade, TU 6-09-5421-90, manufacturer — JSC "Khimreaktiv" (Russia).

3) Reagents used for Adsorption Studies

The following heavy metal salts and organic compounds were used as model pollutants:

- Lead nitrate ($Pb(NO_3)_2$), pure grade (GOST 4236-77), manufacturer — JSC "Khimreaktiv" (Russia);

- Cadmium chloride ($CdCl_2 \cdot 2H_2O$), pure grade (GOST 4330-76), manufacturer — JSC "Khimreaktiv" (Russia);

- Strontium chloride ($SrCl_2 \cdot 6H_2O$), pure grade (GOST 4140-74), manufacturer — JSC "Khimreaktiv" (Russia);

- Potassium permanganate ($KMnO_4$), pure grade (GOST 20490-75), manufacturer — JSC "Khimreaktiv" (Russia);

- Potassium dichromate ($K_2Cr_2O_7$), pure grade (GOST 4220-75), manufacturer — JSC "Khimreaktiv" (Russia);

- Propranolol hydrochloride, pharmaceutical grade, manufacturer — Sigma-Aldrich (USA), CAS No. 318-98-9;

- Bisphenol A, ≥99%, manufacturer — Sigma-Aldrich (USA), CAS No. 80-05-7.

2.2 Aluminosilicate raw materials modification methods

Zeolite/clay sample was grinded in a porcelain mortar to obtain the homogeneous powder, sieved down to less than 100 μm, rinsed with deionized water to remove dust and dried in an oven at 100 °C for 24 h. Before modification with surfactant (DDAB or SLES) the sample was pre-treated with NaCl or HCl solutions.

NaCl-treatment procedure: 10 g of cleaned and dried zeolite/clay was mixed with 1 mol/L NaCl solution at a solid-liquid ratio of 1:10 and stirred for 12 h at 250 rpm and at room temperature. The supernatant was separated by vacuum filtration and solids were washed with room temperature deionized water until negative reaction to Cl^-. $AgNO_3$ was used as an indicator of Cl^- presence. A negative reaction to Cl^- was achieved by a 3-stage washing at s:l = 1:3. The washing waters were reused to prepare a 1 M NaCl solution for subsequent portions of sorbents. The solids

were dried in an oven at 100 °C for 24 h, mixed thoroughly and are denoted as Na-zeolite/ Na-clay.

HCl-treatment procedure: 10 g of cleaned and dried zeolite/clay was mixed with HCl solutions of concentrations 1, 3 or 6 mol/L at a solid-liquid ratio of 1:10 and stirred for 2 h at 250 rpm in an oil bath at 100 ºC. The solids were separated by vacuum filtration and rinsed with deionized water until permanent pH. Constant pH values of 5.6 were achieved by a 3-stage washing with water at s:l = 1:3. The washing waters were reused to prepare acid solutions for the synthesis of subsequent portions of sorbents. Then solids were dried in an oven at 100 °C for 24 h, mixed thoroughly and denoted as 1M H-zeolite, 3M H-zeolite and 6M H-zeolite for zeolite samples, and as 1M H-clay, 3 M H-clay and 6M H-clay, depending on the concentration of the acid used.

Initial or pre-treated zeolite/clay was modified with didodecyldimethylammonium bromide (DDAB) / sodium laureth sulfate solution (SLES), the CMC (critical micelle concentration) of DDAB is 0.1 mmol/L [158], and CMC of SLES is 0.5 mmol/L [157].

Procedure: 10 g of initial or pre-treated zeolite/clay was mixed with 200 mL 0.5 – 10 CMC surfactant solutions of concentrations. The mixture was stirred for 24 h at 250 rpm and at room temperature. The solids were separated from supernatants and then washed with deionized water until a negative reaction to the surfactant traces. Bromine traces were detected with $AgNO_3$, and DDAB were detected with UV–visible spectrometer to avoid leaching into the environment.

A negative reaction to bromides was achieved by a 3-stage washing at s:l = 1:3. The washing waters were reused to prepare surfactant solutions for subsequent portions of sorbents. The solids were dried at 60-70 ºC for 24 h. The amounts of non-adsorbed DDAB were measured using the Adsorption-Spectrophotometric method of cationic surfactant detection introduced by [159] to quantify its content in the adsorbents. The method is based on pre-concentration of the surfactant on silica-gel and then its interaction with the indicator – bromothymol blue dye, the UV-VIS absorbance peaks are measured by the excess dye. The amounts of non-adsorbed SLES were measured by the Du Nuy ring method [160] at the gas/liquid interface using ST-1 (CT-1) power tensiometer.

The above-described method for obtaining all three series of sorbents is shown in detail in the basic process flow diagrams shown in Fig. A1 (for pre-treatment stage) and Fig. A2 (for modification stage) in Appendix A.

2.3 Characterization of the adsorbent materials obtained

A high-resolution scanning electron microscope (FEI Magellan 400, USA) was used to study the morphology of the obtained materials. Elemental analysis was performed using the same equipment by energy dispersive X-ray spectroscopy (EDAX). The average particle size was determined by SEM-microphotographs using an image processing package Fiji of ImageJ software. X-ray diffractometry patterns of the samples were investigated in the two-theta range 10–80° at a step size of 0.05 using a Bruker D8 Advance diffractometer with Cu-Ka source at 40 kV and 40 mA.

FTIR spectra were obtained by a Perkin Elmer Spectrum 65 spectrometer using the KBr method in the IR region of 4000–400 cm^{-1} at 4 cm^{-1} resolution. Raman spectra were obtained by a Solver Spectrum atomic force microscope and a Raman spectrometer in the 3200–100 cm^{-1} region at 4 cm^{-1} resolution.

The specific surface area and pore volume were determined with a Quantachrome Nova 4200e device by nitrogen sorption to its relative pressure of 0.2 atm at -196°C.

The cation-exchange capacity (CEC) was determined by standard NH_4Cl method [16]. 1 g of sample was mixed with 100 mL of 1 M NH_4Cl solution. Suspensions were left for 24 h with periodic shaking and centrifuged, and concentrations of Ca^{2+}, Mg^{2+}, Na^{+} and K^{+} were determined using an atomic absorption spectrometer (Shimadzu 6200, Japan). The CEC was calculated by taking the sum of the concentrations of the released cations and expressed in meq/100 g using the following equation (8):

$$M_{meq/100g} = C_{ppm} / (eq.wt. \times 10) \quad (8)$$

where $M_{meq/100g}$ is the concentration of released cation in meq/100 g, C_{ppm} is the concentration of released cation in mg/L, and eq.wt. is the equivalent weight of released cation – the atomic mass multiplied by its equivalence factor.

The points of zero charge (PZC) were determined using salt addition method [161]. In a series of 50-ml centrifuge tubes, 0.2 g of sample was added to 40.0 ml of 0.1 M $NaNO_3$ solution. The pH was adjusted with 0.1 M HCl and 0.1 M NaOH as needed, to obtain the appropriate pH range of 2, 3, 4, 5, 6, 7, 8, 9, 10, and 11 (± 0.1 pH units). The pH values of the supernatant in each tube were denoted as pH_i. The samples were shaken for 24 h using a lab shaker (PE-6500 Series, Ecros, Russia) at 200 vibrations per minute. After settling, the pH values of the supernatant in each tube were measured and denoted as pH_f. The PZC was obtained from the plot of ΔpH ($=pH_f - pH_i$) against pH_i. Each set of experiments was performed in triplicate and the mean value was recorded.

ζ-potentials of the samples were determined using Malvern Zetasizer NanoZS 90 (Great Britain) device. 0.5 g of z of c were mixed with 50 mL of deionized water for 3 h and then left for

24 h to obtain stable colloid solution. The top turbid part of the solutions (7-10 mL) was analyzed at natural pHs.

2.4 Adsorption experiments of studied pollutants (HM ions, BPA and PRO) onto adsorbents based on Zeolite and Clay

The following equations (9)-(10) were used for all studied systems:

$$E = \frac{C_0 - C_{eq}}{C_0} \times 100\% \quad (9)$$

$$q_e = (C_0 - C_e)*V / m \quad (10)$$

where E is the extraction degree (%), q_e is the amount of adsorbed compound (mg-g), C_0 and C_{eq} are the initial and equilibrium concentrations, respectively (mg/L), V is the volume of solution (L), m is the mass of adsorbent (g).

2.4.1 Adsorption experiments of studied HM ions (Pb^{2+}, Cd^{2+}, Sr^{2+}) onto adsorbents based on Zeolite and Clay

The adsorption of Pb^{2+}, Cd^{2+}, Sr^{2+} on zeolite/clay under ambient conditions was performed by the batch technique.

A weighed amount of sorbent was mixed with $Pb(NO_3)_2$, $Cd(NO_3)_2$, $Sr(NO_3)_2$, $K_2Cr_2O_7$, and $KMnO_4$ solutions of different concentrations (5, 10, 20, 50, 100, 200, 500 mg/L) and mixed for 24 hours using magnetic stirrers at 200 r.p.m. Then the suspensions were centrifuged at 6000 r.p.m and the supernatant was separated for analysis.

The system's pH values were maintained by adding required quantities of HNO_3 or NaOH.

To control the change of concentration in time (kinetics study), aliquots were taken at certain time intervals during the process. To study thermodynamic parameters the adsorption was performed at temperature range 15 - 45 ˚C. All experiments were repeated in triplicate and mean values are taken.

The initial, current and equilibrium concentrations of Pb^{2+}, Cd^{2+}, Sr^{2+} were determined using Atomic Absorption Spectrometer Shimadzu 6200, Japan. The concentrations of MnO_4^- and $Cr_2O_7^{2-}$ were determined using UV-VIS spectrophotometer SPEKOL 1300, Analytic Jena, Germany.

2.4.2 Adsorption experiments of studied organic pollutants (BPA and PRO) onto adsorbents based on Zeolite and Clay

Adsorption experiments were performed in static mode at room temperature and pH=6.1 for PRO and pH=6.8 for BPA (natural pH of the aqueous solutions without any adjustments), pKa values are 9.45 [162] and 9.6 [163] for PRO and BPA respectively.

A weighed amounts of sorbent were mixed with 10 mL of 10-150 mg/L solutions of BPA or PRO in 15 mL centrifuge tubes and mixed for 24 hours using magnetic stirrers at 200 rpm. The suspensions were centrifuged at 6000 rpm, and 5 mL of supernatant were separated for analysis. Concentrations were determined using a Cary 100 Bio UV-VIS spectrophotometer (Agilent Technologies, USA) at maximum adsorption wavelengths of 273 nm for BPA and 289 nm for PRO.

The % of ionization of BPA and PRO are calculated using the modified Henderson-Hasselbalch equation (11) [164]:

$$\%\ ionization = \frac{[A^-]}{[HA]+[A^-]}100 = \frac{100}{1+10^{(pKa-pH)}} \quad (11)$$

2.5 Methods of modeling and statistical processing of adsorption results

2.5.1 Adsorption isotherm theories

When describing the sorption process, adsorption models of sorption isotherms are of great importance. They show how metal ions are distributed between the adsorbent and the liquid phase when they are in equilibrium depending on the concentration (adsorbent/adsorbate).

In recent decades, linear regression has been one of the most viable tools defining the best fitting relationship quantifying the distribution of adsorbates, mathematically analyzing the adsorption systems [165]. Lately, the development of computer technologies allows using non-linear isotherm modeling, which involves the minimization or maximization of error distribution between the experimental data and predicted isotherm.

In the present work, adsorption isotherms were calculated according to the most popular in literature theories. The list of used isotherm models with the equations is in Table 5.

Non-linear equations of isotherm models, as well as the error function analysis were fit to the experimental results using Python 3.

Table 5 – List of used isotherm models

Theory	Linear equation	Non-linear equation	Plot	Reference
Two-parameter models				
Langmuir	$\frac{C_e}{q_e} = \frac{1}{K_L \cdot q_m} + \frac{1}{q_m} C_e$	$q_e = \frac{q_{mL} \cdot K_L \cdot C_e}{1 + K_L \cdot C_e}$	$\frac{C_e}{q_e}\ vs\ C_e$	[166]
Freundlich	$lnq_e = lnK_F + \frac{1}{n} lnC_e$	$q_e = K_F \cdot C_e^{\frac{1}{n}}$	$lnq_e\ vs\ lnC_e$	[167]
Temkin	$q_e = \frac{RT}{B_T} lnK_T + \frac{RT}{B_T} lnC_e$	$q_e = \frac{RT}{B_T} lnK_T C_e$	$q_e\ vs\ lnC_e$	[168]

Table 5 (continued)				
Dubinin-Radushkevich	$lnq_e = lnq_{mDR} - K_{DR}\varepsilon^2$ $\varepsilon = RTln(1+\frac{1}{C_e})$	$q_e = q_{mDR}e^{-K_{DR}\varepsilon^2}$ $\varepsilon = RTln(1+\frac{1}{C_e})$	$lnq_e\ vs\ \varepsilon^2$	[169]
Three-parameter models				
Langmuir-Freundlich	$\frac{q_{mLF}}{q_e} = 1+\frac{1}{(K_{LF}C_e)^\beta}$	$q_e = \frac{q_{mLF}(K_{LF}C_e)^\beta}{1+(K_{LF}C_e)^\beta}$	$\frac{q_{mLF}}{q_e}\ vs\ \frac{1}{C^\beta}$	[170]
Redlich-Peterson	$\frac{C_e}{q_e} = \frac{1}{A}+\frac{B}{A}C_e^\beta$	$q_e = \frac{AC_e}{1+BC_e^\beta}$	$\frac{C_e}{q_e}\ vs\ C_e^\beta$	[171]
Sips	$\frac{q_{mS}}{q_e} = 1+\frac{1}{K_S C_e^\beta}$	$q_e = \frac{q_{mS}K_S C_e^\beta}{1+K_s C_e^\beta}$	$\frac{q_{mS}}{q_e}\ vs\ \frac{1}{C_\beta}$	[172]
Fritz-Schlunder	$\frac{C_e}{q_e} = \frac{1}{K_{FS}q_{mFS}}+\frac{1}{q_{mFS}}C_e^\alpha$	$q_e = \frac{q_{mFS}K_{FS}C_e}{1+K_{FS}C_e^\alpha}$	$\frac{C_e}{q_e}\ vs\ C_e^\alpha$	[173]
Toth	$\left(\frac{C_e}{q_e}\right)^\alpha = \left(\frac{1}{K_T^{\left(\frac{1}{\alpha}\right)}q_{mT}}\right) + \left(\frac{1}{q_{mT}}\right)^\alpha C_e^\alpha$	$q_e = \frac{q_{mT}C_e}{(1/K_T+C_e^\alpha)^{1/\alpha}}$	$\left(\frac{C_e}{q_e}\right)^\alpha\ vs\ C_e^\alpha$	[174]
Four-parameter models				
Fritz-Schlunder	-	$q_e = \frac{AC_e^\alpha}{1+BC_e^\beta}$	-	[173]
Baudu	-	$q_e = \frac{q_{m0}b_0C_e^{(1+x+y)}}{1+b_0C_e^{(1+x)}}$ $b = b_0C_e^x$ $q_{mL} = q_{m0}C_e^y$	-	[175]
Five-parameter model				
Fritz-Schlunder	-	$q_e = \frac{q_{mFS}K_{1FS}C_e^{m1}}{1+K_{2FS}C_e^{m2}}$	-	[173]

Two-parameter isotherm models

The Langmuir model is based on the fact that a monomolecular adsorbate layer is formed on the surface of the studied materials, and all active centers have equal energy and enthalpy [166]. q_e is the amount adsorbed on solid at equilibrium (mg/g), C_e is the equilibrium liquid concentration (mg/L), q_m is the adsorption capacity or maximum adsorption (mg/g), K_L is the adsorption intensity or Langmuir coefficient (L/mg).

Freundlich isotherm [167] is the earliest known experimental equation describing the sorption of material onto animal charcoal. This isotherm could be applied to non-ideal sorption on heterogeneous surfaces as well as multi-layer sorption. q_e is the solute adsorbed (mg/g), C_e is the solute concentration at equilibrium (mg/L); $K_F$is the Freundlich constant, n is the equilibrium constant.

Temkin isotherm assumes that the heat of adsorption of all molecules in the layer could decrease linearly with coverage, i.e. that the adsorption is characterized by a uniform distribution in the binding energies, up to some maximum binding energy [168]. B_T is related to the heat of adsorption (J/mol), R is the gas constant (8.314 J/mol*K), T is the absolute temperature (K) and K_T is the Temkin equilibrium constant corresponding to the maximum binding energy (L/g).

Dubinin-Radushkevich isotherm [169] is an empirical model, which generally applies to express the adsorption mechanism with a Gaussian energy distribution onto a heterogeneous surface. It characterizes an imperative parameter to be specific mean free energy which is utilized to differentiate the physical and chemical adsorption [170]. q_{mDR} (mg/g) is the capacity of saturation theory (mg/g), K_{DR} (mol^2/kJ) is the constant of adsorption energy and ε is the Polanyi potential.

Three-parameter isotherm models

The Langmuir-Freundlich isotherm model is a three-parameter model, where the parameters are defined as follows: q_e is the adsorbed amount at equilibrium (mg/g), q_{mLF} is the Langmuir-Freundlich maximum adsorption capacity (mg/g), C_e is the adsorbate equilibrium concentration (mg/L), K_{LF} is the equilibrium constant for a heterogeneous solid, and β is the heterogeneity parameter that lies between 0 and 1 [170].

The elements from both Langmuir and Freundlich models are combined in the Redlich-Peterson [171] empirical isotherm model. According to this model the mechanism of adsorption is hybrid and does mot follow ideal monolayer adsorption. The equation of Redlich-Peterson isotherm is given in Table 5, where A (L/mg) and B (L/g) are the Redlich-Peterson isotherm constants, β is an exponent lying between 0 and 1, Ce is the equilibrium liquid-phase concentration of the adsorbate (mg/L), and qe is the equilibrium adsorbate loading onto the adsorbent (mg/g).

Sips [172] proposed an equation that solves the problem of the continuing increase in the adsorbed amount with an increase in concentration in the Freundlich equation. It is shown in Table 5 and has a finite limit when the concentration is sufficiently high. The parameters of this equation can be defined as follows: q_e is the adsorbed amount at equilibrium (mg/g), C_e is the equilibrium concentration of the adsorbate (mg/L), q_{mS} is the Sips maximum adsorption capacity (mg/g), K_S is the Sips equilibrium constant (L/mg), and β is the Sips model exponent.

The Fritz-Schlunder [173] isotherm model is three-parameter and consists of Langmuir and Freundlich isotherms. The equation is represented in Table 5 where q_e is the adsorbed amount at equilibrium (mg/g), C_e is the equilibrium concentration of the adsorbate (mg/L), q_{mFS} is the Fritz–Schlunder maximum adsorption capacity (mg/g), K_{FS} is the Fritz–Schlunder equilibrium constant (L/mg), and α is the Fritz–Schlunder model exponent.

The last three-parameter model applied in this work is Toth [174] isotherm model, which is the modified Langmuir equation reducing the error between experimental data and predicted values of equilibrium adsorption data. The Toth correlation is given in Table 5 where q_e is the adsorbed amount at equilibrium (mg/g), C_e is the equilibrium concentration of the adsorbate (mg/L), q_{mT} is the Toth maximum adsorption capacity (mg/g), K_T is the Toth equilibrium constant, and α is the Toth model exponent.

Four-parameter isotherm models

Another four-parameter equation of Langmuir–Freundlich type was developed empirically by Fritz and Schlunder [173] . It is expressed in Table 5 with α and $\beta \leq 1$ where qe is the adsorbed amount at equilibrium (mg/g), Ce the equilibrium concentration of the adsorbate (mg/L), A and B are the Fritz–Schlunder parameters, and α and β are the Fritz–Schlunder equation exponents.

Baudu [175] has remarked that the calculation of the Langmuir coefficients, b and q_{mL}, by the measurement of tangents at different equilibrium concentrations, shows that they are not constants in a broad concentration range. So, he proposed a transformed Langmuir equation shown in Table 5 with $(1 + x + y)$ and $(1 + x) < 1$. Graphical study of $\ln b = f(\ln C_e)$ and $\ln q_{mL} = f(\ln C_e)$ gives access to b_o, q_{mo}, x, and y, where q_e is the adsorbed amount at equilibrium (mg/g), C_e is the equilibrium concentration of the adsorbate (mg/L), q_{m0} is the Baudu maximum adsorption capacity (mg/g), b_o is the equilibrium constant, and x and y are the Baudu parameters.

Five-parameter isotherm models

Fritz and Schlunder [173] have proposed a five- parameters empirical expression which can represent abroad field of equilibrium data (with m1 and $m2 \leq 1$) (Table 5). q_e is the adsorbed amount at equilibrium (mg/g), C_e is the equilibrium concentration of the adsorbate (mg/L), q_{mFS} is the Fritz-Schlunder maximum adsorption capacity (mg/g) and K_{1FS}, K_{2FS}, m_1, and m_2 are the Fritz–Schlunder parameters.

2.5.2 Adsorption kinetic models

Reaction kinetic models. Two models were applied to study the kinetics of Pb(II) ions adsorption on natural zeolite and Chamotte clay: pseudo-first (initially introduced by Lagergren [176]) and pseudo-second order proposed by Ho and McKay [177].

The most used in literature forms are linear forms of the equations (12) and (13) for pseudo-first and pseudo-second order models respectively:

$$\ln(q_e - q_t) = \ln q_e - k_1 t, \tag{12}$$

$$\frac{t}{q_t} = \frac{t}{q_e} + \frac{1}{k_2 q_e^2}, \tag{13}$$

where k_1 and k_2 are the pseudo-first and pseudo-second order rate constants, q_t is the amount of adsorbed solute, q_e is its value at equilibrium.

In 2016 J.P. Simonin [15] published a study where he proved that it is inappropriate to define a suitable kinetic model based only on the values of the correlation coefficients of fitting into linear forms of equations (12) and (13). As pointed out by statisticians [178,179], two fitting models must be compared on the original scale as follows: (14) for K_1 and (15) for K_2:

$$q_t = q_e(1 - \exp(-k_1 t)), \tag{14}$$

$$q_t = \frac{q_e^2 k_2 t}{1 + q_e k_2 t}, \tag{15}$$

In the present context, this principle means that it is irrelevant to compare R^2 values for the two different functions, $y = \ln(q_e - q_t)$ for K1, and $y = t/q_t$ for K2. Instead, the determination coefficient R^2 should be computed using (16) for the same function y = q in both cases K1 and K2 to get a reliable estimator for the comparison of these two models.

$$R^2 \equiv 1 - \frac{\sum_{i=1}^{N}(y_i - \hat{y}_i)^2}{\sum_{i=1}^{N}(y_i - \langle y \rangle)^2}, \tag{16}$$

where N is a number of data; $y_i = \ln(q_e - q_t)$ and $\hat{y}_i = \ln q_e - k_1 t$ for K1 and $y_i = t/q_t$ and $\hat{y}_i = t/q_t + 1/k_2 q_e^2$ K2; $\langle y \rangle \equiv (\frac{1}{N}) \sum_{i=1}^{N} y_i = (1/N)$, i.e. the average value of the y_i's (i = 1. . . .N). For a very bad fit using a non-linear regression R^2 may get result $R^2 < 0$ [179].

Also, when choosing a suitable model, one should take into account the values of AARDy (Absolute Average Relative Deviation), which is calculated by (17):

$$AARD_y \equiv \frac{1}{N} \sum_{i=1}^{N} \left| \frac{\hat{y}_i - y_i}{y_i} \right|, \tag{17}$$

where $y_i \equiv y(t=t_i)$ and $\hat{y}_i \equiv \hat{y}(t=t_i)$.

To determine accurately the order of kinetic processes based on adsorption capacity, the pseudo-nth order kinetic was used. The expression for the non-linear equation of the pseudo-nth order is given below (18) [180]:

$$q_t = q_e - (q_e^{(1-n)} + (n-1)k_n t)^{\frac{1}{(1-n)}}, \quad (18)$$

The values of the accurate order and rate constant K_n were determined using Solver Add-in functions of MS Excel considering that the order is close to 2.

Diffusion kinetic models. It is generally known that a typical solid/liquid adsorption involves film diffusion, intraparticle diffusion, and mass action [181]. However, as the mass action process is very rapid for physical adsorption, diffusion models are mainly constructed to describe the process of film diffusion and/or intraparticle diffusion.

In this work, the results were analyzed using the intraparticle diffusion models of Weber and Morris and Dumwald-Wagner, as well as Chemisorption diffusion models.

The most widely applied intraparticle diffusion equation of Weber and Morris (19) [182] model is:

$$q_t = k_i t^{0.5} + C, \quad (19)$$

where k_i is intraparticle diffusion rate constant (g/mg min), intercept C reflects the boundary layer effect or surface adsorption. If a plot of q_t against the $t^{0.5}$ gives a straight line passing through the origin, then intraparticle diffusion is a rate-determining step for the adsorption process. In case when the plot exhibits two or more intersecting lines, then two or more stages control the adsorption process [183].

The Dumwald-Wagner model is applicable for different adsorption systems and the equation can be expressed as (20) [183]:

$$\ln\left(1 - \frac{q_t}{q_e}\right) = K_{DW} t, \quad (20)$$

where K_{DW} is the film diffusion rate (min^{-1}). If the plot *ln(1-qt/qe)* vs *t* gives a straight line and passes through the origin, then intraparticle diffusion is the rate-limiting step; otherwise, the rate is controlled by film diffusion.

Chemisorption diffusion model is an empirical diffusion-chemisorption kinetic model developed by Sutherland [184]. The following form of the equation (21) was used in this work:

$$\frac{1}{q_t} = \frac{1}{q_e} + \frac{1}{K_{CD} t^{0.5}}, \quad (21)$$

where K_{CD} (mg/g $t^{0.5}$) is the rate of mass transfer of metal ions from the liquid phase to the adsorption site.

2.5.3 Calculation of thermodynamic characteristics of the adsorption process

The following equations (22)-(24) [185] were used to calculate the thermodynamic parameters:

$$\Delta G^0 = -RT ln K_d, \quad (22)$$

where ΔG^0 is the standard free energy change, J/mol; R (8.314 J/mol K) is the gas constant; T is the temperature, K; and K_d is the distribution coefficient for the adsorption process, which is calculated as:

$$K_d = \frac{q_e}{c_e}, \quad (23)$$

The isosteric enthalpy change ΔH^0 and the entropy change ΔS^0 were obtained from the slope and intercept of the linear plot of $\ln K_d$ against 1/T:

$$ln K_d = -\frac{\Delta H^0}{RT} + \frac{\Delta S^0}{R}, \quad (24)$$

2.5.4 Error function analysis of the experimental results

According to several studies [165,170,186] it is necessary to use Error function analysis. In this work, such mathematical error functions as the coefficient of determination (R^2), Sum of squared errors (SEE), Sum of absolute errors (SAE), Average Relative Error (ARE), Mean Square Error (MSE), Root Mean Square Error (RMSE) were employed to compare between the linear and non-linear regression methods. The list of used error functions and their expressions is in Table 6.

Table 6 – List of used error functions

Error function	Expression
Coefficient of correlation (R^2)	$R^2 = \frac{\sum_{i=1}^{n}\left(q_{e.exp} - \overline{q_{e.cal}}\right)_i^2}{\sum_{i=1}^{n}\left(q_{e.exp} - q_{e.cal}\right)_i^2 + \left(q_{e.exp} - \overline{q_{e.cal}}\right)_i^2}$
Sum of squared errors (SEE)	$SEE = \sum_{i=1}^{n}\left(q_{e.exp} - q_{e.cal}\right)_i^2$
Sum of absolute errors (SAE)	$SAE = \sum_{i=1}^{n}\left\lvert q_{e.exp} - q_{e.cal}\right\rvert_i$
Average Relative Error (ARE)	$ARE = \frac{100}{n}\sum_{i=1}^{n}\left\lvert\frac{q_{e.exp} - q_{e.cal}}{q_{e.exp}}\right\rvert_i^2$

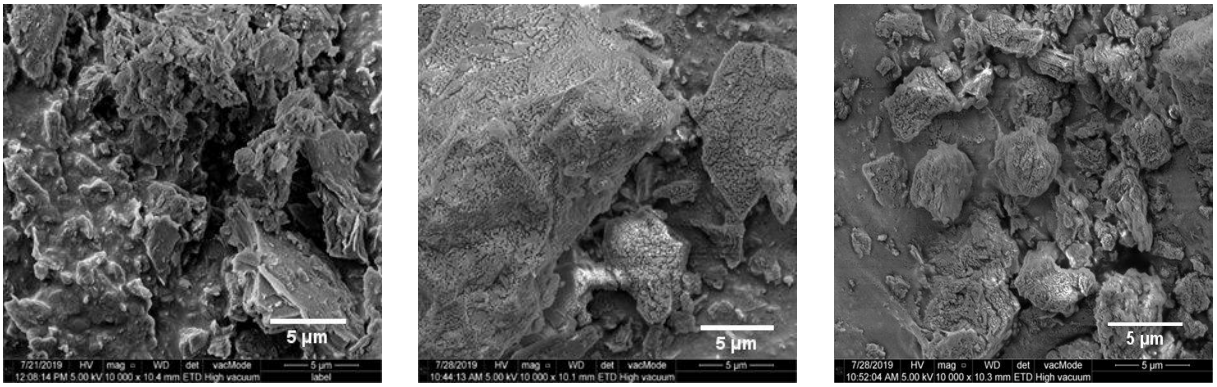
Table 6 (continued)	
Mean Square Error (MSE)	$MSE = \frac{100}{n-2}\sum_{i=1}^{n}\left(q_{e.exp} - q_{e.cal}\right)_i^2$
Root Mean Square Error (RMSE)	$RMSE = \sqrt{\frac{100}{n-2}\sum_{i=1}^{n}\left(q_{e.exp} - q_{e.cal}\right)_i^2}$

3 RESULTS AND DISCUSSION

3.1 Physico-chemical characterization of the obtained adsorbents

3.1.1 Physico-chemical characterization of the obtained Zeolite-based adsorbents

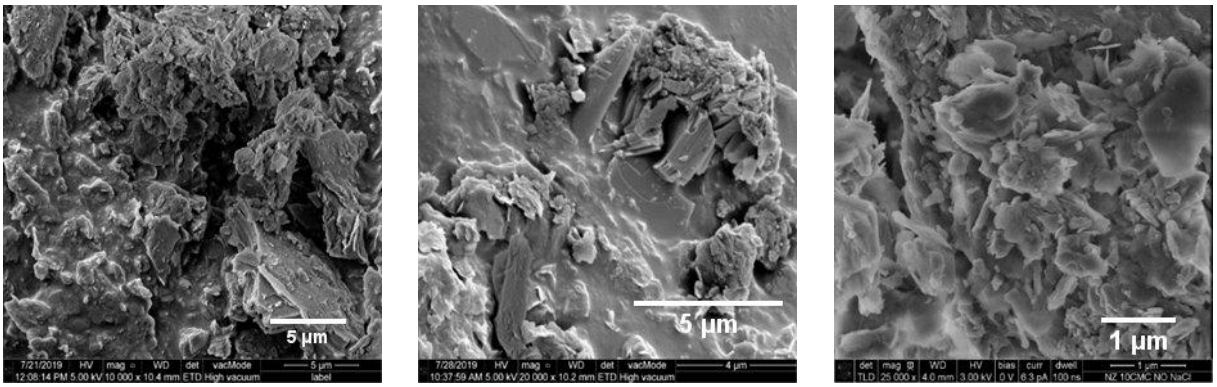
SEM. The SEM micrographs of the initial zeolite and modified adsorbents are presented in Figures 9-11.



a b c

Figure 9 – SEM images of (a) natural zeolite, (b) Na-zeolite and (c) H-zeolite

The morphology of natural zeolite is characterized by dense agglomerates of different shape with some space in between (pores). The particle size distribution spans a broad range from 0.1 to 100 µm with average size of 1.22 ± 0.79 µm [2]. After Na- and H-treatment many very fine points can be seen on the surface of zeolite suggesting increasing porosity of the modified forms. The particle size distribution of the samples is given in Table 7.



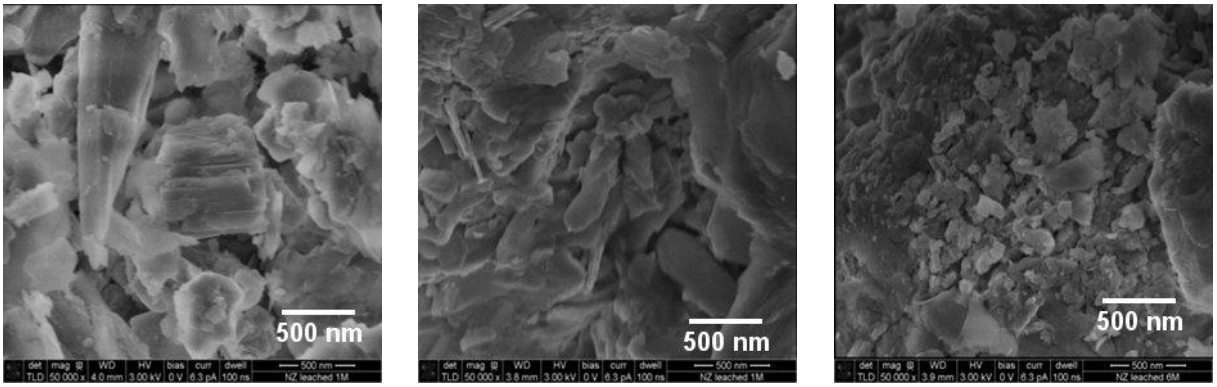
a b c

Figure 10 – SEM images of (a) natural zeolite, (b) SLES-zeolite and (c) DDAB-zeolite.

The SEM micrograph of DDAB-zeolite is presented in Figure 10c. We can see that the surface of the crystalline zeolite is covered by some amorphous particles, which are assumed to be layers of DDAB. After modification with SLES (Figure 10b) the surface of zeolite seems to be covered by a thin film because we can see much less sharp particles.

The images of zeolite treated with different concentrations of HCl (1, 3 and 6 M) are presented in Figure 11. It is very difficult to estimate the influence of the acid concentration on the

zeolite structure from the SEM images. However, it can be noticed that with the increase in acid concentration, the size of the zeolite crystal agglomerates decreases; the particle size distribution is 0.25–1.5 μm for 1 M, 0.1–0.25 μm for 3 M, and 0.05–0.2 μm for 6 M HCl-treated zeolite, and the average particle size (Table *7* – Particle size distribution of composites based on zeolite (Table *7*) decreases accordingly: 0.54 ± 0.16, 0.23 ± 0.05, and 0.12 ± 0.02 μm. These results indicate partial destruction of the zeolite framework.



a b c

Figure 11 – SEM images of HCl-treated zeolite: a) 1 M, b) 3 M, and c) 6 M [187].

Table 7 – Particle size distribution of composites based on zeolite

Sample	Area, μm^2	Standard deviation
zeolite	1.22	0.79
Na-zeolite	1.87	0.50
1M H-zeolite	0.54	0.16
3M H-zeolite	0.23	0.05
6M H-zeolite	0.12	0.02
SLES-zeolite	0.86	0.10
DDAB-zeolite	1.70	0.82

Cation exchange capacity (CEC). According to several studies [13,188,189] ion exchange is one of the main mechanisms that are responsible for the removal of pollutants from water solutions by zeolites. Therefore, the determination of the cation exchange capacity (CEC) of zeolites is very important. The standard method with 1 M NH_4Cl was applied [190], and the results are shown in Table 8.

Table 8 – CEC of zeolite samples (meq/100 g) [187]

Sample	K^+	Na^+	Ca^{2+}	Mg^{2+}	Total
Zeolite	15.7±1.6	116.8±3.5	441.2±10.5	42.3±1.1	616.0±16.7
NaCl-zeolite	16.7±2.0	230.1±6.0	348.4±8.1	29.2±0.6	624.4±16.7
3M HCl-zeolite	10.3±0.7	86.6±2.0	28.2±1.0	4.2	129.2±3.7

The CEC of untreated zeolite is quite high, for calcium, therefore it can be concluded that the zeolite contains more calcium than the other exchange cations. It is also consistent with the elemental analysis (Table 9). However, the second ion in the CEC ranking is sodium, but according to the elemental analysis, the zeolite contains almost three times less sodium than magnesium. This can arise from the fact that sodium reacts in the ion-exchange processes more easily than magnesium, which was the reason for the NaCl treatment of the zeolite that slightly increased the CEC from 616.0 to 624.4 meq/100 g. Notably, because of the NaCl treatment, the release of Na-ions nearly doubled, whereas the release of Mg and Ca ions decreased significantly [187].

Acid treatment led to a very significant reduction in the CEC to 129 meq/100 g due to the leaching of ion-exchange metals. The much greater decrease in the release of calcium and magnesium suggests that they underwent leaching first, followed by potassium and sodium. This trend is in accord with the results of elemental analysis. We suppose that it is related to the fact that Ca and Mg ions interfere with water molecules in the hydrolysis process with formation of insoluble hydroxides and do not return to the zeolite surface during the ion exchange process [187].

Elemental analysis. The results of elemental analysis obtained by EDAX are presented in Table 9. The initial zeolite contains mainly Si, O and Al, as well as small amounts of metals including Na, Mg, K, Ca and Fe. Notably, after treatment of the zeolite with 1 M NaCl, the sodium content increases from 0.51 to 2.31 %, while the content of the other metals decreases: Mg from 1.78 to 0.51 %, K from 1.15 to 0.86 %, and Fe from 6.31 to 1.85 %. This is most likely due to the replacement of these metals with sodium ions. As all the metals in the zeolite structure are potential centers of cation exchange, their content changes after modification with the NaCl solution [187].

The Si/Al ratio, which determines the ion-exchange properties of zeolites, is of interest. The purpose of the acid treatment was to increase the Si/Al ratio, which varies from 2 to 10 for natural zeolites. Highly siliceous zeolites have a larger specific surface area and pore volume [191]. The ratio increases because of the leaching of aluminum, as well as other metals from the zeolite surface. After the acid treatment, the ratio increased in accord with the acid concentration from 4.43 for untreated zeolite, to 4.49 for 1 M, 6.32 for 3 M, and 23.71 for 6 M HCl-treated zeolite (Figure 12). This significant concentration dependence indicates leaching of aluminum from the zeolite with formation of SiO_2.

DDAB- and SLES-modified forms of zeolite contain a little more carbon that indicates the presence of organic surfactants in the composite material.

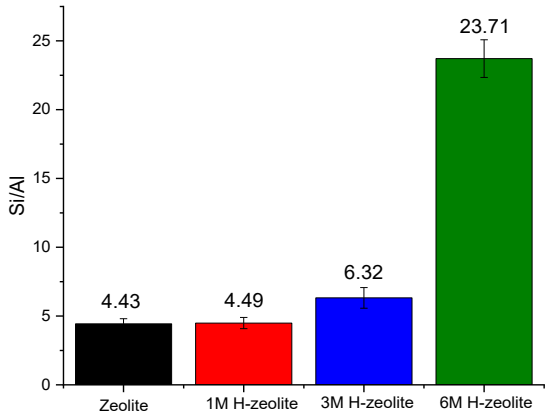


Figure 12 – Si/Al ratio of zeolite treated with HCl solutions of various concentrations [187]

Table 9 – Results of elemental analysis of the adsorbents (Wt.%)

Sample	C	O	Na	Mg	Al	Si	K	Ca	Fe
Zeolite	8.21	40.73	0.51	1.78	6.39	29.38	1.15	5.53	6.32
Na-zeolite	7.24	36.19	2.31	0.51	11.16	34.18	0.86	5.81	1.74
H-zeolite	16.90	32.33	1.46	1.13	9.68	29.72	2.03	3.29	3.46
SLES-zeolite	9.63	39.19	0.38	1.81	8.03	28.90	2.42	3.79	5.85
DDAB-zeolite	7.91	45.71	3.05	3.19	10.30	26.84	0.58	0.91	1.51

X-ray diffractometry (XRD). It is known that XRD is one of the most reliable methods for qualitative diagnosis of minerals. Figure 13 and Figure 15 show the results of XRD analysis.

Parent zeolite showed a similar pattern as the crystalline structure reported in the literature [192,193]. Good agreement between the results shows that the original natural zeolite includes clinoptilolite [192], anorthite sodian [194], and quartz phases. Anorthite is a member of the feldspar group, which often occurs naturally in a mixture with zeolites [195]. After 1 M HCl treatment, most of the peaks, except for the peak at $2\theta° = 41.94$, are maintained. We can notice the increased intensity of some peaks in the $2\theta°$ range of 16 to 35, which might indicate the dissolution of some amorphous impurities and an increase in the crystallinity of the zeolite. Acid treatment of clinoptilolite leads to a partial destruction of Si-O-Si and Si-O-Al bonds, thereby forming additional active centers on the surface, which probably increases sorption capability. After treatment with a stronger concentration of acid (3 and 6 M) there is a loss of many X-ray peaks that reflect the clinoptilolite phase: $2\theta = 11.19$, 13.06, 16.91, 17.36, 19.10, 22.48, 25.03, 26.04,

29.00, and 32.04. Moreover, there is a shift of the 22.48 peak to 21.98, which is characteristic of the non-crystalline phase of SiO_2 [196]; its intensity increases significantly from 3 to 6 M HCl.

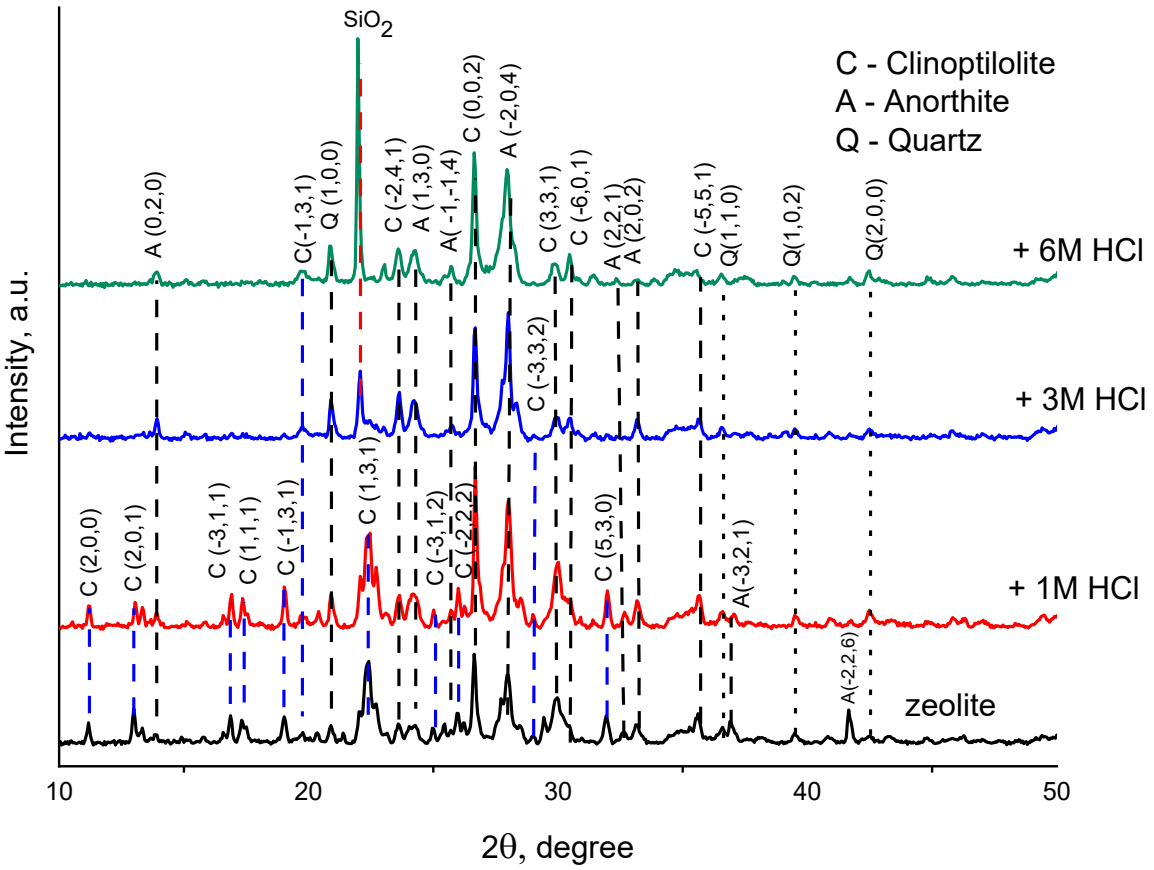


Figure 13 – X-ray diffraction patterns of zeolite treated with various concentrations of hydrochloric acid [187]

Higher acid concentrations lead to dehydration of the zeolite, intersphere cationic restructuring, and partial destruction, which can reduce the sorption activity. It means that at high concentrations of acid, the crystalline zeolite phases partially dissolve with formation of an amorphous silicon oxide phase. This suggestion is supported by the appearance of white-colored particles in the zeolite powder (Figure 14):



Figure 14 – Zeolite (1) before and (2) after treatment with 6 M HCl [187]

Modification of the zeolite with the surfactant DDAB did not change the XRD pattern; both zeolites before and after modification consist of clinoptilolite, anorthite sodian and quartz phases (Figure 15). XRD spectrometry gives information about the crystalline structure of a substance, therefore significant changes in the patterns after the interaction between DDAB and the zeolite surface were not expected.

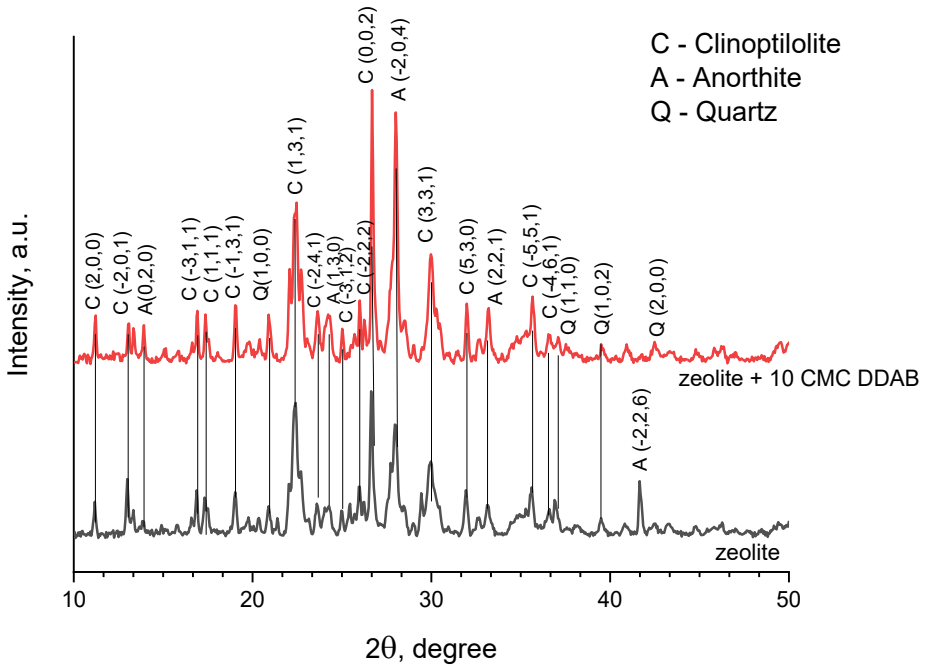


Figure 15 – X-ray diffraction patterns of zeolite before and after modification with DDAB

FTIR and Raman spectroscopy. To gain more information about the probable new bonds formed because of the surfactant modification, FTIR and Raman spectra of the samples were taken (Figures 16-20).

The spectra of untreated zeolite and zeolites treated with acid and NaCl are very typical of clinoptilolite spectra (Figure 16). According to [189] spectra of zeolites can be divided into three groups: 1200–450 cm^{-1} — internal Si–O(Si) and Si–O(Al) bond vibrations in tetrahedra or aluminum and silicon-oxygen bridges (depending on the basic structural unit used to describe the spectrum); 600–800 cm^{-1} — pseudo-lattice vibrations originating from over tetrahedral structural units (rings made of silicon-oxygen and aluminum oxygen tetrahedra); 3000–4000 cm^{-1} and ~1600 cm^{-1} — vibrations related to the presence of OH– groups and zeolite water in the structure. The most intensive peak at 900–1100 cm^{-1} corresponds to O-T-O (where T=Si, Al) bonds. The shift of that peak is sensitive to the change in silicon or aluminum content. The dissolution of Al and Si from the zeolite framework during equilibration periods resulted in an increase in the frequency of this band from 984 to 1033 cm^{-1} for the acid-treated sample [197]. The shift of the peak to the higher frequency area reports the shortening of the bond length. The weak bands in the

750–790 cm^{-1} region correspond to the symmetric stretching vibration of the T—O bonds [198], which also shifts a little for acid-treated zeolite. The peaks at 3580–3300 and 1645–1620 cm^{-1} are assigned to the stretching and deformation vibrations of OH groups adsorbed on the surface of a mineral, respectively [199]. NaCl treatment does not affect the FTIR spectrum of the zeolite, therefore, as FTIR and Raman spectra are usually complementary, Raman spectra of the same samples were taken (Figure 17).

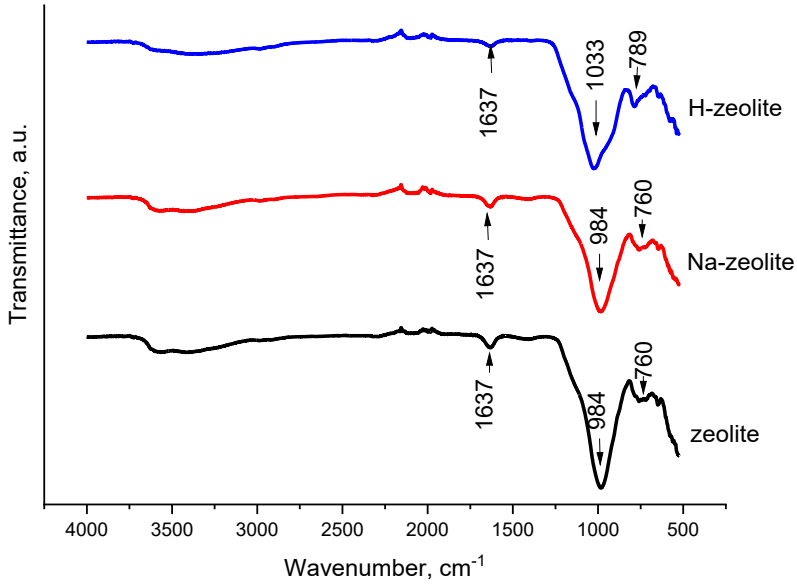


Figure 16 – FTIR spectra of zeolite, Na-zeolite, and H-zeolite [187]

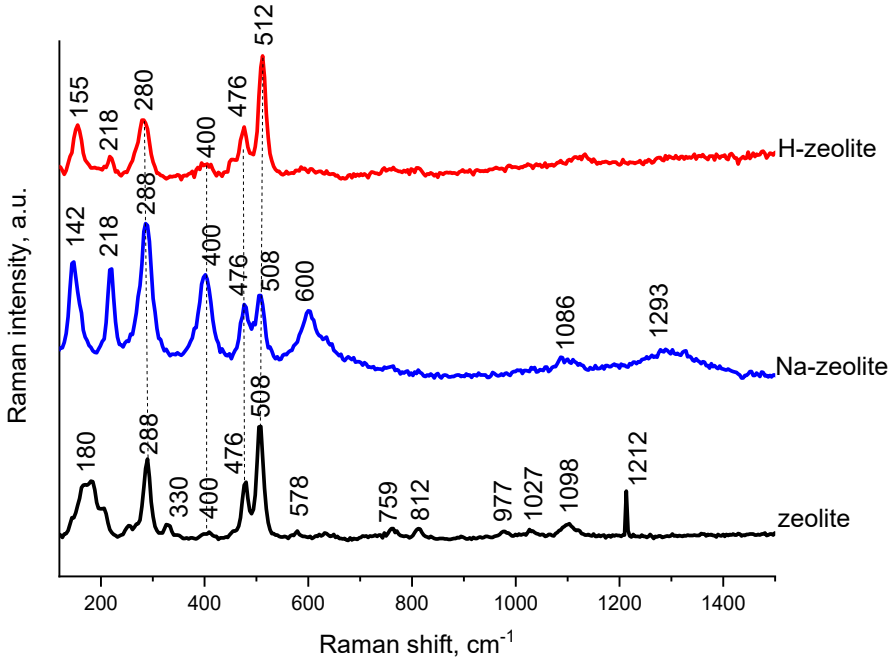


Figure 17 – Raman spectra of zeolite, Na-zeolite, and H-zeolite [187]

The bands at 180, 288, 330, 400, 476, 508, 759, 812, 977, 1027, 1098 and 1212 cm^{-1} are apparent in the Raman spectrum of untreated natural zeolite. The most intense band at 508 cm^{-1} and the band at 476 cm^{-1} are assigned to the bending mode of the characteristic four-membered Si-O-Al rings of clinoptilolite. The band at 812 cm^{-1} is due to the T-O symmetric stretching mode, the band at 1098 cm^{-1} is assigned to asymmetric stretching vibrations of the Si-O-Si bonds, and the band at 288 cm^{-1} corresponds to the bending mode of eight-membered rings [200]. The bands at 180 and 330 cm^{-1} can be assigned to the rocking mode of water adsorbed into an inorganic lattice [189]., and the band at 400 cm^{-1} can refer to internal vibrations of bonds in the TO_4 tetrahedrons [201].

As we can see, quite intense bands at 142, 218 and 600 cm^{-1} appear in the spectrum of Na-zeolite. After NaCl-treatment, a change occurs in the pseudo lattice range of the spectrum (600–800 cm^{-1}) as a result of the ion-exchange process. “Pore-opening” type vibrations are among other modes that occur in this range [189]. Ion exchange causes subsequent adsorption and desorption of water and changes in bands related to vibrations of OH groups and water molecules. Thus, the band at 180 cm^{-1} in the initial zeolite spectrum splits into two bands at 142 and 218 cm^{-1} in the Na-zeolite spectrum. Similar splitting occurs in the spectrum of the acid-treated zeolite: 155 and 218 cm^{-1}, probably due to dehydration of the zeolite. It is known from the literature that the band position and intensity are influenced by the Si/Al ratio [200]. The bands at 288 and 508 cm^{-1}, corresponding to ring vibrations, shift to 280 and 512 cm^{-1}, respectively in the spectrum of acid-treated zeolite. It also supports the conclusion about the partial destruction of zeolite after the acid treatment [187].

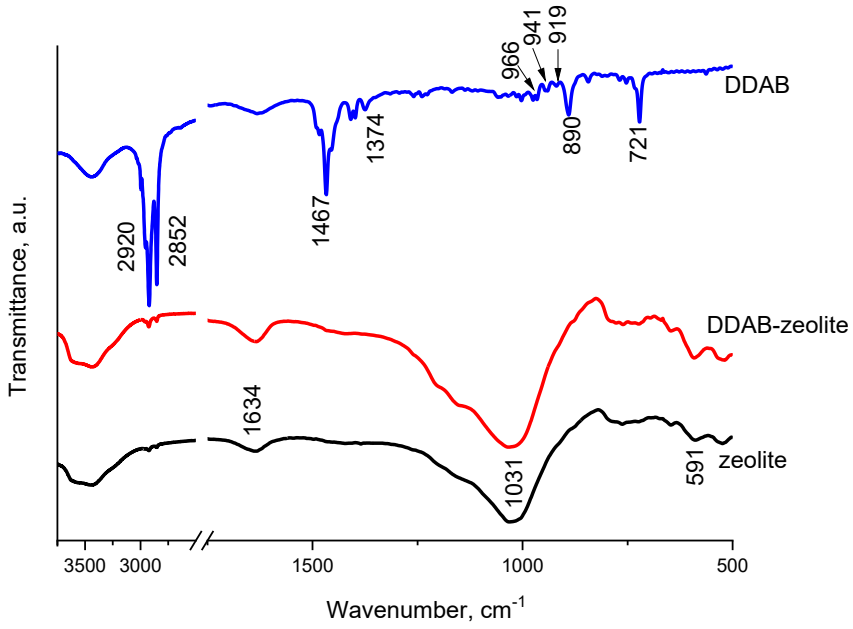


Figure 18 – FTIR spectra of initial zeolite, DDAB powder, and DDAB-zeolite

The FTIR spectra of initial zeolite, DDAB powder, and DDAB-zeolite are presented in Figure 18. Intense peaks in the pure DDAB spectrum at 2920 and 2852 cm^{-1} are related to asymmetric and symmetric stretching vibrations of methylene groups. These peaks are apparent in the surfactant-modified zeolite spectra, which probably indicates coating of the zeolite by DDAB. The very low intensity of these peaks in the SMZ spectrum is probably due to the small concentration of surfactant compared to the amount of zeolite. The peaks located at 721 and 1467 cm^{-1} are assigned to the rocking mode and scissoring motion of the methylene chains, respectively. The peak at 890 cm^{-1} is assigned to the in-plane methyl rocking mode. C-N^{+} stretching bands of DDAB are located at 916, 941 and 966 cm^{-1} [202]. Changes in other bands in the SMZ spectrum are not noticeable [187].

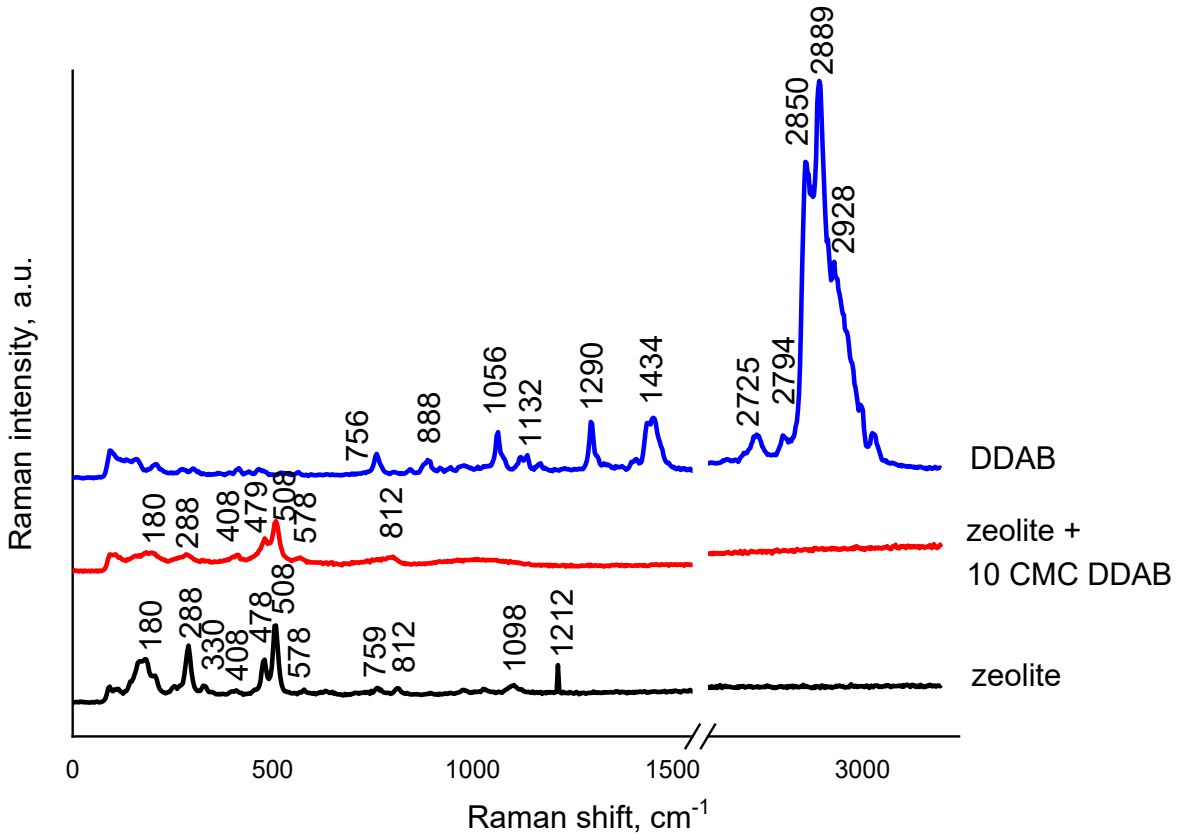


Figure 19 – Raman spectra of initial zeolite, DDAB powder, and DDAB-modified zeolite [187]

The assignment of the bands in the Raman spectrum of powder DDAB is presented in Figure 19. The characteristic bands of the surfactant cannot be seen in the spectrum of SMZ, but we can notice that some of the initial zeolite peaks almost disappeared after modification with DDAB (at 180, 330, 1098 and 1212 cm^{-1}), probably due to coating of the zeolite surface by DDAB micelles, ion-exchange and subsequent change in water content. We can see the decrease in the intensities of the peaks at 288, 476 and 508 cm^{-1}, which refer to the vibrations of four and eight-membered

rings in the structure. It was reported in [189] that the position of this band depends on the degree of zeolite hydration and also on the related position of the cations in the zeolite framework [187].

Table 10 – Raman frequencies for DDAB powder spectrum [203]

Frequency, cm^{-1}	Assignments
756	CH_3 rock from $N^+(CH_3)_3$ group
888	CH_2 rock
1056	C-C asym. stretch + CH_2 wag from (TG_mT) with large *m*
1132	C-C asym stretch + CH_2 wag from (TG_mT) with large *m*
1290	CH_2 twist
1434	-CH_2 bend
2846	C-H sym stretch of –CH_2-
2882	C-H sym stretch of –CH_3
2922	C-H asym stretch of –CH_2-

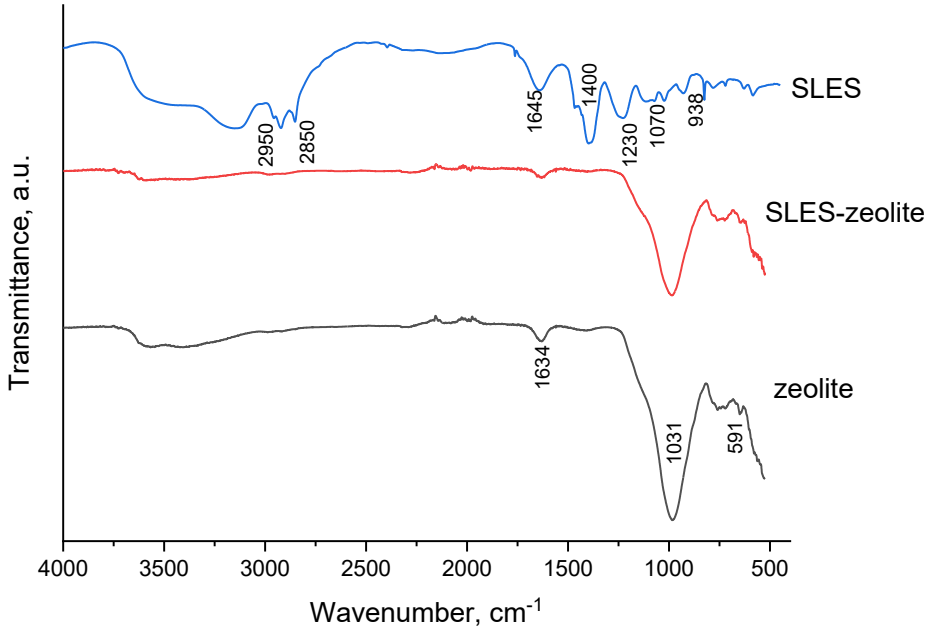


Figure 20 – FTIR spectra of zeolite, SLES, and SLES-zeolite

In the SLES spectrum (Figure 20) peaks characteristic of symmetric and asymmetric CH_2 stretching mode at 2925 cm^{-1} and 2850 cm^{-1} can be seen. A peak at 1645 cm^{-1} is for C=O stretching vibrations. SLES has bands at 1467 cm^{-1} and 1400 cm^{-1} (CH_2 scissoring mode), 1230 cm^{-1} and 1070 cm^{-1} (S=O and -SO_3), 1122 cm^{-1} (antisymmetric C-O-C bridge), and 1022 cm^{-1} (C-O-C bond) [204]. Vibrations in the low-frequency region refer to C=CH_2 (900-650 cm^{-1}), as well as to rocking vibrations of CH_2-groups (772-730 cm^{-1}). No changes were found in the SMZ spectrum after interaction with SLES, except for a decrease in the intensity of the peaks characteristic of zeolite water at 3000–4000 cm^{-1} and ~1600 cm^{-1}. Thus, the interaction between zeolite and SLES occurs due to the separation of OH groups from the surface.

BET results. One of the most important characteristics for the description of sorbents is the specific surface and pore size, which can be obtained by the Brunauer-Emmett-Teller (BET) method. Table 11 shows the values of the specific surface and specific pore volume of the initial zeolite and modified sorbents.

The mean specific surface areas and pore volumes of the samples are presented in Table 11. They indicate changes that occur after the modification of natural zeolite. Modification with DDAB slightly increases the surface area from 4.5 to 8.2 m^2/g, while treatment with SLES has almost no impact on the surface area of zeolite. However, the preliminary acid treatment of the zeolite had the greatest effect – 39.3 m^2/g.

Table 11 – Specific surface area and pore volume of adsorbents [2]

Adsorbent	Surface area, m^2/g	Pore volume, cm^3/g
zeolite	4.5	0.002
Na-zeolite	6.2	0.002
H-zeolite	39.3	0.005
DDAB-zeolite	8.2	0.004
SLES-zeolite	4.6	0.002

Amount of surfactant adsorbed onto zeolite. The amounts of DDAB and SLES in every type of zeolite have been quantified and are given in Table 12.

The amount of DDAB added to each type of zeolite was 20 mmol/kg. As can be seen from the Table 12, most of the surfactant was adsorbed onto zeolite. The best result was observed for untreated zeolite, which is 17.74 mmol/kg (88.7%). The pretreated zeolites adsorbed a little less amount of the surfactant – 16.46 (82.3%) for Na-zeolite and 16.71 (83.55) for 3M HCl-zeolite. It is known from the literature [139] that surfactants are adsorbed onto zeolite via ion-exchange for the first layer, and then via hydrophobic interactions. Worse results for pretreated zeolites are due to:

1. The treatment with Na^+ leads to a homoionic state of zeolite, thus improving its hydrophilicity [144,205].

2. The acid treatment decreases CEC of zeolite, thus decreasing its ability to ion-exchange interactions.

The amount of SLES added to each type of zeolite was 10 mmol/l. In this case initial zeolite adsorbs lowest amount of the surfactant, while Na-zeolite and H-zeolite show similar results.

Treatment with sodium and acid saturates the surface of zeolite with positive charge increasing electrostatic interaction with anionic SLES.

It should be noted that the zeolite adsorbs a larger amount of DDAB than SLES. Since SLES is an anionic surfactant, therefore, electrostatic repulsion can occur, preventing their interaction.

However, most part of surfactants (58-89%) are adsorbed by the studied samples, indicating that they can be applied to the surfactants adsorption from water solutions.

Table 12 – The amounts of DDAB and SLES in adsorbents

Adsorbent	Amount of DDAB in the adsorbent, mmol/kg	Adsorbed amount of DDAB, %	Amount of SLES in the adsorbent, mmol/kg	Adsorbed amount of SLES, %
Zeolite	17.74 ± 0.17	88.7 ± 0.85	5.83 ± 0.33	58.3 ± 3.3
Na-zeolite	16.46 ± 0.29	82.3 ± 1.45	5.92 ± 0.21	59.2 ± 2.1
H-zeolite	16.71± 0.28	83.5 ± 1.40	6.11 ± 0.18	61.1 ± 1.8

PZC and zeta potential. As is known, point of zero charge (PZC) is a pH at which the surface of substance is neutral, i.e. the amount of positive and negative charges are equal to each other. PZC values could help predict the adsorption affinity towards pollutants. Substrates with low PZC values would be best suited to treat effluents contaminated with cations, while substrates with high PZC values would be more appropriate to capture anions [206]. The surface charge is negative at $pH>pH_{pzc}$ and positive at $pH<pH_{pzc}$ [207]. Initial zeolite has PZC value of (7.96±0.05) (Figure 21a, Table 13). The NaCl-treatment slightly increases PZC to (8.85 ±0.06) (Figure 21b), while 3M HCl affects conversely by decreasing it to (3.11±0.02) (Figure 21c). The initial and treated with sodium chloride zeolites have rather high values of the zero-charge point. Therefore, their high efficiency with respect to anionic pollutants can be assumed. However, this may mean a worse fixation of cationic surfactant DDAB on their surface compared to 3M HCl-z.

The zeta potential is the electrical potential developed at the solid-liquid interface in response to relative movement of soil particles and water [208].

It should be stated that the location of zeta potential cannot be determined by the present theories [209]. However, zeta potential of particles is a good indicator of their electrical potential: the higher the zeta potential, the higher the surface potential of charged clay particle [210].

The measurements of zeta potential revealed that the examined z sample surface acquires a negative charge in water at natural pH (zeta potential = -18.1 ± 1 mV). Very similar results were obtained for studied in literature clinoptilolite-type zeolites where zeta potentials varied from -18 to -30 mV [211].

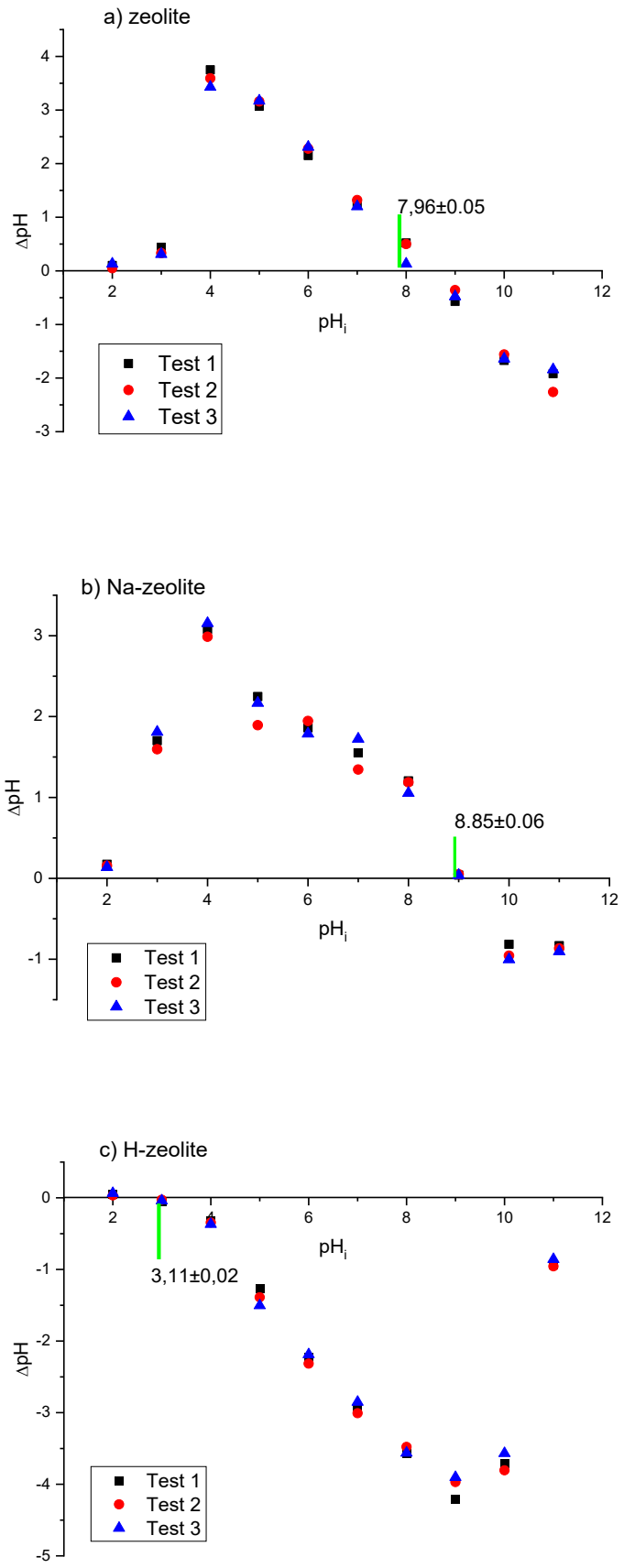


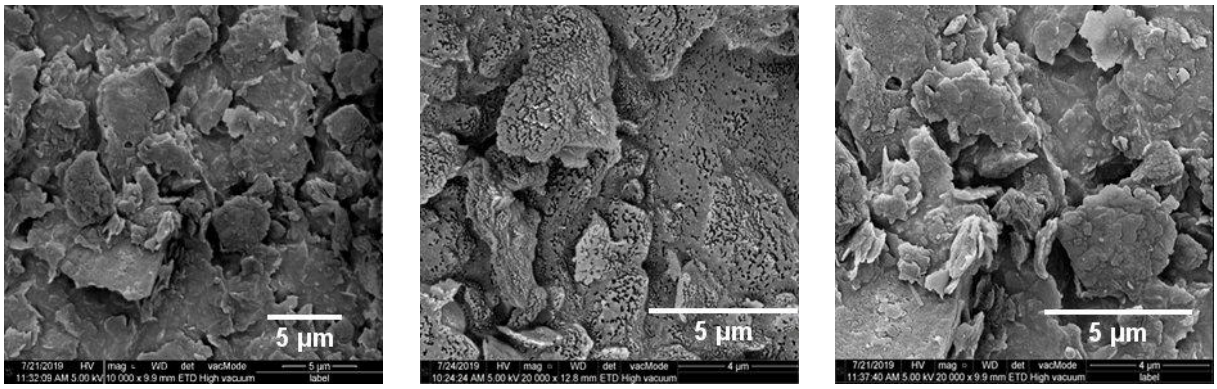
Figure 21 – Plots of ΔpH vs pHi for salt addition method for 0.1 M $NaNO_3$ (mean ± standard deviation, n =3) of a) zeolite; b) Na-zeolite; c) H-zeolite

Table 13 – Points of zero charge and ζ-potential values of the zeolite-based adsorbents

Sample	pH_{PZC}	ζ-potential, mV
zeolite	7.96 ± 0.05	-18.1 ± 1.0
Na-zeolite	8.85 ± 0.06	-
H-zeolite	3.11 ± 0.02	-

3.1.2 Physico-chemical characterization of the obtained Clay-based adsorbents

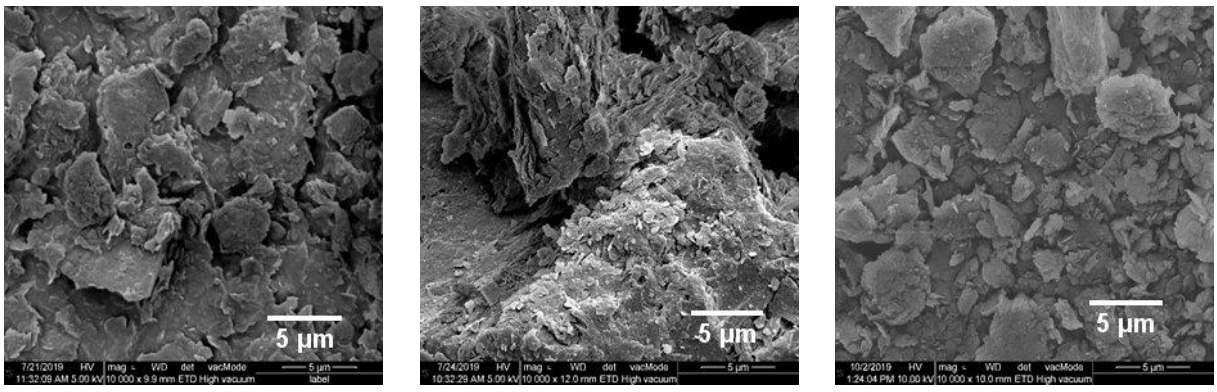
SEM image of Chammote clay is shown in Figures 22-23.



a b c

Figure 22 – SEM-images of (a) clay, (b) Na-clay and (c) H-clay

The layers of flocculent formations of irregular shape and various sizes form Chamotte clay. As is known, clays have a layered structure, therefore they are porous [62]. After treatment with NaCl we can see the appearance of many black holes that can be pores. HCl-treated sample becomes flocculent with appearance of more pores.



a b c

Figure 23 – SEM-images of (a) clay, (b) SLES-clay and (c) DDAB-clay

After modifying with SLES (Figure 23) the size of particles seems to be smaller, and after DDAB the difference is not so significant.

Table 14 shows the data on the particle size distribution of the clay-based materials. Thus, the average area of clay particles is (1.29 ± 1.61) μm^2. Large values of standard deviation are due

to a wide scatter of particle sizes and shapes, which is typical for materials of natural origin. As we can see, treatment with NaCl and HCl leads to decrease in average particle sizes of (0.68 ± 1.46) μm^2 and (0.33 ± 0.40) μm^2 respectively. Modification with surfactants also leads to decrease in size particles. Probably, this can be due to declustering some aggregates during mixing with modifier's solutions.

Table 14 – Particle size distribution of clay-based materials

Sample	Area, μm^2	St dev
clay	1.29	1.61
Na-clay	0.68	1.46
H-clay	0.33	0.40
SLES-clay	0.41	0.68
DDAB-clay	0.17	0.47

Cation exchange capacity (CEC).

Table 15 – CEC of clay-based samples (meq/100 g)

Sample	Na	K	Ca	Mg	Total
Clay	166.9±0.9	11.3±1.0	5.7	50.2±4.0	234.1±5.9
Na-Clay	239.8±2.3	8.7±0.5	1.9	35.6±2.3	286.0±5.1
H-Clay	95.8±3.3	7.5±0.4	0.3	0.7	104.3±3.7

Cation-exchange capacity (CEC) is a value that helps to evaluate the ability of adsorbents to take part in ion-exchange processes [212]. According to reference data [213], the CEC of natural zeolites and clays ranges from 200 to 400 meq/100 g [213]. As we can see from Table 15, the CEC of Chamotte clay is equal to 234.1 meq/100g, which is an average value. However, the studied material shows good CEC by Na^+ ions, which can indicate a good ability for ion exchange. Based on the results of elemental analysis (Table 16), the sodium, potassium, magnesium, and calcium contents of the original clay are approximately equal. Therefore, judging by the CEC data, sodium and magnesium are most actively involved in the ion exchange reaction. After Na-treatment the total CEC rises to 286.0 meq/100 g by increasing the sodium content in the sample. Acid treatment leads to leaching of ion exchange centers and a decrease in the total CEC to 104.3 meq/100 g, which significantly reduces the ability for ion exchange.

Elemental analysis. Table 16 shows elemental composition of clay-based materials. The framework of clay is composed of SiO_2 and Al_2O_3 oxides [62,214], therefore, the content of such elements as silicon, aluminum and oxygen prevails in their composition. There are also metals such as Na, K, Mg, Ca, which act as exchange cations to compensate for the excess charge on the surface of minerals [215]. It should be noted that the Si/Al ratio is 1.2 for clay, which corresponds to the structure of kaolin clay because the framework of the clay is composed of oxides of silicon and aluminum in a ratio of approximately 1:1 [62]. The clay also contains small amounts of iron

and titanium oxides, which can have a good effect on the ability of the clay to sorb heavy metals, in particular As [216].

After treatment with Na, an increase in the sodium content from 0.40 to 0.66% is observed. Acid treatment leads to a decrease in the carbon content, which may indicate a partial dissolution of organic impurities. A decrease in the sodium content associated with ion exchange processes between H^+ and Na^+ ions, is also noticeable.

The fixation of surfactant particles on the clay can be indicated by an increase in the carbon content after modification of clay with surfactants. The carbon content in the sample modified with DDAB is slightly higher than in the SLES treatment. This is because DDAB molecules are larger and contain more carbon than SLES.

Table 16 – Elemental composition of clay-based materials

Sample	C	O	Al	Si	Na	K	Mg	Ti	Fe	Ca
clay	3.71	44.99	20.48	25.76	0.40	0.85	0.66	0.85	2.03	0.27
Na-clay	3.78	47.09	19.84	23.90	0.66	0.83	0.75	0.74	2.26	0.15
H-clay	2.92	42.97	20.88	27.46	0.14	0.91	0.56	1.11	2.66	0.39
SLES-clay	5.03	42.51	21.63	24.96	0.20	0.85	0.71	0.99	2.71	0.41
DDAB-clay	6.19	44.00	20.03	22.96	0.41	1.20	0.96	0.59	3.26	0.40

X-ray diffractometry (XRD). The XRD pattern shown in *Figure 24* suggests that the crystalline structure of clay consists of kaolinite, mullite and quartz. Treatment with salt and acid does not lead to a change in the position of the main peaks. This is most likely because chamotte clay is a resistant material, especially the mineral mullite [217].

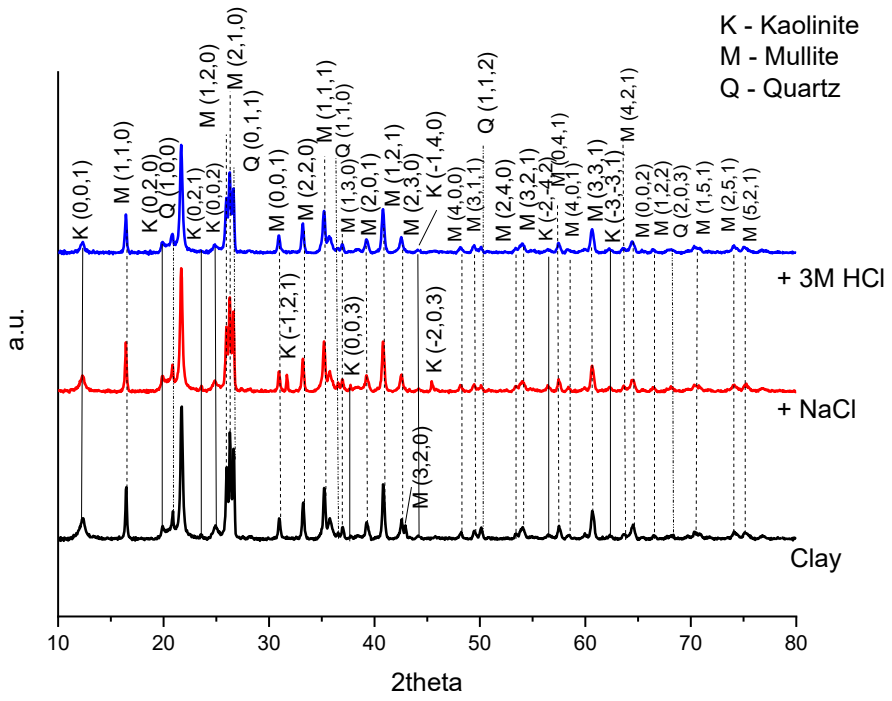


Figure 24 – X-Ray diffraction patterns of clay-based materials

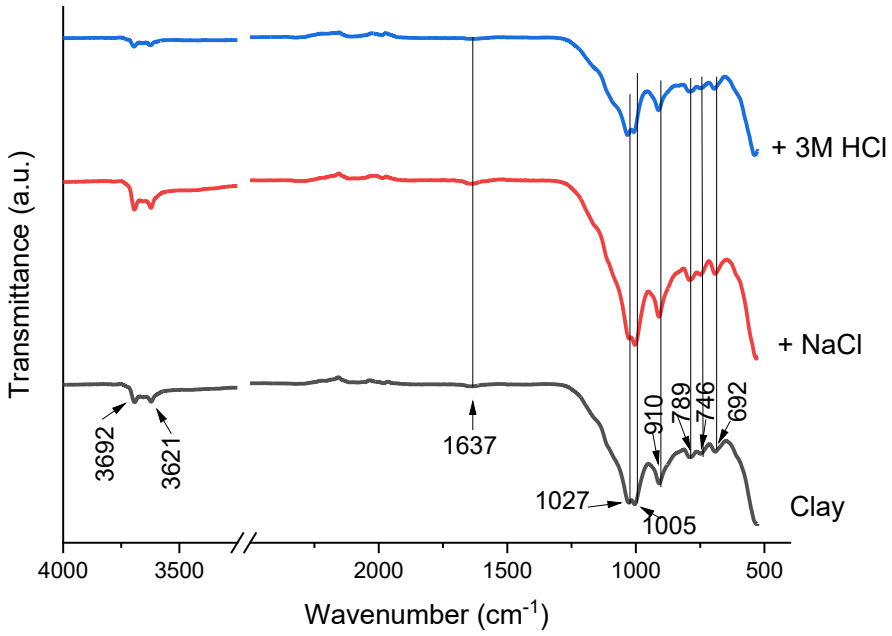


Figure 25 – FTIR spectra of Clay, Na-Clay, and H-Clay

FTIR and Raman spectroscopy. The following bands are present in the spectrum of Chamotte clay (Figure 25): at 3692 and 3621 cm-1 assigned to the stretching vibrations of OH-groups adsorbed on the surface of the mineral; at 1639 cm-1 due to the inner-layer OH(AL-OH) stretching mode; at 1027 and 1005 cm-1 to the Si-O planar stretching; at 910 cm-1 assigned to the inner-surface Al-OH deformation vibrations; at 789 and 746 cm-1 due to symmetric stretching

vibrations of Si-O-Al bonds; and at 692 cm-1 assigned to Mg(Al-OH) vibrations. Na- and H-treatment does not lead to any changes in the FTIR spectrum of clay, which indicates the preservation of the main framework of the material after treatment.

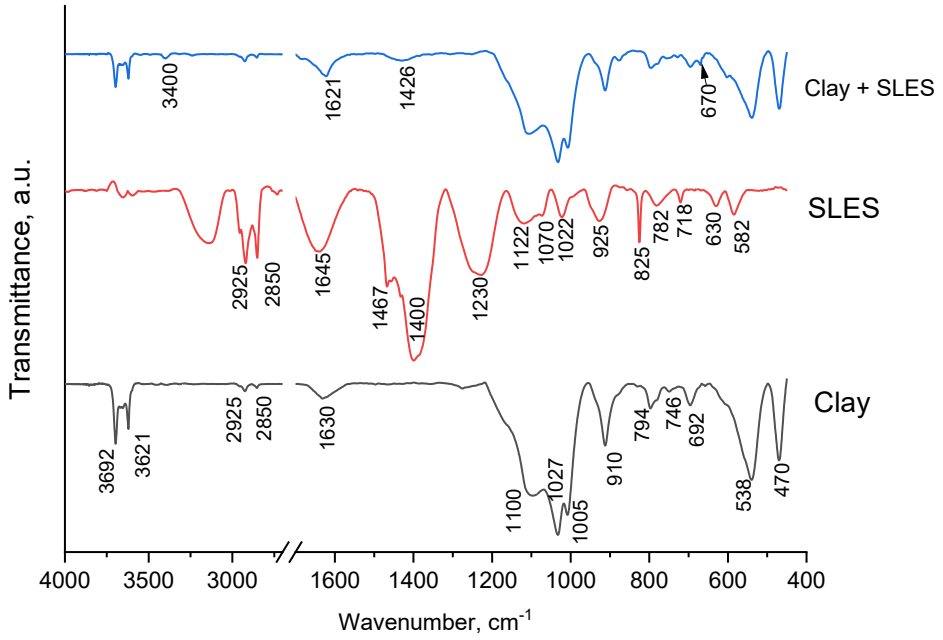


Figure 26 – FTIR spectra of Clay and SLES-Clay

We can notice the appearance of peaks in the region of 1400-1470 cm^{-1} - CH bending, as well as the appearance of a shoulder at 670 cm^{-1} ($C\text{-}CH_2$) in the spectrum of the modified SLES-Clay (Figure 26). This indicates the interaction of SLES molecules with the Clay. It should be noted that the interaction of sulfate groups with the Clay is not observed due to the electrostatic repulsion of anions.

A detailed interpretation of the surfactants' spectra (SLES, DDAB) is presented in paragraph 3.1 of this work.

After modification of clay with DDAB (Figure 27) we can observe changes like with the Zeolite. Intense peaks in the pure DDAB spectrum at 2920 and 2833 cm^{-1} related to asymmetric and symmetric stretching vibrations of methylene groups are apparent in the DDAB-modified clay spectrum, which probably indicates coating of the Clay by DDAB. The very low intensity of these peaks is probably due to the small concentration of the surfactant compared to the amount of the Clay. Changes in other bands in the DDAB-Clay spectrum are not noticeable.

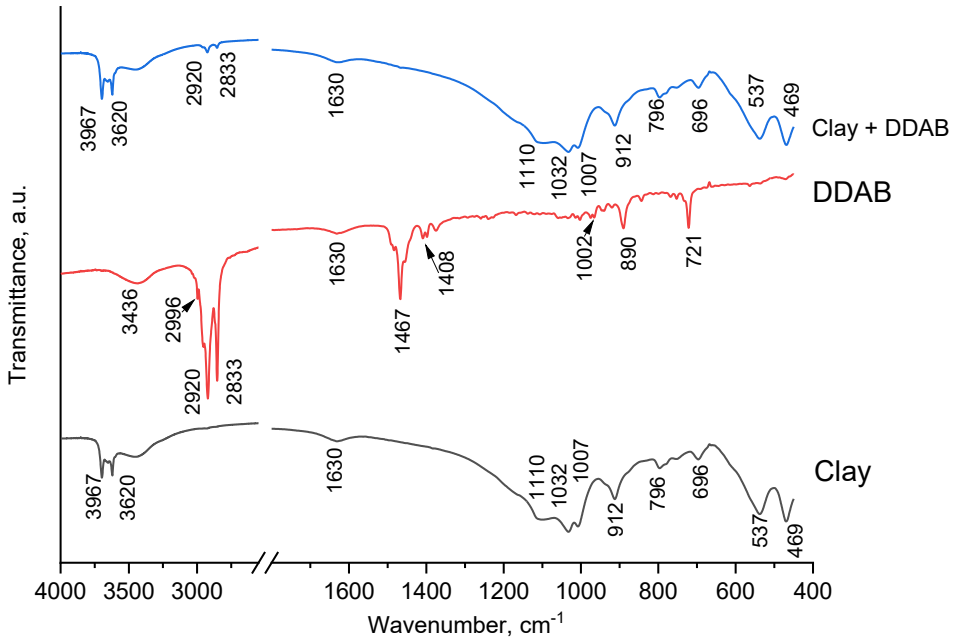


Figure 27 – FTIR spectra of the Clay, DDAB and DDAB-Clay

BET analysis results. The mean specific surface area of the Clay samples (Table 17) indicates changes after treatment. Thus, pre-treatment with sodium and acid increases the surface area from 8.4 m^2/g to 10.9 m^2/g and 15.3 m^2/g, respectively. Na-Clay has bigger pore size (7.2 A) compared to the initial clay (6.9 A). Sodium ions, saturating the surface of the Clay, can lead to electrostatic repulsion, thereby expanding the pores. Acid treatment, on the contrary, leads to a decrease in the pore size to 5.3 A and an increase in the specific surface area due to appearance of secondary porosity.

Modification with DDAB and SLES has no impact on the pore sizes but leads to decrease in surface area to 6.3 and 4.6 m^2/g. This can indicate occupation of part of the adsorption sites on the Clay surface verifying interaction of surfactants with clay during the modification.

Table 17 – Textural properties of the Clay-based materials

Sample	Surface area, m^2/g	Average pore size, Å	Total pore volume, cm^3/g
Clay	8.4	6.9	0.029
Na-Clay	10.9	7.2	0.039
H-Clay	15.3	5.3	0.04
SLES-Clay	6.3	6.9	0.022
DDAB-Clay	4.6	6.9	0.018

Thus, based on the physico-chemical characterization of the obtained adsorbents we can conclude that:

- Na^+-treatment enhances the cation exchange capacity (CEC) of the Zeolite/Clay and their capacity for ion-exchange processes.

- Acid treatment results in a substantial increase in surface area while reducing the exchange capacity relative to the initial materials. High concentrations of acid are unfavorable due to destruction of the Zeolite crystalline framework, while Clay is stable even using high acid concentrations. An optimal acid concentration of 3 mol/L has been determined.

- Pre-treatment with salt or acid provides structural changes to the Zeolite/Clay and affects its interaction with the surfactant modifier.

- The results of IR/Raman spectroscopy and BET analysis provide evidence of the successful modification of Zeolite/Clay with surfactants.

3.2 Heavy metal ions extraction from aqueous solutions onto the adsorbents based on Zeolite and Clay

The following types of sorbents are considered in this work:

- natural zeolite (Zeolite);

- Chamotte clay (Clay);

- Zeolite or Clay modified with an anionic surfactant – sodium laureth sulfate (SLES);

- Zeolite or Clay modified with a cationic surfactant – didodecyl dimethyl ammonium bromide (DDAB).

These types of sorbents were used for adsorption of the following heavy metal (HM) ions: lead (II) [218–220], cadmium (II) [218–220] , strontium (II), manganese (VII) [2], chromium (VI). The original Z and C were used for adsorption of all the above-mentioned HM ions. Modified with anionic SLES – for adsorption of cations (Pb^{2+}, Cd^{2+}, Sr^{2+}), and modified with cationic DDAB – for adsorption of anions ($MnO_4^{2-}, Cr_2O_7^{2-}$). The results are presented in Table 18 [219–221].

Table 18 – The results of HM adsorption onto the obtained adsorbents based on Z and C (C_0 = 100 mg/l, s:l = 1:10, T = 298K, 200 rpm, t = 3 h, pH = 7)

Adsorbent	E, %				
	Pb^{2+}	Cd^{2+}	Sr^{2+}	$Cr_2O_7^{2-}$	MnO_4^-
Zeolite	99.2 ± 0.6	73.4 ± 0.2	49.5 ± 0.4	5.0 ± 0.2	9.2 ± 0.4
Zeolite + SLES	-	97.0 ± 1.5	92.1 ± 0.3	-	-
Zeolite + DDAB	-	-	-	19.6 ± 0.3	12.5 ± 0.6
H-Zeolite + DDAB	-	-	-	80.4 ± 1.3	75.3 ± 0.9
Clay	98.5 ± 1.1	68.3 ± 2.1	41.4 ± 0.7	7.3 ± 0.5	9.9 ± 1.1
Clay + SLES	-	90 ± 0.8	64.3 ± 1.0	-	-
Clay + DDAB	-	-	-	8.2 ± 1.0	13.3 ± 0.7
H-Clay + DDAB	-	-	-	82.5 ± 1.6	78.9 ± 0.8

The initial Zeolite and Clay almost completely extract lead ions from aqueous solutions (the degree of extraction is 98-99%) [219], while they are less effective in relation to cadmium and strontium ions.

Zeolites are reported to have stronger affinity towards Pb ions [222–224]. The adsorption affinity sequence for zeolite and clay can be presented as: $Pb^{2+} > Cd^{2+} > Sr^{2+}$. Let us attempt to explain this trend in terms of acid-base interactions.

It is known that aluminosilicates, in particular zeolites and clays, have acid-base centers. The overwhelming majority of such materials have two types of acid centers – proton-donating Brønsted and Lewis acceptors of electron pairs. As a result of dehydration, during the production process, Lewis acid and basic centers are simultaneously formed on Al-O. In the presence of water molecules, Lewis acid centers are transformed into Brønsted ones [225].

The structure of acid centers of aluminum oxide in the composition of aluminosilicates can be represented as follows (Figure 28):

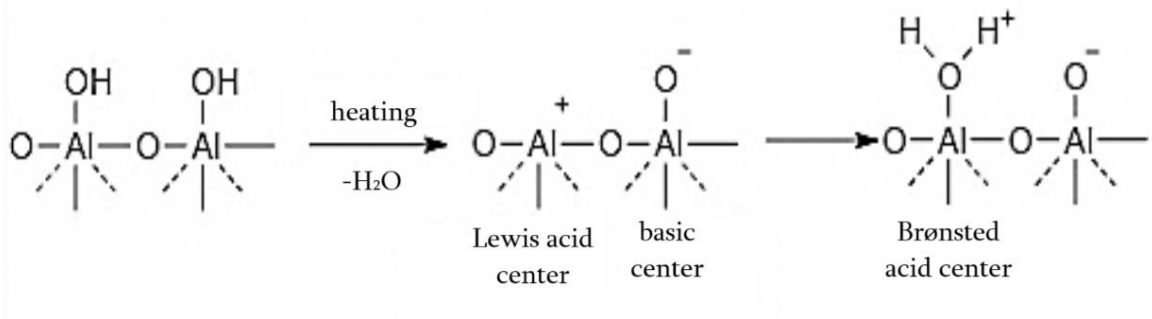


Figure 28 – The structure of aluminum acid centers in aluminosilicates [225]

Thus, the structure of aluminosilicates comprises two categories of basic centers: proton-active (Brønsted) – surface hydroxyl groups (OH-), protonated oxygen bridges (-Si-OH-Al-), and electron-active (Lewis) – coordinatively unsaturated Al^{3+} centers, oxygen anions (≡Si-O^- and ≡Al-O^-). All aforementioned basic centers classify as hard bases under the Pearson LMAO principle, owing to the existence of oxygen groups that are weakly polarized and exhibit enhanced interactions with hard acids. Pb^{2+} is classified as an intermediate acid, Cd^{2+} as a soft Lewis acid, and Sr as a hard Lewis acid, similar to Ca and Ba [226]. According to Pearson's principle [226], the hard basic centers of aluminosilicates are expected to interact more effectively with the hard acid Sr^{2+}, although this is not the case.

Consequently, in the interaction between chamotte clay and the examined metal cations, parameters such as ionic size and charge density assume greater significance.

The adsorption affinity of zeolites for Pb^{2+}, Cd^{2+}, and Sr^{2+} varies due to differences in their ionic properties, hydration energies, and interactions with the zeolite framework. Pb^{2+} has the highest charge density among these ions, which enhances its electrostatic interaction with

negatively charged sites in the zeolite structure. Cd^{2+} is smaller and more hydrated, making its adsorption slightly weaker than Pb^{2+}, while Sr^{2+} has the largest ionic radius and the lowest charge density, leading to weaker electrostatic attraction to zeolites compared to Pb^{2+} and Cd^{2+}.

Hydration energy also plays a crucial role, as lower hydration energy facilitates easier adsorption by allowing ions to shed their water shell and bind to the zeolite surface more readily. Pb^{2+} has a lower hydration energy (−1481 kJ/mol) than Cd^{2+} (−1805 kJ/mol), making it more likely to adsorb onto zeolites. Sr^{2+} has the lowest hydration energy (~−1444 kJ/mol), but its larger size and lower charge density reduce its adsorption strength compared to Pb^{2+}.

In terms of zeolite selectivity and cation exchange capacity (CEC), the adsorption affinity follows the trend $Pb^{2+} > Cd^{2+} > Sr^{2+}$. Pb^{2+} exhibits a strong preference for cation exchange sites due to its high charge density, whereas Cd^{2+} also interacts well but is less preferred than Pb^{2+}. Sr^{2+}, due to its larger size and lower charge density, is generally the least adsorbed of the three.

Modification of Zeolite and Clay by SLES leads to a significant increase in the degrees of extraction of the studied cations – from 73% to 97% for the Zeolite – Cd pair, from 49% to 92% for the Zeolite – Sr pair, from 68% to 90% for the Clay – Cd pair, and from 41% to 64% for the Clay – Sr pair.

Figure 28 shows the interaction scheme of Zeolite/Cclay and SLES. The surface of zeolite contains hydroxyl (OH) groups and cations of exchangeable metals, which are electrostatically bonded to the free oxygen atoms of the SiO_4 tetrahedra. The IR spectra (Figure 20) of Z-SLES and C-SLES (Figure 26) exhibit a reduction in the strength of peaks associated with OH group vibrations in the range of 3000–4000 cm^{-1} and approximately 1600 cm^{-1}. Hydroxyl groups in zeolites and clays exist as water adsorbed within the pores or channels of the aluminosilicate [189]. Consequently, it is assumed that SLES molecules can engage in exchange processes with water molecules, thereby being kept within the mineral's pores (interaction type an in Figure 29):

$$CH_3(CH_2)_{10}CH_2(OCH_2CH_2)_nOSO_3^- + HO\text{-}H = CH_3(CH_2)_{10}CH_2(OCH_2CH_2)_nOSO_3H + OH \quad (25)$$

This hypothesis is also supported by the fact that H-z sorbs a larger amount of SLES than the original Clay (Table 12). That is, the excess positive charge, for example in the form of protons, does indeed lead to better adsorption of SLES on the zeolite/clay surface.

Exchange cations (Na, K, Ca, Mg) are also present in the zeolite channels and clay pores [227], and can also act as a source of excess positive charge for electrostatic attraction of the sulfo group of SLES (interaction type b in Figure 29).

With increasing concentration, SLES can be sorbed in the form of a bilayer (interaction c in Figure 29) due to the hydrophobic interaction of the "tails".

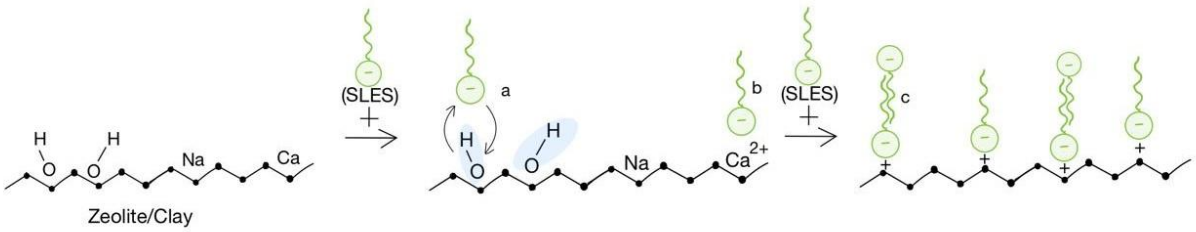


Figure 29 – The interaction scheme of Zeolite/Clay with SLES

Figure 30 shows the interaction scheme of heavy metal ions with Zeolite or Clay modified by SLES. In this case, two types of interaction are possible: 1) electrostatic attraction of the positively charged metal cation to the SLES sulfo group of the second layer; 2) donor-acceptor bond between the metal ion and the free electron pair of oxygen of the SLES ethoxy group.

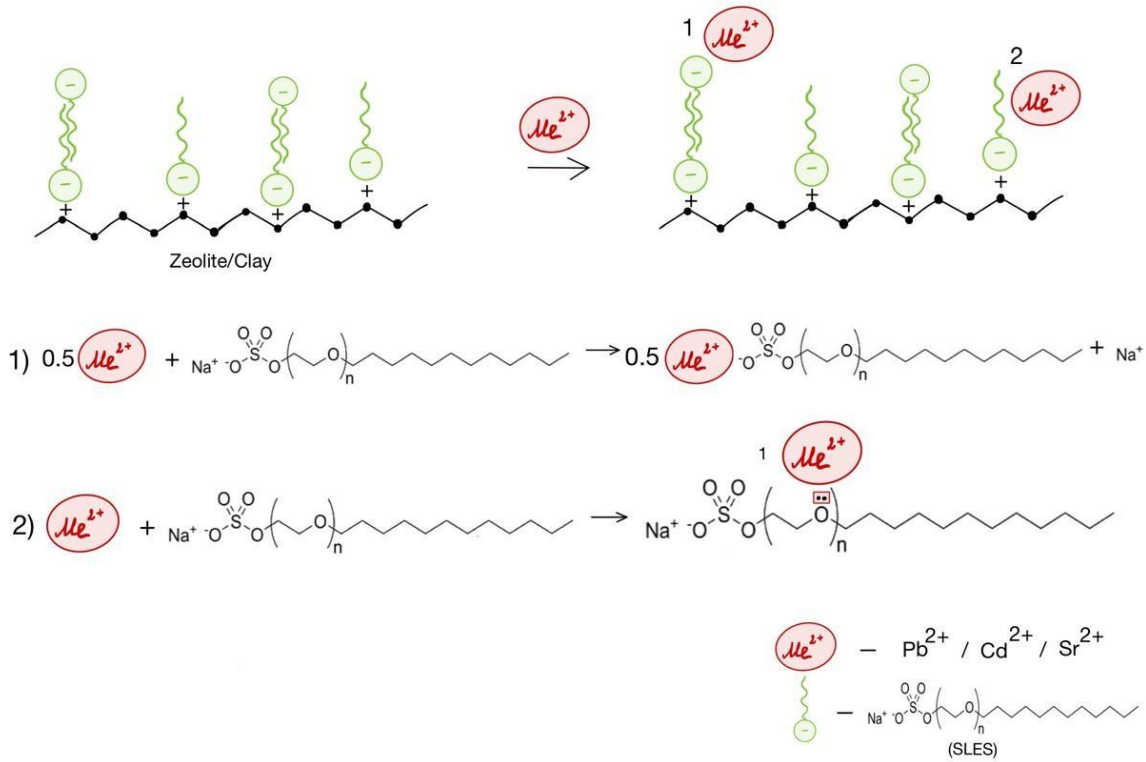


Figure 30 – The interaction scheme of HM cations (Pb, Cd, Sr) and SLES-Zeolite/SLES-Clay

The surface of aluminosilicates is predominantly negatively charged, resulting in insufficient active centers for anion adsorption. The anion extraction efficiencies are 5.0% and 9.2% for Zeolite, and 7.3% and 9.9% for Clay, corresponding to dichromate and permanganate ions, respectively. In this case, adsorption likely occurs due to complexation with cations on the surfaces of Zeolite and Clay.

The incorporation of DDAB into the aluminosilicate composition somewhat enhances the anion extraction efficiency; nevertheless, optimal results (about 75-83% extraction) are attained for Zeolite and Clay that have undergone preliminary acid treatment and subsequent modification with DDAB [221]. Acid treatment is typically conducted to enhance the Si/Al ratio. A low ratio renders the Zeolite surface hydrophilic, whereas a high ratio turns it hydrophobic [35]. Consequently, a more homogeneous dense layer of DDAB is established on acid-treated Zeolite and Clay, which enhances the adsorption of negatively charged anions.

It is assumed that the DDAB molecule can interact with the Zeolite surface through electrostatic attraction with OH-groups adsorbed on the surface (interaction type a in Figure 31). The N+ can also participate in ion-exchange processes with exchangeable metal ions on the zeolite surface (interaction type b in Figure 31). These assumptions are confirmed by the results of Raman spectroscopy (Figure 19), where the disappearance of some zeolite peaks (at 180, 330, 1098 and 1212 cm^{-1}) is noticeable, as well as a decrease in the intensity of peaks at 288, 476 and 508 cm^{-1}. The above changes indicate changes in the degree of zeolite hydration and the related position of the cations in the zeolite framework [187]. Similar changes are noticeable in the IR spectrum of the Chamotte clay after DDAB modification (Figure 27). Subsequent increase in DDAB concentration leads to bilayer formation and recharging of the Zeolite/Clay surface (interaction with), which is typical for surfactant-modified aluminosilicates [30]. Thus, the resulting DDAB bilayer leads to an excess of positive charge on the Zeolite/Clay surface, which attracts dichromate/permanganate anions (Figure 32).

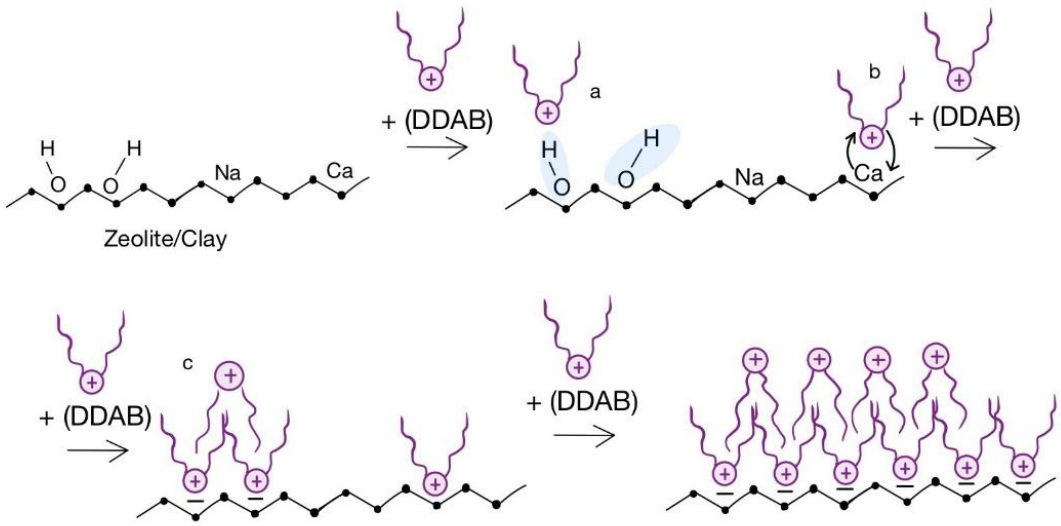


Figure 31 – The interaction scheme of Zeolite/Clay with DDAB

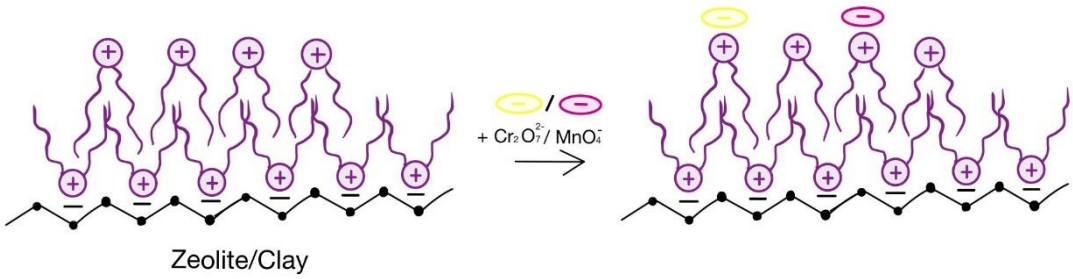


Figure 32 – The interaction scheme of $Cr_2O_7^{2-}/MnO_4^-$ anions with DDAB-Zeolite/DDAB-Clay

As a result, it has been determined that the initial Z/C can serve as excellent sorbents for lead ions without prior treatment. The alteration of Zeolite/Clay with an anionic surfactant, specifically SLES, results in enhanced sorption activity towards heavy metal cations, namely cadmium and strontium. The incorporation of the cationic surfactant DDAB effectively enhances the extraction efficiency of HM anions, specifically dichromate and permanganate.

Thus, surfactants serve as efficient modifiers for regulating the charge and recharge of aluminosilicate surfaces, as well as for the selective adsorption of heavy metal ions on the examined sorbents.

3.3 Investigation of optimum conditions for the adsorption of lead ions onto Clay

Today, elucidation of the mechanisms of various processes, in particular adsorption, is an urgent task of modern chemistry. Since the systems studied in this work are multicomponent, and determining the interaction mechanism is a rather complex task, the simplest adsorbent/pollutant system of Clay + Pb^{2+} was chosen as a model for a more detailed study. The choice of Clay is due to the fact that it consists of the minerals mullite and kaolinite (Figure 24), which are similar in their structure, and mullite is a product of heat treatment of kaolinite [228,229]. The zeolite contains anorthite (Figure 13), which is part of the feldspar group and is a mineral with a completely different structure [187,194]. The selection of lead is based on the observation that it is entirely (100%) removed by the initial materials among the examined heavy metal ions.

3.3.1 Effect of sorbent mass on the adsorption of lead ions onto Clay

It is very important to determine the optimum solid/liquid ratio during adsorption since the most efficient adsorbents are those which show highest pollutant uptake and the lowest cost. Figure 33 displayed the adsorption of Pb^{2+} on Clay as a function of solid content. The adsorption amount (q_e) decreases with solid content increase. This phenomenon can be ascribed to the assumption that more active adsorbent spots remained unsaturated during the Pb^{2+} adsorption process. Similar observations have also been reported for Cr(VI) adsorption to activated carbon [230] and Pb^{2+}/Ni^{2+} adsorption onto zeolite [69]. The adsorption percentage increases with increase of adsorbent mass

and reaches 100% after 0.5 g of clay per 50 ml of solution at initial concentration of Pb^{2+} 50 mg/L. Thus, the solid/liquid ratio of 1:10 is the optimum for efficient adsorption of lead (II) ions onto Clay.

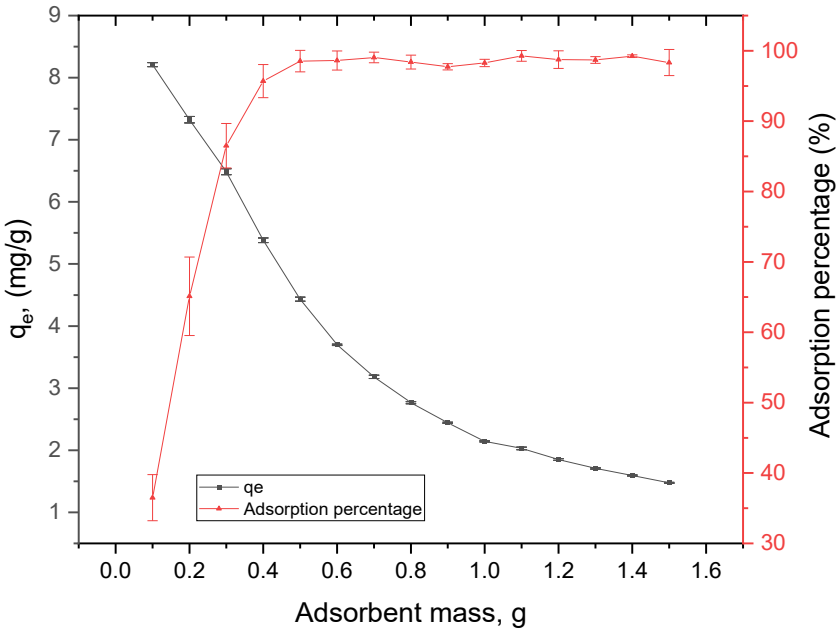


Figure 33 – Effect of adsorbent mass on the adsorption percentage and q_e of Pb(II) on Clay (C_0 = 100 mg/l, T = 298K, 200 rpm, t = 3 h, pH = 7)

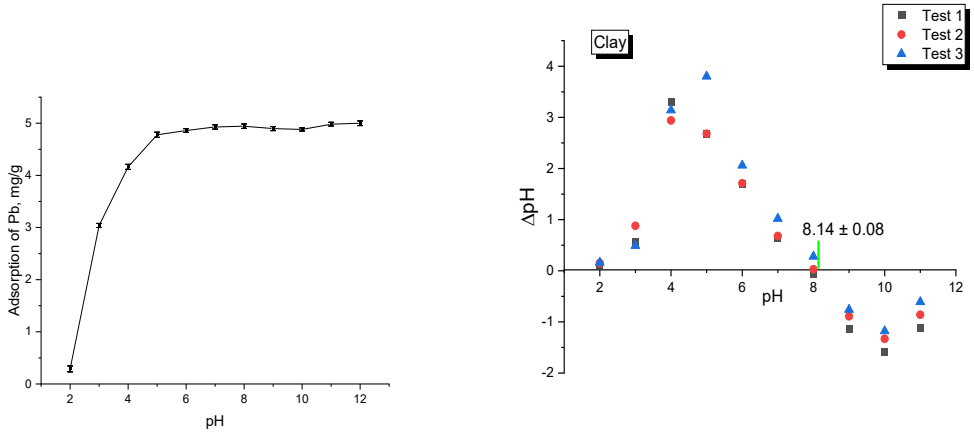
3.3.2 Effect of pH on the adsorption of lead ions onto Clay

The effect of pH on the adsorption of Pb (II) ions onto Clay was studied in the pH range 2-12 (Figure 34a). As we can see from the figure, adsorption values at acidic pH < 5 are low. This is due to the positive charge of clay surface, which causes repulsion of Pb^{2+} cations.

To specify the surface charge, the point of zero charge (PZC) of Clay was determined (Figure 34b). PZC is a pH at which the surface of substance is neutral, i.e. the amount of positive and negative charges is equal to each other. PZC values could help predict the adsorption affinity towards pollutants. Substrates with low PZC values would be best suited to treat effluents contaminated with cations, while substrates with high PZC values would be more appropriate to capture anions [206]. The surface charge is negative at $pH>pH_{pzc}$ and positive at $pH<pH_{pzc}$ [207]. As we can see, the studied material has quite high values of PZC equal to (8.14 ± 0.08), i.e. the adsorption of lead cations would be best at alkaline pH.

Thus, good adsorption performance at pH 6 – 8 is because it is close to PZC value and repulsion between positive charge of the surface and cations is not strong. At pH>8 there are two factors affecting the extraction degree of Pb^{2+} ions: electrostatic attraction between negative surface and positively charged ions, and precipitation of lead hydroxide to the adsorbent surface.

However, it was decided to perform further experiments at natural pH of the $Pb(NO_3)_2$ solution without any adjustment (which is in pH range between 6 and 7), in order to avoid hydroxides precipitation and miscalculate real values of adsorption.



a b

Figure 34 – a) Effect of pH on adsorption of Pb^{2+} on Clay (C_0^{Pb2+} = 50 mg/L, sorbent-solution ratio 1:10, T=298 K, t=3h, 200 rpm); b) PZC value of Clay

3.3.3 Effect of initial concentration and adsorption isotherms of lead ions by Clay

The adsorption performance depends on the concentration of adsorbed substance. The results of studying the process of lead (II) ions adsorption from solutions with concentrations of 5, 10, 20, 50, 100, 200, 500 mg/l are in Figure 35. With the increase in solution concentration, the adsorption capacity of Clay increased gradually. This was because a greater concentration of the solution produces a greater driving force for adsorption [231]. At high concentrations more than 200 mg/L the adsorption tends to equilibrium occupying all available sites on the clay surface.

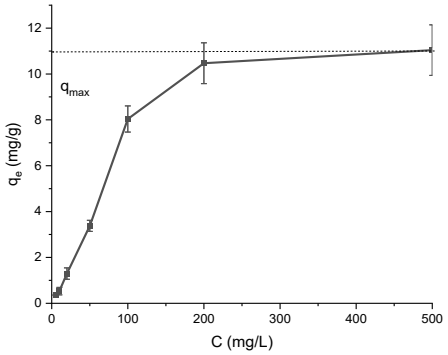


Figure 35 – Pb^{2+} ions adsorption isotherm on Clay
(s:l = 1:10, T = 298K, 200 rpm, t = 3 h, pH = 7)

According to IUPAC classification, the isotherms of lead (II) ions with the studied clay correspond to the type I isotherm. It 'approaches a limiting value' and usually is used to describe adsorption on microporous solid adsorbents having relatively small external surfaces (e.g.

activated carbons, molecular sieve zeolites and certain porous oxides), the limiting uptake being governed by the accessible micropore volume rather than by the internal surface area [232]. Also, such isotherms are called Langmuir isotherm. The adsorption capacity q_{max} reached 11.04 mg/g for Clay.

The parameters obtained from non-linear fittings to the isotherm models are given in Table 19Table *19*.

Table 19 – Parameters obtained when fitting the experimental data to the non-linear equations of isotherm models

Theory	Parameters	Values	Error Functions					
			R^2	SSE	MSE	SAE	ARE	RMSE
Two-parameter models								
Langmuir	K_L, L/mg	1.70	0.981	2.51	0.36	2.96	14.95	0.60
	q_m, mg/g	10.95						
Freundlich	n	5.51	0.819	24.17	3.45	11.26	139.09	1.86
	K_F	4.38						
Temkin	K_T, L/mg	88.91	0.925	9.98	1.43	6.05	28.15	1.19
	B_T, kJ/mol	2.10						
Dubinin-Radushkevich	K_{D-R}, mol^2/kJ^2	3.00 $*10^{-8}$	0.415	78.10	11.16	13.60	71.43	3.34
	q_{mD} , mg/g	11.07						
Three-parameter models								
Langmuir-Freundlich	K_{LF}	1.70	0.981	2.51	0.36	2.96	14.95	0.60
	q_{mLF}, mg/g	10.95						
	β	1.00						
Redlich-Peterson	B, L/g	1.70	0.981	2.51	0.36	2.96	14.95	0.60
	A, L/mg	18.66						
	β	1.00						
Sips	K_S, L/mg	2.39	0.987	1.72	0.25	3.08	39.86	0.50
	q_{mS}, mg/g	10.81						
	β	1.64						
Fritz-Schlunder 3	K_{FS}, L/mg	1.28	0.983	2.28	0.33	3.34	18.71	0.57
	q_{mFS}, mg/g	12.66						
	α	1.03						
Toth	K_T	0.49	0.994	0.80	0.11	1.97	26.68	0.34
	q_{mT}, mg/g	10.76						
	α	3.57						
Four-parameter models								
Fritz-Schlunder 4	B	1.33	0.982	2.37	0.34	3.22	16.00	0.58
	A	16.41						
	α	0.98						
	β	1.00						

Table 19 (continued)								
Baudu	b_0	0.43	0.987	1.72	0.25	3.11	39.60	0.50
	q_{m0}, mg/g	25.21						
	x	-2.62						
	y	1.61						
Five-parameter model								
Fritz-Schlunder 5	K_{1FS}	3.60	0.982	2.37	0.34	3.22	16.00	0.58
	K_{2FS}	1.33						
	q_{m0}, mg/g	4.56						
	m_1	0.98						
	m_2	1.00						

As we can see from Table 19, when comparing R^2 values, the experimental data fit the non-linear equations of the models in the following range: Toth > Sips = Baudu > Fritz-Schlunder 3 > Fritz-Schlunder 4 = Fritz-Schlunder 5 > Langmuir-Freundlich = Langmuir = Redlich-Peterson > Temkin > Freundlich > Dubinin-Radushkevich.

Almost all used models, except for Dubinin-Radushkevich and Freundlich, fit the experimental data quite well. However, the models of Toth, Sips and Baudu describe the isotherm better. It is obvious that the experimental isotherm is the Langmuir type isotherm, assuming monolayer adsorption with limited adsorption capacity. But the values of error functions are much less for Toth model than for the other ones. The Toth model is a modified form of the Langmuir model that allows significantly decrease the errors between experimental data and predicted value [233]. Thus, it is better to use the Toth isotherm model to get more accurate data when fitting the experimental data of Pb(II) ions adsorption onto Clay.

Because the Langmuir model also fits well, we calculated the separation factor (K_R) (eq. (26), which is useful to determine whether the separation is or not favorable in batch systems, can be calculated from the Langmuir isotherms[12,234].

$$K_R = \frac{1}{1 + K_L C_0} \tag{26}$$

where K_L is the Langmuir constant (L/mg), C_0 is the initial concentration of Pb^{2+} (mg/L). If $K_R > 1$ the adsorption is not favorable; if $K_R = 1$ the adsorption is linear; if $0<K_R<1$ the adsorption is favorable; and if $K_R = 0$ it is irreversible. As it can be seen from fig. 8, the separation factors for Clay lie within $0<K_R<1$, i.e. adsorption is favorable. With an increase in the concentration of metal ions the separation factor $K_R \rightarrow 0$, i.e. tends to be irreversible (Figure 36).

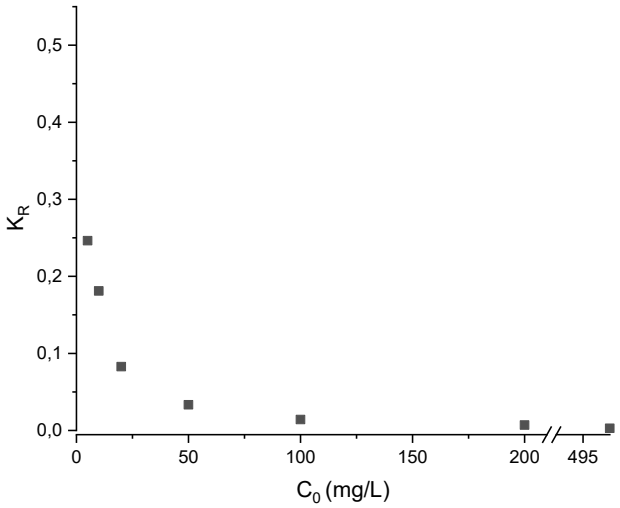


Figure 36 – Separation factors determined from Langmuir isotherms applied to Clay

3.3.4 The effect of contact time and kinetics of Pb adsorption on Clay

a) Reaction kinetic models

By fitting the experimental data to the linear regressions (Equations 12-13) the following results were obtained (Table 20):

Table 20 – Parameters of linear fitting of pseudo-first and pseudo second order models of Pb^{2+} adsorption on zeolite and Clay (s:l = 1:10, T = 298K, 200 rpm, t = 3 h, pH = 7)

C, mg/L	R^2, n=1	R^2, n=2
5	0.425	0.956
10	0.267	0.992
20	0.863	1.000
50	0.414	0.999
100	0.996	1.000

Judging by the values of the correlation coefficient R^2, the adsorption of lead ions is better described by the pseudo-second order model for Clay. However, for some concentrations, controversial values were obtained. For example, at an initial concentration of lead ions of 100 mg /L, the R^2 values are close to one for both kinetic models. The same ambiguity of the results is observed at initial concentrations of lead ions of 20 mg/L.

Based on the results of non-linear regression (Table 21), very similar values of R^2 were obtained for both the pseudo-first and the pseudo-second order models. In this case the error analysis can solve the problem: $AARD_y$ and R^2 are contradictory indicators, i.e. if $R_1^2 > R_2^2$ then $AARD_y1 < AARD_y2$ and vice versa [153]. In the case of metal adsorption of the initial concentration of 100 mg/L, R^2 values equal to 1 were obtained, but the value of $AARD_y2 = 0.0364 < AARD_y1 = 0.1006$. Therefore, in this case, the pseudo-second-order model is better suited for describing the process.

The parameters obtained using pseudo-nth order model (Eq. 18) to get the accurate values are shown in Table 21.

Table 21 – Results of non-linear one-parameter fit using Eqs. 6 – 10 for adsorption of Pb^{2+} on Clay

Kinetic model	Initial concentration, mg/L						
Pseudo-first order	5	10	20	50	100	200	500
$q_{e.exp}$(mg/g)	0.3586	0.5321	1.2957	3.3785	8.0688	10.4740	11.0400
$q_{e.cal}$ (mg/g)	0.3586	0.5321	1.2957	3.3785	8.0688	10.4740	11.0400
K_1 (min^{-1})	0.0281	0.0748	0.1146	0.1107	0.1482	0.0322	0.0275
R^2	0.9649	0.9998	0.9999	0.9999	1.0000	0.9813	0.9618
$AARD_y1$	8.2004	0.8286	0.2086	0.3539	0.1006	16.8019	36.8533
Pseudo-second order							
$q_{e.exp}$(mg/g)	0.3586	0.5321	1.2957	3.3785	8.0688	10.4740	11.0400
$q_{e.cal}$ (mg/g)	0.3547	0.5310	1.2947	3.3754	8.0663	10.3862	10.9234
K_2 (g/mg*min)	0.1799	0.6446	0.7076	0.2244	0.2849	0.0078	0.0059
R^2	0.9998	0.9999	0.9999	0.9999	1.0000	0.9999	0.9998
$AARD_y2$	1.4868	0.2514	0.0921	0.1117	0.0364	1.1414	1.4732
Pseudo-nth order							
Order N	2.0437	2.0000	2.2412	2.7531	2.8313	2.0000	2.0000
$q_{e.exp}$(mg/g)	0.3586	0.5321	1.2957	3.3785	8.0688	10.4740	11.0400
$q_{e.cal}$ (mg/g)	0.3420	0.5289	1.2937	3.3650	8.0568	10.3691	10.9140
K_n ($(mg/g)^{1-n}$/min)	0.2207	0.7009	1.3217	0.7468	1.2651	0.0079	0.0059
R^2	0.9999	0.9999	0.9999	0.9999	1.0000	0.9999	0.9998
$AARD_yn$	0.5419	0.2316	0.6960	1.2306	0.4614	1.1296	1.4667

The orders obtained by the pseudo n-th order kinetic model were found to be very close to 2. Predicted adsorption capacities $q_{e.cal}$ obtained by the pseudo-first order model coincide with experimental equilibrium capacities $q_{e.exp}$ in all cases. However, R^2 and $AARD_y$ values indicate that the pseudo-second order model was more suitable for the complete kinetic curve, not only the final values of q_e. The values of K_n were closer to K_2 of the pseudo-second order model indicating that the adsorption kinetics was close to the second-order.

Also, the values of K_2 tend to increase with the growth of initial concentration and then decrease for initial metal concentration more than 50 mg/L. The increase in the rate is initially associated with an increase in the concentration gradient, the "driving force" of adsorption. The subsequent decrease in the rate of adsorption at high concentrations is because all adsorption centers are quickly filled and form a monolayer according to the Langmuir model, and the process does not proceed further.

b) Diffusion kinetic models

In this work, the results were analyzed using the intraparticle diffusion models of Weber and Morris and Dumwald-Wagner, as well as Chemisorption diffusion model (Table 22).

Table 22 – Diffusion parameters for the adsorption of Pb(II) onto Clay

Diffusion model	Initial concentration of Pb^{2+}, mg/L						
	5	10	20	50	100	200	500
Weber-Morris							
k_i (g/mg $min^{0.5}$)	0.0028	0.0010	0.0010	0.0030	0.0024	0.0675	0.0867
C	0.2748	0.5021	1.2640	3.2729	7.9527	8.4248	8.5225
r^2	0.2122	0.3495	0.4798	0.7570	0.8040	0.3001	0.2089
Dumwald-Wagner							
K_{DW}. min^{-1}	0.0242	0.0161	0.0193	0.0067	0.0067	0.0265	0.0619
r^2	0.8232	0.8365	0.7427	0.9633	0.9911	0.9627	0.9313
Intercept	0.0328	0.6177	0.8622	1.0916	1.5601	0.1425	0.9004
Chemisorption Diffusion							
K_{CD} (mg/g $min^{0.5}$)	0.0533	0.8492	5.6465	14.3266	106.3830	2.7917	1.6477
q_{CD} (mg/g)	0.6599	0.5631	1.3075	3.3956	8.0775	13.6986	20.6612
r^2	0.6321	0.9801	0.8255	0.9447	0.9619	0.7762	0.6688

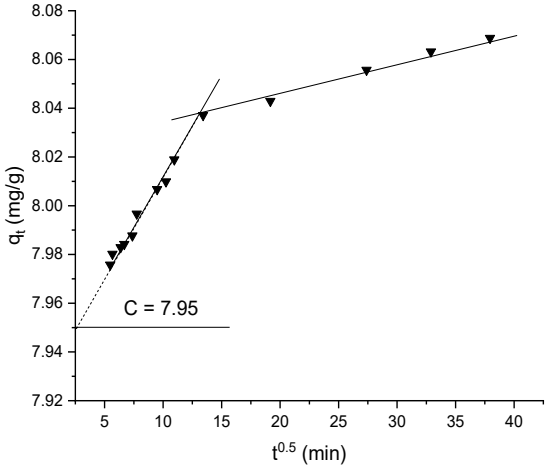


Figure 37 – Intraparticle diffusion plots (Weber-Morris model) for adsorption of Pb(II) onto Clay (b) (C_0 = 100 mg/L, T = 298 K, 50 rpm, pH = 7, t=24 h)

As we can see from Table 22, the plot obtained by Weber-Morris intraparticle diffusion model is not a straight line (R^2 <<1) and intercept value C is not equal to 0, i.e. the plot does not pass through the origin. It means that the adsorption of Pb(II) onto Clay is not controlled by one step. It should be noted that the values of intercept C increase with concentration growth, i.e. the contribution of the surface adsorption in the rate-limiting step is greater for bigger concentrations. It was also observed that the C values are quite big for Clay, which tells about a high amount of surface adsorption onto the Clay. It can be seen from Figure 37, where the plot exhibits two intersecting lines. The first line refers to the diffusion of metal ions from the bulk solution to the

liquid film on the adsorbent surface (surface diffusion). The second line – to the diffusion of metal ions across the liquid film on the adsorbent surface (intraparticle diffusion) [183].

Dumwald-Wagner parameters are given in Table 22. R^2 values, in this case, are much closer to 1, i.e. the plot gives a straight line, but does not pass through the origin. As intercepts are not equal to 0, then we can assume that film diffusion is a rate-limiting step. These results have shown that the mechanism of Pb(II) adsorption onto Clay is complex and involves both film diffusion and intraparticle diffusion steps.

That's why the Chemisorption Diffusion model was applied to experimental data. Values of q_{CD}, K_{CD} and R^2 obtained by Chemisorption Diffusion model are in Table 22. The predicted adsorption capacities q_{CD} were found to be a little higher than the experimental ones. The chemisorption diffusion rates K_{CD} tend to increase with concentration until reach maximum at C_0 = 100 and then decrease. The increasing rate of chemisorption-diffusion (K_{CD}) indicates that both diffusion and chemisorption processes become increasingly important in the rate-determining step. The decrease in high concentration is due to the fulfillment of the Langmuir monolayer. In our case, adsorption occurs due to the ion-exchange processes with the exchange cations present on the surface of Clay.

3.3.5 The effect of temperature and thermodynamics of Pb adsorption on Clay

Thermodynamic parameters were calculated to describe Pb^{2+} adsorption behavior on Clay. The experiments were held at 15˚C, 25 ˚C, 35 ˚C and 45 ˚C.

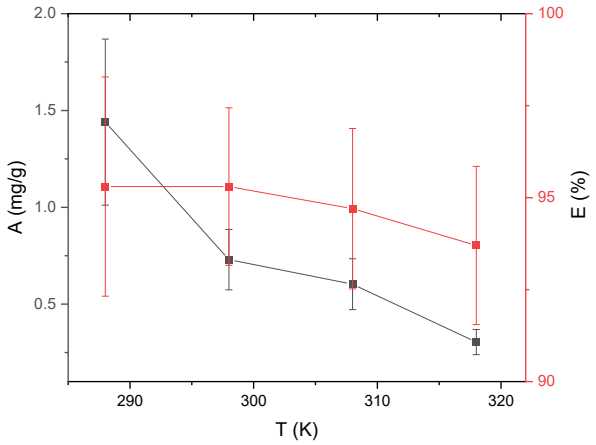


Figure 38 – The effect of temperature on adsorption (A, mg/g) and extraction degree (E,%) of Pb on Clay (C_0 = 100 mg/l, s:l = 1:10, 200 rpm, t = 3 h, pH = 7)

Table 23 – Thermodynamic parameters of Pb^{2+} adsorption on lay

$lnK_d = -\frac{\Delta H^0}{RT} + \frac{\Delta S^0}{R}$	ΔH^0, kJ/mol	ΔS^0, J/mol*K	$-\Delta G^0$, kJ/mol	R^2
$lnK_d = -\frac{2241.30}{T} + 3.35$	-18.63 ± 2.56	27.89 ± 0.07	1.06 – 0.94	0.842

The adsorption and extraction rates of lead ions by Clay decrease with increasing temperature (Figure 38). As can be seen from Table 23, all the ΔG values are negative, i.e. the adsorption process is spontaneous in the forward direction. ΔH° value is found to be negative, which means that adsorption is exothermic. The exothermicity of the Pb^{2+} ions adsorption onto clay minerals has also been reported in Ref. [235]. Generally, an exothermic adsorption process signifies either physisorption or chemisorption, so the absolute values of ΔH° should be concerned [236]. It is known that $\Delta H° \geq 80$ kJ/mol indicated as a starting point for chemisorption enthalpies [183]. In our case, the absolute value of adsorption enthalpy is less than 80 kJ/mol, i.e. it is *physisorption* for Clay.

Positive values of ΔS° show an association between the process of adsorption in this case and increased disorder in the surface of solid/solution [215]. The positive value is due to the passage of a large number of ions from the sorbent into the solution, which indicates active ion-exchange processes. The negative adsorption entropy indicates a decreased randomness at the solid/solution interface during adsorption [237].

Thus, studying the effect of various factors on the process of lead ion adsorption on Clay revealed the following findings:

- The solid/liquid ratio of 1:10 is the optimum for efficient adsorption of lead (II) ions onto Clay.

- Optimal adsorption occurs at pH levels exceeding 6, although pH values above 8 may lead to inaccuracies in the actual adsorption measurements, prompting the decision to conduct additional experiments within the pH range of 6 to 7.

- Saturation of active centers of Clay occurs at initial concentrations of lead solution > 200 mg/L.

- Based on the analysis of various isotherm models, it was established that the adsorption process in the Clay-Pb system is described by the Langmuir isotherm, and the use of the Toth model can significantly reduce the error in modeling the values of sorption capacity.

- A study of process kinetics revealed that the interaction of Clay with Pb aligns with the pseudo-second-order model.

- The application of diffusion kinetic models demonstrated significant surface adsorption (Webber-Morris model), with both film and intraparticle diffusion stages contributing to the rate-limiting step (Dumwald-Wagner model), and adsorption occurring via ion-exchange (Chemisorption Diffusion model).

- An increase in temperature results in a reduction in lead ion extraction, with lead adsorption on Clay being exothermic. The calculated Gibbs energy values indicate the spontaneity of the

adsorption process, the enthalpy value suggests physisorption, and the entropy value reflects active ion-exchange processes.

3.3.6 The mechanism of adsorption of Pb(II) ions on Clay

To consider the mechanism of interaction between Clay and Pb^{2+}, let us briefly consider the structure of Clay. It is known that in the structure of kaolinite, aluminum is present as a binding layer of AlO_6 octahedra [238], or more precisely $[AlO_2(OH)_4]$. Four oxygen atoms in the aluminum-oxygen octahedron $[AlO_2(OH)_4]$ exist in the form of hydroxyl groups and share with the adjacent aluminum atoms, while the other two oxygen atoms are connected to the silicon atoms in the siliconoxygen tetrahedron. Six Al atoms in the Al−O octahedron layer constitute a hexagonal Al ring by sharing O atoms. On the other hand, six Si atoms in the silicon-oxygen tetrahedron layer construct a hexagonal silicon ring by sharing O atoms [238].

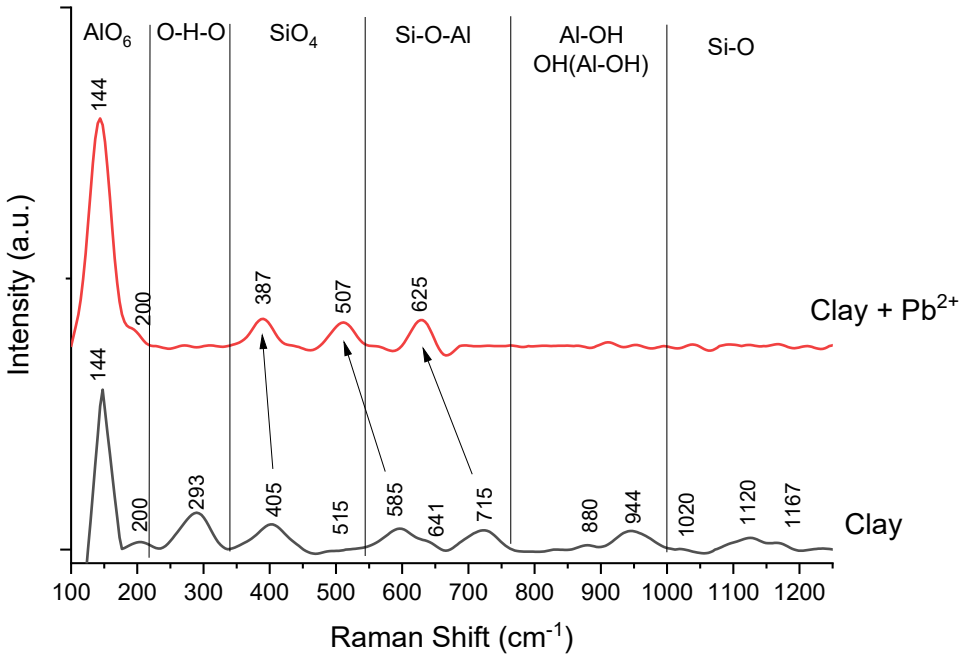
However, Clay is kaolinite that has been processed at very high temperatures. There have been many studies on the thermal conversion process of kaolinite, which is divided into three stages: (1) the elimination of surface adsorbed water, (2) dehydroxylation, and (3) thermal decomposition and conversion. The dehydroxylation of kaolinite is substantially consistent with the removal of water molecules [239].

The dehydroxylation of kaolinite will be accompanied by the transformation of the Al coordination number, and metakaolin will convert to mullite and cristobalite at temperatures higher than 1100 °C. In mullite Al atoms exist in III/IV/V-coordinated forms. Li et.al. [238] established that V/IV-coordinated Al is beneficial for the adsorption of PbO and $PbCl_2$ during coal combustion. Also, PbO is the most stable form of Pb adsorbed on the surface of kaolinite. This conclusion might be true for the system Clay-Pb, and Clay (predominantly mullite) can be considered as a more effective and promising sorbent for lead-containing compounds than kaolinite.

Figures 40-41 show the IR and Raman spectra of Clay before and after adsorption of lead ions.

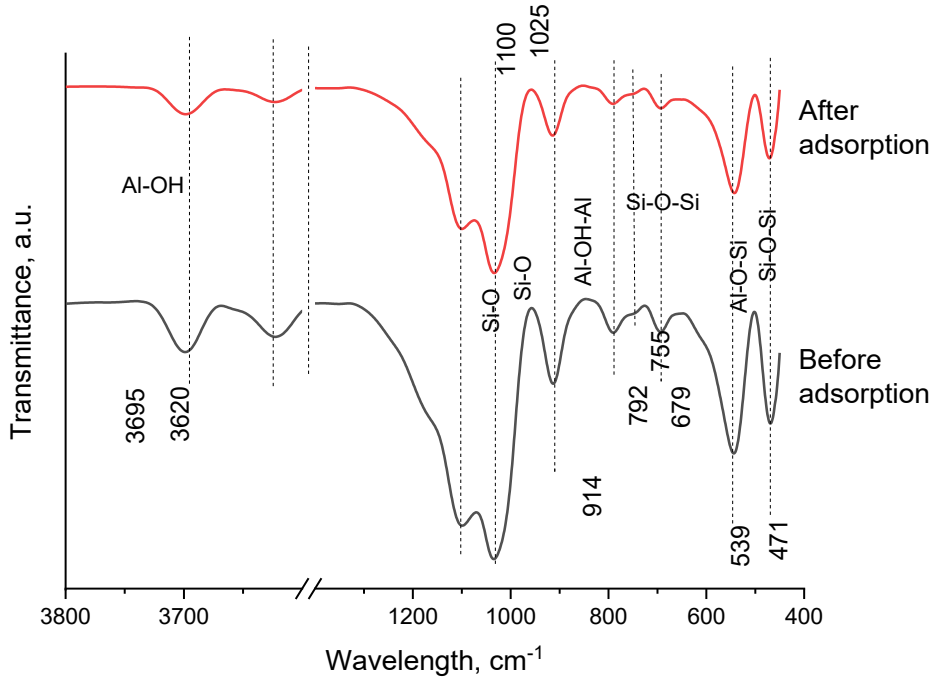
In the IR spectrum of Clay after adsorption, a decrease in the intensity of all peaks characteristic of the inner-layer OH(AL-OH) stretching mode is observed. A decrease in the intensity of the peaks characteristic of Si-O, Si-O-Si bonds indicate the interaction of lead ions with SiO_4 tetrahedra. The intensity of the peaks at 914 cm^{-1} and 539 cm^{-1}, characteristic of stretching vibrations of Al-O and Si-O-Al decreases due to intercalation of Pb ions into the interlayer of the clay [240]. The peaks at 3620 cm^{-1} and 3695 cm^{-1} represent the internal hydroxyl group and inner surface hydroxyl group, respectively. A decrease in the intensity of these peaks also indicates the interaction of OH groups with lead ions. The original form of water in kaolinite

is the hydroxyl group on the Al-O layer [238], hence it is clear that Pb ions combine with AlO_6 octahedrons.



a

Figure 39 – Raman spectra of Clay before and after adsorption of Pb^{2+}



b

Figure 40 – FTIR spectra of Clay before and after adsorption of Pb^{2+}

The Raman spectrum of Clay shows a large peak characteristic of the kaolinite and mullite phases at 144 cm^{-1} from the stretching vibrations of the AlO_6 octahedrons [241]. A small peak at 200 cm^{-1} describes the A_1g mode of AlO_6 octahedron. Peaks at 293, 408, and 944 are characteristic of the crystalline mullite phase, which was formed during calcination of kaolinite at a temperature above 1500 °C and are related to vibrations of the O-H-O triangle, SiO_4 tetrahedron and OH vibration, respectively. The peak at 585 is for SiO_4 tetrahedron stretching mode. A weak peak at 515 corresponds to anatase phase (TiO_2) present in kaolinite [242]. Peak at 715 cm^{-1} corresponds to the Si-O-Al translation [241]. Weak bands at 880 and 1020 cm^{-1} are characteristic for mullite and are in the OH, Al-OH, OH(Al-OH) region. Weak peak at 1167 cm^{-1} is for mullite Al-OH bond. Stronger peak at 1120 is assigned to Si-O-Si stretching vibration [228].

After Pb^{2+} adsorption, a shift of the peaks at 405, 585, and 715 cm^{-1} to a lower frequency region to 387, 507 and 625 cm^{-1} is observed (Figure 40a). This indicates the lengthening and weakening of the Si-O and Si-O-Al bonds due to the interaction of Pb ions with SiO_4 tetrahedra and AlO_6 octahedra [243].

Thus, based on the analysis of the IR and Raman spectra of Clay before and after adsorption of lead ions, it can be assumed that:

Adsorption of lead occurs both on the surface layers of SiO_4 tetrahedrons and in the inner layers of AlO_6 tetrahedrons. Interaction with the surface layers most likely occurs due to ion exchange with metal cations that compensate for the excess negative charge, such as Na, K, Ca, Mg, etc., located in the channels and pores formed by the rings of SiO_4 tetrahedrons. Sorption in the inner layers of AlO_6 octahedrons is possibly due to the contribution of physical adsorption in the pores of the sorbent due to Van der Waals forces.

The proposed mechanism is also confirmed by the results obtained based on kinetic and thermodynamic calculations:

- based on the application of diffusion kinetic models, it was established that there is a high amount of surface adsorption (Webber-Morris model), both film and intraparticle diffusion stages contribute to the rate limiting step (Dumwald-Wagner model), and adsorption occurs via ion-exchange (Chemisorption Diffusion model).

- based on thermodynamic calculations, it was established that the absolute value of enthalpy indicates physisorption, and the value of entropy indicates active ion-exchange processes.

3.4 A new approach to identify contributions of different types of interactions to adsorption mechanisms on aluminosilicates (Na-H method)

Thus, the adsorption mechanism of lead ions by Clay includes two types of interactions, which were confirmed by experimental results. However, to assess the contribution of physical adsorption in pores or ion exchange, the following experiment was carried out: adsorption of lead

ions was performed by treated with NaCl (Na-clay) and acid activated (H-clay) forms of Сдфн (Table 24).

Table 24 – Sorption characteristics of Clay-based materials

Sample	E,%	qe, mg/g	CEC, meq/100g	Surface area (BET), cm^3/g	Mechanism
Clay	99.88 ± 0.01	3.12 ± 0.08	291.3 ± 5.9	8.4 ± 0.4	Ion-exchange
Na-clay	95.58 ± 0.04	3.08 ± 0.01	323.9 ± 5.2	10.9 ± 0.5	Ion-exchange
H-clay	25.44 ± 0.02	0.80 ± 0.07	129.3 ± 3.7	15.3 ± 0.7	No ion-exchange, adsorption in pores

If we consider such characteristics as CEC and specific surface area before and after treatment, we can draw some conclusions about possible adsorption mechanisms. Acid treatment leads to a significant decrease in CEC, an increase in the specific surface area of the sorbent, and a decrease in pore size (Table 24). If adsorption occurred mainly due to adsorption in pores, then an increase in the specific surface area should lead to an increase in the degree of extraction. However, in our case, on the contrary, the extraction degree by the acid-treated form is only 25%. As we can see almost all Pb^{2+} ions are extracted by the original and Na-treated C (99 and 98%, respectively) which have high values of CEC. Salt treatment leads to an increase in CEC but slightly reduces the value of E to 95%. This is probably due to an increase in the specific surface area and expansion of the pores of the clay.

A question may emerge over whether acid-treated clay exhibits diminished sorption of lead ions due to the degradation of its crystalline structure or a significant reduction in pore size. Both questions are rejected, as the XRD study results (Figure 24) demonstrate that the acid treatment did not alter the crystalline structure of the clay. The BET measurements (Table 17) demonstrate a reduction in pore size from 0.79 nm for the original clay to 0.53 nm for the acid-activated clay. Nonetheless, in this context, the diameter of the lead atom measures 0.35 nm, which remains smaller than the pores of all varieties of clay employed.

Nearly all Pb^{2+} ions are extracted by both the original and Na-treated Clay, achieving extraction rates of 99% and 98%, respectively, due to their elevated CEC. Salt treatment results in an elevation in CEC, while somewhat decreasing the extraction degree value to 95%. This is likely attributable to an increase of the specific surface area and an expansion of the clay's pores.

It follows that the greater contribution in the Clay-Pb system is made by ion exchange. The contribution of adsorption in the pores cannot be completely excluded, but it is much smaller than the contribution of ion exchange.

Thus, this method of adsorption with Na- and H-treated (denoted as Na-H method) forms of aluminosilicates can be used as an additional tool to elucidate the adsorption mechanisms.

The algorithm for carrying out this method is as follows:

1) Preparation of three types of aluminosilicates - initial, Na-treated, Acid-activated;

2) Determination of CEC and specific surface area of samples;

3) Carrying out adsorption;

4) Analysis of results.

Na treatment is expected to increase CEC, whilst acid treatment is likely to reduce it and increase specific surface area. Consequently, an increase in CEC will yield a beneficial impact if the adsorption mechanism involving clay is ion exchange. An increase in specific surface area enhances adsorption within the pores of the sorbent. This type of processing does not change the properties of the original clays radically, but only creates a favorable environment for interaction and, as it were, plays the role of an indicator that only enhances what already exists.

It follows that the largest contribution in the C-Pb system is made by ion exchange. The contribution of adsorption in pores cannot be completely excluded, but it is much smaller than the contribution of ion exchange.

Advantages of the Na-H method:

1) Typically, natural aluminosilicate raw materials are modified to improve the purifying efficiency of aqueous solutions. This method enables the rapid identification of which form of interaction between the adsorbent and adsorbate contributes most significantly, hence aiding in the selection of a modifying agent focused on amplifying the predominant type of adsorption.

2) The adsorption mechanism of pollutants by aluminosilicates is generally complicated and involves several types of interactions; thus, this method can elucidate some gaps in mechanisms identified by other approaches and function as an additional instrument for mechanism determination.

3) Understanding the predominant adsorption mechanism of the pollutant might facilitate the selective adsorption of desired chemicals from mixtures by choosing the appropriate modifier for aluminosilicate.

Limitations of the Na-H method:

1) This method is applicable solely to aluminosilicates for which acid treatment yields a reduction in CEC and an enhancement in BET. Otherwise, this method cannot be used.

2) Does not provide data on chemisorption

3) It serves merely as an auxiliary instrument for identifying the predominant form of physisorption, failing to offer a comprehensive understanding of the adsorption mechanism, and should be employed in combination with other established approaches for elucidating the mechanism.

3.5 The study of organic pollutants extraction from aqueous solutions onto the adsorbents based on Zeolite and Clay

The modification of aluminosilicates with surfactants aims to enhance surface charge and hydrophobization, facilitating the adsorption of organic pollutants [3,32,214,244,245].

This study focused on Bisphenol-A and Propranolol as organic contaminants.

The choice of Bisphenol-A (BPA) and Propranolol (PRO) as adsorbates is based on their structure and toxicity. BPA is a good example of hydrophobic anion, since it is a phenolic compound that dissociates and forms anions at sufficiently high pH [29,246]. BPA is an endocrine-disrupting chemical, which can cause abnormalities in the functions of wildlife and human endocrine systems; it is carcinogenic, antioxidant, nonbiodegradable, and highly resistant to chemical degradation [3]. PRO is a beta-adrenergic receptor antagonist, which is widely used to treat cardiovascular diseases such as angina, hypertension, myocardial infarction, and arrhythmias [247]. PRO is considered a rather safe and efficient pharmaceutical, but at higher concentrations it may cause acute and chronic harm to organisms [248]. PRO is a hydrophilic molecule with a hydrophobic aliphatic chain [249], which contains hydroxyl group and secondary amino group, i.e., unlike BPA, PRO may form both anions and cations in aqueous solutions.

The results of BPA and PRO adsorption by the obtained sorbents based on Zeolite and Clay modified with SLES and DDAB are presented in Table 25.

Table 25 – The extraction degrees of BPA and PRO by the studied adsorbents (C_0 = 50 mg/L, V=10 ml, m= 50 mg, contact time =24 h)

Sorbent	E(BPA), %		
	No surfactant	+ DDAB	+ SLES
Zeolite	12.1 ± 1.1	24.8 ± 1.2	1.3 ± 0.1
Na-Zeolite	3.3 ± 0.1	42.0 ± 2.9	0
H-Zeolite	7.3 ± 0.2	47.0 ± 3.2	0
Table 25 (continued)			
Clay	30.9 ± 2.7	35.3 ± 2.6	2.38 ± 0.3
Na-Clay	4.2 ± 0.3	49.7 ± 1.1	6.8 ± 0.6
H-Clay	8.6 ± 0.8	44.5 ± 0.7	5.5 ± 0.3
Sorbent	E(PRO), %		
	No surfactant	+ DDAB	+ SLES

Table 25 (continued)			
Zeolite	26.7 ± 1.3	47.4 ± 2.3	26.4 ± 1.2
Na-Zeolite	36.9 ± 2.6	65.5 ± 4.0	33.2 ± 2.0
H-Zeolite	53.5 ± 3.6	48.4 ± 2.9	35.6 ± 2.3
Clay	41.6 ± 3.1	33.3 ± 0.8	45.5 ± 0.6
Na-Clay	52.2 ± 4.8	51.5 ± 4.3	52.0 ± 3.9
H-Clay	41.6 ± 2.8	45.3 ± 1.1	46.5 ± 1.7

Table 25 illustrates that the original zeolite adsorbs 12% of BPA, while pre-treatment with Na^+ and H^+ results in a reduction of E% to 3.34% and 7.33%, respectively. Low extraction rates are attributed to the presence of BPA in aqueous solution as an anion, resulting in electrostatic repulsion with the negatively charged surface of the zeolite.

BPA uptake is higher for the original clay (35.27%). It can be attributed to a higher specific surface of Clay, which according to a new approach proposed in Section 3.4 (Na-H method), indicates that the main interaction mechanism of Clay with BPA is physisorption in pores.

Modification of Zeolite and Clay with SLES is not effective because it is an anionic surfactant, i.e. there is no interaction with BPA anions. When DDAB is introduced into the sorbents, the values of the degree of BPA extraction increase, since the surface of aluminosilicates is recharged.

Pre-treatment of Zeolute and Clay both with Na^+ and H^+ leads to a decrease in BPA uptake. However, it improves the interaction with DDAB, strengthening the fixation of DDAB on the zeolite surface, thereby increasing the number of adsorption centers for organic molecules. We can see that the best extraction degrees are for Na-Zeolite/Na-Clay +DDAB and H-Zeolite/H-Clay + DDAB.

In the situation of PRO, Zeolite and Clay provide better results: about 27 and 42% respectively. The elevated adsorption values of PRO result from its structure, which includes both negatively and positively charged functional groups, whereas BPA is an anionic molecule.

Pre-treatment with Na^+ and H^+ leads to improvement of PRO adsorption raising E% to 36 and 53% for Na-Zeolite and H-Zeolite, and to 52% for Na-Clay. In the case of H-Clay there is no change in E%. The best results are observed for Na-Zeolite+DDAB (65.49%) and H-Zeolite+DDAB (62.5%).

Thus, sorbents based on Zeolite and DDAB were selected for a more detailed study of the optimal conditions and mechanism of BPA and PRO adsorption.

The effects of different factors, such as DDAB concentration, adsorbent mass, and adsorbate concentration, on the adsorption of BPA and PRO onto Zeolite-based adsorbents were investigated

The effect of DDAB concentration in zeolite-based sorbents on the adsorption of BPA and PRO was investigated (Figure 41).

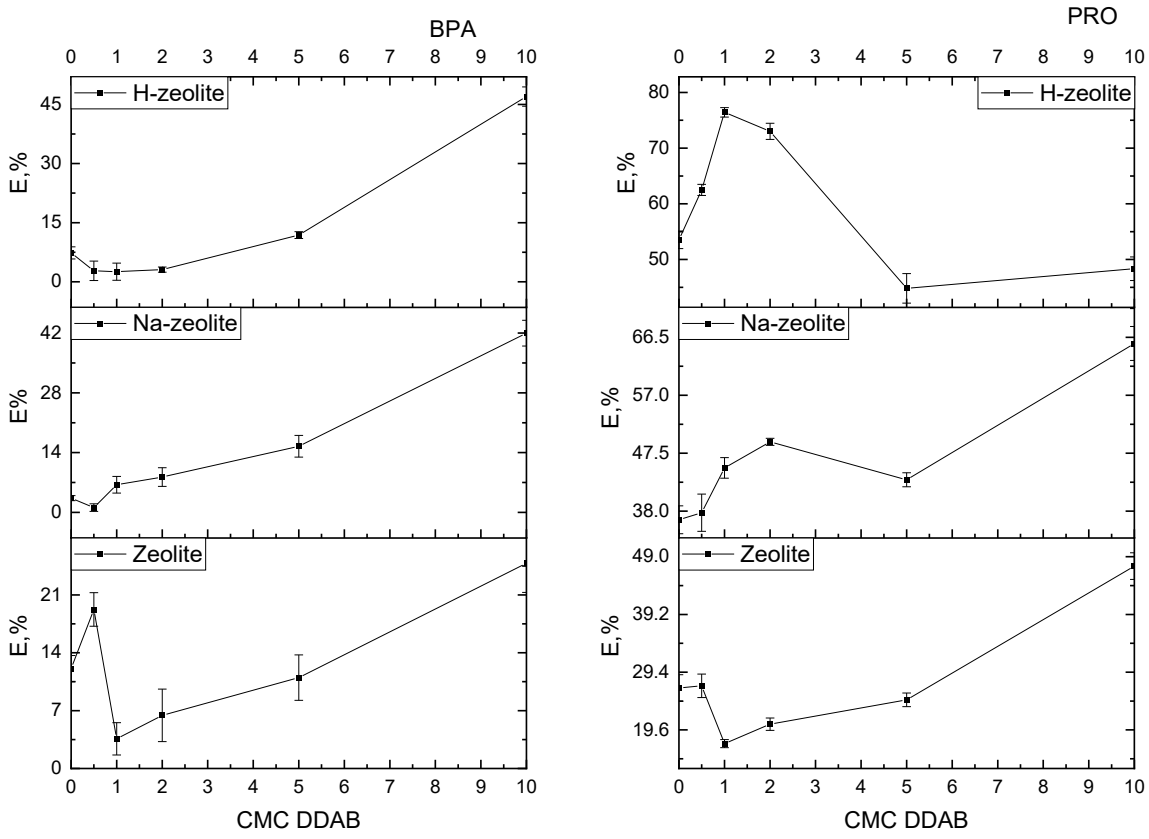


Figure 41 – The effect of DDAB concentration on the adsorption of BPA and PRO (solid:liquid ratio = 1:10; T=298K, pH = 7; 200 rpm)

Maximum extraction rates are recorded at the highest concentration of 10 CMC. However, in the case of the Zeolite+DDAB sorbent, at a DDAB concentration of 0.5 CMC, the BPA extraction rate is 19% and is comparable to the extraction rate at the maximum concentration used of 10 CMC – 24%. For the H-Zeolite+DDAB sorbent, a surfactant concentration of 1 CMC produces a PRO extraction rate of 62%, however at 10 CMC, the extraction rate decreases to 48%. This phenomenon is likely elucidated by the observation that at these concentrations, the zeolite surface is optimally covered with surfactant, resulting in a monolayer with an appropriate surface charge and geometric configuration for the adsorbate (Figure 1a). As DDAB concentration increases, further micelle layers are formed, and the surface coverage may not be suitable for the adsorbate (Figure 1b).

Notable results are likewise evident for all other systems, though at varying surfactant concentrations. In a specific region, there is initially a rise followed by a drop in the level of

extraction. For the Na-Zeolite + DDAB sorbent, the adsorption of PRO reveals a progressive increase in E from 0 to 2 CMC, followed by a decline at 5 CMC and a subsequent rise at 10 CMC. This indicates that selecting the correct concentration of surfactants is essential for modifying sorbents to achieve a layer with the desired charge. Furthermore, by examining the influence of surfactant concentration on adsorption, one can determine the concentration necessary to establish a single surfactant layer.

Consequently, based on the tests conducted, 10 CMC were identified as the ideal DDAB concentrations for all sorbents in the adsorption of BPA and PRO, except for the H-Zeolite + DDAB sorbent for PRO adsorption, for which 1 CMC is optimal.

The effect of adsorbent mass on the adsorption of BPA and PRO (Figure 42) was studied in the interval from 50 to 150 mg per 10 ml of solution using the adsorbents showing the best performance: H-Zeolite + DDAB for BPA and Na-Zeolite + DDAB for PRO. The highest adsorption values are observed with the maximum amount of sorbent (150 mg): 70% for BPA and 80% for PRO. The adsorption reached 7 mg/g for BPA and 8,2 mg/g for PRO.

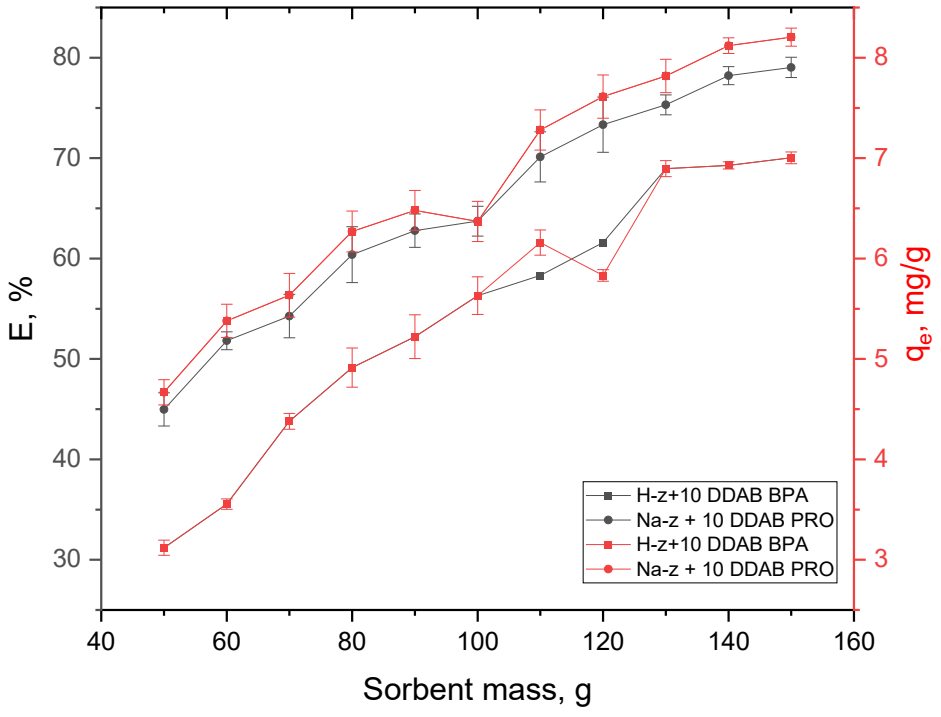


Figure 42 – The effect of adsorbent mass on the extraction of BPA and PRO (C_0 = 50 mg/L, V = 10 ml, contact time = 24 h, T = 298K, pH =7, 200 rpm)

The effect of the adsorbate concentration and adsorption isotherms. Adsorption isotherms of BPA and PRO are presented in Figure 43. As we can see, the isotherms of BPA adsorption and PRO adsorption onto Na-Zeolite + DDAB are the L2 Langmuir type isotherms. Class L isotherms

are characterized by the independence of the heat of adsorption from the degree of surface filling and the absence of competition from the solvent. Class L isotherms are characterized by an initial section curved relative to the concentration axis, since with an increase in the proportion of occupied adsorption sites, it is more difficult for the adsorbate molecules to find a vacant site, especially if they are prone to the formation of large associates with an increase in their concentration in the solution due to intermolecular interaction. L2 isotherms are typical for cases where adsorption reaches its limit at a certain concentration of the adsorbate [250].

The adsorption isotherm of PRO on zeolite belongs to class S2. Class S isotherms have a concave initial section. With an increase in the concentration of the adsorptive in the solution, the adsorption capacity of the sorbent increases sharply, which may be associated with a change in the orientation of the adsorbed molecules relative to the sorbent surface or with a rapid transition to polymolecular adsorption. This is often followed by an inflection point and the appearance of a second plateau, which gives such isotherms a characteristic S-shaped appearance. The reason is the strong interaction between the adsorbed molecules with a simultaneous weakening of the interaction of the adsorptive molecules with the adsorbent, which leads, in general, to an increase in the heat of adsorption [250].

The adsorption isotherm character of PRO on the modified sorbent Na-Zeolite+DDAB changes to type L2. The presence of surfactants in the modified sorbent presumably causes a forced orientation of the PRO particles in relation to the surfactant layer, resulting in monomolecular adsorption limited by the sorbent capacity.

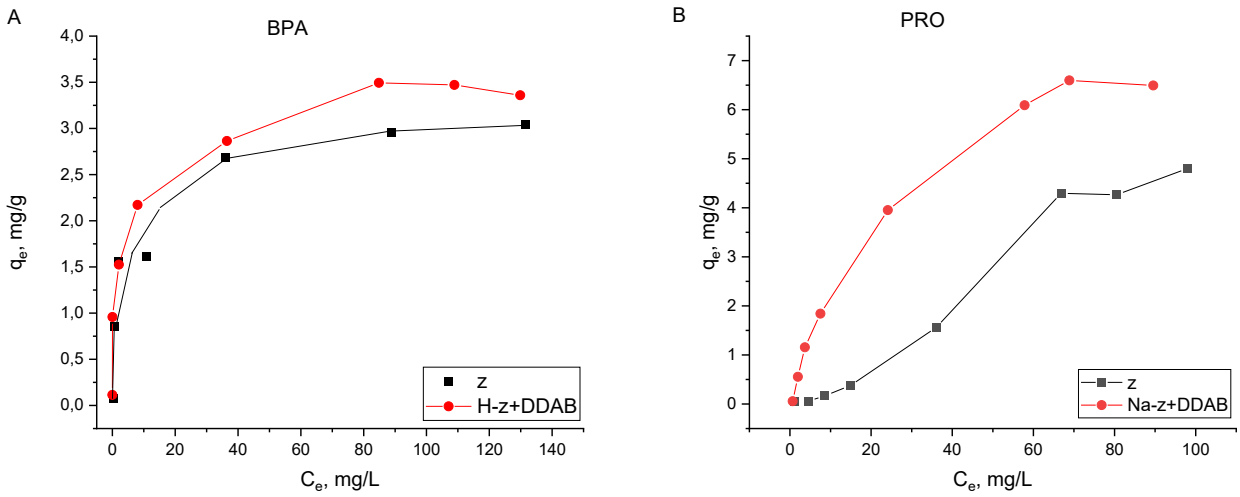


Figure 43 – Isotherms of BPA and b) PRO adsorption onto studied adsorbents (V=10 ml, m = 50 mg, contact time = 24 h, T = 298K, pH =7, 200 rpm)

The results of the non-linear fitting to different isotherm models are in

Table *26*.

Table 26 – The R^2 and ARE values obtained by the non-linear fitting to the isotherm models

Isotherm model	Adsorption system							
	z + BPA		H-Z + DDAB + BPA		z + PRO		Na-Z + DDAB + PRO	
	R^2	ARE	R^2	ARE	R^2	ARE	R^2	ARE, %
Langmuir	0.90	43.31	0.80	23.77	0.93	131.58	0.99	46.66
Freundlich	0.89	110.17	0.97	4.06	0.97	64.72	0.98	54.82
Temkin	**0.94**	**50.98**	**0.98**	**2.15**	0.77	524.35	0.95	67.03
Dubinin-Radushkevich	0.60	40.08	0.71	13.19	0.99	52.22	0.93	45.97
Sips	0.93	74.46	0.98	2.29	**0.99**	**47.11**	1.00	34.72
Fritz-Schlunder 3	0.94	63.40	0.98	2.58	0.97	64.72	**1.00**	**34.36**
Toth	0.93	69.22	0.98	2.38	0.97	95.77	1.00	35.17
Langmuir-Freundlich	0.93	74.46	0.98	2.29	0.96	89.18	1.00	38.48
Redlich-Peterson	0.94	63.40	0.98	2.58	0.97	68.25	1.00	38.48
Fritz-Schlunder 4	0.94	63.39	0.99	2.27	0.96	86.55	1.00	43.95
Fritz-Schlunder 5	0.94	63.39	0.97	4.06	0.97	68.25	1.00	43.95

Based on the analysis of the values of the correlation coefficients and ARE, the most suitable isotherm models are: Temkin for the adsorption of bisphenol-A in the studied systems, Sips for the zeolite + PRO system, and the three parameter Fritz-Schlunder model for the Na-Zeolite + DDAB + PRO system.

The Temkin model presumes that adsorption is a multi-layer process [168]. The Temkin isotherm equation assumes that the heat of adsorption of all the molecules in the layer decreases linearly with coverage due to adsorbent-adsorbate interactions, and that the adsorption is characterized by a uniform distribution of the binding energies, up to some maximum binding energy [148]. Originally, the Temkin model was applied for chemisorption system, taking into consideration the interaction between the adsorbent and the adsorbate by ignoring the extremely low and large value of concentrations. Thus, this model is valid only for an intermediate concentration range [251].The model assumes that heat of adsorption (function of temperature) of all molecules in the layer would decrease linearly rather than logarithmically with coverage [252]. If the bonding energy B_T values are < 8 kJ/mol, adsorption occurs via physisorption mechanism, which is true for the adsorption of BPA onto z and H-z + DDAB systems.

The Sips isotherm model is a combination of the Langmuir and Freundlich models, which predicts the heterogeneity of the adsorption systems as well as have a finite limit at high concentrations [251]. The Sips model does not follow Henry's law due to the reduction to Freundlich model at low concentrations and predicts the monolayer adsorption characterictic of Langmuir model. Sips model is the most applicable 3-parameter isotherm model for monolayer adsorption [253].

The Fritz-Schlunder isotherm model is a Langmuir-Freundlich (i.e., it becomes Freundlich isotherm at low concentrations, whereas transforms to Langmuir at high concentrations) type empirical equation, that can perform more precise simulation of the model variations for application over a wide range of equilibrium data due to the large number of coefficients in the isotherm [251].

Consequently, the modeling of the adsorption process in the analyzed systems will yield minimal mistakes when employing the derived equations (Table 27). Comparison of experimental and predicted isotherm models is presented in Figure 44.

Table 27 – The unknown parameters of the best fit isotherm models to the studied systems

Adsorption system	Isotherm model	Unknown Parameters			Equation
Zeolite + BPA	Temkin	B_T, J/mol	K_T, L/mg	-	$q_e = \frac{RT}{B_T} lnK_T C_e$
		6033.58	10.75		
H-Zeolite+DDAB+BPA	Temkin	5144.44	11.47	-	$q_e = \frac{RT}{B_T} lnK_T C_e$
Zeolite + PRO	Sips	q_{ms}, mg/g	K_S, L/mg	β	$q_e = \frac{q_{mS} K_S C_e^{\beta}}{1 + K_s C_e^{\beta}}$
		5.03	1,54 * 10^{-6}	3.53	
Na-Zeolite+DDAB+PRO	Fritz-Schlunder 3	q_{mFS} ,mg/g	K_{FS}, L/mg	α	$q_e = \frac{q_{mFS} K_{FS} C_e}{1 + K_{FS} C_e^{\alpha}}$
		17.06	16.25 * 10^{-3}	1.14	

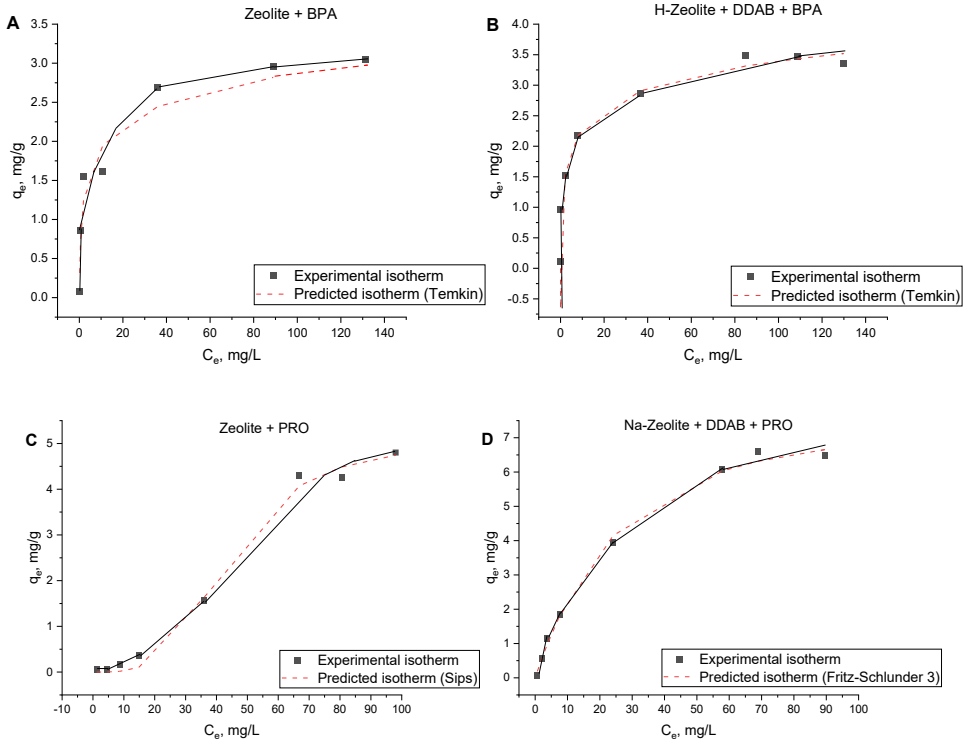


Figure 44 – Comparison of experimental and predicted isotherm models of adsorption of A) BPA onto Zeolite; B) BPA onto H-Zeolite + DDAB; C) PRO onto Zeolite; D) PRO onto Na-Zeolite + DDAB

Thus, by varying the experimental conditions, it is possible to achieve sufficiently high values of BPA and PRO adsorption by obtained sorbents. It was found that

- the optimal concentration of DDAB in the sorbents is 10 CMC (1 mmol/l), and 1 CMC (0.1 mmol/l) for the H-Zeolite + DDAB sorbent during PRO adsorption;

- the optimal adsorbent mass is 15 g/l;

- the adsorption of BPA on Zeolite and H-Zeolite + DDAB is best described by the Temkin isotherm, assuming that adsorption is a multi-layer process, and the calculated values of bonding energy correspond to physisorption;

- the adsorption of PRO on zeolite is best described by the Sips equation, the most applicable 3-parameter isotherm model for monolayer adsorption;

- the adsorption of PRO on Na-Zeolite + DDAB is best described by a three-parameter Fritz-Schlunder equation, which becomes Freundlich isotherm at low concentrations, whereas transforms to Langmuir at high concentrations.

3.6 Study of BPA and PRO adsorption mechanism on zeolite and DDAB based sorbents using Na-H method

Table 28 – BPA and PRO adsorption by natural and modified zeolite (C_0 = 50 mg/L, V = 10 ml, m = 50 mg, contact time = 24 h, T = 298K, pH =7, 200 rpm)

Material	Extraction degree BPA,%	Extraction degree PRO,%
zeolite	12.1 ± 1.1	26.7 ± 1.3
zeolite + DDAB	24.8 ± 1.2	47.4 ± 2.3
Na-zeolite	3.3 ± 0.1	36.9 ± 2.6
Na-zeolite + DDAB	42.0 ± 2.9	65.5 ± 4.0
H-zeolite	7.3 ± 0.2	53.5 ± 3.6
H-zeolite + DDAB	47.0 ± 3.2	48.4 ± 2.9

As shown in Table 28, the extraction degree of BPA decreases in the following order: zeolite > 3 M HCl-zeolite > Na-zeolite. The already relatively low extraction degree of BPA with the parent zeolite decreases four-fold after Na^+ pretreatment, which increases the surface hydrophilicity [144,205], which negatively affects the interaction of the zeolite with the hydrophobic pollutant. The smaller decrease in the extraction degree after acid treatment is probably associated with an increase in the negative charge of the zeolite surface due to the Si/Al ratio growth, which contributes to the electrostatic repulsion of BPA anions from the zeolite surface. However, after DDAB modification, the extraction degree of BPA increases to about 25% for zeolite as a result of coating the surface with a layer of DDAB micelles, partial hydrophobization of the surface, and emergence of new active centers for the adsorption of organic

ions. Modification of Na-zeolite with the surfactant had an even better effect, increasing the degree of BPA extraction to around 42%. This is most likely due to a smoother coating of the zeolite surface as a result of saturation with sodium ions, which is consistent with the assumptions described above. In the case of H-zeolite, the surface coating of DDAB also significantly increased the extraction degree (up to about 47%). However, as the results of Na-zeolite and H-zeolite with DDAB are almost similar, it is practicable to use the simpler NaCl pretreatment [187].

For PRO, the extraction degree coincides with the increase in specific surface (Table 11) – zeolite < Na-zeolite < H-zeolite (4.5, 6.2 and 39.3 m^2/g). It suggests that adsorption in this case is physical and depends on the sorbent porosity [187].

After DDAB modification, the degree of PRO extraction for zeolite increases significantly to ~47%; ~48% for H-zeolite, and about 65% for Na-zeolite. The imposition of surfactant in the zeolite structure leads to the appearance of active centers for the adsorption of PRO and significantly improves the results for zeolite and Na-zeolite [187].

Data with equilibrium pH, ionization % of adsorbates and concentrations of leached cation-exchange ions (Na, K, Ca, Mg) during the adsorption process are presented in Table 29.

The fact about the major impact of physisorption on the PRO adsorption by studied materials can be explained as at the equilibrium pH of adsorption systems PRO molecules are mostly in non-ionized form. However, ion-exchange is also present for PRO, because the concentrations of leached Na and K-ions are a little higher than for systems with water (Table 29) [187].

Table 29 – Ion-exchange properties and equilibrium pH of studied adsorption systems [187]

Adsorbent	Adsorbate	Na, mg/L	K, mg/L	Ca, mg/L	Mg, mg/L	pH_{eq}	pK_a	% ionization
Zeolite	H_2O	0.15	0.01	0.42	0.05	7.92	7.00	89.27
Zeolite	PRO	0.16	0.02	0.37	0.05	7.65	9.45	1.56
Zeolite	BPA	0.27	0.08	0.27	0.05	9.28	9.6	32.37
Na-zeolite	H_2O	0.54	0.00	0.01	0.01	8.18	7.00	93.80
Na-zeolite	PRO	0.65	0	0.07	0.00	7.63	9.45	1.49
Na-zeolite	BPA	0.80	0.05	0.07	0.02	9.53	9.6	45.98
H-zeolite	H_2O	0.00	0.00	0.00	0.00	6.39	7.00	19.71
H-zeolite	PRO	0.00	0.00	0.02	0.01	4.39	9.45	0.00
H-zeolite	BPA	0.00	0.00	0.00	0.00	4.87	9.6	0.00
Zeolite+DDAB	H_2O	0.06	0.00	0.50	0.03	7.73	7.00	84.30
Zeolite+DDAB	PRO	0.10	0.00	0.69	0.02	7.64	9.45	1.53

Zeolite+DDAB	BPA	0.12	0.09	0.25	0.01	8.92	9.6	17.28
Table 29 (continued)								
Na-zeolite+DDAB	H_2O	0.04	0.00	0.09	0.00	7.37	7.00	70.10
Na-zeolite+DDAB	PRO	0.12	0.00	0.35	0.01	7.58	9.45	1.33
Na-zeolite+DDAB	BPA	0.11	0.00	0.12	0.01	8.32	9.6	4.99
H-zeolite +DDAB	H_2O	0.00	0.00	0.00	0.00	5.75	7.00	5.32
H-zeolite +DDAB	PRO	0.00	0.00	0.03	0.01	5.42	9.45	0.01
H-zeolite +DDAB	BPA	0.07	0.03	0.01	0.00	6.29	9.6	0.05

In case of BPA the impact of ion-exchange to the adsorption mechanism is bigger, as ionization % in the studied pH of the systems is much higher than for PRO. That also can be confirmed with the highest concentrations of Na and K ions after the adsorption [187].

In summary, the following types of interactions between the adsorbents and adsorbates may take place:

- electrostatic attraction/repulsion
- hydrophobic/hydrophilic interaction
- ion exchange
- physisorption
- chemisorption.

The simplest interactions between the reacting species are shown in Figures 44-46. It is assumed that the DDAB molecule can interact with the zeolite surface through electrostatic attraction. The N^+ can also participate in ion-exchange processes with exchangeable metal ions on the zeolite surface (Figure 45) [187].

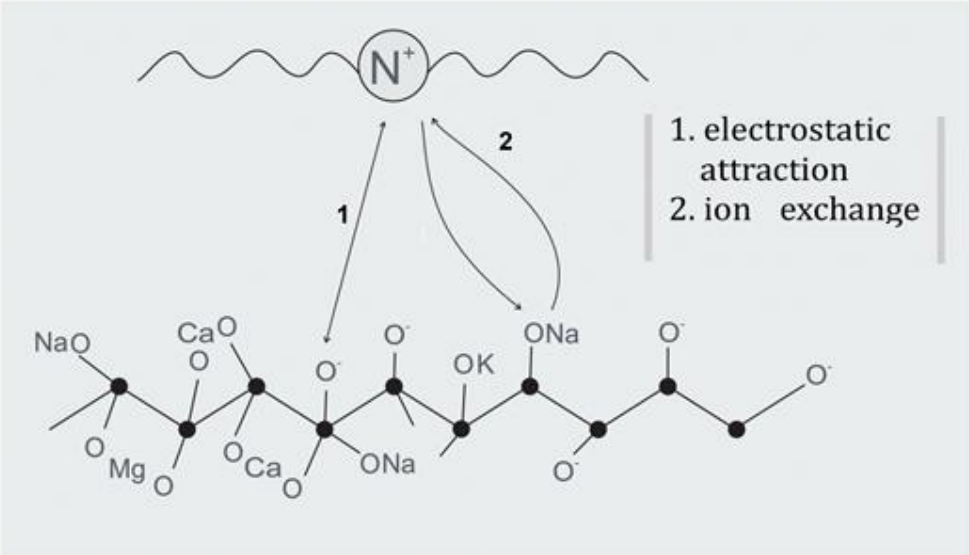


Figure 45 – Scheme of interaction between zeolite and DDAB [187]

The BPA molecules can be adsorbed by the SMZ (zeolite modified with DDAB) by interacting with the zeolite surface, forming bonds between metal zeolite atoms and the oxygen atom of the OH-group in BPA, as well as with DDAB (Figure 46) [187].

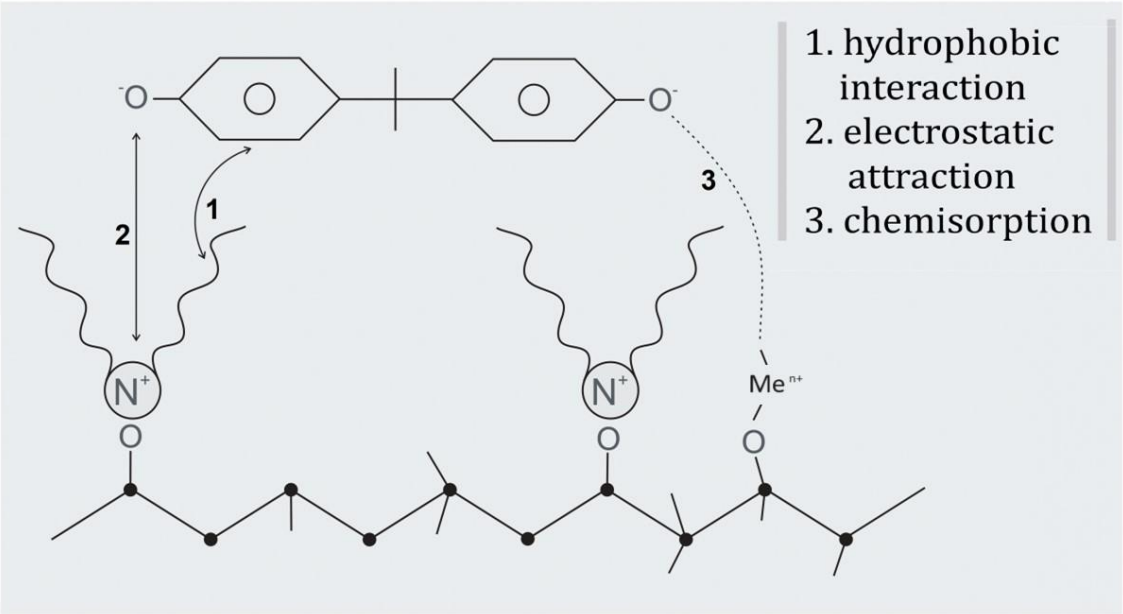


Figure 46 – Scheme of interaction between SMZ and BPA [187]

The latter includes hydrophobic interaction of the surfactant and organic pollutant (BPA) and electrostatic attraction between N^+ of DDAB and O^- of BPA. The adsorption of PRO includes all abovementioned interactions and also physisorption in the zeolite pores (Figure 47) [187].

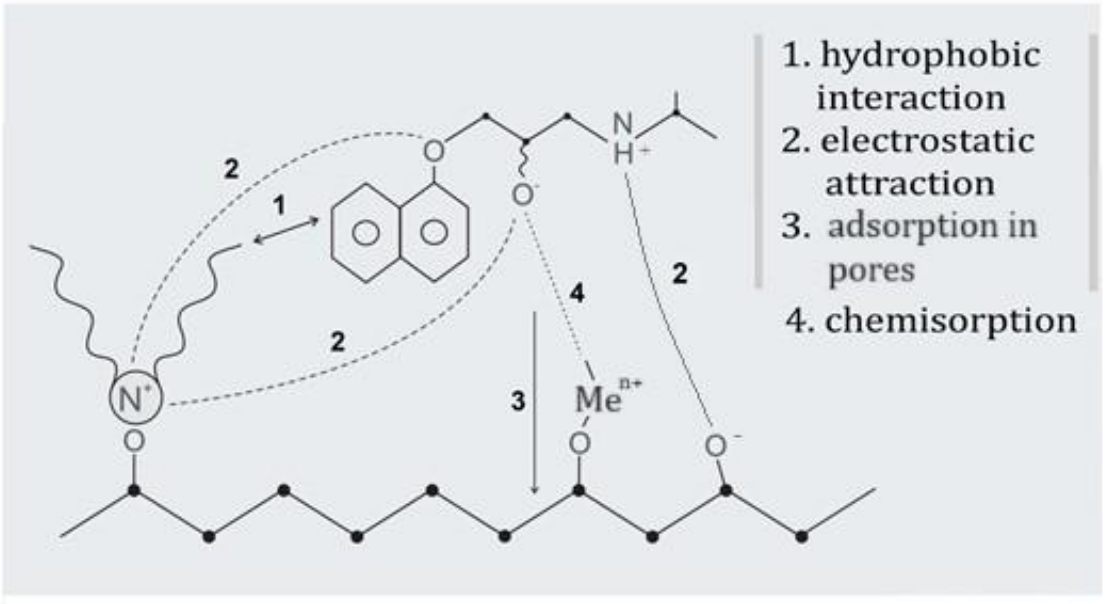


Figure 47 – Scheme of interaction between SMZ and PRO [187]

Thus, based on the results obtained, the following conclusions can be made about the mechanism of adsorption of organic contaminants on zeolite-based sorbents:

- Modification of natural zeolite with cationic surfactant enhances adsorption of organic pollutants by increasing its hydrophobicity.

- As a result of a detailed analysis and description of the physicochemical characteristics and the influence of pretreatment and surfactant modification on the zeolite properties, possible mechanisms of interaction with BPA and PRO were deduced.

- In the case of BPA, the adsorbent-adsorbate interaction mechanism may include chemisorption, electrostatic attraction, and hydrophobic interactions with the surfactant.

- For PRO, the adsorbent-adsorbate interaction mechanism possibly also includes physisorption.

- For PRO, the most effective form of modification was pretreatment of zeolite with NaCl prior to modification with DDAB, however for BPA, slightly better results were obtained with HCl pretreatment [187].

3.7 Practical application of the obtained results

Thus, based on the obtained results, it was established that:

- for the adsorption of Bisphenol-A, the most effective sorbents are those based on Zeolite and Clay, pre-treated with 3 M HCl followed by modification with 10 CMC DDAB;

- for the adsorption of Propranolol, the most effective sorbents are those based on Zeolite and Clay, pre-treated with 1 M NaCl followed by modification with 1 CMC DDAB, as well as those based on Clay pre-treated with 1 M NaCl followed by modification with 10 CMC SLES;

- for the adsorption of Pb^{2+} ions, the original Zeolite and Clay are effective, the degree of extraction reaches almost 100%;

- for the adsorption of Cd^{2+} ions, the most effective sorbents are those based on Zeolite modified with 0.00025 M SLES and Clay modified with 0.01 M SLES;

- for the adsorption of Sr^{2+} ions, the most effective was a sorbent based on Zeolite modified with 0.0005 M SLES;

- for the adsorption of MnO_4^- and $Cr_2O_7^{2-}$ ions, the most effective was Clay pre-treated with 3 M HCl subsequently modified with 20 CMC DDAB.

Table 30 presents a comparative overview of adsorption capacities (q_e, mg/g) and market prices of widely used commercial sorbents (activated carbons, synthetic zeolites, ion exchange resins, and polymeric adsorbents) together with newly developed mineral-based sorbents.

Table 30 – Comparison of the optimal adsorbents based on Zeolite and Clay with commercial adsorbents

Pollutant	Adsorbents							
	This work (parameters not optimized)		Comparative sorbent 1 Active carbon		Commercial sorbent 2 Synthetic zeolite		Commercial sorbent 3 Ion exchange resins	
Pb^{2+}	Sorbent type							
	Shankanay natural zeolite		Commercial grade coconut shell origin granulated activated carbon [254]		Synthetic zeolite *ZSM-5* [255]		Strong Acid Cation exchange resin *Amberlite IR-120* [256]	
	q_e, mg/g	~Cost price, $/kg	q_e, mg/g	~Cost price, $/kg	q_e, mg/g	~Cost price, $/kg	q_e, mg/g	~Cost price, $/kg
	13.8	0.9-1.0*	2.0	$1.3–1.5 (alibaba.com)	74.1	4.5 – 5.5$ (made-in -China.com)	9.8	37.7 (fishersci.com)
	Sorbent type							
Sr^{2+}	Shankanay natural zeolite + 0.5 mmol/L SLES		Commercial granular activated carbon (size>2 mm), Merck, Germany [257]		Synthetic zeolite *NaX* [258]		Polyacrylamide impregnated Nonionic Macropore Adsorption resin *Amberlite XAD-7* [259]	
	q_e, mg/g	~Cost price, $/kg	q_e, mg/g	~Cost price, $/kg	q_e, mg/g	~Cost price, $/kg	q_e, mg/g	~Cost price, $/kg
	15.0	0.8-1.2*	4.4	259.0 (merck.com)	156.0	1.0-2.0 (alibaba.com)	23.0	276.0-297.0 (sigmaaldrich.com, fishersci.com)
Cd^{2+}	Sorbent type							
	Shankanay natural zeolite + 0.25 mmol/L SLES		Commercial activated carbon pellets [260]		Synthetic zeolite *P* [261]		Chelate Cation exchange resin *Duolite ES 467* [262]	
	q_e, mg/g	~Cost price, $/kg	q_e, mg/g	~Cost price, $/kg	q_e, mg/g	~Cost price, $/kg	q_e, mg/g	~Cost price, $/kg
	9.8	1.6*	10.3	1.0-2.0 (alibaba.com)	161.1	35.0-40.0$ (alibaba.com)	13.8	108.0-110.0 (sdfine.com)
$Cr_2O_7^{2-}$	Sorbent type							
	Acid-activated Chamotte clay + 1 mmol/L DDAB		Commercial activated carbon *type PHO 8/35 LBD* [263]		No data		Strong Base Anion exchange resin *Purolite A-400* [264]	
	q_e, mg/g	~Cost price, $/kg	q_e, mg/g	~Cost price, $/kg	q_e, mg/g	~Cost price, $/kg	q_e, mg/g	~Cost price, $/kg
	10.8	6.6*	8.9	1.6-2.2 (imarcgroup.com)	-	-	120.6	13.3 (apswater.com)

Table 30 (continued)

MnO^-	Sorbent type							
	Acid-activated Chamotte clay + 1 mmol/L DDAB		Commercial granular activated carbon [265]		No data		нет данных	
	q_e, mg/g	~Cost price, $/kg	q_e, mg/g	~Cost price, $/kg	q_e, mg/g	~Cost price, $/kg	q_e, mg/g	~Cost price, $/kg
	3.7	6.6*	27.0	1.0-2.0 (alibaba.com)	-	-	-	-
PRO	Sorbent type							
	Na-treated Shankanay natural zeolite + 1 mmol/L DDAB		*Corozo fruit (Bactris guineensis) palm tree* activated carbon [266]		No data		Strong Acid Cation exchange resin *Amberlite IR-120 Plus* [267]	
	q_e, mg/g	~Cost price, $/kg	q_e, mg/g	~Cost price, $/kg	q_e, mg/g	~Cost price, $/kg	q_e, mg/g	~Cost price, $/kg
	6.5	4.4*	134.0	10.0-20.0 (estimated production cost)	-	-	767.0	215.0 (cenmed.com)
BPA	Sorbent type							
	Acid-activated Shankanay natural zeolite + 1 mmol/L DDAB		Charcoal-based carbons from *SorboNorit* [268]		Hydrophobic synthetic zeolite *Wessalith DAY NaY* [269]		Polymeric adsorbent *Amberlite XAD-7 impregnated with Aliquat 336* [270]	
	q_e, mg/g	~Cost price, $/kg	q_e, mg/g	~Cost price, $/kg	q_e, mg/g	~Cost price, $/kg	q_e, mg/g	~Cost price, $/kg
	3.5	4.3*	130.0	1306.0 (fishersci.com)	111.1	100.0-200.0	1.5-1.7	2055.0 (estimated production cost)

* Estimated cost of the obtained adsorbents is calculated using prices in Table B1 in Appendix B

Commercial materials such as ion exchange resins (Amberlite IR-120, Amberlite IRP-69, Duolite ES 467, Purolite A-400) and synthetic zeolites (ZSM-5, NaX, P-type, Wessalith DAY NaY) exhibit high adsorption capacities, in some cases exceeding 700–900 mg/g for organic pollutants such as propranolol. However, these sorbents are associated with relatively high costs, ranging from tens to several hundred US dollars per kilogram in the case of ion exchangers, and up to more than 1000 USD/kg for specialty carbons and polymeric adsorbents (e.g., Amberlite XAD-7). Activated carbons, derived from coconut shells, palm nuts, or coal, represent the most economically accessible group of commercial adsorbents, with bulk prices typically between 1–5 USD/kg, while offering moderate to high adsorption capacities across a broad range of contaminants.

The mineral sorbents developed in this study, based on natural zeolitic and clay-derived materials, show moderate adsorption capacities in the range of tens to several hundred mg/g, depending on the contaminant. Their estimated production costs are significantly lower than those of most commercial resins and specialty zeolites, generally not exceeding 1–6 USD/kg, as they are synthesized from abundant and low-cost raw materials.

Overall, the comparative data demonstrate a trade-off between adsorption efficiency and material cost. While commercial sorbents often provide higher capacities, their elevated market prices may limit large-scale application in cost-sensitive sectors. In contrast, mineral-based sorbents, although less efficient in absolute capacity, offer substantial economic advantages. This suggests their potential suitability for applications where low-cost treatment is prioritized over maximum adsorption efficiency.

The optimum ratio for the sorption of inorganic anions is 10 g/L. Nonetheless, using 10 g of sorbent per 1 L of solution may be economically impractical. Figure 48 illustrates an illustration showing the potential application of a reduced quantity of sorbent per liter of solution throughout several successive stages:

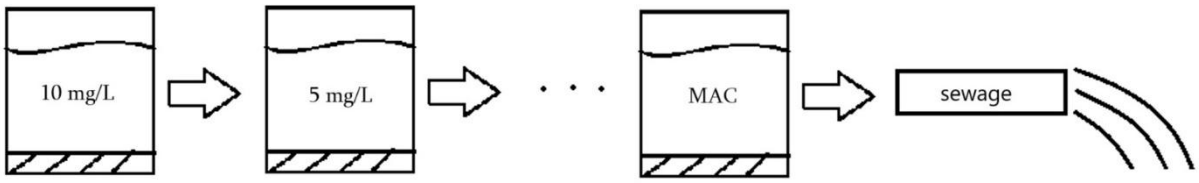


Figure 48 – Scheme of sequential stepwise adsorption of metals by sorbent

The procedure for performing consecutive stepwise sorption, illustrated in Figure 48, is as follows:

A solution containing toxic ions is placed into a vessel with 1 g of sorbent per 1 L of solution, and sorption is carried out. Afterwards, the identical solution is introduced into the subsequent jar

containing 1 g of fresh sorbent and allowed to settle for the duration required to attain equilibrium. The process is repeated until the concentration is reached below the maximum allowable concentration (MAC) level, at which the solution can be discharged as wastewater without harming the environment.

Therefore, to attain a concentration below the MAC threshold for MnO_4^- ions using the H-Zeolite+20 CMC DDAB sorbent, six stages of sequential sorption and, consequently, six grams of sorbent will be necessary. The residual ion concentration after six stages of sorption will be 0.0325 mg/L, which is below the MAC, but utilizing 10 g of sorbent in a single stage is less effective, resulting in a residual concentration of 2.47 mg/L. To extract $Cr_2O_7^{2-}$ ions, 4 stages and, accordingly, 4 g of sorbent are required to achieve a residual concentration of 0.08 mg/l (MAC = 0.1 mg/l). When using 10 g of sorbent in one stage, the residual concentration is 1.918 mg/l.

Using a stepwise sorption process is more advantageous from an economic point of view, since a smaller amount of sorbent is required. However, this scheme takes much more time to achieve the required residual ion concentration.

This study examined the adsorption of different categories of contaminants: heavy metal cations, heavy metal anions, anionic surfactants, cationic surfactants, organic anions, and organic non-ionic compounds. Consequently, the results suggest that the original sorbents (Zeolite and Clay) are suitable for application as multifunctional sorbents in multicomponent systems. The simplest representation of this process is illustrated in Figure 49:

Thus, the initial Zeolite or Clay can be used for the adsorption of the cationic surfactant – DDAB. The results of DDAB adsorption on zeolite are illustrated in Table 12, revealing that the majority of surfactants (58-89%) are adsorbed by the examined samples, suggesting their applicability for surfactant removal from aqueous solutions.

Moreover, Zeolite with DDAB adsorbed on it can be considered as a modified SMZ, suitable for the adsorption of organic pollutants, specifically BPA and PRO, examined in this study. The obtained SMZ can be utilized for the adsorption of inorganic anions, specifically dichromate and permanganate. Following the adsorption of permanganate or dichromate, the sorbent may be used for the subsequent adsorption of heavy metal cations.

This study examined the potential for reusing utilized sorbents. Utilized sorbents are frequently not recycled and accumulate as waste. The zeolite-based sorbents developed in this study exhibited sorption activity towards metal anions. Thus, new active centers may emerge on the sorbent surface due to sorbed anions, facilitating cation adsorption.

Lead (II) ion was chosen as a model cation due to its high toxicity and high share of anthropogenic input into the environment. Moreover, 50% of the total volume of lead emissions into the atmosphere occurs during the combustion of oil and oil products. Also, a significant share

in the global cycle of this element is the input of lead during the smelting of ferrous and non-ferrous metals. Mining waste is also a significant source of anthropogenic input of lead into the environment. The main natural source of input is wind dust.

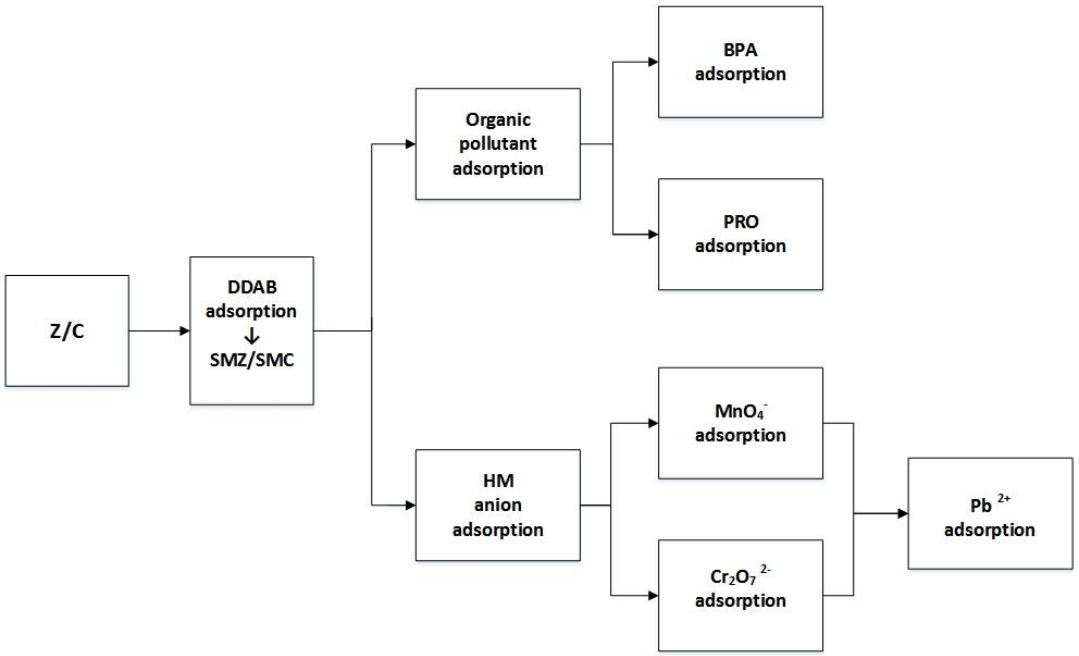


Figure 49 – Schematic diagram of a multi-stage sequential process of adsorption of various contaminants using the initial Zeolite and Clay after the DDAB extraction

The process of sorption of Pb^{2+} ions by the utilized sorbent, pre-treated with 3M HCl and modified with 20 CMC DDAB after extraction of dichromate and permanganate ions, was carried out. The results are presented as a graph of the dependence of the degree of metal extraction (E%) on time in Figure 50.

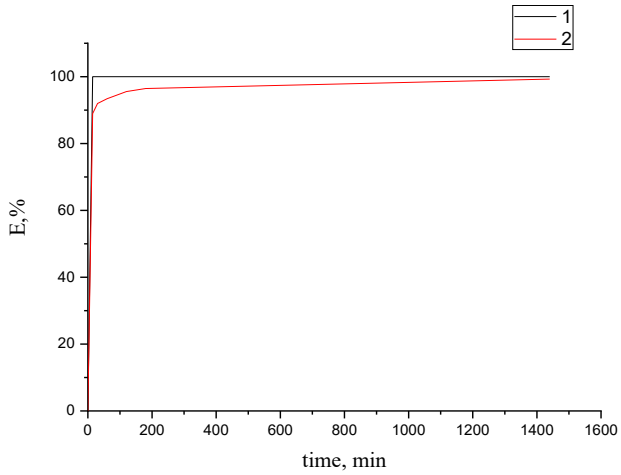


Figure 50 – Dependence of the Pb^{2+} ions uptake by H-Zeolite + DDAB after adsorption of 1) $Cr_2O_7^{2-}$ 2) MnO_4^- on time (T = 293K, pH = 6, C_0 = 10 mg/L, sorbent mass = 1 g/L, 200 rpm)

The used sorbents almost completely extract lead ions, the extraction degree reached 100% for the sorbent containing dichromate ions and 99% for permanganate ions. It follows that the reuse of the utilized sorbents for the extraction of cations is quite possible and effective and is also a promising direction for further research.

Another option for using Zeolite or Clay for sequential adsorption of different compounds may look like this (Figure 51):

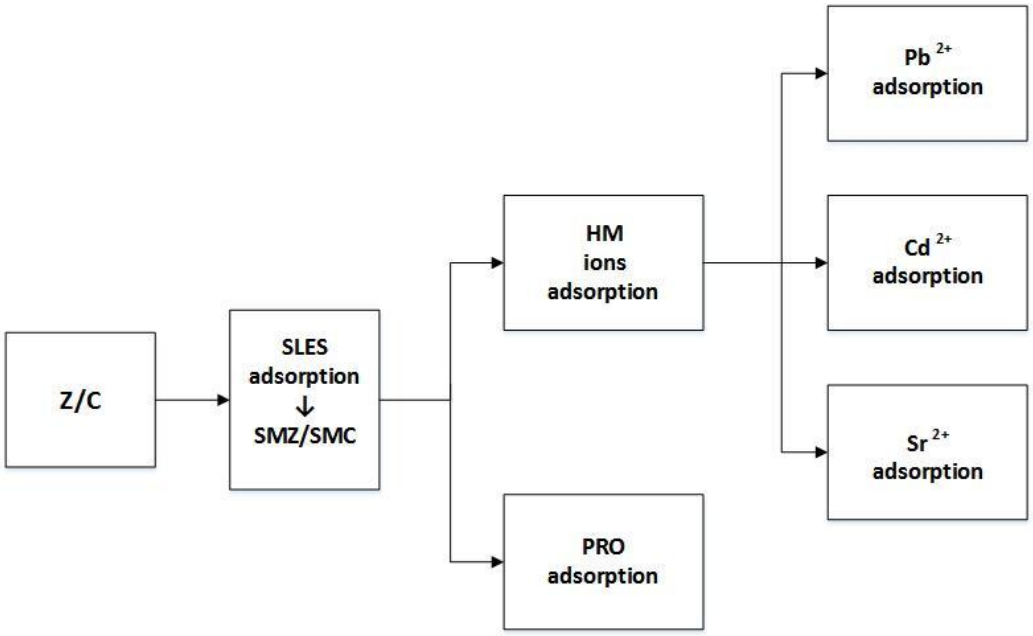


Figure 51 – Schematic diagram of a multi-stage sequential process of adsorption of various contaminants using the initial Zeolite and Clay after the SLES extraction

In this case, HM ions can be adsorbed simultaneously without compromising cleaning efficiency. The sorption of heavy metal ions in the simultaneous presence of natural zeolite and SLES-modified SMZ was investigated, with the findings illustrated in Figure 52.

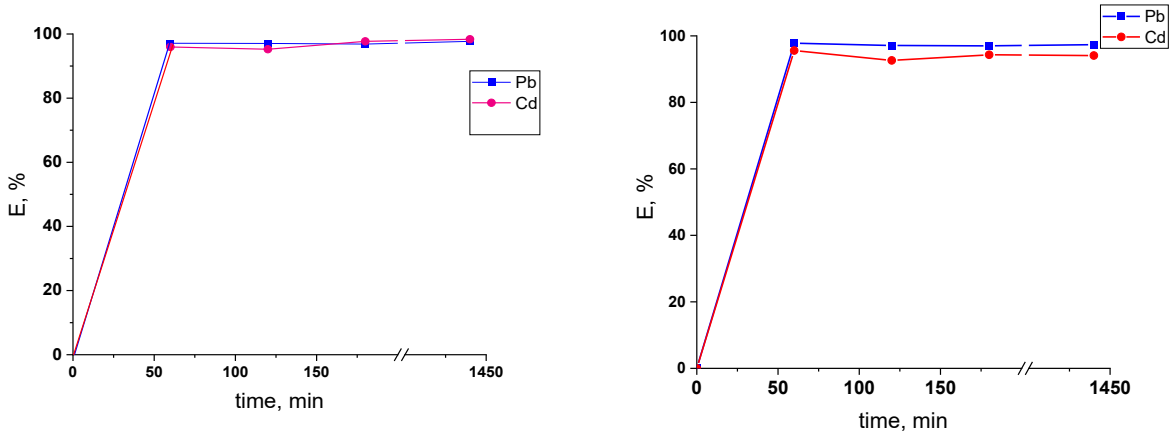


Figure 52 – The dependence of Pb^{2+} and Cd^{2+}uptake by a) Zeolite; b) Zeolite + 0.5 CMC SLES on time (pH = 6,5, T = 298 K, C_0=100 mg/L)

The highest extraction rate of Pb^{2+} ions by natural zeolite was 97.7%, whereas for Cd^{2+} ions it was 98.4%. The extraction rate for Pb^{2+} ions was 97.8%, whereas for Cd^{2+} ions it was 95.6% using SMZ. The extraction of ions in their simultaneous presence and equal concentrations by natural zeolite is significantly high [271].

The investigation of the adsorption of organic pollutants, specifically BPA, an analogue of female reproductive hormones (estrogen) [3], and PRO, a pharmaceutical substance, is also of practical significance. The investigation of the adsorption and desorption of pharmaceutical substances is essential for the targeted delivery of drugs, serving as an alternate approach for effective dosage by regulating their release throughout the body [245,272,273].

The problem of aimless consumption of medicines, as well as the almost complete lack of disposal of medicines after the expiration date, leads to environmental pollution. For example, uncontrolled consumption of antibiotics or anti-inflammatory drugs can lead to resistance to the active form of the medicine, which will subsequently lead to the emergence of super-viruses, for the treatment of which the currently existing medicines are not capable.

Thus, by creating a prolonged-release composite material, it is possible not only to reduce the reckless consumption of drugs, but also to make significant progress in environmental issues. The mechanism of action of the composite material is that, when it enters the human body, a certain amount of the drug is released that is needed at the moment. According to the release mechanism, the obtained forms are divided into prolonged-release drugs and delayed-release drugs. The difference lies in the release time of the drug [274]. Prolonged-release drug forms release over a longer period of time, compared to the usual form. While delayed-release drugs release the active substance in short periods and small doses. Targeted delivery can be found everywhere for the treatment of oncological [275,276], musculoskeletal diseases [276–278], and also in dentistry (periodontics) [279].

In recent years, there has been an increasing trend of widespread use of matrices for the delivery of non-steroidal anti-inflammatory drugs, antibiotics and vitamins [280–284], and it has also been considered as an alternative tool during the COVID19 pandemic [285].

The advantages of targeted delivery include:

- Control of drug dosage.
- Treatment effectiveness.
- Minimizing side effects.
- Eco-friendliness.
- Ease of implementation.

Biocompatible, non-toxic, and accessible materials are used as delivery carriers [286]. These include aluminosilicates, polysaccharides, polymer matrices, and chitosan [287,288]. In the context of clays, two predominant types can be identified: smectite (including montmorillonite, saponite, and hectorite) and kaolinite. Additionally, zeolite is commonly used in matrices of anti-cancer pharmaceuticals and for the administration of anti-inflammatory medicines [276,289].

The practical significance of the results obtained is as follows:

- The potential for targeted application of the most effective sorbents for each individual pollutant.

- The potential for sequential application of the examined sorbents for the remediation of several categories of pollutants. Additional research is required to utilize the examined sorbents as universal agents for cleaning multicomponent systems.

- The feasibility of employing the researched systems for the targeted distribution of pharmaceutical chemicals - BPA and PRO. Still, for the practical application of this concept, additional research on the desorption and pharmacokinetics of BPA and PRO from the synthesized sorbents is required.

CONCLUSIONS

1. Three series of sorbents were synthesized during the study:

The initial series comprises sorbents derived from zeolite/clay, modified with varying quantities of surfactants: cationic didodecyl dimethyl ammonium bromide (DDAB) or anionic sodium laureth sulfate (SLES).

The second series comprise zeolite/clay-based sorbents that have been pre-treated with a 1 mol/L NaCl solution and subsequently modified with surfactants.

The third series comprise zeolite/clay-based sorbents that have undergone acid activation with hydrochloric acid at three distinct concentrations (1 mol/L, 3 mol/L, 6 mol/L), then followed by surfactant treatment.

2. Based on the physico-chemical characterization of the obtained adsorbents we can conclude that:

Na^+ treatment increases the cation exchange capacity (CEC) of the zeolite/clay and the ability to participate in ion-exchange processes.

Acid activation leads to a significant increase of the surface area but decreases the CEC compared to initial materials. High concentrations of acid are unfavorable due to destruction of the zeolite crystalline framework, while clay is stable even at high acid concentrations. The 3 mol/L has been chosen as optimum acid concentration.

Treatment with salt or acid provides structural changes to the zeolite/clay and affects its interaction with the surfactant modifier.

The effective modification of Zeolite/clay with surfactants is evidenced by IR/Raman spectroscopy and BET analysis data.

3. Modified materials were used to extract two types of contaminants – heavy metal (HM) ions – Pb^{2+}, Cd^{2+}, Sr^{2+}, MnO_4^-, $Cr_2O_7^{2-}$ and organic contaminants – Bisphenol-A and Propranolol.

It has been determined that the initial Zeolite/Clay can serve as excellent sorbents for lead ions without prior treatment. The alteration of Zeolite/Clay with an anionic surfactant, specifically SLES, results in enhanced sorption activity towards heavy metal cations, namely cadmium and strontium. The incorporation of the cationic surfactant DDAB effectively enhances the extraction efficiency of HM anions, specifically dichromate and permanganate.

Thus, surfactants serve as efficient modifiers for regulating the charge and recharge of aluminosilicate surfaces, as well as for the selective adsorption of heavy metal ions on the examined sorbents.

4. Thus, based on the results obtained, it was established that:

- For the adsorption of Pb^{2+} ions, the original Zeolite and Clay are effective, the degree of extraction reaches almost 100%.

- For the adsorption of Cd^{2+} ions, the most effective sorbents are those based on Zeolite modified with 0.00025 M SLES and Clay modified with 0.01 M SLES.

- For the adsorption of Sr^{2+} ions, the most effective was a sorbent based on Zeolite modified with 0.0005 M SLES.

- For the adsorption of MnO_4^- and $Cr_2O_7^{2-}$ ions, the most effective was a sorbent pre-treated with 3 M HCl subsequently modified with 20 CMC DDAB.

- For the adsorption of Bisphenol-A, the most effective sorbents are those based on Zeolite and Clay, pre-treated with 3 M HCl followed by modification with 10 CMC DDAB.

- For the adsorption of Propranolol, the most effective sorbents are those based on Zeolite and Clay, pre-treated with 1 M NaCl followed by modification with 1 CMC DDAB, as well as those based on Clay pre-treated with 1 M NaCl followed by modification with 10 CMC SLES.

5. Studying the effect of various factors on the process of lead ion adsorption on Clay revealed the following findings:

- The solid/liquid ratio of 1:10 is the optimum for efficient adsorption of lead (II) ions onto Clay.

- Optimal adsorption occurs at pH levels exceeding 6, although pH values above 8 may lead to inaccuracies in the actual adsorption measurements, prompting the decision to conduct additional experiments within the pH range of 6 to 7.

- Saturation of active centers of Clay occurs at initial concentrations of lead solution > 200 mg/L.

- Based on the analysis of various isotherm models, it was established that the adsorption process in the Clay-Pb system is described by the Langmuir isotherm, and the use of the Toth model can significantly reduce the error in modeling the values of sorption capacity.

- A study of process kinetics revealed that the interaction of Clay with Pb aligns with the pseudo-second-order model.

- The application of diffusion kinetic models demonstrated significant surface adsorption (Webber-Morris model), with both film and intraparticle diffusion stages contributing to the rate-limiting step (Dumwald-Wagner model), and adsorption occurring via ion-exchange (Chemisorption Diffusion model).

- An increase in temperature results in a reduction in lead ion extraction, with lead adsorption on Clay being exothermic. The calculated Gibbs energy values indicate the spontaneity of the adsorption process, the enthalpy value suggests physisorption, and the entropy value reflects active ion-exchange processes.

6. Analysis of IR and Raman spectra of Clay before and after lead ion adsorption suggests that lead adsorption occurs on both the surface layers of SiO_4 clay tetrahedrons and within the inner layers of AlO_6 tetrahedrons. Interaction with the surface layers presumably occurs through ion exchange with metal cations, such as Na, K, Ca, and Mg, which compensate for the excessive negative charge present in the channels and pores created by the SiO_4 tetrahedron rings. The sorption within the inner layers of AlO_6 octahedrons may be attributed to physical adsorption in the sorbent's pores, facilitated by Van der Waals forces.

7. A novel Na–H method is proposed to differentiate and assess the contributions of ion exchange and pore adsorption in aluminosilicate–pollutant systems. By altering CEC and surface area via Na^+ and H^+ treatments, it serves as a rapid diagnostic tool for identifying dominant adsorption mechanisms and refining the theoretical understanding of sorption processes.

8. By varying the experimental conditions, it is possible to achieve sufficiently high values of BPA and PRO adsorption by the obtained sorbents. It was found that:

- The optimal concentration of DDAB in the sorbents is 10 CMC (1 mmol/l), and 1 CMC (0.1 mmol/l) for the H-Zeolite + DDAB sorbent during PRO adsorption.

- The optimal adsorbent mass is 15 g/l.

- The adsorption of BPA on zeolite and H-Zeolite + DDAB is best described by the Temkin isotherm, assuming that adsorption is a multi-layer process, and the calculated values of bonding energy correspond to physisorption.

- The adsorption of PRO on zeolite is best described by the Sips equation, the most applicable 3-parameter isotherm model for monolayer adsorption.

- The adsorption of PRO on Na-Zeolite + DDAB is best described by a three-parameter Fritz-Schlunder equation, which becomes Freundlich isotherm at low concentrations, whereas transforms to Langmuir at high concentrations.

9. During the study of the mechanism of BPA and PRO adsorption on zeolite-based sorbents, the following was established:

- Modification of natural zeolite with cationic surfactant enhances adsorption of organic pollutants by increasing its hydrophobicity.

- As a result of a detailed analysis and description of the physicochemical characteristics and the influence of pretreatment and surfactant modification on the zeolite properties, possible mechanisms of interaction with BPA and PRO were deduced.

- In the case of BPA, the adsorbent-adsorbate interaction mechanism may include chemisorption, electrostatic attraction, and hydrophobic interactions with the surfactant.

- For PRO, the adsorbent-adsorbate interaction mechanism possibly also includes physisorption.

- For PRO, the most effective form of modification was pretreatment of zeolite with NaCl prior to modification with DDAB, however for BPA, slightly better results were obtained with HCl pretreatment.

10. The practical significance of the results obtained is as follows:

- The potential for targeted application of the most effective sorbents for each individual pollutant.

- The potential for sequential application of the examined sorbents for the remediation of several categories of pollutants. Additional research is required to utilize the examined sorbents as universal agents for cleaning multicomponent systems.

- The feasibility of employing the researched systems for the targeted distribution of pharmaceutical chemicals - BPA and PRO. Still, for the practical application of this concept, additional research on the desorption and pharmacokinetics of BPA and PRO from the synthesized sorbents is required.

REFERENCES

1 Ussipbekova Ye.Zh., Zhagiparova A.D., Rakhym A.B., Kenessova A.K., Seilkhanova G.A., Osmanzhan G.O. Issledovanie adsorbcii ionov medi i cinka sorbentami na osnove rastitel'nyh othodov – zhmyha i luzgi semyan podsolnuha (Study of adsorption of copper and zinc ions by sorbents based on plant waste - cake and husk of sunflower seeds) // Eurasian Journal of Ecology. - 2021. - Vol. 2, Is. 67. - P. 22–30. (in Russian)

2 Csavdari A., Rakhym A., Seilkhanova G. Preliminary assessment of modified Kazakh natural zeolites as possible sorbents for MnO_4^- removal from aqueous solutions // Studia Universitatis Babeș-Bolyai Chemia. - 2018. - Vol. 63, Is. 4. - P. 181–192.

3 Dong Y., Wu D., Chen X., Lin Y. Adsorption of bisphenol A from water by surfactant-modified zeolite // Journal of Colloid and Interface Science. - 2010. - Vol. 348, Is. 2. - P. 585–590.

4 Reeve P.J., Fallowfield H.J. Natural and surfactant modified zeolites: A review of their applications for water remediation with a focus on surfactant desorption and toxicity towards microorganisms // Journal of Environmental Management. - 2018. - Vol. 205. - P. 253–261.

5 Kong H., Wu D., Xie Q., Xie J., Wang Z., Zhang Z. Adsorption of organic pollutants by surfactant modified zeolite as controlled by surfactant chain length // Microporous and Mesoporous Materials. - 2013. - Vol. 179. - P. 144–150.

6 Sun K., Shi Y., Wang X., Li Z. Sorption and retention of diclofenac on zeolite in the presence of cationic surfactant // Journal of Hazardous Materials. - 2017. - Vol. 323. - P. 584–592.

7 Breck D.W. Zeolite molecular sieves: structure, chemistry, and use // New York: Wiley, 1974.

8 Brosillon S., Manero M.-H., Foussard J.-N. Mass transfer in VOC adsorption on zeolite: experimental and theoretical breakthrough curves // Environmental science & technology. - 2001. - Vol. 35, Is. 17. - P. 3571–3575.

9 Uddin M.K. A review on the adsorption of heavy metals by clay minerals, with special focus on the past decade // Chemical Engineering Journal. - 2017. - Vol. 308. - P. 438–462.

10 Lopes A.C., Martins P., Lanceros-Mendez S. Aluminosilicate and aluminosilicate based polymer composites: present status, applications and future trends // Progress in surface science. - 2014. - Vol. 89, Is. 3–4. - P. 239–277.

11 Dionisiou N.S., Matsi T. Natural and surfactant-modified zeolite for the removal of pollutants (mainly inorganic) from natural waters and wastewaters // Environmental Materials and Waste. - 2016. - P. 591–606.

12 Díaz-Nava C., Olguín M.T., Solache-Ríos M., Alarcón-Herrera M.T., Aguilar-Elguezabal A. Phenol sorption on surfactant-modified Mexican zeolitic-rich tuff in batch and continuous systems // Journal of Hazardous Materials. - 2009. - Vol. 167, Is. 1–3. - P. 1063–1069.

13 Godelitsas A., Armbruster T. HEU-type zeolites modified by transition elements and lead // Microporous and Mesoporous Materials. - 2003. - Vol. 61, Is. 1–3. - P. 3–24.

14 Díaz-Nava C., Olguín M.T., Solache-Ríos M., Alarcón-Herrera M.T., Aguilar-Elguezabal A. Phenol sorption on surfactant-modified Mexican zeolitic-rich tuff in batch and continuous systems // Journal of hazardous materials. - 2009. - Vol. 167, Is. 1–3. - P. 1063–1069.

15 Agatayeva A.A. Razrabotka sorbcionnoj tekhnologii izvlecheniya ceolitom poleznyh komponentov iz fosforsoderzhashchego zhidkogo othoda: dis. ... d-ra filosofii (PhD): 6D072000 – Himicheskaya tekhnologiya neorganicheskih veshchestv (Development of sorption technology for extracting useful components from phosphorus-containing liquid waste using zeolite: diss. ... Doctor of Philosophy (PhD): 6D072000 – Chemical technology of inorganic substances) / A. A. Agatayeva. – Almaty, 2016. – 150 p. (in Russian)

16 Momčilović M., Kragović M., Stojmenović M., Marković M., Petrović M., Nedeljković B., Pašalić S. Natural and Modified Zeolite—Alginate Composites. Application for Removal of Heavy Metal Cations from Contaminated Water Solutions // Minerals. - 2018. - Vol. 8, Is. 1. - P. 11.

17 Guo L., Huang Y., Lan J., Cao D., Zhang L., Zeng X. Heavy metal ion removal of wastewater by zeolite-imidazolate frameworks // Separation and Purification Technology. - 2017. - Vol. 194, Is. September 2017. - P. 462–469.

18 Shang H., Javadi S., Zhao Q. Organic Surfactant Modified Zeolite as a Permeable Reactive Barrier Component—A Laboratory Study // Geotechnical Frontiers 2017. – 2017. – C. 443-449.

19 Ospanov K.T., Muhanova G.N. Obezvrezhivanie osadkov stochnyh vod ot tyazhelyh metallov s pomoshch'yu prirodnogo ceolita (Protection of waste water sediments from heavy metals using natural zeolite) // Voda i ekologiya: problemy i resheniya. (Water and ecology: problems and solutions) - 2015. - Is. 4. - P. 56–61. (in Russian)

20 He Y., Lin H., Dong Y., Wang L. Preferable adsorption of phosphate using lanthanum-incorporated porous zeolite: Characteristics and mechanism // Applied Surface Science. - 2017. - Vol. 426. - P. 995–1004.

21 Li Z., Anghel I., Bowman R.S. Sorption of oxyanions by surfactant-modified zeolite // Journal of Dispersion Science and Technology. - 1998. - Vol. 19, Is. 6–7. - P. 843–857.

22 Liu J., Cheng X., Zhang Y., Wang X., Zou Q., Fu L. Zeolite modification for adsorptive removal of nitrite from aqueous solutions // Microporous and Mesoporous Materials. - 2017. - Vol. 252. – P. 179-187.

23 Naghash A., Nezamzadeh-Ejhieh A. Comparison of the efficiency of modified clinoptilolite with HDTMA and HDP surfactants for the removal of phosphate in aqueous solutions // Journal of Industrial and Engineering Chemistry. - 2015. - Vol. 31. – P. 185-191.

24 Fungaro D.A., Borrely S.I., Carvalho T.E.M. Surfactant Modified Zeolite from Cyclone Ash as Adsorbent for Removal of Reactive Orange 16 from Aqueous Solution // American Journal of Environmental Protection. - 2013. - Vol. 1, Is. 1. - P. 1–9.

25 Jumaeri J., Santosa S.J., Sutarno S. Adsorption of Congo Red Dye on HDTMA Surfactant-Modified Zeolite A Synthesized from Fly Ash // Defect and Diffusion Forum. - 2018. - Vol. 382. - P. 307–311.

26 Zarei M., Djafarzadeh N., Khadir L. Removal of direct blue 129 from aqueous medium using surfactant-modified zeolite: a neural network modeling // Environmental Health Engineering and Management. - 2018. - Vol. 5, Is. 2. - P. 101–113.

27 Xie Q., Xie J., Chi L., Li C., Wu D., Zhang Z., Kong H. A new sorbent that simultaneously sequesters multiple classes of pollutants from water: Surfactant modified zeolite // Science China Technological Sciences. - 2013. - Vol. 56, Is. 7. - P. 1749–1757.

28 Dong Y., Wu D., Chen X., Lin Y. Adsorption of bisphenol A from water by surfactant-modified zeolite // Journal of Colloid and Interface Science. - 2010. - Vol. 348, Is. 2. - P. 585–590.

29 Genç N., Kılıçoğlu Ö., Narci A.O. Removal of Bisphenol A aqueous solution using surfactant-modified natural zeolite: Taguchi's experimental design, adsorption kinetic, equilibrium and thermodynamic study // Environmental Technology (United Kingdom). - 2017. - Vol. 38, Is. 4. - P. 424–432.

30 Bazbaz I.A., Yousef R.I., Musleh S.M. Modification of jordanian zeolitic tuff using cationic surfactants and their capacity for phenols removal // Asian Journal of Chemistry. - 2011. - Vol. 23, Is. 6. - P. 2553–2557.

31 Li Z., Anghel I., Bowman R.S. Sorption of oxyanions by surfactant-modified zeolite // Journal of Dispersion Science and Technology. - 1998. - Vol. 19, Is. 6–7. - P. 843–857.

32 Bowman R.S. Applications of surfactant-modified zeolites to environmental remediation // Microporous and Mesoporous Materials. - 2003. - Vol. 61, Is. 1–3. - P. 43–56.

33 Haggerty G.M., Bowman R.S. Sorption of Chromate and Other Inorganic Anions by Organo-Zeolite // Environmental Science and Technology. - 1994. - Vol. 28, Is. 3. - P. 452–458.

34 Ghiaci M., Abbaspur A., Kia R., Seyedeyn-Azad F. Equilibrium isotherm studies for the sorption of benzene, toluene, and phenol onto organo-zeolites and as-synthesized MCM-41// Separation and Purification Technology. - 2004. - Vol.40, Is. 3. – P. 217-229.

35 Jiang N., Shang R., Heijman S.G.J., Rietveld L.C. High-silica zeolites for adsorption of organic micro-pollutants in water treatment: A review // Water Research. - 2018. - Vol. 144. - P. 145–161.

36 Hernández-Huesca R., Díaz L., Aguilar-Armenta G. Adsorption equilibria and kinetics of CO_2, CH_4 and N_2 in natural zeolites // Separation and Purification Technology. - 1999. - Vol. 15, Is. 2. - P. 163–173.

37 Ertan A., Çakicioğlu-Özkan F. CO_2 and N_2 Adsorption on the Acid (HCL, HNO_3, H_2SO_4 and H_3PO_4) Treated Zeolites // Adsorption. - 2005. - Vol. 11. - P. 151–156.

38 Mansouri N., Rikhtegar N., Ahmad Panahi H., Atabi F., Shahraki B.K. Porosity, characterization and structural properties of natural zeolite - Clinoptilolite - as a sorbent // Environment Protection Engineering. - 2013. - Vol. 39, Is. 1. - P. 139–152.

39 Dávila-Estrada M., Ramírez-García J.J., Solache-Ríos M.J., Gallegos-Pérez J.L. Kinetic and Equilibrium Sorption Studies of Ceftriaxone and Paracetamol by Surfactant-Modified Zeolite // Water, Air, and Soil Pollution. - 2018. - Vol. 229, Is. 4. – P.123.

40 Sultanbaeva G.Sh., Dzhunusbekova G.B., Chernyakova R.M., Dzhusipbekov U.Zh. Fiziko-himicheskie issledovaniya ceolita, aktivirovannogo solyanoj kislotoj (Physical and chemical studies of ceolite activated by hydrochloric acid) // Academic Scientific Journal of Chemistry. - 2006. - Is. 4. - P. 68–72. (in Russian)

41 Hedlund J., Sterte J., Anthonis M., Bons A.-J., Carstensen B., Corcoran N., Cox D., Deckman H., De Gijnst W., de Moor P.-P. High-flux MFI membranes // Microporous and Mesoporous Materials. - 2002. - Vol. 52, Is. 3. - P. 179–189.

42 Hedlund J., Korelskiy D., Sandström L., Lindmark J. Permporometry analysis of zeolite membranes // Journal of Membrane Science. - 2009. - Vol. 345, Is. 1–2. - P. 276–287.

43 Korelskiy D., Ye P., Zhou H., Mouzon J., Hedlund J. Reprint of: An experimental study of micropore defects in MFI membranes // Microporous and mesoporous materials. - 2014. - Vol. 192. - P. 69–75.

44 Zamzow M.J., Eichbaum B.R., Sandgren K.R., Shanks D.E. Removal of heavy metals and other cations from wastewater using zeolites // Separation science and technology. - 1990. - Vol. 25, Is. 13–15. - P. 1555–1569.

45 Bureš F. Quaternary Ammonium Compounds: Simple in Structure, Complex in Application // Topics in Current Chemistry. - 2019. - Vol. 377, Is. 3. - P. 1–21.

46 Bai R., Sun Q., Wang N., Zou Y., Guo G., Iborra S., Corma A., Yu J. Simple Quaternary Ammonium Cations-Templated Syntheses of Extra-Large Pore Germanosilicate Zeolites // Chemistry of Materials. - 2016. - Vol. 28, Is. 18. - P. 6455–6458.

47 Shen X., Mao W., Ma Y., Peng H., Xu D., Wu P., Han L., Che S. Mesoporous MFI Zeolite with a 2D Square Structure Directed by Surfactants with an Azobenzene Tail Group // Chemistry - A European Journal. - 2018. - Vol. 24, Is. 34. - P. 8615–8623.

48 Sullivan E.J., Hunter D.B., Bowman R.S. Fourier transform Raman spectroscopy of sorbed HDTMA and the mechanism of chromate sorption to surfactant-modified clinoptilolite // Environmental Science and Technology. - 1998. - Vol. 32, Is. 13. - P. 1948–1955.

49 Li C., Dong Y., Wu D., Peng L., Kong H. Surfactant modified zeolite as adsorbent for removal of humic acid from water // Applied Clay Science. - 2011. - Vol. 52, Is. 4. - P. 353–357.

50 Tran H.N., Viet P. Van, Chao H.P. Surfactant modified zeolite as amphiphilic and dual-electronic adsorbent for removal of cationic and oxyanionic metal ions and organic compounds // Ecotoxicology and Environmental Safety. - 2018. - Vol. 147, Is. August 2017. - P. 55–63.

51 Ghiaci M., Kia R., Abbaspur A., Seyedeyn-Azad F. Adsorption of chromate by surfactant-modified zeolites and MCM-41 molecular sieve // Separation and Purification Technology. - 2004. – Vol.40. – P. 285-295.

52 Zheng Y., Liu W., Wang Q., Sun Y., Li G., Wu T., Li Y. Study of STAB- and DDAB-modified sepiolite tructures and their adsorption performance for emulsified oil in produced water // Colloid and Interface Science Communications. - 2020. - Vol. 34. - P. 100231.

53 Melanson J.E., Baryla N.E., Lucy C.A. Double-chained surfactants for semipermanent wall coatings in capillary electrophoresis // Analytical Chemistry. - 2000. - Vol. 72, Is. 17. - P. 4110–4114.

54 Karnjanakom S., Maneechakr P. Adsorption behaviors and capacities of Cr(VI) onto environmentally activated carbon modified by cationic (HDTMA and DDAB) surfactants // Journal of Molecular Structure. - 2019. - Vol. 1186. - P. 80–90.

55 Hedayati M.S., Li L.Y. Removal of polycyclic aromatic hydrocarbons from aqueous media using modified clinoptilolite // Journal of Environmental Management. - 2020. - Vol. 273, Is. March. - P. 111113.

56 Garoma T., Kocher J. Investigation of surfactant-modified activated carbon for recycled water disinfection // Water Science and Technology. - 2010. - Vol. 62, Is. 8. - P. 1755–1766.

57 Huang Y., Zeng X., Guo L., Lan J., Zhang L., Cao D. Heavy metal ion removal of wastewater by zeolite-imidazolate frameworks // Separation and Purification Technology. - Elsevier, 2018. - Vol. 194. - P. 462–469.

58 Assi M.A., Hezmee M.N.M., Sabri M.Y.M., Rajion M.A. The detrimental effects of lead on human and animal health // Veterinary world. - 2016. - Vol. 9, Is. 6. - P. 660.

59 Schock M.R. Causes of temporal variability of lead in domestic plumbing systems // Environmental monitoring and assessment. - 1990. - Vol. 15. - P. 59–82.

60 Montes-Atenas G., Valenzuela F. Wastewater Treatment through Low Cost Adsorption Technologies // Physico-Chemical Wastewater Treatment and Resource Recovery. - 2017. - P. 213–238.

61 Seilkhanova G.A., Imangaliyeva A.N., Mastai Y., Rakhym A.B. Bentonite polymer composite for water purification // Bulletin of Materials Science. - Indian Academy of Sciences, 2019. - Vol. 42, Is. 60. - P. 1–8.

62 Gu S., Kang X., Wang L., Lichtfouse E., Wang C. Clay mineral adsorbents for heavy metal removal from wastewater : a review // Environmental Chemistry Letters. - 2019. - Vol. 17, Is. 2. - P. 629–654.

63 Seilkhanova G.A., Imangaliyeva A.N., Akbayeva D.N. Modified raw materials: synthesis, characterization and application for Cd^{2+} ions removal // Studia Universitatis Babes-Bolyai Chemia. - 2017. - Vol. 62, Is. 1. - P. 35–50.

64 Shirzadi H., Nezamzadeh-Ejhieh A. An efficient modified zeolite for simultaneous removal of Pb(II) and Hg(II) from aqueous solution // Journal of Molecular Liquids. - 2017. - Vol. 230. - P. 221–229.

65 Kragović M., Daković A., Marković M., Krstić J., Gatta G.D., Rotiroti N. Characterization of lead sorption by the natural and Fe(III)-modified zeolite // Applied Surface Science. - 2013. - Vol. 283. - P. 764–774.

66 Franco D.S.P., Fagundes J.L.S., Georgin J., Salau N.P.G., Dotto G.L. A mass transfer study considering intraparticle diffusion and axial dispersion for fixed-bed adsorption of crystal violet on pecan pericarp (Carya illinoensis) // Chemical Engineering Journal. - Elsevier, 2020. - Vol. 397, Is. May. - P. 125423.

67 Budianta W., Andriyani N.D., Ardiana A., Warmada I.W. Adsorption of lead and cadmium from aqueous solution by Gunungkidul zeolitic tuff, Indonesia // Environmental Earth Sciences. - 2020. - Vol. 79, Is. 8. - P. 1–11.

68 Obiri-Nyarko F., Kwiatkowska-Malina J., Malina G., Wołowiec K. Assessment of zeolite and compost-zeolite mixture as permeable reactive materials for the removal of lead from a model acidic groundwater // Journal of Contaminant Hydrology. - 2020. - Vol. 229, Is. November 2019. - P. 103597.

69 Khan S., Idrees M., Bilal M. Revealing and elucidating chemical speciation mechanisms for lead and nickel adsorption on zeolite in aqueous solutions // Colloids and Surfaces A: Physicochemical and Engineering Aspects. - 2021. - Vol. 623, Is. December 2020. - P. 126711.

70 Friberg L., Piscator M., Nordberg G.F., Kjellström T. Cadmium in the Environment. - 1974. – No. 2nd edition. – 248 pp.

71 Dal Bosco S.M., Jimenez R.S., Carvalho W.A. Removal of toxic metals from wastewater by Brazilian natural scolecite // Journal of Colloid and Interface Science. - 2005. - Vol. 281, Is. 2. - P. 424–431.

72 Mier M.V., Callejas R.L., Gehr R., Cisneros B.E.J., Alvarez P.J.J. Heavy metal removal with mexican clinoptilolite:: multi-component ionic exchange // Water research. - 2001. - Vol. 35, Is. 2. - P. 373–378.

73 Wingenfelder U., Nowack B., Furrer G., Schulin R. Adsorption of Pb and Cd by amine-modified zeolite // Water research. - 2005. - Vol. 39, Is. 14. - P. 3287–3297.

74 Cortés-Martínez R., Martínez-Miranda V., Solache-Ríos M., García-Sosa I. Evaluation of natural and surfactant-modified zeolites in the removal of cadmium from aqueous solutions // Separation Science and Technology. - 2004. - Vol. 39, Is. 11. - P. 2711–2730.

75 Nguyen T.C., Loganathan P., Nguyen T.V., Vigneswaran S., Kandasamy J., Naidu R. Simultaneous adsorption of Cd, Cr, Cu, Pb, and Zn by an iron-coated Australian zeolite in batch and fixed-bed column studies // Chemical Engineering Journal. - 2015. - Vol. 270. - P. 393–404.

76 Velarde L., Nabavi M.S., Escalera E., Antti M.-L., Akhtar F. Adsorption of heavy metals on natural zeolites: A review // Chemosphere. - 2023. - Vol. 328. - P. 138508.

77 İnan S. Inorganic ion exchangers for strontium removal from radioactive waste : a review // Journal of Radioanalytical and Nuclear Chemistry. - 2022. - Vol. 331, Is. 3. - P. 1137–1154.

78 Munthali M.W., Johan E., Aono H., Matsue N. Cs^{+} and Sr^{2+} adsorption selectivity of zeolites in relation to radioactive decontamination // Journal of Asian Ceramic Societies. - 2015. - Vol. 3, Is. 3. - P. 245–250.

79 Shichalin O.O., Papynov E.K., Ivanov N.P., Balanov M.I., Dran'kov A.N., Shkuratov A.L., Zarubina N. V, Fedorets A.N., Mayorov V.Yu., Lembikov A.O., Shi Y., Tananaev I.G., Ivanets A.I. Study of adsorption and immobilization of Cs^{+}, Sr^{2+}, Co^{2+}, Pb^{2+}, La^{3+} ions on Na-Faujasite zeolite transformed in solid state matrices // Separation and Purification Technology. - 2024. - Vol. 332. - P. 125662.

80 RSE "Kazhydromet" Information bulletin on the state of the environment of Kazakhstan for May 2025: [Electronic resource] - Almaty, 2025. Access mode: https://www.kazhydromet.kz/ru/ecology/informacionnye-byulleteni-o-sostoyanii-okruzhayuschey-sredy-respubliki-kazahstan. - Date of access: 09/15/2025.

81 Kučić D. Batch Adsorption of Cr(VI) Ions on Zeolite and Agroindustrial Waste // Chemical and Biochemical Engineering Quarterly. - 2018. - Vol. 31, Is. 4. - P. 497–507.

82 Thanos A.G., Katsou E., Malamis S., Drakopoulos V., Paschalakis P., Pavlatou E.A., Haralambous K.J. Cr(VI) removal from aqueous solutions using aluminosilicate minerals in their Pb-exchanged forms // Applied Clay Science. - Elsevier, 2017. - Vol. 147, Is. July. - P. 54–62.

83 Salama T.M., Ali I.O., Bakr M.F., El-Sheikh S.M., Fodial M.H. Functionalization of Synthesized NaP Zeolite with Silver Nanoparticles Capped with Alkyl Dimethyl Hydroxyethyl Ammonium for Sorption and Reduction of Chromate(VI) Oxoanions // Journal of Inorganic and Organometallic Polymers and Materials. - 2018. - Vol. 28, Is. 1. - P. 334–351.

84 Shi T., Yang D., Yang H., Ye J., Cheng Q. Preparation of chitosan crosslinked modified silicon material and its adsorption capability for chromium(VI) // Applied Clay Science. - 2017. - Vol. 142. - P. 100–108.

85 Prikry J.D., Bertetti F.P., Pabalan R.T. Effects of Surfactant Modification on the Sorption Behavior of Natural Zeolites for Strontium(2+) and Uranium(6+) // MRS Online Proceedings Library. - 2011. - Vol. 608, Is. 1. - P. 281.

86 Leyva-Ramos R., Jacobo-Azuara A., Diaz-Flores P.E., Guerrero-Coronado R.M., Mendoza-Barron J., Berber-Mendoza M.S. Adsorption of chromium(VI) from an aqueous solution on a surfactant-modified zeolite // Colloids and Surfaces A: Physicochemical and Engineering Aspects. - 2008. - Vol. 330, Is. 1. - P. 35–41.

87 Zeng Y., Woo H., Lee G., Park J. Adsorption of Cr(VI) on hexadecylpyridinium bromide (HDPB) modified natural zeolites // Microporous and Mesoporous Materials. - 2010. - Vol. 130, Is. 1. - P. 83–91.

88 Haggerty G.M., Bowman R.S. Sorption of chromate and other inorganic anions by organo-zeolite // Environmental Science & Technology. - 1994. - Vol. 28, Is. 3. - P. 452–458.

89 Velarde L., Nabavi M.S., Escalera E., Antti M.-L., Akhtar F. Adsorption of heavy metals on natural zeolites: A review // Chemosphere. - 2023. - Vol. 328. - P. 138508.

90 Asgari G., Ramavandi B., Rasuli L., Ahmadi M. Cr (VI) adsorption from aqueous solution using a surfactant-modified Iranian zeolite: characterization, optimization, and kinetic approach // Desalination and Water Treatment. - 2013. - Vol. 51, Is. 31–33. - P. 6009–6020.

91 AL-Aoh H.A. Adsorption of MnO_4^- from aqueous solution by Nitraria retusa leaves powder; kinetic, equilibrium and thermodynamic studies // Materials Research Express. - 2019. - Vol. 6, Is. 11. - P. 115102.

92 Mfoumou C.M., Tonda-Mikiela P., Ngoye F., Lionel M.B., Spenseur B.M., Sachse A., Mignard S., Tchouya G.R.F. Dynamic Adsorption on Fixed-Bed Column of Manganese Oxoanions (MnO_4^-) in Aqueous Media on Activated Carbon Prepared from Palm Nut Shells // Journal of Environment Pollution and Human Health. - 2022. - Vol. 10, Is. 2. - P. 58–70.

93 Verma R.K., Kapoor R., Gupta S.K., Chaudhari R.R. An efficient technique for removal of K^+ and MnO_4^- ions through adsorption in aqueous solution by using activated charcoal // Pharm. Chem. J. - 2014. - Vol. 1, Is. 2. - P. 20–25.

94 Mfoumou C.M., Ngoye F., Tonda-Mikiela P., Berthy M.L., Spenseur B.M., Tchouya G.R.F. Fixed-Bed Column Adsorption Modeling of MnO_4^- Ions from Acidic Aqueous Solutions on Activated Carbons Prepared with the Biomass // Open Journal of Inorganic Chemistry. - 2023. - Vol. 13, Is. 2. - P. 25–42.

95 Chen F., Hong M., You W., Li C., Yu Y. Simultaneous efficient adsorption of Pb^{2+} and MnO_4^- ions by MCM-41 functionalized with amine and nitrilotriacetic acid anhydride // Applied Surface Science. - 2015. - Vol. 357. - P. 856–865.

96 Li X., Zhang S., Zhang L., Yang Y., Zhang K., Cai Y., Xu Y., Gai Y., Xiong K. Viologen-Based Cationic Metal–Organic Framework for Antibiotics Detection and MnO_4^- Removal in Water // Crystal Growth & Design. - 2022. - Vol. 22, Is. 7. - P. 3991–3997.

97 Jovanovic M., Arcon I., Kovac J., Tusar N.N., Obradovic B., Rajic N. Removal of manganese in batch and fluidized bed systems using beads of zeolite a as adsorbent // Microporous and Mesoporous Materials. - 2016. - Vol. 226. - P. 378–385.

98 Massoudinejad M., Asadi A., Vosoughi M., Gholami M., kakavandi B., Karami M.A. A comprehensive study (kinetic, thermodynamic and equilibrium) of arsenic (V) adsorption using $KMnO_4$ modified clinoptilolite // Korean Journal of Chemical Engineering. - 2015. - Vol. 32, Is. 10. - P. 2078–2086.

99 Bergaya F., Lagaly G. Handbook of clay science. - Newnes, 2013. – Vol.5.

100 Gu S., Kang X., Wang L., Lichtfouse E., Wang C. Clay mineral adsorbents for heavy metal removal from wastewater: a review // Environmental Chemistry Letters. - 2019. - Vol. 17, Is. 2. - P. 629–654.

101 Alshameri A., Wei X., Wang H., Fuguo Y., Chen X., He H., Yan C., Xu F. A review of the role of natural clay minerals as effective adsorbents and an alternative source of minerals // Minerals. - 2019. - Vol. 3. - P. 49–64.

102 Kinoti I.K., Karanja E.M., Nthiga E.W., M'Thiruaine C.M., Marangu J.M. Review of Clay-Based Nanocomposites as Adsorbents for the Removal of Heavy Metals // Journal of Chemistry. - 2022. - Vol. 2022, Is. 1. – P. 7504626.

103 Ewis D., Ba-Abbad M.M., Benamor A., El-Naas M.H. Adsorption of organic water pollutants by clays and clay minerals composites: A comprehensive review // Applied Clay Science. - 2022. - Vol. 229. – P. 106686.

104 Khatamian M., Divband B., Shahi R. Ultrasound assisted co-precipitation synthesis of Fe3O4/bentonite nanocomposite: Performance for nitrate, BOD and COD water treatment // Journal of Water Process Engineering. - 2019. - Vol. 31. - P. 100870.

105 Ain Q.U., Rasheed U., Yaseen M., Zhang H., Tong Z. Superior dye degradation and adsorption capability of polydopamine modified Fe3O4-pillared bentonite composite // Journal of hazardous materials. - 2020. - Vol. 397. - P. 122758.

106 Bhattacharyya K.G., Gupta S. Sen Adsorption of a few heavy metals on natural and modified kaolinite and montmorillonite: A review // Advances in Colloid and Interface Science. - 2008. - Vol. 140, Is. 2. - P. 114–131.

107 Chai J.-B., Au P.-I., Mubarak N.M., Khalid M., Ng W.P.-Q., Jagadish P., Walvekar R., Abdullah E.C. Adsorption of heavy metal from industrial wastewater onto low-cost Malaysian kaolin clay–based adsorbent // Environmental Science and Pollution Research. - 2020. - Vol. 27, Is. 12. - P. 13949–13962.

108 Chen M., Yang T., Han J., Zhang Y., Zhao L., Zhao J., Li R., Huang Y., Gu Z., Wu J. The Application of Mineral Kaolinite for Environment Decontamination: A Review // Catalysts. - 2023. - Vol. 13, Is. 1. – P. 123.

109 Omotoyinbo, Ajibade J. L.O. Working Properties of Some Selected Refractory Clay Deposits in South Western Nigeria. // J Min and Mat Char and Eng. - 2008. - Vol. 7, Is. 3. - P. 233–245.

110 Musil S.S., Kriven W.M. In situ mechanical properties of chamotte particulate reinforced, potassium geopolymer // Journal of the American Ceramic Society. - 2014. - Vol. 97, Is. 3. - P. 907–915.

111 Kotova O.B., Ustyugov V.A., Sun S., Ponaryadov A. V. Mullite production: phase transformations of kaolinite, thermodynamics of the process // Journal of Mining Institute. - 2022. - Vol. 254. - P. 129–135.

112 Santos F.D., da Conceição L.R. V., Ceron A., de Castro H.F. Chamotte clay as potential low cost adsorbent to be used in the palm kernel biodiesel purification // Applied Clay Science. - 2017. - Vol. 149. - P. 41–50.

113 Rathinavelu A., Venkateswaran V. A Comparative Study on the Removal of Cr (VI) using Fire Clay-TiO_2 Nanocomposite and Fire Clay // J. Environ. Nanotechnol. - 2015. - Vol. 4, Is. 3. - P. 24–31.

114 Bajpai S.K. Removal of hexavalent chromium by adsorption onto fireclay and impregnated fireclay // Separation Science and Technology. - 2001. - Vol. 36, Is. 3. - P. 399–415.

115 Rahmani A.R., Foroughi M., Noorimotlagh Z., Adabi S. Hexavalent Chromium Adsorption onto Fire Clay. - 2016.

116 Venkateswaran V., Rathinavelu A. Studying on The Removal of Pb (II) using Fire Clay–TiO2 Nanocomposite and Fire Clay // J. Environ. Nanotechnol. - 2015. - Vol. 4, Is. 4. - P. 45–51.

117 Rathinavelu A., Venkateswaran V. Studies on the Removal of Ni (II) from Aqueous Solution using Fire Clay-TiO2 Nanocomposite and Fire Clay // Chemical Science. - 2016. - Vol. 5, Is. 3. - P. 555–566.

118 Sharma P., Olufemi A.F., Qanungo K. Development of green geo-adsorbent pellets from low fire clay for possible use in methylene blue removal in aquaculture // Materials Today: Proceedings. - 2022. - Vol. 49. - P. 1556–1565.

119 Sharma P., Qanungo K. Development of Eco-friendly Adsorbent Pellets from Low Fire Clay and Potato Starch for Potential Use in Methylene Blue Removal in Aquaculture. // Nature Environment & Pollution Technology. - 2021. - Vol. 20.

120 Li Z., Bowman R.S. Retention of inorganic oxyanions by organo-kaolinite // Water Research. - 2001. - Vol. 35, Is. 16. - P. 3771–3776.

121 Al-Qaradawi S., Salman S.R. Photocatalytic degradation of methyl orange as a model compound // Journal of Photochemistry and photobiology A: Chemistry. - 2002. - Vol. 148, Is. 1–3. - P. 161–168.

122 Wang J., Gao M., Shen T., Yu M., Xiang Y., Liu J. Insights into the efficient adsorption of rhodamine B on tunable organo-vermiculites // Journal of hazardous materials. - Elsevier, 2019. - Vol. 366. - P. 501–511.

123 Chotzen R.A., Polubesova T., Chefetz B., Mishael Y.G. Adsorption of soil-derived humic acid by seven clay minerals: a systematic study // Clays and Clay minerals. - 2016. - Vol. 64. - P. 628–638.

124 Shen T., Gao M., Zang W., Ding F., Wang J. Architecting organo silica nanosheets for regenerable cost-effective organics adsorbents // Chemical Engineering Journal. - Elsevier, 2018. - Vol. 331. - P. 211–220.

125 Wu C., Spongberg A.L., Witter J.D. Adsorption and degradation of triclosan and triclocarban in soils and biosolids-amended soils // Journal of agricultural and food chemistry. - 2009. - Vol. 57, Is. 11. - P. 4900–4905.

126 Wang J., Gao M., Ding F., Shen T. Organo-vermiculites modified by heating and gemini pyridinium surfactants: Preparation, characterization and sulfamethoxazole adsorption // Colloids and Surfaces A: Physicochemical and Engineering Aspects. - 2018. - Vol. 546. - P. 143–152.

127 Sharma R., Kamal A., Abdinejad M., Mahajan R.K., Kraatz H.-B. Advances in the synthesis, molecular architectures and potential applications of gemini surfactants // Advances in colloid and interface science. - 2017. - Vol. 248. - P. 35–68.

128 Zhao W., Wang Y. Coacervation with surfactants: From single-chain surfactants to gemini surfactants // Advances in colloid and interface science. - 2017. - Vol. 239. - P. 199–212.

129 Gu Z., Gao M., Luo Z., Xue G., Lu L., Liu Y. Gemini surfactant modified montmorillonite as highly efficient adsorbent for anionic dyes // Separation Science and Technology. - 2014. - Vol. 49, Is. 18. - P. 2878–2889.

130 Adamson A.W., Gast A.P. Physical chemistry of surfaces. - New York: Interscience publishers, 1967. - Vol. 150. – 180 pp.

131 Dąbrowski A. Adsorption—from theory to practice // Advances in colloid and interface science. - 2001. - Vol. 93, Is. 1–3. - P. 135–224.

132 Gregg S.J., Sing K.S.W., Salzberg H.W. Adsorption surface area and porosity // Journal of the electrochemical society. - 1967. - Vol. 114, Is. 11. - P. 279.

133 Ali I., Gupta V.K. Advances in water treatment by adsorption technology // Nature protocols. - 2006. - Vol. 1, Is. 6. - P. 2661–2667.

134 Crini G., Lichtfouse E. Advantages and disadvantages of techniques used for wastewater treatment // Environmental chemistry letters. - 2019. - Vol. 17. - P. 145–155.

135 Langmuir I. The constitution and fundamental properties of solids and liquids. II. liquids. // Journal of the American Chemical Society. - 1917. - Vol. 39, Is. 9. - P. 1848–1906.

136 Ho Y.S., Mckay G. Pseudo-second order model for sorption processes // Process Biochemistry. - 1999. - Vol. 34. - P. 451–465.

137 Belkassa K., Khelifa M., Batonneau-Gener I., Marouf-Khelifa K., Khelifa A. Understanding of the mechanism of crystal violet adsorption on modified halloysite: Hydrophobicity, performance, and interaction // Journal of Hazardous Materials. - 2021. - Vol. 415. - P. 125656.

138 Ren H., Jiang J., Wu D., Gao Z., Sun Y., Luo C. Selective adsorption of Pb (II) and Cr (VI) by surfactant-modified and unmodified natural zeolites: a comparative study on kinetics, equilibrium, and mechanism // Water, Air, & Soil Pollution. - 2016. - Vol. 227, Is. 101. - P. 1–11.

139 Sullivan E.J., Hunter D.B., Bowman R.S. Fourier transform Raman spectroscopy of sorbed HDTMA and the mechanism of chromate sorption to surfactant-modified clinoptilolite // Environmental Science and Technology. - 1998. - Vol. 32, Is. 13. - P. 1948–1955.

140 Kushwaha A., Rani R., Patra J.K. Adsorption kinetics and molecular interactions of lead [Pb(II)] with natural clay and humic acid // International Journal of Environmental Science and Technology. - 2020. - Vol. 17, Is. 3. - P. 1325–1336.

141 Xu H., Hu X., Chen Y., Li Y., Zhang R., Tang C., Hu X. Cd(II) and Pb(II) absorbed on humic acid-iron-pillared bentonite: Kinetics, thermodynamics and mechanism of adsorption // Colloids and Surfaces A: Physicochemical and Engineering Aspects. - 2021. - Vol. 612. – P. 126005.

142 He Y., Lin H., Dong Y., Wang L. Preferable adsorption of phosphate using lanthanum-incorporated porous zeolite: Characteristics and mechanism // Applied Surface Science. - 2017. - Vol. 426. - P. 995–1004.

143 Dinh V., Nguyen P., Tran M., Luu A. HTDMA-modified bentonite clay for effective removal of Pb (II) from aqueous solution // Chemosphere. - 2022. - Vol. 286, Is. July 2021. – P. 131766.

144 Peng S., Tang Z., Jiang W., Wu D., Hong S., Xing B. Mechanism and performance for adsorption of 2-chlorophenol onto zeolite with surfactant by one-step process from aqueous phase // Science of the Total Environment. - 2017. - Vol. 581–582. - P. 550–558.

145 Liu P., Zhang A., Liu Y., Liu Z., Liu X., Yang L., Yang Z. Adsorption Mechanism of High-Concentration Ammonium by Chinese Natural Zeolite with Experimental Optimization and Theoretical Computation // Water (Switzerland). - 2022. - Vol. 14, Is. 15. – P. 2413.

146 Zhong Z., Li J., Ma Y., Yang Y. The adsorption mechanism of heavy metals from coal combustion by modified kaolin: Experimental and theoretical studies // Journal of Hazardous Materials. - 2021. - Vol. 418. – P. 126256.

147 Otten D.E., Shaffer P.R., Geissler P.L., Saykally R.J. Erratum: Elucidating the mechanism of selective ion adsorption to the liquid water surface // Proceedings of the National Academy of Sciences of the United States of America. - 2012. - Vol. 109, Is. 8. - P. 3190.

148 Benmessaoud A., Nibou D., Mekatel E.H., Amokrane S. A comparative study of the linear and non-linear methods for determination of the optimum equilibrium isotherm for adsorption of Pb2+ ions onto Algerian treated clay // Iranian Journal of Chemistry and Chemical Engineering. - 2020. - Vol. 39, Is. 4. - P. 153–171.

149 Karnjanakom S., Maneechakr P. Adsorption behaviors and capacities of Cr(VI) onto environmentally activated carbon modified by cationic (HDTMA and DDAB) surfactants // Journal of Molecular Structure. - 2019. - Vol. 1186. - P. 80–90.

150 Günay A., Arslankaya E., Tosun I. Lead removal from aqueous solution by natural and pretreated clinoptilolite: Adsorption equilibrium and kinetics // Journal of Hazardous Materials. - 2007. - Vol. 146, Is. 1–2. - P. 362–371.

151 Bhattacharyya K.G., Sen Gupta S. Pb(II) uptake by kaolinite and montmorillonite in aqueous medium: Influence of acid activation of the clays // Colloids and Surfaces A: Physicochemical and Engineering Aspects. - Elsevier, 2006. - Vol. 277, Is. 1–3. - P. 191–200.

152 Yang J., Huang B., Lin M. Adsorption of Hexavalent Chromium from Aqueous Solution by a Chitosan/Bentonite Composite: Isotherm, Kinetics, and Thermodynamics Studies // Journal of Chemical and Engineering Data. - 2020. - Vol. 65, Is. 5. - P. 2751–2763.

153 Simonin J.P. On the comparison of pseudo-first order and pseudo-second order rate laws in the modeling of adsorption kinetics // Chemical Engineering Journal. - 2016. - Vol. 300. - P. 254–263.

154 Lima E.C., Hosseini-Bandegharaei A., Moreno-Piraján J.C., Anastopoulos I. A critical review of the estimation of the thermodynamic parameters on adsorption equilibria. Wrong use of equilibrium constant in the Van't Hoof equation for calculation of thermodynamic parameters of adsorption // Journal of Molecular Liquids. - 2019. - Vol. 273. - P. 425–434.

155 Griffin L.R., Browning K.L., Truscott C.L., Clifton L.A., Webster J., Clarke S.M. A comparison of didodecyldimethylammonium bromide adsorbed at mica/water and silica/water interfaces using neutron reflection // Journal of Colloid and Interface Science. - 2016. - Vol. 478. - P. 365–373.

156 El-Sharkawy G.F. Awareness of Sodium Lauryl Sulfate & Sodium Laureth Sulfate Health Hazards among Users // Journal of American Science. - 2011. - Vol. 7, Is. 4. - P. 535–541.

157 Aoudia M., Al-Haddabi B., Al-Harthi Z., Al-Rubkhi A. Sodium lauryl ether sulfate micellization and water solubility enhancement towards naphthalene and pyrene: effect of the degree of ethoxylation // Journal of Surfactants and Detergents. - 2010. - Vol. 13. - P. 103–111.

158 Griffin L.R., Browning K.L., Truscott C.L., Clifton L.A., Webster J., Clarke S.M. A comparison of didodecyldimethylammonium bromide adsorbed at mica/water and silica/water interfaces using neutron reflection // Journal of Colloid and Interface Science. - 2016. - Vol. 478. - P. 365–373.

159 Chebotarev A.N., Paladenko T. V., Shcherbakova T.M. Adsorption-photometric determination of cationic surfactant traces // Journal of Analytical Chemistry. - 2004. - Vol. 59, Is. 4. - P. 309–313.

160 Schwartz A. M., Perry J. W., Berch J. Surface active agents and detergents. – New York : Interscience, 1958. – Vol. 253.

161 Bakatula E.N., Richard D., Neculita C.M., Zagury G.J. Determination of point of zero charge of natural organic materials // Environmental Science and Pollution Research. - Environmental Science and Pollution Research, 2018. - Vol. 25, Is. 8. - P. 7823–7833.

162 Osol A., Hoover, J.E. Et. al. Remington's Pharmaceutical Sciences. 15th ed. Easton, Pennsylvania: Mack Publishing Co., 1975. - 835 p.

163 Zeng G., Zhang C., Huang G., Yu J., Wang Q., Li J., Xi B., Liu H. Adsorption behavior of bisphenol A on sediments in Xiangjiang River, Central-south China // Chemosphere. - 2006. - Vol. 65, Is. 9. - P. 1490–1499.

164 Iovino P., Canzano S., Capasso S., Erto A., Musmarra D. A modeling analysis for the assessment of ibuprofen adsorption mechanism onto activated carbons // Chemical Engineering Journal. - 2015. - Vol. 277. - P. 360–367.

165 Foo K.Y., Hameed B.H. Insights into the modeling of adsorption isotherm systems // Chemical Engineering Journal. - 2010. - Vol. 156, Is. 1. - P. 2–10.

166 Langmuir I. The constitution and fundamental properties of solids and liquids. II. Liquids // Journal of the American chemical society. – 1917. – Vol. 39, Is. 9. – P. 1848-1906.

167 Freundlich H.M.F. Over the Adsorption in Solution // The Journal of Physical Chemistry. - 1906. - Vol. 57. - P. 385–471.

168 Temkin M.I., Pyzhev V. Kinetics of Ammonia Synthesis on Promoted Iron Catalysts. // Acta Physicochimica USSR. - 1940. - Vol. 12. - P. 327–356.

169 Dubinin M.M., Radushkevich L.V. The equation of the characteristic curve of the activated charcoal // Proceedings of the Academy of Sciences, Physical Chemistry Section. - 1947. - Vol. 55. - P. 331–337.

170 Benmessaoud A., Nibou D., Mekatel E.H., Amokrane S. A comparative study of the linear and non-linear methods for determination of the optimum equilibrium isotherm for adsorption of Pb^{2+} ions onto Algerian treated clay // Iranian Journal of Chemistry and Chemical Engineering. - 2020. - Vol. 39, Is. 4. - P. 153–171.

171 Redlich O., Peterson D.L. A Useful Adsorption Isotherm // Journal of Physical Chemistry. - 1959. - Vol. 63, Is. 6. - P. 1024–1026.

172 Sips R. On the Structure of a Catalyst Surface // Journal of Chemical Physics. - 1948. - Vol. 16. - P. 490–495.

173 Fritz W., Schlunder E.U. Simultaneous adsorption equilibria of organic solutes in dilute aqueous solu- ¨ tion on activated carbon // Chem. Eng. Sci. - 1974. - Vol. 29. - P. 1279–1282.

174 Toth J. Calculation of the BET-Compatible Surface Area from Any Type I Isotherms Measured Above the Critical Temperature // J. Colloid Interf. Sci. - 2000. - Vol. 225. - P. 378–383.

175 Baudu M. Study of Interactions Solute-Fibres of Active Carbon // Application and Regeneration. University of Rennes I. - 1990.

176 Lagergren S.Y. Zur Theorie der sogennanten Adsorption gelöster Stoffe // Kungliga Svenska Vetenskapsakad. Handlingar. - 1898. - Vol. 24. - P. 1–39.

177 Ho Y.S., Mckay G. Pseudo-second order model for sorption processes // Process Biochemistry. - 1999. - Vol. 34. - P. 451–465.

178 A Scott C.W. Transformations and R^2 // Am. Stat. - 1991. - Vol. 45. - P. 127–129.

179 Simonin J.P. On the comparison of pseudo-first order and pseudo-second order rate laws in the modeling of adsorption kinetics // Chemical Engineering Journal. - 2016. - Vol. 300. - P. 254–263.

180 Tseng R.-L., Wu P.-H., Wu F.-C., Juang R.-S. A convenient method to determine kinetic parameters of adsorption processes by nonlinear regression of pseudo-nth-order equation // Chemical Engineering Journal. - 2014. - Vol. 237. - P. 153–161.

181 Qiu H., Lv L., Pan B.C., Zhang Q.J., Zhang W.M., Zhang Q.X. Critical review in adsorption kinetic models // Journal of Zhejiang University: Science A. - 2009. - Vol. 10, Is. 5. - P. 716–724.

182 Weber W.J., Morris J.C. Kinetics of Adsorption on Carbon from Solution // Journal of the Sanitary Engineering Division. - 1963. - Vol. 89, Is. 2. - P. 31–59.

183 Ali O., Mohamed S. Adsorption of copper ions and alizarin red S from aqueous solutions onto a polymeric nanocomposite in single and binary systems // Turkish Journal of Chemistry. - 2017. - Vol. 41, Is. 6. - P. 967–986.

184 Sutherland C. Removal of heavy metals from water using low-cost adsorbents: process development : diss. – Trinidad, 2004.

185 Genç N., Kılıçoğlu Ö., Narci A.O. Removal of Bisphenol A aqueous solution using surfactant-modified natural zeolite: Taguchi's experimental design, adsorption kinetic, equilibrium and thermodynamic study // Environmental Technology (United Kingdom). - 2017. - Vol. 38, Is. 4. - P. 424–432.

186 Mahmoud A.E.D. Graphene-based nanomaterials for the removal of organic pollutants: Insights into linear versus nonlinear mathematical models // Journal of Environmental Management. - 2020. - Vol. 270, Is. May. - P. 110911.

187 Rakhym A.B., Seilkhanova G.A., Mastai Y. Physicochemical evaluation of the effect of natural zeolite modification with didodecyldimethylammonium bromide on the adsorption of Bisphenol-A and Propranolol Hydrochloride // Microporous and Mesoporous Materials. - 2021. - Vol. 318. - P. 111020.

188 Moshoeshoe M., Nadiye-Tabbiruka M.S., Obuseng V. A review of chemistry, structure, properties and applications of zeolites // American journal of Materials Science. - 2017. - Vol. 7, Is. 5. - P. 191–221.

189 Król M., Mozgawa W., Barczyk K., Bajda T., Kozanecki M. Changes in the vibrational spectra of zeolites due to sorption of heavy metal cations // Journal of Applied Spectroscopy. - 2013. - Vol. 80, Is. 5. - P. 644–650.

190 Kragović M., Pašalić S., Marković M., Petrović M., Nedeljković B., Momčilović M., Stojmenović M. Natural and modified zeolite—alginate composites. Application for removal of heavy metal cations from contaminated water solutions // Minerals. - 2018. - Vol. 8, Is. 1. - P. 11.

191 Wang C., Leng S., Guo H., Yu J., Li W., Cao L., Huang J. Quantitative arrangement of Si/Al ratio of natural zeolite using acid treatment // Applied Surface Science. - 2019. - Vol. 498, Is. May. - P. 143874.

192 Koyama K., Takéuchi Y. Clinoptilolite: The distribution of potassium atoms and its role in thermal stability // Zeitschrift fur Kristallographie - New Crystal Structures. - 1977. - Vol. 145, Is. 3–4. - P. 216–239.

193 Costa-Marrero Y., Andrade M., Ellena J., Duque-Rodríguez J., Farias T., Autié-Castro G. Zeolite/ZnO composites based on a Cuban natural clinoptilolite and preliminary evaluation in methylene blue adsorption // Materials Research Express. - 2020. – Vol.7, Is.1. – P. 015066.

194 Borg I.Y., Smith D.K. Calculated powder patterns. Part II. Six potassium feldspars and barium feldspar // American Mineralogist. - 1969. - Vol. 54, Is. 1–2. - P. 163–181.

195 Gennaro R. De, Dondi M., Cappelletti P., Cerri G., Gennaro M. De, Guarini G., Langella A. Zeolite – feldspar epiclastic rocks as flux in ceramic tile manufacturing // Microporous and Mesoporous Materials. - 2007. - Vol. 105. - P. 273–278.

196 Romano Rinaldi, J.J.Pluth J.V.S. Zeolites of the Phillipsite Family. Refinement of the Crystal Structures of Phillipsite and Harmotome // Acta Cryst. - 1974. - Vol. B30. - P. 2426–2433.

197 Polatoglu I. Chemical behavior of clinoptilolite rich natural zeolite in aqueous medium. - Izmir Institute of Technology (Turkey), 2005.

198 Pechar F., Rykl D. Infrared spectra of natural zeolites of the natrolite group // Casopis pro Mineralogii a Geologii. - 1981. - Vol. 35, Is. 2. - P. 189–202.

199 Tarasevich B.N. IR Spectra of Main Classes of Organic Compounds: Reference Materials. - Moscow: M.V.Lomonosov Moscow State University, 2012. - 55 p.

200 Yu Y., Xiong G., Li C., Xiao F.S. Characterization of aluminosilicate zeolites by UV Raman spectroscopy // Microporous and Mesoporous Materials. - 2001. - Vol. 46, Is. 1. - P. 23–34.

201 Rykl D., Pechar F. Raman polarization spectra of the natural zeolite analcime // Chem. zvesti. - 1981. - Vol. 35, Is. 1. - P. 45–50.

202 Zhang L., Sun X., Song Y., Jiang X., Dong S., Wang E. Didodecyldimethylammonium bromide lipid bilayer-protected gold nanoparticles: Synthesis, characterization, and self-assembly // Langmuir. - 2006. - Vol. 22, Is. 6. - P. 2838–2843.

203 Foucault R., Birke R.L., Lombardi J.R. SERS of Surfactants in Monolayer and Multibilayer Forms on an Electrified Ag Surface // Langmuir. - 2003. - Vol. 19, Is. 21. - P. 8818–8827.

204 Florea-Spiroiu M., Achimescu D., Stanculescu I., Purica M., Gavrila R., Peretz S. Anti-fog chitosan/sodium lauryl ether sulfate films // Polymer Bulletin. - 2013. - Vol. 70, Is. 12. - P. 3305–3316.

205 Fard R.F., Aminabad M.S., Hadi M., Gholami M., Mirzaei N. Sorption of acid dye by surfactant modificated natural zeolites // Journal of the Taiwan Institute of Chemical Engineers. - 2015. - Vol. 59. - P. 186–194.

206 Bakatula E.N., Richard D., Neculita C.M., Zagury G.J. Determination of point of zero charge of natural organic materials // Environmental Science and Pollution Research. - 2018. - Vol. 25, Is. 8. - P. 7823–7833.

207 Gulicovski J.J., Čerović L.S., Milonjić S.K. Point of zero charge and isoelectric point of alumina // Materials and Manufacturing Processes. - 2008. - Vol. 23, Is. 6. - P. 615–619.

208 Sparks D.L. Kinetics of reactions in pure and in mixed systems. // Soil physical chemistry. - 1986. - P. 83–145.

209 Shang J.Q. Zeta potential and electroosmotic permeability of clay soils // Canadian Geotechnical Journal. - 1997. - Vol. 34, Is. 4. - P. 627–631.

210 Yukselen Y., Kaya A. Zeta Potential of Kaolinite in the Presence of Alkali, Alkaline Earth and Hydrolyzable Metal Ions // Water, Air, and Soil Pollution. - 2003. - Vol. 145, Is. 1. - P. 155–168.

211 Rožić M., Ivanec Šipušić Đ., Sekovanić L., Miljanić S., Ćurković L., Hrenović J. Sorption phenomena of modification of clinoptilolite tuffs by surfactant cations // Journal of Colloid and Interface Science. - 2009. - Vol. 331, Is. 2. - P. 295–301.

212 Chapman H.D. Cation-Exchange Capacity // Black, C.A., Ed., Methods of Soil Analysis, American Society of Agronomy, Madison. - 1965. - P. 891–901.

213 Noori M., Zendehdel M., Ahmadi A. Using natural zeolite for the improvement of soil salinity and crop yield // Toxicological and Environmental Chemistry. - 2006. - Vol. 88, Is. 1. - P. 77–84.

214 Reeve P.J., Fallowfield H.J. Natural and surfactant modified zeolites: A review of their applications for water remediation with a focus on surfactant desorption and toxicity towards microorganisms // Journal of Environmental Management. - 2018. - Vol. 205. - P. 253–261.

215 Zarei M., Djafarzadeh N., Khadir L. Removal of direct blue 129 from aqueous medium using surfactant-modified zeolite: a neural network modeling // Environmental Health Engineering and Management. - 2018. - Vol. 5, Is. 2. - P. 101–113.

216 Li Y., Cai X., Guo J., Zhou S., Na P. Fe/Ti co-pillared clay for enhanced arsenite removal and photo oxidation under UV irradiation // Applied Surface Science. - 2015. - Vol. 324. - P. 179–187.

217 Ribeiro M.J., Tulyagavov D.U., Ferreira J.M., Labrincha J.A. High temperature mullite dissolution in ceramic bodies derived from Al-rich sludge // Journal of the European Ceramic Society. - 2005. - Vol. 25, Is. 5. - P. 703–710.

218 Rakhym A.B., Seilkhanova G.A., Kurmanbayeva T.S. Adsorption of lead (II) ions from water solutions with natural zeolite and chamotte clay // Materials Today: Proceedings. - 2020. - Vol. 31, Is. Part 3. - P. 482–485.

219 Rakhym A.B., Bekturganova U.Z., Seilkhanova G.A., Csavdari A. Chamotte clay sorbent for the extraction of lead and cadmium ions from aqueous solutions // International Journal of Biology and Chemistry. - 2019. - Vol. 12, Is. 2. - P. 129–134.

220 Telkhozhayeva M.S., Seilkhanova G.A., Rakhym A.B., Imangaliyeva A.N., Akbayeva D.N. Sorbciya ionov svinca i kadmiya iz vodnyh rastvorov modificirovannym ceolitom (Sorption of lead and cadmium ions from aqueous solutions by modified zeolite) // Chemical Bulletin of KazNU - 2018. - Vol. 4, Is. 91. - P. 16–22. (in Russian)

221 Rakhym A.B., Seilkhanova G.A., Csavdari A. Adsorbciya bihromat- i permanganat-anionov organo-ceolitom mestorozhdeniya Shankanaj (Adsorption of dichromate and permanganate anions by organo-zeolite from Shankanai deposit) // Eurasian Journal of Ecology. - 2018. - Vol. 4, Is. 57. - P. 58–68. (in Russian)

222 Hamidpour M., Kalbasi M., Afyuni M., Shariatmadari H., Furrer G. Sorption of lead on Iranian bentonite and zeolite: kinetics and isotherms // Environmental Earth Sciences. - 2011. - Vol. 62. - P. 559–568.

223 Wingenfelder U., Nowack B., Furrer G., Schulin R. Adsorption of Pb and Cd by amine-modified zeolite // Water research. - 2005. - Vol. 39, Is. 14. - P. 3287–3297.

224 Pandey P.K., Sharma S.K., Sambi S.S. Removal of lead (II) from waste water on zeolite-NaX // Journal of Environmental Chemical Engineering. - 2015. - Vol. 3, Is. 4. - P. 2604–2610.

225 Grishko A.N. Nekotorye svojstva geterogennyh katalizatorov (Some properties of heterogeneous catalysts) // iPolytech Journal. - 2011. – Vol. 59, Is. 12. - P. 187–191.

226 Pearson R.G. Hard and soft acids and bases // Journal of the American Chemical society. - 1963. - Vol. 85, Is. 22. - P. 3533–3539.

227 Koyama K., Takeuchi Y. Clinoptilolite: the distribution of potassium atoms and its role in thermal stability // Zeitschrift für Kristallographie-Crystalline Materials. - 1977. - Vol. 145, Is. 1–6. - P. 216–239.

228 Chargui F., Hamidouche M., Belhouchet H., Jorand Y., Doufnoune R., Fantozzi G. Mullite fabrication from natural kaolin and aluminium slag // Boletín de la Sociedad Española de Cerámica y Vidrio. - 2018. - Vol. 57, Is. 4. - P. 169–177.

229 Percival H.J., Duncan J.F., Foster P.K. Interpretation of the Kaolinite-Mullite Reaction Sequence from // Journal of the American Ceramic Society. - 1974. - Vol. 57, Is. February. - P. 57–61.

230 Gorzin F., Bahri M.M., Abadi R. Adsorption of Cr(VI) from aqueous solution by adsorbent prepared from paper mill sludge: Kinetics and thermodynamics studies // Adsorpt. Sci. Technol. - 2017. - Vol. 36. - P. 149–169.

231 Kang Y.R., Mu B., Zhu G., Zhu Y.F., Wang A.Q. Preparation and Properties of Antibacterial Polyhexamethylene Biguanide/Palygorskite Composites as Zearalenone Adsorbents // Clays and Clay Minerals. - 2022. – Vol. 70, Is. 2. – P. 182-195.

232 Stafford K., Sing W. Reporting Physisorption Data for Gas / Solid Systems with Special Reference to the Determination of Surface Area and Porosity // Pure and Applied Chemistry ·. - 1982. - Vol. 54, Is. 11. - P. 2201–2218.

233 Rajahmundry G.K., Garlapati C., Kumar P.S., Alwi R.S., Vo D.V.N. Statistical analysis of adsorption isotherm models and its appropriate selection // Chemosphere. - 2021. - Vol. 276. – P. 130176 .

234 Ho Y.S., Huang C.T., Huang H.W. Equilibrium sorption isotherm for metal ions on tree fern // Process Biochemistry. - 2002. - Vol. 37, Is. 250. - P. 1421–1430.

235 Gupta S. Sen, Bhattacharyya K.G. Interaction of metal ions with clays: I. A case study with Pb(II) // Applied Clay Science. - 2005. - Vol. 30, Is. 3–4. - P. 199–208.

236 Bentiss F., Lebrini M., Lagrenée M. Thermodynamic characterization of metal dissolution and inhibitor adsorption processes in mild steel/2,5-bis(n-thienyl)-1,3,4-thiadiazoles/ hydrochloric acid system // Corrosion Science. - 2005. - Vol. 47, Is. 12. - P. 2915–2931.

237 Turku I., Sainio T., Paatero E. Thermodynamics of tetracycline adsorption on silica // Environ Chem Lett. - 2007. - Vol. 5. - P. 225–228.

238 Li J., Zhong Z., Ma Y., Lai X., Li Z. Adsorption Mechanism of PbO/PbCl2 on Kaolinite Surfaces during Coal Combustion Based on Frontier Orbital Theory // Energy & Fuels. - 2020. - Vol. 34, Is. 9. - P. 11258–11269.

239 Yu M., Huang Y., Xia W., Zhu Z., Fan C., Liu C., Dong L., Xu L., Liu L., Zha J. PbCl2 capture by kaolin and metakaolin under different influencing factors of thermal treatment // Energy & Fuels. - 2020. - Vol. 34, Is. 2. - P. 2284–2292.

240 Zhong Z., Li J., Ma Y., Yang Y. The adsorption mechanism of heavy metals from coal combustion by modified kaolin: Experimental and theoretical studies // Journal of Hazardous Materials. - 2021. - Vol. 418. - P. 126256.

241 Frost R.L., Vassallo A.M. The dehydroxylation of the kaolinite clay minerals using infrared emission spectroscopy // Clays and Clay minerals. - 1996. - Vol. 44. - P. 635–651.

242 Shoval S., Boudeulle M., Panczer G. Identification of the thermal phases in firing of kaolinite to mullite by using micro-Raman spectroscopy and curve-fitting // Optical Materials. - 2011. - Vol. 34, Is. 2. - P. 404–409.

243 Liebau F., Liebau F. Chemical bonds in silicates // Structural Chemistry of Silicates: Structure, Bonding, and Classification. - 1985. - P. 14–51.

244 Apreutesei R.E., Catrinescu C., Teodosiu C. Surfactant-modified natural zeolites for environmental applications in water purification // Environmental Engineering and Management Journal. - 2008. - Vol. 7, Is. 2. - P. 149–161.

245 Vargas A.M., Cipagauta-Ardila C.C., Molina-Velasco D.R., Ríos-Reyes C.A. Surfactant-modified natural zeolites as carriers for diclofenac sodium release: A preliminary feasibility study for pharmaceutical applications // Materials Chemistry and Physics. - 2020. - Vol. 256, Is. April. - P. 123644.

246 Ortiz-Martínez K., Reddy P., Cabrera-Lafaurie W.A., Román F.R., Hernández-Maldonado A.J. Single and multi-component adsorptive removal of bisphenol A and 2,4-dichlorophenol from aqueous solutions with transition metal modified inorganic-organic pillared clay composites: Effect of pH and presence of humic acid // Journal of Hazardous Materials. - 2016. - Vol. 312. - P. 262–271.

247 Vishwakarma K., Kalra J., Gupta R., Sharma M., Sharma T., Clinic S., Pradesh U., Clinic S. Financial support and sponsorship Piloerection : A Rare Ictal Phenomenon – Case Report and Review of Literature // Annals of Indian Academy of Neurology. - 2017. - Vol. 20, Is. 2. - P. 169–172.

248 Maszkowska J., Stolte S., Kumirska J., Łukaszewicz P., Mioduszewska K., Puckowski A., Caban M., Wagil M., Stepnowski P., Białk-Bielińska A. Beta-blockers in the environment: Part II. Ecotoxicity study // Science of the Total Environment. - 2014. - Vol. 493. - P. 1122–1126.

249 Ubrich N., Bouillot P., Pellerin C., Hoffman M., Maincent P. Preparation and characterization of propranolol hydrochloride nanoparticles: A comparative study // Journal of Controlled Release. - 2004. - Vol. 97, Is. 2. - P. 291–300.

250 Neckina O.V. Praktikum po fizicheskoj himii NGU. Himicheskaya termodinamika i kinetika. Adsorbciya iz rastvorov na tverdoj poverhnosti: Metodicheskoe posobie. Novosib. Gos. Un-t. (Practical training in physical chemistry of NSU. Chemical thermodynamics and kinetics. Adsorption from solutions on a solid surface: Methodical manualNovosib. State University) – Novosibirsk: RIC NGU, 2015. - 17 p. (in Russian)

251 Al-Ghouti M.A., Da'ana D.A. Guidelines for the use and interpretation of adsorption isotherm models: A review // Journal of Hazardous Materials. - 2020. - Vol. 393. - P. 122383.

252 Foo K.Y., Hameed B.H. Insights into the modeling of adsorption isotherm systems // Chemical Engineering Journal. - 2010. - Vol. 156, Is. 1. - P. 2–10.

253 Wang J., Guo X. Adsorption isotherm models: Classification, physical meaning, application and solving method // Chemosphere. - Elsevier Ltd, 2020. - Vol. 258. - .

254 Dwivedi C.P., Sahu J.N., Mohanty C.R., Mohan B.R., Meikap B.C. Column performance of granular activated carbon packed bed for Pb(II) removal // Journal of Hazardous Materials. - 2008. - Vol. 156, Is. 1. - P. 596–603.

255 Priyadi P., Iskandar I., Suwardi S., Mukti R.R. Characteristics of heavy metals adsorption Cu, Pb and Cd using synthetics zeolite Zsm-5 // Journal of Tropical Soils. - Lampung University, 2015. - Vol. 20, Is. 2. - P. 77–83.

256 Kocaoba S. Comparison of Amberlite IR 120 and dolomite's performances for removal of heavy metals // Journal of Hazardous Materials. - 2007. - Vol. 147, Is. 1. - P. 488–496.

257 Chegrouche S., Mellah A., Barkat M. Removal of strontium from aqueous solutions by adsorption onto activated carbon: kinetic and thermodynamic studies // Desalination. - 2009. - Vol. 235, Is. 1. - P. 306–318.

258 Vasylyeva H., Mironyuk I., Strilchuk M., Tryshyn V., Gaidar O., Vasyliev O. Adsorption of zirconium ions by X-type zeolite // Biointerface Research in Applied Chemistry. - 2021. - Vol. 11, Is. 5. - P. 13421–13431.

259 Sivaiah M. V, Venkatesan K.A., Krishna R.M., Sasidhar P., Murthy G.S. Ion exchange properties of strontium on in situ precipitated polyantimonic acid in amberlite XAD-7 // Separation and Purification Technology. - 2005. - Vol. 44, Is. 1. - P. 1–9.

260 Gutiérrez-Segura E., Colín-Cruz A., Fall C., Solache-Ríos M., Balderas-Hernández P. Comparison of Cd–Pb adsorption on commercial activated carbon and carbonaceous material from pyrolysed sewage sludge in column system // Environmental technology. - 2009. - Vol. 30, Is. 5. - P. 455–461.

261 Mimura H., Akiba K. Adsorption behavior of cesium and strontium on synthetic zeolite P // Journal of Nuclear Science and Technology. - 1993. - Vol. 30, Is. 5. - P. 436–443.

262 Rao K.S., Chaudhury G.R., Mishra B.K. Kinetics and equilibrium studies for the removal of cadmium ions from aqueous solutions using Duolite ES 467 resin // International Journal of Mineral Processing. - 2010. - Vol. 97, Is. 1. - P. 68–73.

263 Babel S., Kurniawan T.A. Cr(VI) removal from synthetic wastewater using coconut shell charcoal and commercial activated carbon modified with oxidizing agents and/or chitosan // Chemosphere. - 2004. - Vol. 54, Is. 7. - P. 951–967.

264 Balan C., Volf I., Bilba D. Chromium (VI) removal from aqueous solutions by purolite base anion-exchange resins with gel structure // Chemical Industry and Chemical Engineering Quarterly. - 2013. - Vol. 19, Is. 4. - P. 615–628.

265 Mfoumou C.M., Tonda-Mikiela P., Ngoye F., Lionel M.B., Spenseur B.M., Sachse A., Mignard S., Tchouya G.R.F. Dynamic Adsorption on Fixed-Bed Column of Manganese Oxoanions (MnO_4^-) in Aqueous Media on Activated Carbon Prepared from Palm Nut Shells // Journal of Environment Pollution and Human Health. - 2022. - Vol. 10, Is. 2. - P. 58–70.

266 Franco D.S.P., Georgin J., Ramos C.G., Eljaiek S.M., Badillo D.R., de Oliveira A.H.P., Allasia D., Meili L. The synthesis and evaluation of porous carbon material from corozo fruit (bactris guineensis) for efficient propranolol hydrochloride adsorption // Molecules. - 2023. - Vol. 28, Is. 13. - P. 5232.

267 Burke G.M., Mendes R.W., Jambhekar S.S. Investigation of the Applicability of Ion Exchange Resins as a Sustained Release Drug Delivery System For Propranolol Hydrochloride // Drug Development and Industrial Pharmacy. - 1986. - Vol. 12, Is. 5. - P. 713–732.

268 Bautista-Toledo I., Ferro-García M.A., Rivera-Utrilla J., Moreno-Castilla C., Vegas Fernández F.J. Bisphenol A Removal from Water by Activated Carbon. Effects of Carbon Characteristics and Solution Chemistry // Environmental Science & Technology. - 2005. - Vol. 39, Is. 16. - P. 6246–6250.

269 Tsai W.-T., Hsu H.-C., Su T.-Y., Lin K.-Y., Lin C.-M. Adsorption characteristics of bisphenol-A in aqueous solutions onto hydrophobic zeolite // Journal of Colloid and Interface Science. - 2006. - Vol. 299, Is. 2. - P. 513–519.

270 Batra S., Datta D., Sai Beesabathuni N., Kanjolia N., Saha S. Adsorption of Bisphenol-A from aqueous solution using amberlite XAD-7 impregnated with aliquat 336: Batch, column, and design studies // Process Safety and Environmental Protection. - 2019. - Vol. 122. - P. 232–246.

271 Mendigaliyeva G.E., Rakhym A.B., Seilkhanova G.A. Kompozitnyj material na osnove ceolita, modificirovannogo polietilenglikolem dlya ochistki vodnyh rastvorov ot ionov Pb^{2+} i Cd^{2+} (Composite material based on zeolite modified with polyethylene glycol for purification of aqueous solutions from Pb^{2+} and Cd^{2+} ions // Herald of the Kazakh-British Technical University. – 2019. – Vol.16, Is. 1. – P. 63-71. (in Russian)

272 Hayakawa K., Mouri Y., Maeda T., Satake I., Sato M. Surfactant-modified zeolites as a drug carrier and the release of chloroquin // Colloid and Polymer Science. - 2000. - Vol. 278, Is. 6. - P. 553–558.

273 de Gennaro B., Catalanotti L., Cappelletti P., Langella A., Mercurio M., Serri C., Biondi M., Mayol L. Surface modified natural zeolite as a carrier for sustained diclofenac release: A

preliminary feasibility study // Colloids and Surfaces B: Biointerfaces. - 2015. - Vol. 130. – P. 101-109.

274 García-Villén F., Carazo E., Borrego-Sánchez A., Sánchez-Espejo R., Cerezo P., Viseras C., Aguzzi C. Clay minerals in drug delivery systems // Modified Clay and Zeolite Nanocomposite Materials: Environmental and Pharmaceutical Applications. - 2018. - P. 129–166.

275 Crespi D., Mennini T., Gobbi M. Carrier-dependent and Ca^{2+}-dependent 5-HT and dopamine release induced by (+)-amphetamine, 3,4-methylendioxy-methamphetamine, p-chloroamphetamine and (+)-fen¯uramine // British journal of pharmacology. – 1997. – Vol. 121, Is. 8. – P. 1735-1743.

276 Karimi M., Habibizadeh M., Rostamizadeh K., Khatamian M., Divband B. Preparation and characterization of nanocomposites based on different zeolite frameworks as carriers for anticancer drug: zeolite Y versus ZSM-5 // Polymer Bulletin. - 2019. - Vol. 76, Is. 5. - P. 2233–2252.

277 Kaur M., Datta M. Diclofenac Sodium Adsorption onto Montmorillonite: Adsorption Equilibrium Studies and Drug Release Kinetics // Adsorption Science & Technology. – 2014. – Vol. 32, Is. 5. – P. 365-387.

278 Yang L., Fassihi R. Modulation of diclofenac release from a totally soluble controlled release drug delivery system // Journal of Controlled Release. - 1997. - Vol. 44. - 135–140 p.

279 Orekhova L.Yu., Kudryavceva T.V., Burlakova Yu.S. Sistemy lokal'noj dostavki lekarstvennyh preparatov v parodontologii (Local drug delivery systems in periodontology)// Parodontologiya. - 2016. - Vol. 5, Is. 1(78). - P. 34–39. (in Russian)

280 França D. B. et al. Monitoring diclofenac adsorption by organophilic alkylpyridinium bentonites // Chemosphere. – 2020. – Vol. 242. – P. 125109.

281 Silva Filho E.C. Clays as Biomaterials in Controlled Drug Release: A Scientific and Technological Short Review // Biomedical Journal of Scientific & Technical Research. - 2019. - Vol. 15, Is. 2. – P. 11237-11242 .

282 Attama A.A., Nkemnele M.O. In vitro evaluation of drug release from self micro-emulsifying drug delivery systems using a biodegradable homolipid from Capra hircus // International Journal of Pharmaceutics. - 2005. - Vol. 304, Is. 1–2. - P. 4–10.

283 Calabrese I., Gelardi G., Merli M., Liveri M.L.T., Sciascia L. Clay-biosurfactant materials as functional drug delivery systems: Slowing down effect in the in vitro release of cinnamic acid // Applied Clay Science. - 2017. - Vol. 135. - P. 567–574.

284 Massaro M., Colletti C.G., Lazzara G., Riela S. The use of some clay minerals as natural resources for drug carrier applications // Journal of Functional Biomaterials. - 2018. - Vol. 9, Is. 4. – P.58.

285 Teodorescu M., Morariu S. Drug delivery system based on PVA and clay for potential treatment of COVID-19 // Journal of Polymer Research. - 2022. - Vol. 29, Is. 2. – P.67.

286 Kushnir A.A., Sypko K.S., Gubin A.S., Sheremet E.O., Sukhanov P.T. The use of sorbents of various natures for the extraction of non-steroidal anti-inflammatory drugs from aqueous media (review) // Sorbtsionnye i Khromatograficheskie Protsessy. - 2021. - Vol. 21, Is. 2. - P. 196–215.

287 Cheikh D., García-Villén F., Majdoub H., Zayani M.B., Viseras C. Complex of chitosan pectin and clay as diclofenac carrier // Applied Clay Science. - 2019. - Vol. 172. - P. 155–164.

288 Khlibsuwan R., Pongjanyakul T. Chitosan-clay matrix tablets for sustained-release drug delivery: Effect of chitosan molecular weight and lubricant // Journal of Drug Delivery Science and Technology. - 2016. - Vol. 35. - P. 303–313.

289 Krajišnik D., Daković A., Malenović A., Kragović M., Milić J. Ibuprofen sorption and release by modified natural zeolites as prospective drug carriers // Clay Minerals. - Mineralogical Society, 2015. - Vol. 50, Is. 1. - P. 11–22.

APPENDIX A

Flow-chart diagrams for optimal adsorbents synthesis

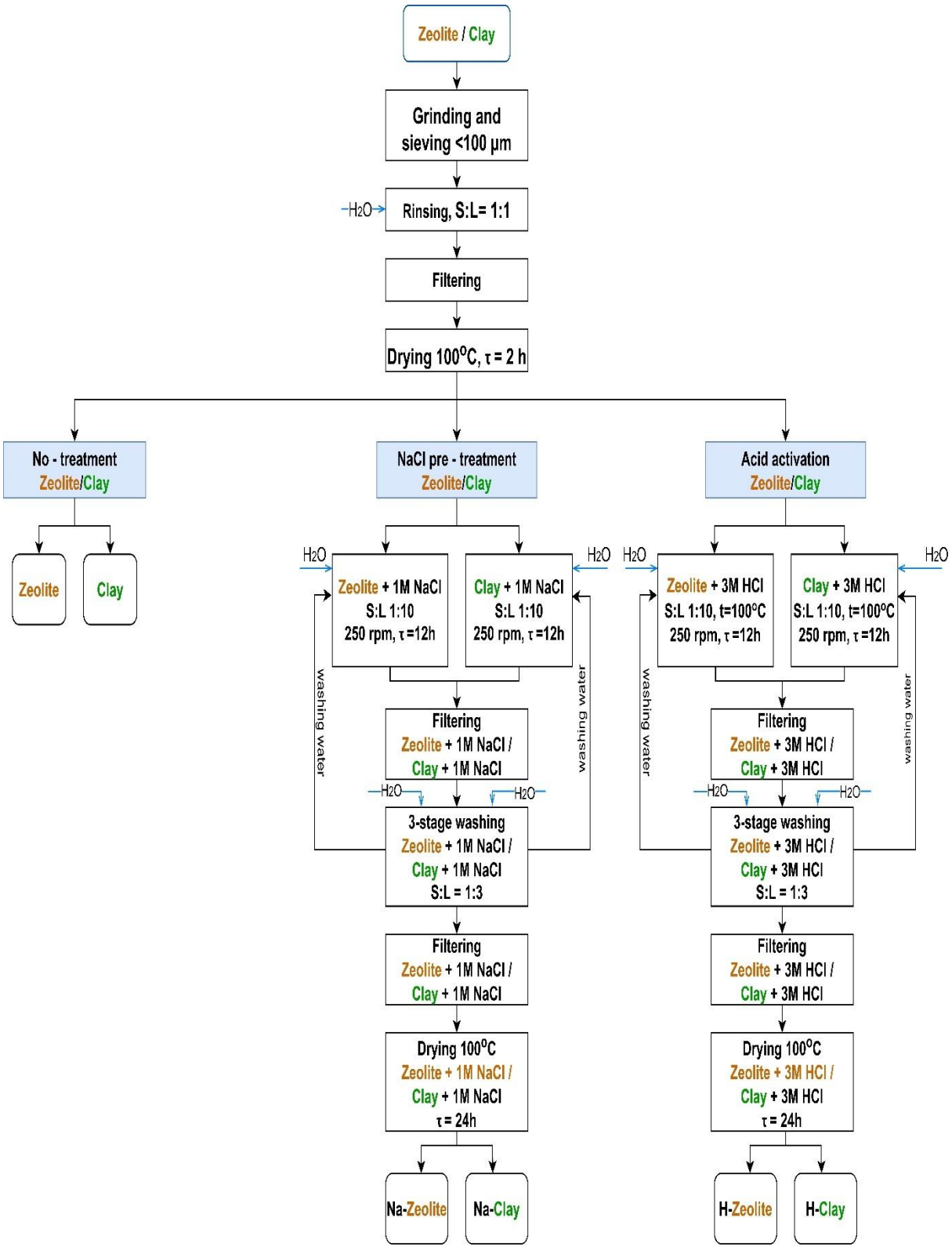


Figure A1 – Flow-chart diagram for pre-treatment stage of adsorbents preparation

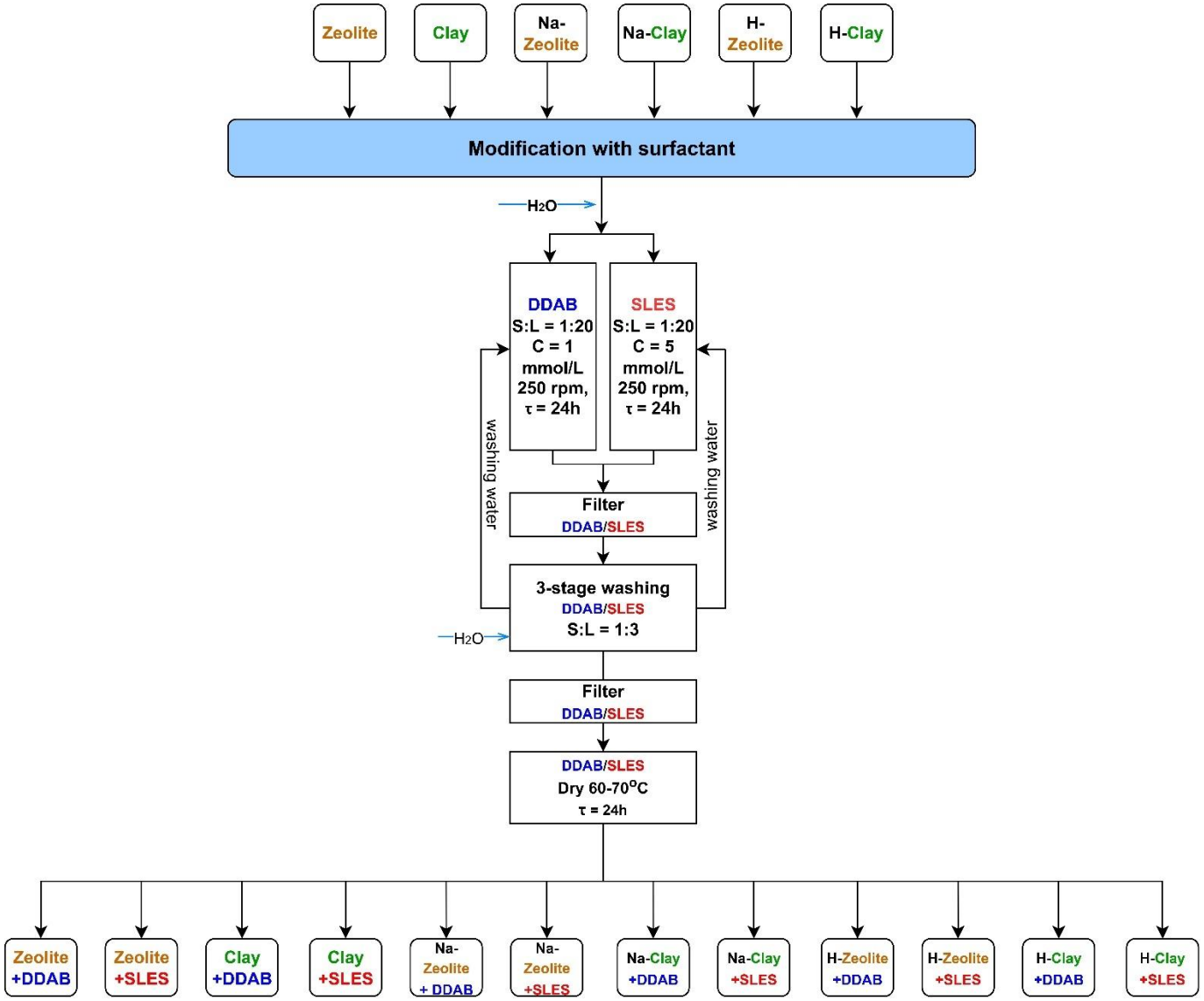


Figure A2 – Flow-chart diagram for modification stage of adsorbents preparation

APPENDIX B

Data for cost price calculation of modified adsorbents preparation

Table B1 – Cost structure of 1 kg of modified adsorbents

Cost Item	Subcategory / Material	Unit	Quantity per 1 kg	Unit Price, USD	Amount, USD
Raw Materials	Zeolite Shankanai	kg	1.00	0.30	0.30
	Chamotte clay	kg	1.00	0.15	0.15
	HCl (tech. 36%)	kg	1.10	0.30	0.33
	NaCl	kg	0.60	0.20	0.12
	H_2O (deionized)	m^3	0.010	1.00	0.01
	DDAB	kg	0.00924	200.00	1.85
	SLES	kg	0.035	3.00	0.11
Energy	Electricity	kW·h	20.0	0.05	1.00
Labor	Manual and operator labor	$/h	1	0.50	0.50
Amortization	Equipment	-	-	-	0.15
Processing Losses	Output loss	-	5%	-	0.20
Quality Control	Testing, reagents ($AgNO_3$, UV)	-	-	-	0.10
Packaging	Bags, big bags	pcs	1	0.20	0.20
Logistics	Transportation	$/kg	1	0.20	0.20
Administrative	Rent, accounting, overhead	-	-	-	0.40
TOTAL COST PRICE					**4.5-6.0**
Commercial markup (30%)					1.5-2.0
TOTAL WHOLESALE PRICE					**~6.0-8.0**

Table B1 provides a calculated breakdown of the production cost of 1 kg of modified sorbent, based on natural zeolite from the Shankanai deposit or chamotte clay. It includes the main cost items: raw materials, reagents, energy consumption, labor, equipment amortization, packaging, logistics, quality control, processing losses, and administrative expenses.

Raw materials include zeolite (0.30 $/kg), chamotte clay (0.15 $/kg), and chemical reagents such as hydrochloric acid (HCl), sodium chloride (NaCl), deionized water, and surfactants — cationic DDAB and anionic SLES. The prices are based on market rates as of 2025.

Energy costs are calculated based on two drying stages and 24-hour stirring at 250 rpm, with a total energy consumption of approximately 20 kWh per kilogram of product.

Other items include estimated labor costs for small-scale or pilot production (0.50 $/kg), equipment amortization (0.15 $/kg), material losses during washing, filtration, and drying (~5%), packaging and transportation costs (0.20 $/kg each), as well as quality control of residual surfactant and chloride ions (0.10 $/kg). Administrative overheads are estimated at approximately 10% of the total cost.

The final production cost of the modified sorbent is approximately 4.5-6.0 $/kg. With a typical commercial markup of 30%, the recommended wholesale price ranges from 6 to 8 $/kg, depending on production volume and delivery conditions.